THE ROLE OF MUSCLE IN AMYOTROPHIC LATERAL SCLEROSIS: PATHOGENESIS AND THERAPEUTIC POTENTIAL

A thesis submitted to the University of London

for the degree of Doctor of Philosophy

in the Faculty of Biomedical Science

By

Joanna Riddoch-Contreras BSc (Hons)

Sobell Department of Motor Neuroscience and Movement Disorders

Institute of Neurology,

University College London

October 2007

ProQuest LLC
789 East Eisenhower Parkway
P.O. Box 1346
Ann Arbor, MI 48106-1346

ACKNOWLEDGEMENTS

My gratitude goes to my supervisors, Dr Linda Greensmith and Professor Michael Duchen, for their encouragement and peerless support throughout my PhD.

Thank you to Jim Dick for kindly teaching me all the necessary laboratory skills which were invaluable to my thesis. Many thanks to my valued colleagues at the Institute of Neurology, who shared their practical experience and were all great friends namely, Jim, Dr Jo Dekkers, Dr Dairin Kieran, Dr Bernadett Kalmar, Dr Lynsey Bilsland, Dr Niran Nirmalananthan and Dr Virginie Bros, Jing Yip, Emem Edet-Amana, Dr Sarah Al-Izki, Dr Gita Prahu and Dr Nikki Potter. Thank you to my colleagues in the department of physiology, UCL, Dr Andrey Abramov, Dr Michelangelo Campanella, Dr Zoe Mann, Rosie Milton, Rosella Abeti, Dr Andrew Hall, Dr Parjam Zolfaghari and Sam Ranasinghe. Special thanks to Dr Jonny Wright, for his constant encouragement making everything seem achievable.

Most of all I thank my parents Rita Contreras Cruz and Dr John Riddoch, for all the outstanding support, particularly over this past year. I appreciated all the encouragement you gave me and having exceptional confidence in me.

ABSTRACT

Amyotrophic Lateral Sclerosis (ALS) is a progressive neurodegenerative disorder, characterised by the loss of motoneurons in the motor cortex, brainstem and spinal cord, leading to muscle atrophy and eventual paralysis. Despite intensive research the mechanisms that underlie the selective vulnerability of motoneurons in ALS remain unclear. Recent results have shown the involvement of non-neuronal cells in the central nervous system, such as glia in the pathogenesis of ALS. However the role of other cells in the peripheral nervous system, which also functionally interact with motoneurons, such as skeletal muscle, has not yet been established. In this thesis the role of skeletal muscle in ALS pathogenesis was investigated.

Transgenic $SOD1^{G93A}$ mice are a commonly used model of ALS, which closely resemble several features of human ALS. In this Thesis, experiments were performed to examine the effect of mutant SOD1 expression in muscles and examined the effect of motoneurons on the cellular properties of muscles, using an *in vitro* co-culture system. The results presented in **Chapter 3** show that mitochondrial dysfunction and aberrant calcium signalling arises in mutant SOD1 motoneurons and is influenced by muscles at an early stage in development.

Furthermore the loss of target derived neurotrophic support has been implicated in ALS and promising effects have been obtained from IGF-I in $SOD1^{G93A}$ mice. The potential neuroprotective effect of MGF, a splice variant of IGF-I was investigated *in vivo* in $SOD1^{G93A}$ mice. The results presented in **Chapter 4** show that MGF has potent neuroprotective effect in $SOD1^{G93A}$ mice. Both IGF-I and MGF were effective in improving muscle strength, increasing motor unit survival and delaying the progression of the disease. However the muscle restricted expression of MGF significantly improved motoneuron survival to a greater extent that IGF-I in $SOD1^{G93A}$ mice. The results of this research highlight skeletal muscle as an appropriate target to deliver therapeutic strategies to prevent motoneuron degeneration in ALS and suggest that early deficits, in muscle in particular, in mitochondrial function may play a role in ALS pathogenesis.

DECLARATION

I, Joanna Riddoch-Contreras, confirm that the work presented in this Thesis is my own. Where information has been derived from other sources, I confirm that this has been indicated in the Thesis.

Joanna Riddoch-Contreras

CONTENTS

LIST OF FIGURES

LIST OF TABLES

ABBREVIATIONS

½ RT	Half relaxation time
4-AP	4-aminopyridine
A	
a.u	Arbitrary units
AAV	adenosine viral vector
Acetyl CoA	Acetyl coenzyme A
ACh	Acetylcholine
AChE	Acetylcholinesterase
AChR	Acetylcholine Receptor
AD	Alzheimer's disease
AIF	Apoptosis inducing factor
ALS	Amyotrophic Lateral Sclerosis
AM	acetoxy-methyl
AMPA	α-amino-3-hydroxy-5-methylisoxazole-4-propionate
Apaf-1	Apoptotic protease-activator 1
AraC	Cytosine arabinoside
ATP	Adenosine triphosphate
B	
BDNF	Brain-derived neurotrophic factor
bHLH	basic helix-loop-helix
BMP4	Morphogenetic protein 4
BoTx	Botulinum A toxin
C	
Ca^{2+}	Calcium
Ca^{2+}ATPase	Calcium pump
Ca^{2+}_c	Cytosolic calcium
Caspases	Cysteine-dependent, aspartate-specific proteases
CCS	Copper chaperone for SOD1
ChAT	Choline acetyltransferase

CICR	Calcium induced calcium release
CN^-	Cyanide
CNS	Central nervous system
CNTF	Ciliary neurotrophic factor
COX	Cytochrome C oxidase
Cu/Zn SOD1	Copper/zinc superoxide dismutase
CX3CL1	Chemokine fractalkine
CX3CR1	Chemokine fractalkine receptor
D	
DAB	3-3'-diaminobenzidine
DAPI	4',6-diamidino-2-phenylindole
DCTN1	Dynactin
DHPR	Dihydropyridine receptors
DIV	Days *in vitro*
DMEM	Dulbecco's Modified Eagle Medium
DMSO	Dimethylsulfoxide
DNA	Deoxyribonucleic acid
DNCHC1	Dynein heavy chain
E	
E	Embryonic day
E-C coupling	Excitation-contraction coupling
EDL	Extensor digitorum longus
EEAT2	Excitatory amino acid transporter 2
EGTA	Ethylene glycolbis (2-aminoethylether)-N,N,N',N'-tetraacetic acid)
EPSP	Excitatory post synaptic potential
ERK	Extracellular-signal-regulated kinase
ESC	Embryonic stem cells
F	
FCCP	Carbonyl cyanide p-trifluoromethoxyphenyl hydrazone
FCS	Fetal Calf Serum
FGF2	Fibroblast growth factor 2

G

G93A	Glycine ^{93} to Alanine substitution
GAP-43	Growth associated protein-43
GDNF	Glial cell line-derived neurotrophic factor
GFAP	Glial fibrillary acidic protein
GH	Growth Hormone
GLT1	glial glutamate transporter

H

H_2O_2	Hydrogen peroxide
HB9	Homeobox 9
HBSS	Hanks' Balanced Salt Solution
HD	Huntington's disease
$HO^{\bullet}$	Hydroxyl radical
HSF1	Heat shock transcription factor-1
Hsp	Heat Shock protein
HSP	Hereditary Spastic Paraplegia
hUCB	Human umbilical cord blood

I

IGFBP	Insulin-like growth factors binding protein
IGF-I	Insulin-like growth factor I
IGF-Ia	Main systemic IGF-1 isoform
IGF-Ib	Mechano growth factor
IGF-II	Insulin-like growth factor II
IGF-IR	IGF-I receptor
IgG	Immunoglobulin
IL-6	Interleukin-6
IP_3	Inositol 1, 4, 5-trisphosphate
IP_3R	IP_3 receptor
IRSs	Insulin receptor substrate proteins

K

KA	Kainate

kD	Kilo daltons
L	
LB	Luria Bertani medium
LIF	Leukaemia inhibitory factor
Loa	Legs at odd angles
LPS	Lipopolysaccharide
LSM	Laser scanning microscope
LV	Lentiviral Vector
M	
MAPK	mitogen-activated protein kinase
mg	milligram
MGF	Mechano Growth Factor
MHC	Myosin heavy chain
MN	Motoneuron
MNR2	Motoneuron restricted 2
MOM	Mouse on mouse
MRF	Myogenic regulatory factor
mRNA	Messenger RNA
mtDNA	Mitochondrial DNA
MuSK	Muscle-specific tyrosine kinase
N	
Na^+	Sodium
NAD^+	NADH oxidised state
NADH	Nicotinamide adenine dinucleotide
NDGA	Nordihydroguaiaretic acid
NF-H	Neurofilament heavy polypeptide
NF-L	Neurofilament light polypeptide
NF-M	Neurofilament medium polypeptide
NGF	Nerve growth factor
NHS	Normal Horse Serum
NMDA	N-methyl-D-aspartate

nNOS	Neuronal nitric oxide
NO	Nitric oxide
NT3	Neurotrophin-3
NT4	Neurotrophin-4
O	
$O_2^{\bullet -}$	Superoxide
$ONOO^-$	Peroxynitrite
P	
Pax	Paired box transcriptional factors,
PBS	Phosphate Buffered Saline
PCR	Polymerase chain reaction
PD	Parkinson's disease
PI3-K	Phosphatidylinositol 3-kinase
PMT	Photomultiplier tube
PNS	Peripheral nervous system
PTP	Permeability transition pore
R	
rAVV	Recombinant adeno-associated virus
RM	Recording medium
RNA	Ribonucleic acid
RNAi	Interfering RNA
ROI	Region of interest
ROS	Reactive Oxygen Species
RyR	Ryanodine receptors
S	
SALS	Sporadic Amyotrophic lateral Sclerosis
SBMA	Spinal bulbar muscular atrophy
SDH	Succinate dehydrogenase
SEM	Standard error of the mean
SERCA	Sarco-endoplasmic reticulum Ca^{2+}-ATPases
SETX	Senataxin

Shh	Sonic hedgehog
SMA	Spinal Muscular Atrophy
SOD2	Manganese superoxide dismutase
SR	Sarcoplamic reticulum
sRNAi	Small interfering RNA
T	
TA	Tibialis anterior
TDP-43	TAR-DNA binding protein
THG	Thapsigargin
TMRM	Tetramethylrhodamine methyl ester
TNF-α	Tumor necrosis factor-α
TRAIL	TNF-related apoptosis inducing ligand
TTP	Time to peak
T-tubule	Transverse Tubule
TTX	Tetrodotoxin
U	
UCP	Uncoupling Proteins
UCP3	Uncoupling Protein 3
UV	Ultra violet
V	
VAMP	Vesicle-associated membrane protein
VAPB	VAMP (vesicle-associated membrane protein)-associated protein B
VEGF	Vascular endothelial growth factor
W	
WT	Wild type
Z	
zVAD-fmk	N-benzylocarbonyl-Val-Ala-Asp-fluoromethylketone
α-BTX	alpha-bungarotoxin
$\Delta\Psi_m$	Mitochondrial membrane potential

CHAPTER 1

GENERAL INTRODUCTION

Introduction

In this thesis the experiments described examine the mechanisms underlying the pathogenesis of Amyotrophic Lateral Sclerosis (ALS). This progressive neurodegenerative disorder is characterised by the selective degeneration of motoneurons. There is no cure or effective treatment for ALS, so improving our understanding of the mechanisms that underlie this disorder may prove beneficial for developing future therapeutic strategies and improve our understanding of other neurodegenerative conditions with common mechanisms. Despite extensive research, the mechanisms that underlie the selective vulnerability of motoneurons in ALS remain unclear. Increasing evidence suggests that ALS is a neurodegenerative condition not exclusive to motoneurons. Non-neuronal cells in the central nervous system, such as glia, are involved in the pathogenesis of ALS. The role of other non-neuronal cells, such as skeletal muscles, which reside in the peripheral nervous system and interact with motoneurons, has not yet been established. The unique interaction between motoneurons and muscles in ALS remains unresolved. Therefore in this thesis the role of skeletal muscle in ALS pathogenesis is investigated.

Neurodegeneration can recapitulate many early developmental events, and I will therefore give a brief outline of the development of the neuromuscular system, concentrating on motoneurons and muscles and their critical interaction. It is possible that the mechanisms that exist during development, which underlie the critical dependence, between motoneurons and muscles, may also be important in adult motoneuron survival.

1.1 Development of the neuromuscular system

The main components of the neuromuscular system are the motoneuron, the motor axon, the neuromuscular junction and the target muscle. The functional role of the neuromuscular system is to initiate muscle contraction, to generate and coordinate movement. In the early stages of the developing neuromuscular system, motoneurons and muscles are derived from embryologically distinct cell populations and develop

independently of each other. As motoneurons form functional contacts with muscle fibres a critical interaction arises and further functional specialisation of both cell types occurs. The important interaction between development motoneurons and muscles is addressed in this introduction.

1.1.1 Early motoneuron development

The vertebrate nervous system originates from the neural plate a sheet of neuroepithelial cells, which during neurulation, folds up to form the neural tube. Motoneurons are derived from the multi-potent neuroepithelial precursor cells in the ventral region of the neural tube (Langman J and Haden CC, 1970). Distinct classes of motoneurons and interneurons arise in a dorsal-ventral orientation in the ventral neural tube. The generation of neuronal patterning is due to a graded, secreted, signalling Sonic Hedgehog (Shh) protein, which establishes distinct regions of homeodomian transcription factor production along a dorsal-ventral axis. Shh is expressed by cells of the notochord and floor plate adjacent to the neural tube. Shh initially converts medial neural cells into a population of ventral progenitors (Ericson et al., 1996). It appears that the Shh-induced pathway of motoneuron differentiation occurs independent of the process of neurogenesis (Tanabe et al., 1998). The differentiation of motoneurons from ventral progenitors requires the prolonged expression of Shh in the S phase of the final cell division (Ericson et al., 1996). The program of motoneuron differentiation requires the repression of the interneurons fate and Shh induces the expression of homeodomain proteins, motoneuron restricted 2 (MNR2) and Homeobox 9 (HB9) in motoneuron progenitors. The expression of MNR2 is sufficient to direct somatic motoneuron differentiation (Tanabe et al., 1998).

1.1.2 Skeletal Muscle Formation in Vertebrates

In invertebrates, during embryonic development, skeletal muscle is derived from the paraxial mesoderm. The paraxial mesoderm forms laterally to the neural tube and notochord, giving rise to specialized structures referred to as somites, which form in a rostral-caudal orientation, at embryonic day eight in the mouse (Buckingham et al., 2003; Cossu et al., 1996).

During myogenesis upregulation of transcription factors, including the basic helix-loop-helix (bHLH) transcriptional activators of the myogenic regulatory factor family (MRF); MyoD, Myf-5, myogenin, Myf-6 (MRF-4), and the Paired box (Pax) transcriptional factors, $Pax3^+$ and $Pax7^+$ ensure specification to the myogenic lineage by regulating gene expression. Myogenesis is also controlled by positive and negative signalling factors from the surrounding environment. Wnts, produced by the surface ectoderm and Shh from notochord and floor, are positive effectors of myogenesis (Buckingham et al., 2003), whereas repressive signalling factors such as Bone morphogenetic protein 4 (BMP4) produced from the neural tube and lateral plate mesoderm are inhibitory to myogenic gene expression (Shi and Garry, 2006).

In response to signalling factors from the neighbouring lineages (neural tube, notochord and surface ectoderm) segmentation and differentiation of the somites occurs. The somites differentiate to form dorsally the dermomyotome, where the skeletal muscle progenitor cells resided, and later form the skin and skeletal muscles of the trunk and limbs (Buckingham et al., 2003). Ventrally the sclerotome is formed which gives rise to the skeleton. The muscles in the head are derived from anterior unsegmented, paraxial mesoderm and from the prechodal mesoderm. The muscle progenitor cells from the dorsal medial region of the somites migrate under the dermomyotome to form the myotome and rapidly differentiate and adopt the myogenic lineage. The cells that have migrated from the dorsal myotome will give rise to the expaxial myotome (the source of back and trunk musculature), the Myf5 expressing cells. The cells derived from the ventral lateral region of the myotome form the hypaxial myotome (the source of limb musculature) and are the MyoD expressing cells (Buckingham et al., 2003). Pax3 is also necessary for the activation of MyoD in the absence of Myf5 and is crucial for the survival and establishment of cells in the hypaxial myotome (Buckingham, 2001). After the induction of Myf5 and MyoD in the myotome domains, the cells are committed to a myogenic lineage (myoblasts). The proliferating myoblasts withdraw from the cell cycle to become terminally differentiated myocytes, which express myogenin and MRF-4 "late" MRF's (Kassar-Duchossoy et al., 2004). The other proliferating cells that

specifically express $Pax3^+$ and $Pax7^+$ migrate from the central dermomyotome to the central region of the myotome and continue to proliferate without differentiating or expressing any markers of the MyoD family; these cells are thought to be the source of satellite cells in adult muscle (Shi and Garry, 2006).

1.1.3 Muscle Development

The basic contractile units of skeletal muscle are muscle fibers, which arise from the fusion of the mononucleated myocytes which form multinucleated myotubes and are the constitutive units of muscle fibers. The first muscle fibers that form are primary fibres (embryonic day (e) 11-14 in the mouse limb) and form prior to innervation and express both fast and slow Myosin heavy chain (MHC) isoforms (Torgan and Daniels, 2001). These fibers are the supporting structure for the formation of the secondary muscle fibers (e14-16) which occurs around the time of innervation. These fibers comprise the bulk of skeletal muscle (Buckingham et al., 2003). During the development and maturation of the secondary muscle fibers, they sequentially express different MHC isoforms, primarily embryonic followed by neonatal and then adult fast and slow MHC isoforms (Torgan and Daniels, 2001).

1.1.4 Formation of the neuromuscular junction

Motor axons reach the target muscle, which consists of newly formed myotubes. Upon contact between the motor axon's growth cone and myotube, synaptic transmission is initiated immediately. Spontaneous and evoked neuromuscular transmission begins within seconds after nerve contacts muscle (Kidokoro and Yeh, 1982; Chow and Poo, 1985; Xie and Poo, 1986). Initially synaptic transmission is not very efficient, but following presynaptic and postsynaptic specialisation, there is increased transmission efficiency at the synapse.

1.1.5 Postsynaptic Differentiation

Following contact with the motor nerve, the postsynaptic site begins to mature and specialise. The distribution of acetylcholine receptor (AChR) on the newly formed

myotube is diffuse prior to innervation. The redistribution of AChRs on the myotube following innervation is regulated by the motor nerve in three distinct signalling processes that include agrin, neuregulin, and acetylcholine.

Agrin released from motor nerve localises the muscle-specific tyrosine kinase (MuSK), to the synaptic site. Agrin also stimulates MuSK, which recruits rapsyn, a MuSK effector protein, to the synapse, and this complex mediates the AChR clustering and stabilisation of synaptic AChR (Anderson and Cohen, 1977; Gautam et al., 1995). Neuregulin can stimulate the expression of genes coding for AChR subunits. Neuregulin released from motor nerve interacts with erbB kinase to induce selective expression of AChR subunit genes (Martinou et al., 1991; Loeb and Fischbach, 1995). As AChR cluster at the synapse the density of extrasynaptic AChR declines. Release of acetylcholine activates AChRs, leading to depolarisation, referred to as the excitatory post synaptic potential (EPSP). If EPSP reaches threshold, it can trigger an action potential which propagates along the length of the muscle, leading to the opening of voltage gated calcium channels and increased levels of cytosolic calcium. Increased calcium then initiates a muscle contraction. Calcium also activates a cascade of protein kinases that transduce signals that reach extrasynaptic nuclei and repress AChR subunit gene transcription (Huang et al., 1994; Adams and Goldman, 1998).

1.1.6 Presynaptic Differentiation

Changes in the presynaptic terminal also take place following contact between developing motor nerves and muscle fibres, which lead to maturation of the neuromuscular system. The presynaptic differentiation of the motor nerve terminal results in an increased number of synaptic vesicles. Many synaptic vesicles become clustered in dense areas on the presynaptic membrane called active zones (Kelly and Zacks, 1969; Ko, 1985; Buchanan et al., 1989; Lupa and Hall, 1989). Presynaptic differentiation only occurs at sites where there is contact with muscle fibres, which suggests that a target-derived factor is involved in regulating differentiation of the presynaptic nerve terminal (Lupa et al., 1990). Presynaptic differentiation may be mediated by muscle-derived agrin, or laminin β2, which stimulate the accumulation of

synaptic vesicles, or fibroblast growth factor (FGF2), which induces the clustering of synaptic vesicles (Dai and Peng, 1995; Porter et al., 1995). Presynaptic differentiation of the nerve terminal is also thought to be triggered by an elevation in intracellular calcium (Dai and Peng, 1993). Furthermore synapsins, vesicle-associated proteins that act to modulate transmitter release, may also regulate the structural and functional maturation of the motor nerve terminal (Lu et al., 1996).

1.1.7 Synapse elimination

Even after contact between the motor nerve and muscle fibers has been made at the endplate region, the endplate region develops but successive axons follow the routes laid down by the initial pathfinder axons and each muscle fibre consequently becomes innervated by axons from several motoneurons. The reorganisation of synaptic contacts, during postnatal development, leads to a single endplate region on each muscle fibre, but each endplate is innervated by several motor axons. This is termed polyneuronal innervation. In mature synapses each muscle fibre is innervated by a single motor axon. Thus each muscle fibre is activated by a single motoneuron, although each motor axon can branch to innervate many muscle fibres (Navarrete and Vrbova, 1993). The elimination of superfluous nerve terminals during postnatal development is not the result of motoneuron death, rather a reduction in the size of the peripheral field of motoneurons. Motoneurons with a larger network of terminals will be less able to provide sufficient support to their individual terminals than those with a smaller peripheral field (O'Brien et al., 1982), so that each mature motoneuron is innervated by fewer muscle fibres than during early development. This coincides with a period of increased neuromuscular activity and it has been shown to be dependent on neuromuscular activity (Navarrete and Vrbova, 1983).

Elimination of polyneuronal innervation can be increased by increasing neuromuscular activity, for example by chronic electrical stimulation (O'Brien and Vrbova, 1978). A reduction in neuromuscular activity e.g. following application of TTX to the motor nerve, reduces the rate of synaptic elimination (Callaway et al., 1987). The activity of the target muscle can also be reduced pharmacologically by blocking

acetylcholinesterase (AChE), the enzyme that hydrolyses ACh therefore increasing the duration of ACh activity and under these conditions there is a greater rate of elimination of polyneuronal innervation (Duxson and Vrbova, 1985; Greensmith and Vrbova, 1991; O'Brien et al., 1982). Inhibiting AChR by curare or BoTX, reduces the rate of elimination of polyneuronal innervation (Gordon et al., 1974). Thus, a large body of evidence demonstrates that neuromuscular activity regulates the process by which excess synaptic input is limited. However the mechanisms by which all but one nerve terminal is eliminated remained unclear until recent results have shown that the synaptic efficacy of individual innervating axon branches may be the determining factor underlying synapse elimination (Buffelli et al., 2003; Kasthuri and Lichtman, 2003). Thus, the axon with the greatest efficacy, determined by the amount of neurotransmitter released and the ability of axons to excite postsynaptic muscle fibres will succeed over weaker axon branches. Weaker axon branches will detach from the neuromuscular junction and undergo protease-mediated degradation (Buffelli et al., 2003). Evidence suggests that the molecular mechanism of activity dependent synapse reduction involves proteases, such as calcium-activated neutral proteases, which are involved in breaking down cytoskeletal proteins (Connold et al., 1986; Tyc and Vrbova, 1995; Swanson and Vrbova, 1987). Other evidence recently indicates that thrombin, a serine protease, may play a more important role in electrical activity-dependent synapse reduction (Liu et al., 1994; Glazner et al., 1997; Zoubine et al., 1996).

1.1.8 Determination of motor unit phenotype

Following the establishment of the adult pattern of innervation of muscle fibres, muscle fibres undergo a process of differentiation. This development of muscle fibres is determined by the activity of the motoneuron. Thus, the activity pattern of the motoneuron leads to the differentiation of slow and fast motor units (Navarrete and Vrbova, 1983). During the first few weeks of postnatal development, the pattern of firing of motoneurons which supply both slow and fast muscle is at a low frequency, irregular firing pattern. At this stage both slow and fast muscles contract slowly and achieve maximal tensions at low rates of stimulation (Brown, 1973; Close R., 1964). The contractile properties of muscles match the activity pattern of their motoneurons at

this stage in development. During the second to third postnatal week there is a progression towards the adult motor unit firing pattern. Slow muscles retain their 'tonic' motor unit activity pattern and increase the duration of low frequency firing (Navarrete and Vrbova, 1983). In fast muscles the activity of motor units becomes 'phasic' with a higher firing frequency of motor units, but continue to fire for short periods of time. Elimination of polyneuronal innervation and down-regulation of gap junctions on motoneurons, is required for motoneurons to exclusively exert influence over the muscle fibre it supplies (Navarrete and Vrbova, 1993).

1.1.9 Target dependence of motoneurons

Once developing motoneurons make contact with their target muscle fibres they become critically dependent on interaction with muscle fibres for their survival and maturation. This dependence of motoneurons on their target muscle is age-dependent. Thus neonatal nerve injury results in extensive motoneuron cell death (Lowrie et al., 1987). However this dependency on target interaction declines rapidly and in rodent injury to the sciatic nerve at 5 days of age, results in no motoneuron death (Greensmith and Vrbova, 1996). The extent of motoneuron cell death also depends on the site and severity of axonal injury (Kashihara et al., 1987). Thus the closer the axonal injury occurs to the cell body, the more likely that motoneuron cell death will occur, whereas distal lesions were followed by least cell death. Furthermore more motoneurons die when nerve is severed (axotomy) than when it is only crushed (Greensmith and Vrbova, 1996).

The functional dependence of motoneurons on their target muscle during development may be related to the release neurotrophins from muscles (Oppenheim, 1991). In early development, and following neonatal axotomy, neurotrophic factors such as brain-derived neurotrophic factor (BDNF), ciliary neurotrophic factor (CNTF), glial cell line-derived neurotrophic factor (GDNF), leukaemia inhibitory factor (LIF), interleukin-6 (IL-6), neurotrophin-3 (NT-3) and neurotrophin-4 (NT-4) rescued motoneurons at least in the short-term (Hughes et al., 1993; Li et al., 1994; Ikeda et al., 1996; Koliatsos et al., 1993; Koliatsos et al., 1994; Sendtner et al., 1990; Sendtner et al., 1992; Tan et al., 1996;

Vejsada et al., 1995; Yan et al., 1992; Baumgartner and Shine, 1998). However the effects are relatively short lived and long term treatment with neurotrophic factors failed to promote long-term survival of target-deprived motoneurons (Greensmith and Vrbova, 1996). Neurotrophic factors have been shown to enhance the expression of the cholinergic phenotype in motoneurons. The neurotrophins are able to increase the activity of ACh-synthesizing enzyme choline acetyltransferase (ChAT), in motoneurons *in vivo* and *in vitro* (Zurn et al., 1994; Martinou et al., 1992; Wong et al., 1993; Neff et al., 1993; Arakawa et al., 1990). Furthermore neurotrophins can prevent the injury-induced decrease in ChAT in motoneurons following axotomy (Yan et al., 1995). BDNF and NT3 have been shown to enhance the release of transmitter at the developing neuromuscular junction (Lohof et al., 1993). Thus, exogenous application of neurotrophins not only increases neuronal survival, but can also enhance the expression of the cholinergic phenotype and neuromuscular transmission, which may in turn influence motoneuron survival.

Interaction with the target may also influence motoneuron survival by regulating the motoneuron phenotype. The increase in the expression of proteins associated with neuromuscular transmission coincides with a period of increased neuromuscular and locomotor activity. During this critical period of development, the upregulation of transmitter related proteins, including ACh-synthesizing enzyme choline acetyltransferase (ChAT) and acetylcholinesterase (AChE) (Burt, 1975; O'Brien and Vrbova, 1978; Linseman et al., 2002), is associated with a decrease in proteins associated with axonal growth including growth associated protein-43 (GAP-43) and α-tubulin (Caroni and Becker, 1992). Motoneurons therefore change their phenotype from growing cells into transmitting cells which are independent of the target muscle for survival. Preventing neuromuscular interaction either by reducing transmitter release from the nerve terminals by applying $MgSO_4$ to the neuromuscular junction, or by blocking AChR on the muscle membrane with α-bungarotoxin (Greensmith and Vrbova, 1992), during early postnatal development, results in significant motoneuron death (Greensmith et al., 2000; Greensmith and Vrbova, 1992). Moreover increasing transmitter release of the nerve terminals by treatment with a potassium channel blocker

4-aminopyridine (4-AP), which is known to enhance transmitter release, reduces the vulnerability of motoneurons to nerve injury (Greensmith et al., 1996). Thus muscle influences motoneurons by regulating the release of ACh transmitter from the developing motor nerve. Therefore as transmission normally increases the expression of growth associated proteins decreases and motoneurons become less vulnerable to nerve injury (Sharp et al., 2003). Thus growing motoneurons are vulnerable to injury induced cell death, whereas mature transmitting motoneurons are more resistant to cell death. It is possible that interaction between the motoneuron and its target muscle, which results in this change in the phenotype of the motoneuron, enables the motoneuron to handle increased levels of excitation that occur in the developing spinal cord.

Glutamate is the main excitatory transmitter in the spinal cord. It is well established that glutamate excitotoxicity plays a role in the death of neurons (Choi, 1992). Evidence indicates that motoneurons are also particularly vulnerable to the toxic effects of glutamate. Motoneurons that are denied contact with target muscle in the first week of postnatal development are susceptible to glutamate induced cell death (Greensmith et al., 1994a). Furthermore blocking NMDA glutamate receptors can protect motoneurons from injury-induced cell death (Mentis et al., 1993; Greensmith et al., 1994b). Therefore during early postnatal development, the motoneuron is critically dependent on the target muscle for its survival and maturation.

1.2. Motoneuron degeneration

It is clear that during embryonic and postnatal development motoneurons and muscles are critically dependent on interaction for maturation. Preventing this interaction leads to motoneuron death. Motoneuron cell death can therefore occur (i) during embryonic development (programmed cell death) and (ii) early in postnatal development following axonal injury. However adult motoneurons can also undergo degeneration as a consequence of disease, for example in motoneuron diseases such as Amyotrophic Lateral Sclerosis.

1.2.1 Motoneuron diseases

The motoneuron diseases are a heterogeneous group of diseases which affect motoneurons and include Spinal Muscular Atrophy (SMA), Hereditary Spastic Paraplegia (HSP), Spinal bulbar muscular atrophy (SBMA, also known as Kennedy's Disease), Primary Lateral Sclerosis and Amyotrophic Lateral Sclerosis (ALS). The **Table 1.1** provides an overview of the different motoneuron disorders. The results described in this thesis are focused particularly on ALS.

1.2.2 Amyotrophic Lateral Sclerosis

Amyotrophic lateral sclerosis (ALS) first described by Jean-Martin Charcot in 1869, is the most common adult motoneuron disease in humans. ALS is a progressive neurodegenerative disorder, characterized by the loss of motoneurons in the motor cortex, brainstem and spinal cord ultimately leading to paralysis and death, typically within 2-5 years of disease onset (Cleveland and Rothstein, 2001). In the typical form of ALS there is evidence of both spinal and cortical involvement. The disease presents usually either in one limb, with wasting of the hand muscles or foot drop and, particularly common in women presenting after the age of 50, a combination of bulbar and corticobulbar symptoms, including dysphagia, dysarthria, tongue wasting, and brisk jaw jerk (Talbot, 2002). The asymmetrical weakness and wasting in the limbs is associated with clinical evidence of corticospinal tract damage, with increased tone and brisk reflexes.

1.2.3 Genetics of ALS

Although the majority of cases of ALS are sporadic, approximately 10% of cases are familial. The identified mutations in the genes that have been reported to cause ALS are shown in **Table 1.2**. These genes encode for the following proteins; copper/zinc superoxide dismutase (SOD1), alsin, senataxin (SETX), synaptobrevin/VAMP (vesicle-associated membrane protein)-associated protein B (VAPB) and dynactin (DCTN1) for references refer to **Table 1.2**. Mutations in angiogenin, neurofilament light subunit, survival motor neuron and vascular endothelial growth factor (VEGF) have also been implicated in sporadic ALS (Pasinelli and Brown, 2006). However, most of our

understanding of the pathogenesis of ALS has come from the study of the mutant SOD1 model of ALS.

Table 1.1 Classification of hereditary and sporadic motoneuron diseases

The table summarises the group of motoneuron disorders. There are two types of motoneurons (MN), upper and lower motoneurons which are known to degenerate. The lower motoneurons are located in the anterior horn of the spinal cord and brainstem. The upper motoneurons are located in the cerebral cortex of the brain, principally in the primary motor cortex. The age of onset varies from juvenile to adult and can be hereditary or sporadic in cause.

TABLE 1.1

Motoneuron disease	**Inheritance**	**Age of onset**	**MN affected**
Amyotrophic Lateral Sclerosis	Sporadic	Adult	Upper and lower MN
ALS familial adult onset	Autosomal dominant & Autosomal recessive	Adult	Upper and lower MN
ALS familial juvenile onset	Autosomal recessive	Juvenile	Upper and lower MN
Primary Lateral Sclerosis	Sporadic	Adult	Upper MN
Spinal Muscular Atrophy			
Type I Werdnig-Hoffmann	Autosomal recessive	Infantile	Lower MN
Type II Intermediate	Autosomal recessive	Infantile	Lower MN
Type III Kugelberg-Welander	Autosomal recessive	Infantile /Juvenile	Lower MN
Type VI Adult onset	Autosomal recessive & Autosomal dominant	Adult	Lower MN
Hereditary Spastic Paraplegia	Autosomal recessive	Adult	Upper MN
Spinal and Bulbar Muscular Atrophy	X-linked	Adult	Lower MN

1.2.4 Cu/Zn superoxide dismutase (SOD1)

Approximately 20% of familial ALS cases arise from mutations in copper/zinc superoxide dismutase (Cu/Zn SOD, SOD1) on chromosome 21q22.1 (Rosen, 1993). SOD1 is a ubiquitously expressed, predominantly cytosolic protein consisting of 153 amino-acids that functions as a homodimer. The enzymatic activity of SOD1 requires two co-factors, copper and zinc. Each subunit of SOD1 binds one copper and one zinc atom. SOD1 acts as a cellular antioxidant by catalysing the conversion of superoxide radicals, a toxic by-product of mitochondrial oxidative phosphorylation, to water or hydrogen peroxide.

The normal activity of Cu/Zn superoxide dismutase is shown by the reaction below:

$$SOD1\text{-}Cu^{2+} + O_2^{\bullet -} \rightarrow SOD1\text{-}Cu^{+} + O_2$$

$$SOD1\text{-}Cu^{2+} + O_2^{\bullet} \rightarrow SOD1\text{-}Cu^{2+} + H_2O_2$$

$$H_2O_2 \xrightarrow{\text{Glutathione peroxidase Catalase}} H_2O$$

Table 1.2 Genetics of ALS

The identified loci and genes containing the mutations leading to ALS are listed in the table. For each, chromosome location, the inheritance pattern, and type of onset are indicated. The names of genes are included where possible.

(Cu/Zn superoxide dismutase (SOD1), Senataxin (SETX), synaptobrevin/VAMP (vesicle-associated membrane protein)-associated protein B (VAPB) and dynactin (DCTN1)

TABLE 1.2

ALS	Gene	Chromosome	Inheritance	Clinical Features	References
ALS1	SOD1	21q22	Autosomal dominant	Typical ALS	(Rosen, 1993)
ALS2	ALS2	2q33	Autosomal recessive	Juvenile onset	(Hadano et al., 2001) (Yamanaka et al., 2006) (Yang et al., 2001)
ALS4	SETX	9q34	Autosomal dominant	Adult onset slowly progressive	(Chance et al., 1998) (Chen et al., 2004)
ALS8	VAMP	20q13	Autosomal dominant	Typical ALS	(Nishimura et al., 2004a) (Nishimura et al., 2004b)
ALS	DCTN1	2p13	Autosomal dominant	Adult onset	(Puls et al., 2003)
ALS5	Unknown	15q15.1-q21.1	Autosomal recessive	Juvenile slowly progressive	(Hentati et al., 1998)
ALS6	Unknown	16q12	Autosomal dominant	Typical ALS	(Abalkhail et al., 2003) (Ruddy et al., 2003) (Sapp et al., 2003)
ALS7	Unknown	20p13	Autosomal dominant	Typical ALS	(Sapp et al., 2003)

There are more than 125 different mutations that have been identified, across all five exons of SOD1 (Pasinelli and Brown, 2006). Although most mutations are missense, 12 mutations are nonsense or deletion mutations that produce a truncated SOD1 protein (Pasinelli and Brown, 2006). There is no clear association between the levels of SOD1 enzymatic activity and clinical progression or disease phenotype, as the mutations that have been identified have either reduced dismutase activity or retain their full catalytic activity (Pasinelli and Brown, 2006).

Several lines of transgenic mice have been generated to express the mutant human SOD protein, under the control of the human or mouse SOD1 gene promoter, at levels equal to or higher than the endogenous SOD1 protein. These transgenic mice exhibit a phenotype and pathology that resemble those observed in ALS patients (Gurney et al., 1994). Transgenic $SOD1^{G93A}$ or $SOD1^{G37R}$ mice develop motoneuron disease, despite elevations in SOD1 enzyme levels (Cleveland, 1999). Moreover, mice that express WT human Cu/Zn SOD at levels comparable $SOD1^{G93A}$ and act as a control for elevated levels of human SOD (Dal Canto and Gurney, 1995) and do not develop motoneuron disease. SOD1 knock-out mice also do not develop motoneuron disease (Reaume et al., 1996). Therefore the SOD1-mediated toxicity is not due to a loss of function, but rather a toxic gain of function.

1.2.5 Apoptosis

ALS motoneurons are known to die by apoptosis (Guegan et al., 2001). Apoptosis is a controlled, programmed, ATP dependent form of cell death, involving the use of signal transduction pathways in both its initiation and execution. The principle molecular components that regulate apoptosis include the Bcl-2 family of proteins that is composed of both pro- apoptotic and anti-apoptotic members that regulate the process of programmed cell death. Bcl-2 and Bcl-X_L are inhibitors of cell death and Bax is pro-apoptotic. The other components include Apaf-1 (apoptotic protease-activator 1) and a specific class of caspases (cysteine-dependent, aspartate-specific proteases), which are required for apoptosis (Green and Kroemer, 2004).

There are two pathways that can lead to caspase activation, the extrinsic and intrinsic pathways. In the extrinsic pathway, also known as the 'death-receptor pathway', apoptosis is triggered by ligand-induced activation of death receptors at the cell surface. The death receptors include TNF receptor 1, CD95/Fas as well as the TNF-related apoptosis inducing ligand (TRAIL) receptors 1 and 2 (Kroemer et al., 2007). In the intrinsic pathway, also known as the 'mitochondrial pathway', apoptosis results from an intracellular cascade were mitochondrial permeabilization is a crucial component. Cytochrome *C* has been shown to play a key role in mediating cell death when released from the mitochondria into the cytosol, where it binds to Apaf-1 to become part of the apoptosome (Cozzolino et al., 2006). Cytochrome *C* is released either because pro-apoptotic proteins such as Bax and t-Bid translocate to mitochondria or the opening of the mitochondrial permeability transition pore increases mitochondrial permeability and can induce the release of pro-apoptotic molecules (Zamzami et al., 1996). In cytosol the apoptosome binds pro-caspase-9 and activates caspase-9, which cleaves pro-caspase-3 to generate active caspase-3, the finial executor of cells (Green and Kroemer, 2004).

1.2.6 Apoptosis in ALS

There is evidence to suggest that apoptosis contributes to neuronal death in ALS. Apoptosis is characterised by four features (i) cell shrinkage, (ii) the condensation of chromatin, (iii) cellular fragmentation, and (iv) phagocytosis of cellular remnants (Kroemer et al., 2007). However, in ALS patients and animal models it is difficult to detect morphological and biochemical markers of apoptosis (Migheli et al., 1999). There is evidence for the activation of apoptotic pathways involving mitochondrial dependent changes in ALS and $SOD1^{G93A}$ mice (Guegan et al., 2001). In brain mitochondria of symptomatic $SOD1^{G93A}$ mice, there is a decreased association of cytochrome c within the inner mitochondrial membrane, which may increase the susceptibility of mitochondria to initiating apoptosis (Kirkinezos et al., 2005). In early symptomatic $SOD1^{G93A}$ mice, levels of cytosolic cytochrome c are increased and at the same time mitochondria levels are reduced (Kirkinezos et al., 2005). In post-mortem spinal cord tissue from sALS patients, cytochrome c immunoreactivity in the surviving

motoneurons is faint, indicating a cytosolic localisation (Guegan et al., 2001). The translocation of cytochrome c from mitochondria to the cytosol is crucial for the mitochondrial dependent activation of caspases. The redistribution of Bax occurs prior to the translocation of cytochrome c, which may possibly act as the initiating signal for permeabilisation of the outer mitochondrial membrane and release of cytochrome c (Guegan et al., 2001).

In post-mortem spinal cord tissue from ALS patients, the expression of Bax mRNA is up-regulated and Bcl2 mRNA, an anti-apoptotic protein, is reduced (Martin, 1999). In the spinal cord of symptomatic $SOD1^{G93A}$ mice, the immunoreactivity of Bad and Bax were also shown to be markedly increased and Bcl-2 and Bcl-xL were reduced (Vukosavic et al., 1999).

Immunoprecipitation studies using human and mouse spinal cord, showed that both WT and mutant $SOD1^{G93A}$ directly interact with Bcl2, the anti-apoptotic protein. Bcl2 was also found to be bound to mutant SOD1 aggregates in spinal cord mitochondria found in post-mortem spinal cord tissue from an ALS patient with the A4V mutation as well in $SOD1^{G93A}$ mice (Pasinelli et al., 2004). Therefore depletion of the anti-apoptotic protein Bcl2 in motoneurons may increase their susceptibity to cell death. In $SOD1^{G93A}$ mice treated with a recombinant adeno-associated virus (rAVV) encoding Bcl2, which resulted in sustained Bcl2 expression in motoneurons, there was an increase in motoneuron survival, although lifespan remained unchanged (Azzouz et al., 2000).

It has also been suggested that motoneuron death can be triggered by a specific pathway down-stream of the Fas death receptor (Raoul et al., 2002). An increased vulnerability to motoneuron cell death via the Fas receptor requires nitric oxide, the Fas death domain-associated protein Daxx and p38 kinase activation (Raoul et al., 1999; Raoul et al., 2002; Raoul et al., 2006). Mutant SOD1 motoneurons *in vitro* have an increased susceptibility to the activation of Fas leading, via phosphorylation of p38, via Daxx, and further nitric oxide synthesis, to a Fas/nitric oxide feedback loop required for motoneuron cell death (Raoul et al., 2002; Raoul et al., 2006).

1.3 Pathogenesis of ALS

Several key mechanisms are thought to play a role in ALS; mitochondrial dysfunction, oxidative damage, glutamate excitotoxicity, protein aggregation, cytoskeletal proteins, axonal transport deficits and neuroinflammation. Many of these mechanisms are thought to be involved in other neurodegenerative conditions (Kanazawa, 2001). The precise molecular mechanisms underlying the specific vulnerability of motoneurons in ALS remain unknown. However, several mechanisms have been implicated in the pathogenesis of ALS. Our understanding of the pathogenesis of ALS has been greatly increased by substantial post-mortem and biopsy evidence from ALS patients. However much of the current understanding of the pathogenesis of ALS comes from the study of transgenic SOD1 mice, which exhibit a phenotype and pathology that resemble those observed in ALS patients (Gurney et al., 1994). The clinical and pathological similarities of familial and sporadic ALS suggest that there may be a common pathogenesis. However there is recent evidence that transgenic SOD1 mice do not recapitulate the same mechanisms/deficits that are shown in human familial and sporadic ALS. In human ALS, the TAR-DNA binding protein (TDP-43), a nuclear factor that functions as a regulator of transcription, is mislocalised to the cytoplasm where it appears diffusely or as a component of ubiquitinated inclusion in affected neurons (Arai et al., 2006; Neumann et al., 2006). However mutant SOD1 mice fail to recapitulate the TDP-43 abnormalities observed in human ALS (Robertson et al., 2007).These results suggest that mutant SOD1 mice may not share the same mechanisms, as those which occur in the human disease.

1.3.1 Mitochondrial dysfunction

Mitochondria have a central role in cellular function, providing cellular ATP, participating in cellular calcium signalling, and apoptotic cell death (Duchen, 2004). It follows that disruption to mitochondrial function will result in cellular dysfunction or cell death (Duchen, 2004). There is now evidence to show that mitochondria are key players in the mechanisms that lead to motoneuron death in ALS. Thus apoptosis,

oxidative stress, glutamate excitotoxicity, protein aggregation and axonal transport disruption, are all mechanisms that are linked in some manner to mitochondrial physiology (Dupuis et al., 2004). Alterations in mitochondrial structure and function are not restricted to motoneurons in ALS, and occur in muscle of ALS patients and SOD1 mice (Siklos et al., 1996b; Afifi et al., 1966; Dupuis et al., 2003). Detailed discussions of the role of mitochondrial deficits in ALS are discussed in **Chapter 3**.

1.3.2 Oxidative damage

Oxidative stress arises from the imbalance between the production of reactive oxygen species (ROS) and the detoxifying defence. Typical markers of oxidative damage include increased ROS, decreased glutathione levels, lipid peroxidation, and DNA damage (Barber et al., 2006). Evidence from post mortem studies, shows increased oxidative damage to proteins in tissue from ALS patients. For example; protein carbonyl levels have been found to be elevated in both spinal cord and motor cortex (Shaw et al., 1995) from SALS patients. Levels of 3-nitrotyrosine, a marker for oxidative damage mediated by peroxynitrite are also elevated in motoneurons of spinal cord tissue from ALS patients (Abe et al., 1995; Abe et al., 1997; Beal et al., 1997; Ferrante et al., 1997). Similarly, in mutant SOD1 mice, free 3-nitrotyrosine immunoreactivity and markers of lipid peroxidation are elevated even at presymptomatic stages of disease (Bruijn et al., 1997a; Hall et al., 1998).

In cells mitochondria are the major site for the generation of ROS, including $O_2^{\bullet-}$ $OH^{\bullet}$ and H_2O_2. This is a normal consequence of oxidative phosphorylation and results in the generation of unpaired electrons. The mitochondrial enzyme SOD2 is localized to the mitochondrial matrix and is crucial for scavenging $O_2^{\bullet-}$ within mitochondria. A partial deficiency in SOD2 can exacerbate the clinical phenotype and reduces the lifespan in the mutant $SOD1^{G93A}$ mice (Andreassen et al., 2000). Whereas the overexpression of SOD2 attenuates cell death in neuroblastoma cells expressing $SOD1^{G37R}$ (Flanagan et al., 2002) and attenuates levels of mitochondrial superoxide levels in the neuroblastoma cell line (Zimmerman et al., 2007). These studies show that increasing the SOD2 expression levels acts to reduce levels of mitochondrial superoxide and thus protects against

neuronal cell death. Furthermore reductions in SOD2 levels may mediate mutant SOD1 toxicity, by increased oxidative stress, thus exacerbating the disease progression in ALS.

Recently it has been shown that cells expressing mutant SOD1 have a decrease in peroxiredoxin 3, a mitochondrial-targeted anti-oxidant (Wood-Allum et al., 2006). Ebselen, an anti-oxidant, is effective in reducing hydroperoxides, and acts to mimic peroxiredoxin 3, ameliorating the toxicity of mutant SOD1 in (NSC34) motoneuron-like cells (Wood-Allum et al., 2006). In mutant SOD1 neuroblastoma cells (Beretta et al., 2003) and mutant SOD1 motoneurons (Kruman et al., 1999) the relative levels of mitochondrial peroxynitrite and hydroxyl radicals were shown to be increased. Relative levels of mitochondrial oxidative stress and production of reactive oxygen species were determined by the fluorescent probe dihydrorhodamine-123 (Kruman et al., 1999). Levels of membrane lipid peroxidation were assessed using a thiobarbituric acid reactive substance and were shown to be increased in mutant SOD1 motoneurons (Kruman et al., 1999). Increased levels of protein carbonylation and lipid hydroperoxides, markers of oxidant-induced damaged proteins and lipids were identified in spinal cord and brain mitochondria isolated from $SOD1^{G93A}$ mice (Kirkinezos et al., 2005; Mattiazzi et al., 2002). These results suggest that involvement of mitochondrial oxidative stress may mediate the toxicity of mutant SOD1 in motoneurons.

The generation of transgenic *c.elegans* expressing mutant SOD1 were shown to be more vulnerable to oxidative stress, induced by paraquat than WT *c.elegans* (Oeda et al., 2001). Oxidative stress in the mutant SOD1 *c.elegans* strains, induced discrete aggregates in muscle, identified by green fluorescent protein. Oxidative stress resulted in aberrant accumulations of mutant proteins identified in *c.elegans* model of ALS. These results suggest that a disruption of the mitochondrial anti-oxidant defence mechanism may generate oxidative stress within motoneurons and other non-neuronal cells and contribute to the pathogenesis in ALS.

1.3.3 Glutamate Excitotoxicity

Glutamate-mediated excitotoxicity has been implicated in neuronal cell death, where the prolonged exposure to the excitatory amino acid glutamate can activate calcium-permeable glutamate receptors, resulting in elevated intracellular calcium (Ca^{2+}) (Cleveland and Rothstein, 2001). Elevated intracellular Ca^{2+} can activate proteases, nucleases and lipases and ultimately lead to neuronal death (Choi, 1992).

Glutamate induced excitotoxicity occurs through the over-activation of N-methyl-D-aspartate (NMDA) receptor, α-amino-3-hydroxy-5-methyl-4-isoxazole propionic acid (AMPA) and kainate (KA) receptors. In most neurons the NMDA receptor is associated with glutamate excitotoxicity, however motoneurons are believed to be more vulnerable to the AMPA/KA receptors (Rothstein et al., 1993; Vandenberghe et al., 2000b; Van Den and Robberecht, 2000; Van Den et al., 2000). Activation of AMPA receptors which lack the subunit GluR2 of the receptor have high permeability to Ca^{2+} (Carriedo et al., 1996) and are therefore vulnerable to excessive glutamate stimulation (Heath et al., 2002). The susceptibility of motoneurons to glutamate-mediated excitotoxicity may be related to a higher density of Ca^{2+} -permeable AMPA receptors compared to dorsal horn neurons (Vandenberghe et al., 2000b; Vandenberghe et al., 2000a).

It has been shown that motoneurons express atypical Ca^{2+}-permeable AMPA receptors which may contribute to an increase in calcium influx into motoneurons and eventual excitotoxicity and cell death (Williams et al., 1996). Furthermore, defective GluR2 editing has been found selectively in motoneurons in post-mortem spinal cord tissue from ALS patients (Kawahara et al., 2004). Thus, changes in the composition of AMPA receptor subunits may alter glutamate stimulation resulting in excitotoxicity and motoneuron cell death.

There is further evidence that suggests that there is an underlying deficit in glutamate metabolism in ALS. Abnormal glutamate transporter GLT-1 (EAAT-2) mechanisms may result in an elevated extracellular glutamate and consequently induce excitotoxicity. The loss of the glial glutamate transporters has been identified in the motor cortex and spinal cord of ALS patients (Fray et al., 1998; Maragakis et al., 2004; Sasaki et al.,

2000; Rothstein et al., 1995) and transgenic models of ALS (Bruijn et al., 1997; Howland et al., 2002) which may provoke glutamate induced excitotoxicity. There is evidence that glutamate transporters become irretrievably impaired by oxidative stress. SOD1 mutants expressed in *Xenopus oocytes* selectively inactivate the glial glutamate transporter GLT1 in the presence of H_2O_2 (Trotti et al., 1999). These results suggest interdependence between oxidative stress and excitotoxicity, whereby neuronal vulnerability to glutamate is increased by oxidative stress. Intracellular calcium can be buffered by calcium binding proteins and as described in **Chapter 3,** a decrease in calcium buffering capacity may contribute to the selective vulnerability of motoneurons in ALS, by exacerbation of glutamate-mediated excitotoxicity.

1.3.4 Motoneuron specific protein aggregations

Protein aggregation is a common feature of ALS. In post-mortem spinal cord tissue from ALS patients intracellular cytoplasmic aggregates containing ubiquitin can be observed in cell bodies and proximal axons of motoneurons (Leigh et al., 1991). Intracellular aggregates containing mutant SOD1 have also been found in motoneurons and astrocytes of SOD1 mice (Bruijn et al., 1997; Cheroni et al., 2005; Watanabe et al., 2001). The formation of protein aggregates may result from an inhibition of protein degradation and may exert toxicity by acquiring an aberrant chemistry (Bruijn et al., 1998). However, it has also been suggested that aggregates may in fact have a protective role in sequestering misfolded proteins in models of Huntington's disease and Parkinson's disease (Tanaka et al., 2004; Arrasate et al., 2004). Aggregates may potentially protect neurons by decreasing the toxic effects of misfolded proteins.

However the predominant view is that protein aggregations are indeed pathological. The correct folding of proteins is maintained by 'molecular chaperones', which mediate the folding or assembly of proteins into their final configuration. Molecular chaperones can also target misfolded proteins and prevent protein aggregation. Heat shock proteins (Hsps) act as molecular chaperones and associate with misfolded proteins to either promote their refolding or direct proteins to the ubiquitin-proteasome pathway for degradation (Kim et al., 2007). Hsps are constitutively expressed in motoneurons and

glial cells, but a defective heat shock response in motoneurons may contribute to the formation of aggregates and lead to motoneuron degeneration (Shinder et al., 2001). The overexpression of Hsp70 and Hsp40 has *in vitro* been shown to suppress the formation of mutant SOD1 aggregates in cell lines and reduce cell death (Bruening et al., 1999; Takeuchi et al., 2002). Arimoclomol, a co-inducer of Hsp expression delays disease progression and extends lifespan in $SOD1^{G93A}$ mice by 22% (Kieran et al., 2004). Arimoclomol induces the phosphorylation-mediated activation of the heat shock transcription factor-1 (HSF1), resulting in an increase in expression of Hsp70 and Hsp90 in the lumbar spinal cords of $SOD1^{G93A}$ mice. However simply raising the levels of Hsp70 by crossing Hsp70 overexpressing mice with SOD1 mice proved unsuccessful at ameliorating disease progression (Liu et al., 2005). These results suggest that the prolonged activation of HSF-1 may be required and the consequent activation of various Hsp and co-chaperones may be necessary to exert the neuroprotective actions of Hsp.

The formation of protein aggregates may be the consequence of impaired proteasomal function. In the lumbar spinal cord of $SOD1^{G93A}$ mice, a specific reduction in the level of 20S proteasome was found in presymptomatic mice (Kabashi et al., 2004). This may lead to the accumulation of aberrant ubiquitinated protein. Indeed a decrease in proteasomal activity correlated with the accumulation of mutant SOD1 in spinal cord homogenates of symptomatic $SOD1^{G93A}$ mice (Cheroni et al., 2005). Furthermore in the ventral horn of symptomatic $SOD1^{G93A}$ mice, a decreased immunostaining for 20s proteasome was found to be associated with a marked increased in ubiquitin, indicating an accumulation of ubiquitinated protein (Cheroni et al., 2005).

1.3.5 Dysfunction of cytoskeletal proteins

(i)Evidence of neurofilaments involvement in ALS

Neurofilaments (NF) are the most abundant structural protein in the neuronal cytoskeleton. There are 3 neurofilament subunits, classified according to their molecular weight: (i) NF-Light (NF-L); 61 kD (ii) NF-Medium (NL-M); 90 kD (iii) NF-Heavy (NF-H); 115 kD. Neurofilaments are synthesized in the neuronal soma, then co-assemble into neurofilament polymers to be subsequently transported to the axon by slow axonal

transport. They are essential for the maintenance of cell shape, axonal calibre and axonal transport (Zhang et al., 1997). Aberrant accumulation of neurofilaments is a common feature of both familial and sporadic ALS (Hirano, 1991; Hirano et al., 1984a; Hirano et al., 1984b) and has also been identified in mutant SOD1 mice (Bruijn et al., 1997; Dal Canto and Gurney, 1994b). Large myelinated neurofilament rich axons have been shown to be most vulnerable to the risk of degeneration in both mutant SOD1 mice and ALS patients.

Surprisingly, increased levels of wild-type (WT) NF-L or NF-H subunits in mice resulted in age-dependent motoneuron pathology with the accumulation of neurofilaments in motoneurons (Cote et al., 1993; Xu et al., 1993). A point mutation in the NF-L subunit in mice also resulted in progressive paralysis (Lee et al., 1994). In SOD1 mice a deletion of the NF (M/H) tail domain resulted in a delay in disease onset compared to WT SOD1 mice (Lobsiger et al., 2005). In these mice there are more surviving ventral root motor axons and motoneurons, a protective effect on the axonal calibre and an improvement in the number of innervated endplates (Lobsiger et al., 2005). The improvement observed in SOD1 mice following the removal of the NF-L and NF-H tail domain may result from an enhancement of anterograde transport and a restoration of axonal transport (Lobsiger et al., 2005).

ii)Peripherin

Peripherin is a 57kD intermediate filament, which is normally expressed in motoneurons (Troy et al., 1990a; Troy et al., 1990b). Peripherin levels increase in response to neuronal injury or in response to inflammatory cytokines (Sterneck et al., 1996). Peripherin has been identified within neurofilaments in the neuronal inclusions in post-mortem spinal cord tissue from ALS patients (Corbo and Hays, 1992) and SOD1 mice (Tu et al., 1996; Robertson et al., 2003). In mice, overexpression of peripherin induces the selective degeneration of motoneurons (Beaulieu et al., 1999). Furthermore, an assembly-disrupted frame shift mutation in the peripherin gene has been reported in one sporadic ALS patient (Gros-Louis et al., 2004). However the precise involvement of peripherin in ALS remains unclear, as overexpression or ablation of peripherin does not

affect disease progression or lifespan in $SOD1^{G37R}$ mice (Lariviere et al., 2003) suggesting that peripherin is not a contributing factor in mutant SOD1-mediated ALS.

1.3.6 Altered axonal transport in ALS

A unique feature of motoneurons is the functional contact that they form with skeletal muscle. In humans, in order to innervate distal muscles, some motor axons extend for more than one metre in length. Therefore proteins/vesicles synthesized in the motoneuron cell body are subsequently transported away from the cell body along the axon using kinesin motors by anterograde transport. A reciprocal retrograde transport is driven by the dynein motor and directs movement of cargos towards the motoneuron cell body. These motors travel along microtubule 'tracks' and transport cargos which include neurofilaments, vesicles, organelles, neurotrophic factors, and receptors (Chevalier-Larsen and Holzbaur, 2006). Motoneurons require axonal transport for normal cellular homeostasis. Several lines of evidence now show that impaired axonal transport plays a role in the pathogenesis of ALS (Sasaki and Iwata, 1996; Williamson and Cleveland, 1999; Boillee et al., 2006; Chevalier-Larsen and Holzbaur, 2006).

Ultrastructural evidence showing accumulated membrane bound cytoplasmic organelles suggested an impairment in fast axonal transport in the proximal axons of anterior horn neurons, identified in post-mortem spinal cord tissue from ALS patients (Sasaki and Iwata, 1996). Axonal transport has also been shown to be disrupted in mutant SOD1 mice (Sasaki et al., 2005; Ligon et al., 2005; Williamson and Cleveland, 1999; Murakami et al., 2001). A recent study has also identified perturbations in fast axonal transport in $SOD1^{G93A}$ motoneurons (De Vos et al., 2007). Mutant SOD1 in motoneurons impairs the transport of mitochondria reducing the content of mitochondria in axons and resulting in an accumulation of mitochondria in the motoneuron cell bodies (De Vos et al., 2007). This accumulation of mitochondria also results in altered mitochondrial function. The mitochondrial membrane potential is reduced, suggesting impaired mitochondrial function, and may also act to enhance axonal stress, by limiting the local availability of mitochondrial metabolites and ATP generation (De Vos et al., 2007).

Mutations in the dynein and dynactin complex are known to result in progressive motoneuron degeneration in both humans and mice. Point mutations in the gene encoding the $p150^{Glued}$ subunit of dynactin (DCTN1) have been identified in families with a slowly progressing, autosomal dominant form of lower motoneuron disease (Puls et al., 2005; Munch et al., 2004). The $p150^{Glued}$ subunit of dynactin binds to dynein and directly to microtubules, serving to increase the efficiency of dynein-mediated motility (Karki and Holzbaur, 1995; Waterman-Storer et al., 1995; Waterman-Storer et al., 1997; Muresan et al., 2001). Disruption of the dynein-dynactin complex, by the overexpression of the dynamitin (p50) subunit of dynactin in transgenic mice, inhibits axonal transport in motoneurons and causes late-onset progressive motoneuron degeneration (LaMonte et al., 2002). Homozygous expression of a missense mutation in the dynein heavy chain (DNCHC1) gene in Legs at odd angles (*Loa*) significantly reduces the rate of axonal transport in motoneurons, and results in motoneuron degeneration (Hafezparast et al., 2003). In $SOD1^{G93A}$ mice, retrograde axonal transport defects are present in embryonic motoneurons (Kieran et al., 2005). Quite surprisingly, crossing $SOD1^{G93A}$ mice with Loa/+ mice, delays the disease progression and significantly increases life span in $Loa/SOD1^{G93A}$ mice (Kieran et al., 2005). Moreover, there is a complete recovery in axonal transport deficits in motoneurons of these mice, which may be responsible for the amelioration of disease (Kieran et al., 2005). These results suggest that an improvement of the defects in axonal transport may have beneficial effects in ALS.

1.4 The role of non-neuronal cells in ALS pathogenesis

Although ALS is characterised by the degeneration of motoneurons, increasingly evidence shows that ALS is a non-cell autonomous disease in which non-neuronal cells in the CNS play a significant role (Boillee et al., 2006). Evidence that more than one cell type was required for the disease came from experiments in which the selective expression of mutant SOD1 in either neurons (Lino et al., 2002; Pramatarova et al., 2001) or astrocytes (Gong et al., 2000) does not result in motoneuron degeneration. These studies suggest that mutant SOD1 expression in motoneurons or astrocytes alone does not mediate ALS. In addition the generation of chimeric mice in which there is a

mixture of mutant SOD1 and WT in motoneurons and non-neuronal cells, mutant SOD toxicity to motoneurons was found to be dependent upon the expression of mutant SOD1 within non-neuronal cells (Clement et al., 2003). The proportion of non-neuronal cells with mutant SOD1 directly influenced disease manifestation. An increased proportion of WT non-neuronal cells resulted in no disease. Non-neuronal cells with mutant SOD1 were also shown to induce the formation of ubiquitinylated intracellular aggregates in WT motoneurons (Clement et al., 2003). Thus astrocytes play an important role in the pathogenesis of ALS.

1.4.1 Evidence supporting the involvement of astrocytes in ALS pathogenesis

The degeneration of motoneurons in ALS is accompanied by significant astrocytosis which can be observed in both ALS post-mortem tissue (Hirano, 1996; Schiffer et al., 1996; Hall et al., 1998b) as well as the spinal cord of mutant SOD1 mice. In SOD1 mice astrogliosis is present at symptom onset and increases with disease progression, yet it is unclear whether it is detrimental or a beneficial (Hall et al., 1998c; Levine et al., 1999; Alexianu et al., 2001). Recent evidence suggests that astrogliosis is detrimental to the pathogenesis of ALS.

The mechanism by which the expression of mutant SOD1 in astrocytes influences motoneuron survival is currently the focus of much research. In a co-culture model of embryonic stem cells (ESC) differentiated into motoneurons with $SOD1^{G93A}$ astrocytes, the survival of ESC motoneurons was significantly reduced by $SOD1^{G93A}$ astrocytes (Di Giorgio et al., 2007). These results show that $SOD1^{G93A}$ astrocytes have a negative effect on motoneuron survival (Di Giorgio et al., 2007). Primary astrocyte cultures expressing mutant SOD1 contain diffusible factors that are toxic to primary and ESC derived motoneurons, which were specific to $SOD1^{G93A}$ astrocytes, and not to muscles, microglia, cortical neurons or fibroblasts (Nagai et al., 2007). The soluble factors produced in mutant SOD1 astrocyte-conditioned medium, are toxic to ESC motoneurons via a Bax-dependent cell death pathway (Nagai et al., 2007). These findings suggest that astrocytes may play a role in the specific degeneration of spinal motoneurons.

1.4.2 Microglia activation and evidence for the involvement of inflammation

Neuroinflammation is a prominent feature in ALS with increased number of activated microglia, the innate immune cells, occurring as the disease progresses (Appel and Simpson, 2001; Beers et al., 2006; Xiao et al., 2007; Zhao et al., 2006). Microglial activation has been identified in post-mortem studies in the brain and spinal cord of ALS patients, (Engelhardt and Appel, 1990; Henkel et al., 2004; Kawamata et al., 1992; McGeer et al., 1991; Troost et al., 1993; Turner et al., 2004) and in spinal cords of mutant SOD1 mice (Hall et al., 1998a; Henkel et al., 2006; Kriz et al., 2002).

Microglial activation is associated with increased production of cytotoxic substances, including nitric oxide, superoxide, as well as pro-inflammatory cytokines such as tumor necrosis factor-α (TNF-α,), IL-1β and IL-6. However microglia may also be neuroprotective for example promoting the release of trophic factors, such as IGF-I (Butovsky et al., 2005; Zhao et al., 2006). The precise role of microglial in ALS remains unclear.

Results do however show that microglial activation may deleterious in models of ALS, chronic administration of a microglia activator lipopolysaccharide (LPS), exacerbated SOD1 mutant mediated disease in mice (Nguyen et al., 2004). The cytokine TNFα has been shown to be produced at higher levels by adult human $SOD1^{G93A}$ microglial cells when stimulated with LPS compared to WT microglial cells (Weydt et al., 2004). A direct toxic effect of activated microglia has been shown in a primary co-culture system of motoneurons and microglia. Following activation LPS, activated $SOD1^{G93A}$ microglia release more cytotoxic (superoxide) and pro-inflammatory molecules (nitric oxide), and less neurotrophic factors (IGF-I) compared to wild-type microglia (Xiao et al., 2007). Activated $SOD1^{G93A}$ microglia, can also induce a greater proportion of motoneuron cell death compared with WT microglia (Xiao et al., 2007). A recent study has revealed the significance of the neuron-to microglia signalling molecule chemokine fractalkine (CX3CL1) which is released by neurons and its receptor (CX3CR1) is expressed on microglia. Fractalkine is known to be involved in inhibiting microglial activation and cell death, and when $SOD1^{G93A}$ mice are bred with the deleted fractalkine receptor, there

is a rapid disease progression in $SOD1^{G93A}$ mice (Cardona et al., 2006). These results suggest that neuron-to-microglia signalling through the fractalkine receptor, may play a role in protecting against motoneuron cell death. Furthermore, treatment of $SOD1^{G93A}$ mice with the tetracycline derivative Minocycline, which inhibits microglial activation (Yrjanheikki et al., 1999) increased survival, inhibiting microglial activation, as well as exerting anti-apoptotic effects (Kriz et al., 2002; Van Den et al., 2002b; Zhu et al., 2002). Together these data provide strong evidence that microglial activation is detrimental to the progression of the disease.

1.4.3 Muscle involvement in ALS

Muscle weakness and eventual paralysis is a defining feature of ALS. One of the earliest pathological events observed in SOD1 mice, is the withdrawal of the motor axon from the neuromuscular synapse (Frey et al., 2000; Fischer et al., 2004; Pun et al., 2006). In view of these early structural changes in muscle and the loss of neuromuscular junction it has been suggested that ALS is a "dying–back" axonopathy (Fischer et al., 2004) and therefore targeting the muscle and neuromuscular junction could potentially be of therapeutic benefit in ALS.

The possibility that preventing muscle atrophy in $SOD1^{G93A}$ mice by enhancing muscle mass and strength, was tested in a study, in which mice were injected with an antibody to myostatin, a protein that inhibits muscle growth (Holzbaur et al., 2006). The results showed that inhibiting myostatin delayed muscle atrophy, but only transiently, failing to sustain muscle mass through the disease progression. It is possible that the failure to sustain the long term inhibition of myostatin resulted in the unsuccessful extension of lifespan of $SOD1^{G93A}$ mice (Holzbaur et al., 2006).

Mutant SOD1 is expressed in skeletal muscle but the precise contribution of the muscle in the pathogenesis of ALS remains unclear. The specific knockdown of mutant SOD1, using siRNA, specifically in muscle, has no effect on disease onset or progression (Miller et al., 2006). However using siRNA of mutant SOD1 in both muscles and motoneurons was sufficient to delay disease progression (Miller et al., 2006). These

results suggest that muscle alone is not the primary target for SOD1 mutant mediated disease. It may be more likely that impairments in muscle are a contributing factor to the pathogenesis of ALS, rather than a primary cause. If there is early metabolic dysfunction in skeletal muscle this may heighten the progression of the disease in vulnerable motoneurons. The involvement of muscle in the pathogenesis of ALS is discussed in more detail in **Chapter 3**.

Many therapeutic strategies have been targeted in muscle. There is increasing evidence that skeletal muscle is a potential target for gene therapy approaches in ALS. Muscle directed gene therapy has been shown to be successful in delivering neurotrophic factors to motoneurons (Wang et al., 2002; Kaspar et al., 2003; Kaspar et al., 2005; Acsadi et al., 2002; Azzouz et al., 2004).

1.5 Therapeutic strategies for ALS

Riluzole is currently the only licenced drug for treatment of ALS patients, although its effects on disease are modest since riluzole does not improve quality of life or muscle strength (Carri et al., 2006). Considerable research had therefore been focused on the identification and development of novel targets and agents that interfere with specific mechanisms that are implicated in ALS pathogenesis, so agents which are anti-oxidant, anti-glutamate, anti-apoptotic and anti-inflammatory have been tested. However as the pathogenesis of ALS may be multi-factorial targeting multiple pathways, by combined therapies (refer to Table 1.4) is likely to be the most effective approach (Carri et al., 2006). Transgenic animal models, in particular the $SOD1^{G93A}$ mice (Gurney et al., 1994) have been widely used for the assessment of a number of potential therapies for ALS. Table 1.3 summarises the therapeutic approaches that have been tested in models of ALS and for a recent review (Nirmalananthan and Greensmith, 2005; Bedlack et al., 2007). Table 1.4 summarises the combined therapies, transgenic overexpressing mice and viral therapies that have also shown improvements in lifespan.

Table 1.3 Therapeutic approaches in ALS

The most effective pharmacological therapies tested in transgenic SOD1 mice are summarised in the Table 1.3. The treatments are designed to intercept one or more of the pathological mechanisms including mitochondrial dysfunction, oxidative damage, glutamate excitotoxicity, protein aggregation, impaired neurotrophic support and neuroinflammation. The treatments tested in the SOD1 mice are judged in terms of their ability to prolong lifespan.

TABLE 1.3

Therapy	Mechanism	ALS model	Increase lifespan (%)	References
d-penicillamine	Copper chelator	$SOD1^{G93A}$	8%	(Hottinger et al., 1997)
AR-R 17,477	Inhibits nNOS activity	$SOD1^{G93A}$	13%	(Facchinetti et al., 1999)
Coenzyme Q_{10}	Anti-oxidant	$SOD1^{G93A}$	10%	(Matthews et al., 1998)
Riluzole	Anti-glutamate	$SOD1^{G93A}$	10.5%	(Gurney et al., 1998)
RPR 119990	Anti-glutamate	$SOD1^{G93A}$	12.7%	(Canton et al., 2001)
NBQX	Anti-glutamate	$SOD1^{G93A}$	10%	(Van Damme et al., 2003)
β-lactam	Anti-glutamate	$SOD1^{G93A}$	8%	(Rothstein et al., 2005)
Creatine	stabilizes mitochondrial creatine kinase	$SOD1^{G93A}$	17.8%	(Klivenyi et al., 1999)
Arimoclomol	HSP co-inducer	$SOD1^{G93A}$	22%	(Kieran et al., 2004)
Celecoxib	COX2 inhibitor	$SOD1^{G93A}$	25%	(Drachman et al., 2002)
Minocycline	Anti-apoptotic, Anti-inflammatory	$SOD1^{G93A}$	9-16%	(Kriz et al., 2002) (Van Den et al., 2002b) (Zhu et al., 2002)
NDGA	Inhibition of TNFα release	$SOD1^{G93A}$	32%	(West et al., 2004)
WHI-PI3I	Tyrosine kinase inhibitor	$SOD1^{G93A}$	49%	(Trieu et al., 2000)
hUCB	Immunomodulatory	$SOD1^{G93A}$	22%	(Garbuzova-Davis et al., 2003)
VEGF	Growth factor	$SOD1^{G93A}$ (Rat)	8%	(Storkebaum et al., 2005)
ZVAD-fmk	Caspase inhibitor	$SOD1^{G93A}$	22%	(Li et al., 2000)

Table 1.4 Alternative therapeutic approaches in ALS

The table summarises the combined therapies, transgenic overexpressing mice that have been generated to intercept one or more of the pathological mechanisms of ALS and viral therapies that have shown improvements in lifespan.

TABLE 1.4

Combined therapies		ALS model	lifespan (%)	References
Riluzole, minocycline + nimodipine		$SOD1^{G37R}$	12%	(Kriz et al., 2003)
Creatine +celecoxib or rofecoxib		$SOD1^{G93A}$	29%	(Klivenyi et al., 2004)
Creatine + minocycline		$SOD1^{G93A}$	28%	(Zhang et al., 2003)
Exercise and IGF-I		$SOD1^{G93A}$	31%	(Kaspar et al., 2005)
Transgenic overexpression				
Human NF-H	Neurofilament	$SOD1^{G37R}$	65%	(Couillard-Despres et al., 1998)
Bcl-2	Inhibits caspase/apoptosis activation	$SOD1^{G93A}$	15%	(Kostic et al., 1997)
ICE	Inhibits caspase 1	$SOD1^{G93A}$	8%	(Friedlander et al., 1997)
Viral Therapies	Mechanism			
AAV – Bcl2	Anti-apoptotic	$SOD1^{G93A}$	0%	(Azzouz et al., 2000)
AAV – GDNF	Neurotrophic factor	$SOD1^{G93A}$	14%	(Wang et al., 2002)
Ad – GDNF	Neurotrophic factor	$SOD1^{G93A}$	12%	(Acsadi et al., 2002)
AAV – IGF-I	Neurotrophic factor	$SOD1^{G93A}$	18%	(Kaspar et al., 2003)
LV- VEGF	Growth Factor	$SOD1^{G93A}$	15%	(Azzouz et al., 2004)
LV – siRNA	Ablation of mSOD1	$SOD1^{G93A}$	77%	(Ralph et al., 2005)

1.5.1 Growth Factors -VEGF

There are various studies that have implicated vascular endothelial growth factor (VEGF), a cytokine crucial for angiogenesis in ALS, and highlighted its therapeutic potential. A targeted deletion of the hypoxia response element within the VEGF promoter in mice ($VEGF^{\delta/\delta}$) was shown to have a phenotype similar to SOD1 mutant mice, with severe motor deficits and pathological changes including neurofilament accumulation in brainstem and spinal motoneurons (Oosthuyse et al., 2001). The double transgenic $SOD1^{G93A}/VEGF^{\delta/\delta}$ mice have extensive motoneuron degeneration and exhibit accelerated disease progression (Lambrechts et al., 2003). The treatment of $SOD1^{G93A}$ mice injected with a lentiviral vector containing VEGF into various muscles delayed the onset and slowed the disease progression (Azzouz et al., 2004). $SOD1^{G93A}$ rats treated with VEGF delivered intracerebroventricular, also showed an improvement in disease progression and lifespan (Storkebaum et al., 2005). These findings strengthen the notion that a loss of growth factor support, such as VEGF might be a key factor in the pathogenesis of ALS and therapies to augment growth factors may prove beneficial.

1.6 Gene therapies in ALS

Gene therapy as a therapeutic strategy has yielded promising results in mouse models of ALS. Several approaches have been investigated using viral gene therapy, direct infusion of anti-sense oligonucleotides, gene silencing with siRNA, and histone deacetylase inhibitors.

1.6.1 Viral gene therapy

The ability to transfer genes, using viral vectors, allows therapeutic genes to be delivered to the nervous system. Viral gene therapy has been examined in ALS, using three different viral vectors (i) recombinant adenovirus (Ad), (ii) adeno-associated virus (AAV) and (iii) lentivirus. The benefits of using viral vectors include the long term transgene expression, an efficient transduction capacity and low risk of immune reaction by expression of viral genes. Furthermore the viral vectors can be retrogradely transported, which is ideal for targeting motoneurons by delivering the virus via

injections to skeletal muscle, although such an approach may be difficult in patients. Muscle directed gene therapy has been shown to be successful in delivering neurotrophic factors to motoneurons (Wang et al., 2002; Kaspar et al., 2003; Kaspar et al., 2005; Acsadi et al., 2002; Azzouz et al., 2004). The use of gene therapy to deliver neurotrophic factors appears to be a promising therapeutic strategy for ALS.

1.6.2 Gene silencing

The emergence of small interfering RNA (siRNA) technology, which specifically silences gene expression at the mRNA level, is emerging as a novel therapeutic approach in ALS. Using viral vectors to mediate expression of siRNA to silence the mutant SOD1 expression *in vivo* has proved successful (Ralph et al., 2005; Raoul et al., 2005; Miller et al., 2005). Lentiviral-delivered siRNA injected into several muscle groups of $SOD1^{G93A}$ mice silenced the mutant SOD1 expression *in vivo* and delayed onset and extended survival by 77% in the $SOD1^{G93A}$ mice (Ralph et al., 2005). The gene silencing of mutant SOD1, provides the greatest therapeutic efficacy in terms of increased lifespan in the $SOD1^{G93A}$ mice, observed to date. This approach also highlights the ablation of mutant SOD1 *in vivo* as a potential therapeutic approach in mutant SOD1-mediated ALS.

1.6.3 Anti-sense oligonucleotide therapy for ALS

An alterative approach is the use of synthetic anti-sense oligonucleotides which target and assist the degradation of mRNA. Small nucleotide sequences of DNA target mRNA in a sequence dependent manner, ultimately leading to the degradation of mRNA by endogenous RNaseH. The synthetic anti-sense oligonucleotide delivered by the direct infusion into the brain (intracerebroventricular) to $SOD1^{G93A}$ rats, was shown to be successful at reducing mutant SOD1 expression levels in the brain and spinal cord, resulting in a delay in the progression of the disease (Smith et al., 2006). The dosage of antisense oligonucleotides can be regulated, which overcomes one of the limitations of viral vectors, where there are no mechanisms for altering the dose (Xia et al., 2006).

1.7 Aims of this Thesis

This thesis examines the involvement of skeletal muscle in the pathogenesis of ALS. Experiments will be presented in which I examine

(i) The effect of mutant SOD1 expression in myotubes on the functional properties of mitochondria and

(ii) The effect of motoneurons on mitochondrial function in muscles in an *in vitro* co-culture model

(iii) The effect of increasing the expression of a muscle specific neurotrophic factor, MGF on the disease progression in $SOD1^{G93A}$ mice.

CHAPTER 2

MATERIALS AND METHODS

2.1 Transgenic SOD1 mouse colony

2.1.1 Breeding and maintenance

All experimental animals used in this study were maintained and bred in the Biological Services Unit at Institute of Neurology, University College London. Every effort was made to ensure methods of reduction, refinement and replacement took place to minimize the number of animals used and maximize their welfare. All experimental procedures conducted in this study were performed in accordance with the UK Animal (Scientific procedure) Act 1986, and following approval from the ethical review panel of the Institute of Neurology.

The mice were housed in conventional plastic and stainless steel cages, with woodchip bedding and cardboard tubes for environmental enrichment. The mouse room was maintained on a 12 hour light cycle, lights on from 7am-7pm, the temperature was kept between 19-23 °C, humidity of ~ 40-70%, 12-15 air changes per hour. The mice were feed a pellet diet from hoppers placed in food racks, and water was provided in bottles both suspended from the cage lid and above the floor of the cage. At end-stage, when mice had considerable muscle weakness and could not support their own weight to reach the pellets, the mice were given pellets which were soaked in water, and the sodden pellets were left on the floor of the cage. This ensured that the mice were able to feed and rehydrated despite not being able to reach water bottles or pellets.

Transgenic male mice carrying a high copy number of the mutant allele for human SOD1 containing the Gly93 -->Ala (SOD^{G93A}) substitution often referred to as B6SJL-TgN[SOD1G93A]1Gur) were originally purchased from Jackson Laboratories (Bar Harbour, ME) and were bred with female B6SJLF1 hybrids. The transgenic progeny were identified by polymerase chain reaction (PCR) of the tail DNA with specific primers for human SOD1. In those experiments where overexpressing SOD^{WT} mice were genotyped the standard SOD PCR was used as it does not differentiate DNA between SOD^{WT} and $SOD1^{G93A}$ mice.

2.1.2 DNA isolation and polymerase chain reaction

To obtain a sample of DNA from the mice, ethyl chloride was used to anaesthetize the tip of the mice's tail and approximately 0.5cm of tail was removed. The tail was digested by one of two methods, either by the standard protocol for weaning mice or the rapid DNA extraction method used for embryos or neonatal mice.

The standard protocol consists of the tails digested with 15µl proteinase K (20mg/ml) in 300µl TNES buffer (50mM Tris pH 8, 100mM EDTA, 100mM NaCl, and 1% lauryl sulphate) overnight at 55 °C. Following the overnight digestion the samples were centrifuged at 14,000 rpm for 4 minutes and the supernatant decanted, 4µl of the supernatant was diluted to 200 µl with distilled water.

The alterative rapid DNA extraction method was modified protocol (McClive and Sinclair, 2001). Neonatal mice tail snips were digested at 55 °C for 5 mins with digestion buffer contained KCl (50mM), Tris-HCl (10mM pH 8.3), NP40 (0.45%), Tween-20 (0.45%) and proteinase K (20mg/ml). Samples were vortexed and subsequently incubated for a following 10mins at 95 °C, the digested samples were then centrifuged 14000g for 3 mins, the supernatant removed to add to the PCR mix.

The PCR reaction mixture was prepared using a modified version of the Jackson Laboratories protocol, each reaction mixture for the PCR included per sample 17.65µl sterile water, 2.5µl (10x) PCR buffer, 0.75µl $MgCl_2$ (10x), 0.5µl dNTP (10mM), 0.25µl primer 1 IMR0042 (1µg/µl), 0.25µl primer 2 IMR0043(1µg/µl), 0.25µl primer 3 IMR0113(1µg/µl), 0.25µl primer 4 IMR0114(1µg/µl), 0.1µl *Taq* Polymerase(0.5 units) total volume 22.5 µl. The PCR reaction mixture was kept on ice and 22.5µl aliquoted into 0.2ml PCR tubes and 2.5 µl DNA sample was added to each tube.

The primer sequences for wild-type (WT) forward is IMR0042, 5'- CTA GGC CAC AGA ATT GAA AGA TCT -3' and the WT reverse (common) Primer 2 IMR0043, 5'-GTA GGT GGA AAT TCT AGC ATC ATC C -3'. The PCR primers for the analysis of

SOD1 is IMR0113, 5'- CAT CAG CCC TAA TCC ATC TGA -3' and IMR0114, 5'- CGC GAC TAA CAA TCA AAG TGA -3'

The program for amplification was as follows 95°C for 3 mins (cycle 1) , 95°C for 30 sec (cycle 2), 60°C for 30 sec (cycle 3), 72°C for 45 sec, cycles 2-4 were repeated for 35 cycles, 72°C for 2 mins, then held at 4°C . The PCR products were separated by DNA electrophoresis on an agarose gel (2%) at 60 volts for 30 mins. The expected PCR product for Tg SOD is 236 base pairs and the internal standard (WT) 324 base pairs.

2.2 *In vitro* experiments

2.2.1 Preparation of culture plates

In the fume hood glass coverslips were sterilised by passing through the flame of a Bunsen burner, and placing each coverslip into a well of a culture plate. A solution of polyornithine 1:1000 (1.5mg/ml in sterile water), was prepared and added to each well, ensuring the coverslip were fully covered. The plates were left overnight in the incubator. The following day the polyornithine was removed and left to dry. Laminin 1:200 (1mg/ml) was placed on the coverslips in the wells ensuring all the coverslip were covered and the plates were left in the incubator for at least 2 hours. Prior plating the cells, laminin was removed and replaced with culture media.

2.2.2 Primary Muscle culture

Primary myotubes were obtained from postnatal day 0-2 (P0-P2) mice which were sacrificed by decapitation. The mice were immersed in 70% ethanol and the hind-limbs removed under a dissection microscope, in dissection solution containing Dulbecco's Phosphate Buffered Saline (PBS) with penicillin streptomycin (5000units/ml) and amphotericin B (2.5mg/L). All skin and bone was separated with sterile forceps and the muscle collected in a culture dish in calcium, magnesium free Hanks' Balanced Salt Solution (HBSS) HEPES (1M 1%) (Invitrogen), EDTA (0.02%) (VWR).

To dissociate the muscle cells, a sharp blade was used to finely chop the muscle into ~ 0.2mm^3 pieces. The collected muscle was then incubated for 50 mins on a shaking platform at 37 °C in trypsin (4mg/ml) and collagenase (0.5mg/ml) (Invitrogen), in Ca–Mg free HBSS and HEPES (VWR), EDTA (0.02%). BSA (24mg/ml) was added to the cell suspension to inhibit trypsin activity. The cell suspension was triturated using flamed Pasteur pipette and filtered using N100 nylon mesh to remove large pieces of undigested tissue, remaining skin or bone. The collected cell suspension was centrifuged at 900 RPM (180g) for 5 mins and the supernatant removed and the pellet was re-suspended in Dulbecco's Modified Eagle Medium (DMEM) (Invitrogen), Fetal Calf Serum (FCS)(10% PAA laboratories), Normal Horse Serum (NHS) (10% PAA laboratories), penicillin/streptomycin (0.1%). The cells were seeded at a density of 5x10 ^{6} /ml onto laminin (Invitrogen), coated 75cm^2 culture flask and cells maintained in culture medium containing DMEM, Fetal Calf Serum (10%) , Normal Horse Serum (10%), penicillin/streptomycin (0.1%) .

Cultures were maintained for 1-2 days or until spindle-shaped myoblasts had proliferated and aligned themselves for fusion (~70% confluent) the cells were rinsed a couple of times with HBSS, HEPES (1M), then incubated for 5 min with fresh, filtered dispase a neutral protease (0.5mg/ml) at 37 °C or until 75% of cells detached when the medium was swirled in the flasks. 1ml FCS was added to inhibit the dispase activity. Cells were collected and DMEM (79%), FCS (10%), NHS (10%), penicillin/streptomycin (1%) were added to cells. The cell suspension was centrifuged at 800 RPM (160g) for 5 mins, the supernatant removed and the pellet re-suspended in DMEM (79%), FCS (10%), NHS (10%), and penicillin/streptomycin (1%). The cells were seeded on an uncoated cell culture dish for 30 min at 37 °C and subsequently mechanical agitated to dislodge and collect loosely attached cells. Cells were seeded at a density of 10x10^4/ml onto 22mm diameter laminin coated coverslips in 6 well plates. The culture medium DMEM (79%), FCS (10%), NHS (10%), penicillin/streptomycin (1%) was changed after 24hrs and cultures maintained at 37 °C and 5% CO_2. The cells became completely confluent within 2-3 days and the culture medium was changed to DMEM (94%), NHS (5%), penicillin/streptomycin (1%) to differentiate the myoblasts

and myotubes formed within 2-3 days in culture. Following 2 days in culture the residual fibroblasts are eliminated by replacing the culture growth medium with medium containing cytosine arabinoside (AraC) (10μM) DMEM (94%), NHS (5%), penicillin/streptomycin (1%).

2.2.3 Acetylcholine Receptor and Immunofluorescence labeling

Prior to fixation for immunofluorescence, AChR on the myotubes surface were labelled with $5x10^{-8}$Alexa 488 conjugated α-bungarotoxin (Molecular Probes) for 1hr at 37°C. Myotube cultures were rinsed in PBS and fixed in -20°C methanol for 5 mins. Cultures were washed twice for 2 mins in PBS, and incubated in permeabilization solution (BSA (0.1%) and saponin (0.5%)) for 15mins and the mouse-mouse (MOM) protocol followed as detailed below:

2.2.4 Mouse-mouse Immunocytochemistry

Specific localization of mouse primary monoclonal antibodies on mouse tissue can be optimized by the use of a mouse-on-mouse immunodetection kit (MOM kit, Vector Laboratories, cat #BMK-2202). This kit blocks endogenous mouse immunoglobulins in the mouse tissue, permitting the accurate detection of the mouse primary antibody by the anti-mouse secondary antibody. Cells were incubated in H_2O_2 (0.3%) for 30 mins, to block endogenous peroxidase activity, and then incubated for 1hr in mouse-on mouse (MOM) mouse Ig blocking reagent at room temperature. Following two rinses in PBS for 2 mins each the cells were incubated in working solution MOM diluent for 5mins before removing excess MOM diluent. Cells were then incubated in the, monoclonal anti-Myosin (skeletal slow) antibody (Clone NOQ7.5.4.D (1:1000)) diluted in MOM, for 30 mins at room temperature. The cells were then washed twice with PBS for 2 minutes each time and MOM biotinylated IgG reagent was applied for 10mins. The sections were washed twice 2 mins in PBS and incubated in fluorescent Avidin Alexa 488 (1:200) or Texas Red (1:200 for 1hr in the dark and subsequently washed twice for 2 mins in PBS. The nucleus was counterstained with 4',6-diamidino-2-phenylindole (DAPI) (1:1000) for 20mins, and the sections mounted with Dakocytomation Fluorescent mounting medium (cat #S3023).

All reagents were supplied from Sigma-Aldrich unless otherwise stated.

2.2.5 Primary cultures of mixed ventral horn cells

The primary cultures of mixed ventral horn cells were obtained from mutant SOD1 transgenic mice embryos at E13 using a protocol adapted from that described by (Camu and Henderson, 1992). Time-mated pregnant females were terminally anaesthetized with pentobarbitione (140mg/kg) and embryos removed by hysterectomy and placed in a petri dish with sterile dissection solution. The embryos were extracted from placenta and each embryo placed in a clean Petri-dish labelled with a number, for identification purposes and the tail biopsies taken for genotyping. Under a dissection microscope the embryo was placed on a dissection dish and with sharp forceps the head of the embryo was removed, above the cerebellum, and visceral tissue removed. The embryo was then placed "face down" and the dorsal meninges and thin tissue overlying the spinal cord was scored along both sides of spinal cord and gently removed. The tip of forceps was scored along carefully dorsal meninges, releasing the meninges and opening out the cord. The spinal cord was released from underlying tissue by passing closed forceps underneath the cord and then opening up the forceps releasing them from the tissue. The spinal cord once removed from the body was placed ventral side up and the meninges pulled off carefully. The dorsal horns were cut from the spinal cord with a fine ophthalmic scalpel blade. The remaining ventral horn portion of the spinal cord was collected in a petri dish with sterile PBS and grouped according to genotype following PCR of tails.

The ventral horn tissue was cut into small pieces and transferred into 15 ml polystyrene tube and 1 ml sterile PBS added to trypsin (0.025% final concentration) and incubated for 10 mins at 37°C, agitating the tube after first 5 mins. Immediately after trypsin incubation, the spinal cord fragments were transferred into a polystyrene tube containing 800µl L-15 medium, 100µl BSA (4% w/v), 100µl DNAse (1mg/ml)

The tissue suspension was triturated twice and allowed to settle for 2 min, the supernatant transferred to a fresh 15 ml tube. To the tube containing the tissue fragments, 900µl L-15 medium, 100 µl BSA (4% w/v), 20 µl DNAse (1mg/ml) was added. The tissue suspension was triturated 8 times; fragments settled and the supernatant transferred to the fresh tube. Using a long Pasteur pipette, 1 ml BSA (4%) was added to the bottom of the tube which contained the pooled supernatants, to form a cushion when spinning the suspension. The tube was centrifuged for 5 min at 1500 rpm at room temperature. The supernatant was removed and the pellet re-suspended (~6 times) in 1 ml complete neurobasal medium with normal horse serum (2%), 50 units/ml penicillin 50µg/ml streptomycin 2-mercaptoethanol (0.2%), B27 supplement (2%), glutamine (0.5mM), GDNF (0.1ng/ml), CNFT (0.1ng/ml) and 20 µl DNAse (1mg/ml). The cells should be completely dissociated. The expected yield is approximately 1-2 million cells per spinal cord. Cells were seeded at a density of $10x10^4$, onto polyornithine and laminin coated coverslips. The cultures were maintained in the incubator at 37°C and 5% CO_2 and replaced twice a week with complete Neurobasal medium (CNM).

2.2.6 Establishment of motoneuron and muscle co-cultures

The motoneuron and muscle co-culture model was established from mutant SOD^{G93A} and WT mice. One day prior to plating mixed ventral horn neurons, the myotube medium was replaced with CNM. Mixed ventral horn neurons were plated on the top of the myotube cultures at 7 DIV and were seeded at a density of $10x10^4$. Co-cultures were maintained in the incubator at 37°C and 5% CO_2 and replaced twice a week with CNM. The co-cultures were maintained for approximately 3 weeks in culture.

2.3 Cellular fluorescence imaging

The cellular properties in primary myotube and motoneurons cultures were examined using a variety of fluorophores and images acquired using a confocal laser scanning microscope (Zeiss 510).

2.3.1 Assembly of the imaging chamber and Fluorophore loading

Prior to the imaging experiments, the recording medium (RM), a HEPES buffered salt solution, was prepared [NaCl (156mM) KCl (3mM), $MgSO_4$ (2mM), KH_2PO_4 (1.25mM), $CaCl_2$ (2mM) , glucose(10mM), Hepes (10mM)] and pH adjusted to 7.35 with NaOH. In some experiments $CaCl_2$ was omitted from the bath solution and EGTA (1mM) was added with appropriate pH correction.

The cultured cells on 22mm coverslips were removed from the culture dish and were washed in warmed recording medium (~37°C). The coverslips were mounted in a custom built imaging chamber, which held a circular base with a slight indentation where the 22mm coverslip, was securely held. A middle insert with a rim around the periphery, contained a rubber O ring, which formed a waterproof barrier between the imaging chamber and the objective lens. Placed on top of the base and middle insert was the mounting ring which screwed securely to form a waterproof seal.

Once the cultured cells were mounted in the custom built imaging chamber they were loaded with fluorimetric indicators listed in **Table 2.1** (Molecular probes, Paisley UK). Tetramethyl-rhodamine methyl ester (TMRM) is highly lipid soluble cation and membrane permanent. TMRM crosses the cell membrane easily and localizes to the mitochondrial compartment in response to the electrochemical potential gradient. The cells loaded with TMRM were allowed to equilibrate for approximately 30 mins in the presence of TMRM. The cytosolic Ca^{2+} indicator Fluo 4 is negatively charged and water-soluble and therefore cannot easily diffuse across cell membrane. The fluorimetric indicator Fluo 4 is therefore loaded as acetoxy-methyl AM ester which is membrane permeant. Loading AM esters into the cells requires the incubation with Pluronic F-127 (0.005%), a nonionic detergent, which facilitates the loading of the AM ester. The AM ester once inside the cell, is hydrolyzed by intracellular esterases, and releases the fluorophore.

Once the cells had been loaded for the required time, the cells were washed twice in recording medium and incubated again in 500μM, except for the TMRM experiments where the TMRM had to be maintained in the imaging chamber at all times.

Drugs applied during the experiments were made in recording medium and all experiments were performed using a 37°C heated stage.

The concentration of TMRM (20nM) used in theses experiments is unlikely to be subject to auto-quenching (Duchen, 2004). Auto-quenching is a phenomenon whereby energy is transferred by collision between monomeric dye molecules and the high concentration of dye may promote the aggregation of dye which is non-fluorescent. Upon mitochondrial depolarisation, the quench is mode is relieved and there is an increase in fluorescence, as the dye is redistributed from the mitochondria to the cytosol (Duchen, 2004). As relatively high concentrations (10-20μM) of TMRM are required for auto-quenching and a low concentration was used in these experiments (20nM), a decrease in TMRM fluorescence indicates a reduced $\Delta\Psi_m$.

Table 2.1 Fluorophore loading conditions

Fluorophore	Concentration	Pluronic	Loading Time	Parameter
TMRM	20nM	No	20-30 mins	Mitochondrial Membrane Potential
Fluo-4AM	5μm	Yes (0.005%)	20 mins	Cytosolic Ca^{2+} levels (high affinity)

2.3.2 Confocal imaging

Images were acquired using a Zeiss 510 Laser Scanning microscope (Oberkocken, Germany). The Zeiss Axiovert 200M inverted microscope comprised quartz 40x (numerical aperture 1.3 and glass 60x (numerical aperture 1.4) plan-apochromat, oil immersion objective lenses. The available laser UV laser (line 351 and 364), laser diode 405nm (line 405), Argon lasers (lines 458, 477, 488, and 514) and two helium-neon lasers (lines at 543nm and 633nm). A diagram representing the setup for the confocal laser scanning microscope is shown in **Fig 2.1**.

Figure 2.1 Schematic diagram of a confocal laser scanning microscope

The excitation light provided by a laser, reflects off a dichroic mirror onto the objective lens, which focuses the light onto a small spot within the specimen. The scan generator rapidly moves the laser beam across the specimen, line by line, by means of two mirrors which are mounted on motors. The same mirrors rapidly scan the emitted light, which is reflected onto a dichroic mirror and passes through either a bandpass or longpass filter. The bandpass filter transmits wavelengths within an indicated wavelength band and rejects longer wavelengths. Longpass filter transmits wavelengths longer than a specific threshold value and rejects shorter wavelengths. The emitted light is then focused onto the pinhole and the light that passes through the pinhole is collected by a photomultiplier tube (PMT).

The placing of a pinhole in front of the PMT detection system is the basis of confocal scanning. This pinhole limits the emitted light detected, so that only 'in focus' light originating from the sample specimen will pass through the pinhole. In contrast, light originating from 'out of focus' planes will not be detected, therefore improving the quality of the images obtained. Photocathodes in the PMTs detect the light passing through the pinhole and release electrons that accelerate towards an electron multiplier, which consists of a series of dynodes. The current output from the electron multiplier is proportional to the number of electrons striking the photocathode. This analogue signal is then digitised 512x 512 pixels to produce an image on the computer monitor.

FIGURE 2.1

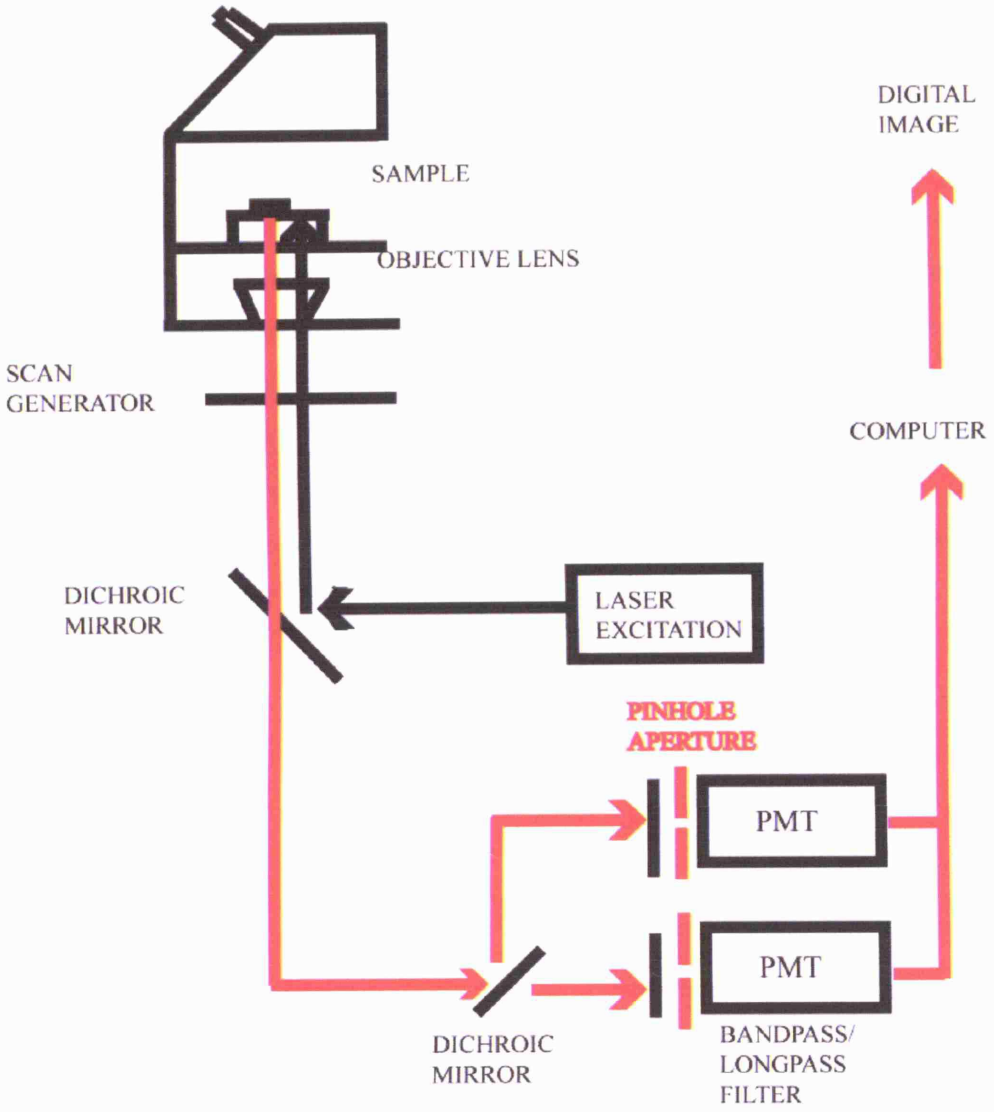
DIGITAL
IMAGE
SAMPLE
OBJECTIVE LENS
SCAN
GENERATOR
COMPUTER
DICHROIC
MIRROR
LASER
EXCITATION
PINHOLE
APERTURE
PMT
PMT
DICHROIC
MIRROR
BANDPASS/
LONGPASS
FILTER

2.3.3 Image acquisition

Images (stack size: 512 x 512 pixels) (105μm x105μm) were acquired at a pixel speed of 6.4μs and the signal digitized to pixel depth 12 bits (4096 grey levels) for an improved resolution of the signal. The pinhole was kept open to give an optical slice of approximately 3μm. In experiments where autofluorescence was measured, the pinhole was fully opened. When acquiring images the multi-tracking function was used, whereby images from different optical configurations were collected successively on 2 channels and the cross-talk between the excitation/emission spectra from different fluorophores was prevented. The multi-taking function allows up to 4 fluorophores to be measured simultaneously within a time series. The parameters that were kept constant throughout the experiments were detector gain (PMT sensitivity), amplifier offset (black level setting) and amplifier gain (electronic post amplification). The intensity of the laser (laser power) could be independently controlled and was maintained for the wavelength 405nm between 0.05-2%, 488nm at 0.05%-1% and 543nm 0.05-4%. The optical configurations for each fluorophore and drug concentration used in the experiments are summarized in **Table 2.2**.

Table 2.2 The optical configuration for each Fluorophore and drug concentration

Fluorophore	Laser excitation wavelength (nm)	Microscope dichroic filter (nm)	Bandpass /Longpass Emission filter
TMRM	543	560	LP 560
Fluo 4-AM	488	490	BP 505-550
NADH	350	450	BP 435-485
FAD	450	550	LP 505

Drug	Concentration	Drug action
Glutamate	5μM	Glutamate receptor agonist
FCCP	1 μM	Mitochondrial uncoupler (proton ionophore)
Cyanide	1mM	Inhibitor of complex IV
Caffeine	1mM and 10mM	Activate Ca^{2+} release from RyR

2.3.4 Imaging processing

Images were acquired using Zeiss LSM software. The fluorescent calcium imaging experiments was analyzed using Lucida Version 5 image analysis software (Kinetic Imaging, Liverpool, UK). The first image in a time series often contained transient Ca^{2+} activity therefore, a virtual image was created from the darkest value of each pixel throughout the time series. To normalize the fluorescence signal, all images of the time series were divided by the darkest image. The changes in the fluorescence intensity over time were identified by choosing regions of interest (ROI) within the cells. ROI were selected and the average changes in fluorescent signals in the time series were exported in a macro and a line plot generated in Microsoft Excel.

Measurements of mitochondrial membrane potential were determined using cells loaded with the potentimetric indicator TMRM and were analyzed using LSM Image Examiner. For each experiment a 'z stack' was acquired through the entire cell and a 3D projection made. The maximum intensity value of each pixel was taken through each point in the cell and a single compressed image was generated. An image threshold value for the background fluorescence was subtracted from the fluorescence signal. Regions of interest for each cell were selected and the mean pixel intensity value obtained, corresponded to the fluorescence signal. The fluorescence signal was corrected for the laser power and the resulting value corresponded to the mitochondrial membrane potential.

2.3.5 Fluorescent calcium imaging

The use of a single excitation wavelength high affinity calcium indicator (Fluo-4) was used to assess calcium activity in our experiments. Fluo-4 shows a shift in the fluorescence intensity on binding with calcium; unbound free indicator has weak fluorescence intensity. The cytosolic calcium concentration is related to the fluorescence intensity by the following equation.

$$[Ca^{2+}] = kd\ (F-Fmin)/(Fmax-F)$$

Kd is the dissociation constant, F is the fluorescence observed, Fmin is lowest fluorescence attained in the absence of calcium and Fmax is the highest fluorescence obtained in the presence of calcium. By calibrating the fluorescence intensity, a quantitative measurement can be made and an increase in fluorescence is directly related to an increase in concentration of calcium. Since a calibration for each cell is required there is a potential risk of damaging the cultured cells. Therefore fluorescence intensity measured was shown as a relative change in fluorescence intensity thereby allowing a qualitative analysis.

2.4 Generation of MGF and IGF-I constructs

MGF and IGF-1Ea cDNA constructs were inserted into pcDNA3.1/NT vectors (Invitrogen, USA) modified by the insertion of the myosin light chain enhancer, upstream of the human cytomegalovirus (CMV) promoter. The plasmids were multiplied in Escherichia coli and purified using the Endofree Plasmid Maxi Kit (Qiagen, Germany), as detailed below.

2.4.1 Bacterial culture and transformation

Liquid cultures of *E.Coli* were grown in Luria Bertani medium (LB) containing ampicillin (100 μg/ml) or overnight at 37°C in an orbital incubator shaking at 250 rpm. Bacteria were grown on solid culture medium of 1.5% (w/v) bacto-agar on LB on 90 mm Petri dishes at 37°C to isolate individual colonies. Transformed bacteria were stored at –70°C in 15% (w/v) glycerol in LB.

500ng-1μg plasmid DNA was transformed into 50μl *E.coli* (Invitrogen Life Technologies) and incubated on ice for 2 min. The cells were heat-shocked at 37°C for 1 min and returned to ice for 5 min. 900μl of sterile LB (Invitrogen Life Technologies) was added and the cells were incubated at 37°C with shaking for 2-3 hrs to allow the antibiotic resistance gene on the plasmid construct to be sufficiently expressed. The cells were centrifuged at 11,000 rpm for 5 min, resuspended in a further 50μl LB and streaked

out on to LB agar plates containing 100 μg/ml ampicillin. The plates were then incubated overnight at 37°C.

2.4.2 Plasmid DNA purification

The QIAGEN Plasmid Endofree Maxi Kit™ (Qiagen, Germany) was used to separate plasmid DNA from bacterial genomic DNA, the endotoxin free kit was selected for gene transfer *in vivo*. Bacteria from overnight cultures were harvested by centrifugation at 6000 rpm for 15 min at 4°C in a Sorvall GSA centrifuge rotor. The supernatant discarded and the bacterial pellet resuspended in chilled buffer P1 (50mM Tris.Cl, pH 8,10mM EDTA, 100μg/ml RNaseA). In order to allow maximum lysis of bacteria, they were incubated in buffer P2 (200mM NaOH, SDS (1%) (w/v) at room temperature (RT) for 5 min and the lysate was neutralised using buffer P3 (3M potassium acetate, pH 5.5) at 4°C. The lysate was then transferred to a QIAfilter Maxi cartridge and incubated 10 min at RT. The lysate, which contained the plasmid DNA, proteins, cell debris and SDS was cleared by filtering through the cartridge and loaded directly onto a QIAGEN-tip that had been pre-equilibrated with buffer QBT (750mM NaCl, 50mM MOPS pH 7, 15% isopropanol v/v) and was allowed to flow through by gravity. This tip contains resin which bound the negatively charged plasmid DNA. After washing twice with buffer QC (1M NaCl, 50mM MOPS pH 7, 15% isopropanol v/v) to remove any contaminating genomic DNA, RNA and protein, bound DNA was eluted with buffer QN (1.6 NaCl, 50mM MOPS pH 7,15% isopropanol v/v). The eluted plasmid DNA was desalted by isopropanol precipitation and centrifuged at 11,000rpm Sorvall SS-34 rotor for 30 min at 4°C. The resulting DNA pellet was washed in 70% (v/v) ethanol and centrifuged at 11,000rpm for 10 min at 4°C. The ethanol was decanted and the DNA air-dried for 5-10 min at RT prior to resuspension in an appropriate volume of ddH_2O. The endotoxin-free Qiagen Maxi-prep Kit integrates the endotoxin removal into the standard QIAGEN plasmid purification procedure. Typically, 500ml of culture would be used, resulting in approximately 500μg of pure plasmid DNA.

2.4.3 Determination of yield

The concentration plasmid DNA was quantified by spectrophotometer (Nanodrop (ND1000, Wilmington USA) using 1µl sample. The ratio of 260nm/280nm was used to assess the purity of the DNA sample. A ratio of ~1.8 is generally accepted as pure DNA. The plasmid concentration was diluted in sterile ddH_2O to a concentration 1µg/µl and frozen at -20°C until required.

2.5 *In vivo* Experiments

2.5.1 Assessment of disease progression

The progression of disease in $SOD1^{G93A}$ mice in this study was evaluated by assessing body weight over the course of disease and observation of behavioral changes. At 120 days of age, $SOD1^{G93A}$ muscle force and phenotype, motor unit and motoneuron survival were examined *in vivo* in live anesthetized mice to determine the extent of disease progression on hind limb muscle function.

2.5.2 Body weight

The mice were weighed on a weekly basis until a decline in body weight was first observed. From then on the mice were weighed on a daily basis to monitor the decrease of body weight.

2.5.3 Disease Endpoint

In theses experiments for humane purposes, mice were determined to have reached 'endpoint' when they (i) decreased body weight by 20% from maximum and (ii) inability to right themselves within 30 seconds when placed on their sides. Therefore the mice were not allowed to die of natural causes, but reached an objectively determined criteria defined as endpoint.

2.5.4 *In vivo* surgery

At 70 days of age mice were weighed and anesthetized with halothane (4% induction concentration and then maintained at 0.8%-2%) in 2l/min oxygen. The hind limbs were

cleaned with sterile NaCl and muscles in both hind limbs injected intramuscularly with either MGF, IGF-I or vehicle plasmid, using a 0.5ml insulin syringe. Several injections sites were made for the different muscles in each hind limb. The total volume delivered was 200µl (1µg/µl) to each leg.

2.5.5 Physiological assessment of Muscle force

In vivo physiological assessment of hind-limb muscle function was carried out on deeply anaesthetised live animals at 120 days of age. The mice were given anaesthetic (4.5% chloral hydrate 1ml/100g of body weight, intra peritoneal injection) both the paw pinch reflex and the eye blink reflex used to determine the level of anaesthesia.

When the mice were deeply anaesthetised, the legs were shaven. The mice were placed face down on a cork board and the distal tendons of both the TA and the EDL muscle were dissected and attached to isometric force transducers using silk thread. The sciatic nerve was exposed, sectioned and all the branches cut except for the deep peroneal nerve which innervates the TA and EDL muscles. The mice were pinned to the cork board through the knee joint and ankle joint with dressmaker's pins to securely attach the hind limbs whilst the recordings were being made. The nerve was then positioned on fine silver electrodes for stimulation. The length of the muscles was adjusted for maximal twitch tension and the muscle and nerves were kept moist throughout the recordings with saline. All experiments were carried out at room temperature (23°C) and the levels of anaesthesia were maintained.

2.5.6 Muscle force and contractile characteristics

Isometric contractions were elicited by stimulation of the nerve to the EDL and TA using square-wave pulses of 0.02ms duration and supra-maximal intensity via silver wire electrodes. Tetanic contractions of both the EDL and TA muscles were then recorded to determine maximal muscle force. Contractions were elicited by trains of stimuli at a frequency of 40, 80 and 100Hz. The twitch and maximum tetanic tension as well as the time to peak and half relaxation time values were measured with aid of a computer and appropriate software. The time to peak was calculated by measuring the

time taken (ms) for the muscle to elicit peak twitch tension. The half relaxation time was calculated as the time taken (ms) for the peak twitch tension to decrease to half its original value.

2.5.7 Motor unit number

The number of motor units innervating EDL muscles was determined by stimulating the motor nerve with stimuli of increasing intensity, resulting in stepwise increments in twitch tension due to successive recruitment of motor axons. The number of stepwise increments recorded on an oscilloscope was counted to give an estimate of the number of motor units present in each muscle.

2.5.8 Fatigue test

The fatigue pattern of the EDL muscles was also assessed by repeatedly stimulating the muscle at 40Hz for 250ms every second for 3 mins, and the contractions recorded on a pen recorder (Lectromed multitrace 2, UK Ltd).

2.5.9 Muscle freezing

At the end of the in-vivo physiology experiments the EDL and TA muscles from both hind limbs were dissected out and weighed. The tendons of the muscles were cut with a scalpel, to leave the central third of the muscle, to enable the muscles to be mounted upright on a piece of cork board and covered in tissue-tek (Agar scientific, Stanstead UK). The muscles were then quickly snap-frozen in isopentane cooled in liquid nitrogen and stored at -80 °C until processed.

2.5.10 Removal of spinal cord

Following the removal of the hind limbs muscles the mice were terminally anesthetised and perfused transcardially with 4% paraformaldehyde in 0.1 M phosphate buffer saline; (PBS Oxoid Ltd, Basingstoke, Hampshire, England). The spinal cord was the removed and the lumbar region (L2-L5) post-fixed for 4 hrs in the same fixative and then cryoprotected in sucrose (30% in 0.1M PBS) at 4°C for at least 4 hours. In some cases fresh spinal cord was taken for western blot analysis. In these experiments following

removal of the muscles, the spinal cords were perfused transcardially with saline, then extracted rapidly and the lumbar spinal cord region inserted into eppendorf tubes and snap frozen in liquid nitrogen. The tissue was stored at -80 °C until processing.

2.5.11 Spinal cord histology

Transverse serial sections (20μm) from the lumbar spinal cord were cut and stained with Gallocyanin (Nissl stain), which identifies ribosomes (Nissl substance) as dark blue in colour giving the neuronal cytoplasm a granular appearance. The spinal cord sections were stained with gallocyanin stain for approximately 15 minutes. The sections were washed briefly in distilled water and dehydrated in increasing concentrations of alcohol for 1 minute each and cleared in two changes of histoclear solution for 2 minutes each. The spinal cord sections were subsequently mounted using DPX mounting solution and left to dry.

2.5.12 Criteria for counting sciatic motoneurons

The numbers of motoneurons present in the sciatic motor pool of the ventral horn of the spinal cord were determined by counting every third section and counting motoneurons which had a clearly visible nucleolus and distinctly labeled cytoplasm (Coggeshall RE, 1984). Only large (diameter ~20μm) polygonal motoneurons were incorporated in the counts. The localization of the motor nuclei supplying the hind-limb muscles of the mouse have been comprehensively mapped (McHanwell and Biscoe, 1981). The sciatic motoneurons form a continuous, cell column in the dorsolateral quadrant of the ventral horn extending from rostral L6 into the caudal third of L3 over a longitudinal distance of about 6.3 to 7.5 mm. This column in the rat, has a width of 0.5 mm, in mid-L4 (Swett et al., 1986). Using this description as a guide for the location of the sciatic motor pool, motoneurons in the dorsolateral position within the ventral spinal cord, which formed a tightly defined motor pool, were counted. The surviving motoneurons counted in the sciatic motor pool gave an estimation of the proportion of the sciatic motoneurons rather than an accurate assessment of the total number of sciatic motoneuron. The total population of sciatic motoneurons of the rat contains approximately 2000 motoneurons (Swett et al., 1986) as determined by retrograde transport of HRP.

2.5.13 Muscle histochemistry

Transverse sections of TA and EDL muscle were cut (12μm) on a cryostat and collected on polyornithine coated glass slides. Muscle sections were allowed to dry, and then stored at -20°C until they were processed for various histochemical stains.

i) Haematoxylin & Van Gieson

The muscle sections were fixed in 90% alcohol for 30 mins prior to staining. The sections were rinsed in 70% alcohol and then placed in Weigerts Iron Haematoxylin (1% Haematoxylin in absolute alcohol and 30% aqueous solution of ferric chloride) for 20-40 mins. The sections were then rinsed in tap water and differentiated for a couple of seconds in 1% acid alcohol (1% conc. HCL in 70% alcohol) and washed for 10 mins in running tap water. The sections were stained in Van Gieson (saturated aqueous solution of picric acid and 1% fuchsin) for 3 mins and wash very briefly in water to remove fuchsin 1-2 seconds. This is followed by one change of 90% alcohol and two changes of absolute alcohol for about 10 seconds in each. Finally the sections had two washes of histoclear (2mins each) and section mounted with DPX mounting medium.

ii) Succinic dehydrogenase

Succinic dehydrogenase (SDH), a working solution was prepared phosphate buffer pH 7.6 (0.1M), sodium succinate (1M), nitroblue-tetrozolium (15mM), potassium cyanide (0.1M)and phenazine methosulphate(10mM), using previously described protocol (Nachlas et al., 1957) The working solution is light sensitive and must be kept in the dark. Before staining the muscle sections the SDH stain was warmed to 37°C. A few drops of the working solution were used to cover the muscle sections and incubated for 5 mins at 37°C in an incubator. The sections were then rinsed in NaCl (0.9%) for 1 minute followed by acetone (70%) and acetone (90%) for 1 minute each. The sections were then dehydrated in increasing concentrations of alcohol for 1 minute each and twice in histoclear solution for 2 minutes each time. The muscle sections were subsequently mounted using a coverslip and DPX mounting solution and left to dry.

2.5.14 Western Blot

Snap frozen spinal cord and muscle tissue samples were homogenised in lysis buffer SDS (2%), EDTA (2mM), EGTA (2mM) , Tris pH 6.8 (5mM) and protease inhibitor cocktail at 1:100. The samples were spun in centrifuge for 5 min, approx 8000rpm. The supernatant was collected and the protein levels determined using BioRad assay (cat: 500-0116) and a series of BSA standards. The protein samples concentrations were adjusted and were aliquoted and kept in -80C.

Protein samples were boiled in sample buffer TRIS (62.5mM) pH 6.8, Glycerol (25%), SDS (2%), Bromophenol-blue (0.01%), β-Mercapto-ethanol (1:20) for 5mins prior to SDS PAGE. The concentration of protein loaded was 50μg and separated at 160V for 1hr on an Acrylamide gel (12.5%). Protein was then electrophoretically transferred to Hybond ^{TM} ECL^{TM} nitocellulose membranes. The nitocellulose membranes were fixed for 1hr in glutaraldehyde (1%) fixative in PBS and blocked with non-fat dried milk (5%) and tween-20 (0.1%) in PBS for 1hr at room temperature. The blots were incubated in primary antibody made up in non-fat dried milk (5%) and tween-20 (0.1%) in PBS overnight at 4°C. The following day the membranes were washed three times for 10 mins tween-20 (0.1%) in PBS and incubated for 2hrs in HRP- conjugated secondary antibody at 1:1000. The membranes were subsequently washed three times for 10mins tween-20 (0.1%) in PBS. The blot was visualised with a chemiluminescent detection reagent kit (Amersham ECL reagent cat no: RPN 2106). The blots were then exposed to Kodak film in the dark for approx 2-10 min and film developed using Kodak developer and fixer in the dark room.

2.6 Statistical Analysis

Statistical comparisons of the data collected were performed using a Mann-Whitney U test, a non-parametric alternative to the T-Test used for small sample sizes. The test assumes a null hypothesis and tests the samples to see whether there is significance for an alternative hypothesis (i.e. that the samples are from different populations). 'P' represents the probability that these samples are from the same population. The data are presented as the mean with the standard error of the mean (SEM). Statistical significance was set at 95% i.e $P \leq 0.05$.

Chapter 3

The effect of mutant SOD1 expression on the cellular properties of mitochondria in skeletal muscle and motoneurons *in vitro*

3.1 INTRODUCTION

ALS is characterised by the progressive degeneration of motoneurons and accompanied by muscle weakness and eventual paralysis. A unique feature of motoneurons is their contact with skeletal muscle during development motoneurons and muscle fibres are highly dependent on this functional interaction for their survival and maturation.

Since recent evidence has shown that non-neuronal cells in the CNS which interact with motoneurons play an important role in the pathogenesis of ALS, it is possible that muscle fibres that interact with motoneurons in the periphery, also contribute to disease. There is substantial post-mortem and biopsy evidence from patients with ALS, indicating mitochondrial dysfunction occurring specifically in nerve terminals (Atsumi, 1981), as well as in skeletal muscle (Afifi et al., 1966). In addition to their principle role as metabolic powerhouses of the cell, mitochondria also have the ability to sequester and release large quantities of calcium, under pathological conditions and during normal cellular calcium homeostasis. The involvement of both mitochondrial dysfunction and disrupted calcium signalling in the pathogenesis of ALS has not yet been resolved.

Early changes in mitochondrial morphology occur in motoneurons from transgenic mice expressing mutant SOD1, prior to neuronal generation (Dal Canto and Gurney, 1995; Wong et al., 1995; Kong and Xu, 1998). Impairments to the mitochondrial electron transport chain complexes, in particular reduced complex VI activity (Menzies et al., 2002; Jung et al., 2002; Kirkinezos et al., 2005; Mattiazzi et al., 2002), and alterations in mitochondrial calcium capacity in isolated brain and spinal cord mitochondria (Damiano et al., 2006) have been reported to be involved in mutant SOD1 mediated motoneuron degeneration. However, the contribution of mitochondrial dysfunction and disrupted calcium signalling within skeletal muscle to ALS pathogenesis is poorly understood. Therefore, to examine the effect of mutant SOD1 expression on the cellular properties of skeletal muscle and motoneurons, *in vitro* primary myotubes and co-cultures of motoneurons and myotubes from SOD1 mice were established. Using these *in vitro* cultures, mitochondrial function and calcium signalling were assessed.

3.1.1 Mitochondrial involvement in ALS

The earliest reported evidence implicating mitochondrial abnormalities in ALS was identified at the ultrastructural level by electron microscopy studies from muscle biopsies of patients with ALS. The presence of large abnormal mitochondria as well as mitochondrial aggregates in the subsarcolemmal regions were reported in skeletal muscle (Afifi et al., 1966) and a reduced mitochondrial number was identified in intramuscular nerves (Atsumi, 1981). Further evidence from autopsy studies from ALS patients later reported morphological and ultra-structural abnormalities of mitochondria in spinal cord anterior horns cells (Sasaki and Iwata, 1996). Increased mitochondrial volume and mitochondrial calcium were identified in motor nerve terminals taken from muscle biopsies of ALS patients (Siklos et al., 1996a).

Skeletal muscle biopsies from patients with ALS were reported to have a reduced in Complex I (NADH: CoQ oxidoreductase) activity compared to age-matched controls (Wiedemann et al., 1998). These findings were further supported by imaging the intrinsic Flavoprotein/NAD(P)H autofluorescence, which indicated the existence of a reduced state in the mitochondrial redox state in ALS muscles (Wiedemann et al., 1998). The findings of this study indicate a deficiency of complex I in the mitochondrial respiratory chain in ALS muscles. Interestingly, these observed mitochondrial abnormalities were specific to SALS and were not identified in patients with spinal muscular atrophy, suggesting that the findings are not simply due to muscle denervation.

Abnormal mitochondrial DNA (mtDNA) has also been reported in ALS patients (Vielhaber et al., 2000). Muscle biopsies of ALS patients were screened and diminished levels of mtDNA were identified (Vielhaber et al., 2000). One ALS patient was reported to have multiple mtDNA deletions. Interestingly there were diminished levels of manganese superoxide dismutase 2 (SOD2) in skeletal muscle ALS patients (Vielhaber et al., 2000). As SOD2 is crucial for ROS detoxification, and the mitochondrial respiratory chain is the major site for ROS generation, reduced levels of SOD2 could result in increased ROS generation and have a deleterious effect, resulting in degradation of mtDNA.

A marked upregulation of mitochondrial uncoupling protein 3 (UCP3) mRNA was also identified in muscle biopsy samples from ALS patients (Dupuis et al., 2003). Uncoupling proteins (UPSs) are members of a novel family of proteins known as mitochondrial carrier proteins (Esteves and Brand, 2005), which are key regulators of mitochondrial respiration and may act to attenuate the mitochondrial production of reactive oxygen species (ROS) species. UCP3 when activated by products of ROS metabolism such as superoxide (O_2•) radicals are thought to increase the proton conductance in muscle mitochondria and mild uncoupling acts as a feedback mechanism to decrease the overproduction of ROS although, this mechanism still remains highly controversial (Echtay et al., 2002). An increased expression of UCP3 may prove to be protective against oxidative stress through the uncoupling of mitochondria. However it is unclear whether UCP3 upregulation may be detrimental to the metabolic function of skeletal muscle. If there is an underlying dysfunction in the mitochondria, uncoupling the respiratory chain might potentially be deleterious. It remains unclear whether activation of UCP's is beneficial or indeed detrimental to metabolic function.

3.1.2 Mitochondrial localisation of mutant SOD1

The intracellular localisation of WT and mutant SOD1 has been detected at the ultrastructural level by electron microscopy in lumbar spinal cord sections (Higgins et al., 2002) and are associated with vacuolated mitochondria (Jaarsma et al., 2001). A significant proportion of enzymatically active SOD1 localised to the intermembrane space in mitochondria isolated from brain in SOD^{G93A} mice (Mattiazzi et al., 2002; Okado-Matsumoto and Fridovich, 2002; Okado-Matsumoto and Fridovich, 2001) In disagreement with these earlier findings it was reported (Liu et al., 2004), that only mutant SOD1 but not wild type SOD1 was associated preferentially with spinal cord mitochondria in several overexpressing transgenic mice $SOD1^{G37R}$, $SOD1^{G85R}$, $SOD1^{G93A}$, SOD^{H46R} and post-mortem tissue from a familial ALS patient. It was proposed that mutant SOD1 progressively accumulates and aggregates on the outer membrane of the mitochondria, which results in the clogging of protein translocation machinery of mitochondria (Liu et al., 2004). Further experimental evidence is required

to reconcile these discrepancies in terms of the localisation of wild-type SOD1. The conflicting findings may be due to the different experimental strategies used to purify mitochondria and to detect SOD1. However recent evidence however corroborates the finding that both WT and mutant SOD1 localise to mitochondria (Vijayvergiya et al., 2005). In addition, mutant not wild-type SOD1, was found to form large molecular weight aggregates in the matrix of brain mitochondria (Vijayvergiya et al., 2005).

3.1.3 Mitochondrial dysfunction in mutant SOD1

Mitochondria may be the target for SOD1 mediated toxic damage. Early pathological changes in mitochondrial of $SOD1^{G93A}$ and $SOD1^{G37R}$ transgenic mice include swelling, vacuolisation and degeneration of mitochondria specifically in motoneurons and endoplasmic reticulum (Dal Canto and Gurney, 1995; Wong et al., 1995). These early pathological changes in motoneurons mitochondria may be associated with changes which also occur in muscle mitochondria, leading to mitochondrial dysfunction in both motoneurons and muscles.

Indeed preceding the onset of the disease in $SOD1^{G93A}$ mice there is disorganisation and dilation of mitochondria cristae (Kong and Xu, 1998). As the disease progresses, the onset of muscle weakness is correlated with substantial vacuolisation of mitochondria in the spinal cord (Kong and Xu, 1998). The mitochondrial vacuolar pathology is characterised by expansion of the mitochondrial intermembrane space and results in the swelling, and vacuolisation of the mitochondria. This mitochondrial pathology is a specific feature of 'high expressor line' $SOD1^{G93A}$ mice which contain high copy numbers of the mutated enzyme and the $SOD1^{G37R}$ mice (Dal Canto and Gurney, 1995). Interestingly, transgenic mice expressing high levels of the wild-type human SOD, do not develop the motoneuron disease phenotype but do exhibit mitochondrial vacuolar pathology (Dal Canto and Gurney, 1995; Jaarsma et al., 2000). Indeed not all the transgenic mice exhibit abnormal mitochondria, such as $SOD1^{G85R}$ (Brujin et al 1997). These findings suggest that mitochondrial swelling and vacuolisation, which occurs in 'high expressor' lines $SOD1^{G93A}$ and $SOD1^{G37R}$ mice, may result from a high concentration of SOD1 as opposed to the toxic properties of mutant SOD1.

Evidence of disrupted mitochondrial respiratory complexes, was found in isolated brain mitochondria of transgenic $SOD1^{G93A}$ mice, which had decreased mitochondrial respiration, specifically complex IV (Kirkinezos et al., 2005). In addition cytochrome C was shown to have a reduced association in inner mitochondrial membranes, following disruption of the outer mitochondrial membrane (Kirkinezos et al., 2005).

The mitochondrial enzyme SOD2 is localized to the mitochondrial matrix and is crucial for scavenging superoxide radicals ($0_2^{\cdot}$) within mitochondria. A partial deficiency in SOD2 can exacerbate the clinical phenotype and reduces the lifespan in the mutant $SOD1^{G93A}$ mice (Andreassen et al., 2000). Interestingly, it has been reported that there are diminished levels of SOD2 in skeletal muscle ALS patients (Vielhaber et al., 2000) although recent findings failed to find this reduction (Soraru et al., 2007). It therefore remains unclear whether diminished levels SOD2 are indeed altered in skeletal muscle ALS patients.

There is evidence of mitochondrial dysfunction in SOD1 muscle, at an early symptomatic stage. UCP3 mRNA was reported to be specifically up-regulated in muscle in $SOD1^{G86R}$ mice (Dupuis et al., 2003). Further mitochondrial dysfunction in muscle of $SOD1^{G86R}$ mice was observed, including reduced ATP levels, and significant reduction in the respiratory control ratio (ratio between state III and state II respiration) which is in line with mitochondrial uncoupling (Dupuis et al., 2003).

There is considerable evidence to support the involvement of SOD1 induced toxicity in mitochondria dysfunction in both *in vivo* and *in vitro* studies. Mutant SOD1 transfected into neuroblastoma SH-SY5Y cells causes a significant decrease in mitochondrial membrane potential and a net increase in cytosolic calcium concentration (Kruman et al., 1999). Furthermore, primary mixed spinal cord cultures from $SOD1^{G93A}$ mice, were shown to have enhanced oxyradical production, lipid peroxidation, increased intracellular calcium levels, and decreased intra-mitochondrial calcium levels (Kruman et al., 1999). In addition, expression of mutant SOD1 in transfected NSC-34

(motoneuron-like cell line) confirmed that levels of $SOD1^{G93A}$ comparable to those in the human condition, were sufficient to increased ROS formation and decrease mitochondrial membrane potential (Rizzardini et al., 2005). These findings suggest that $SOD1^{G93A}$ toxicity promotes increased levels of oxidative stress and membrane lipid peroxidation and reduces mitochondrial membrane potential. This may result may be due to inhibition of respiration, reduced substrate availability or alternatively, mitochondrial uncoupling. Therefore expression of mutant SOD1 in a variety of cell types can result in mitochondrial dysfunction.

3.1.4 Mitochondria and Calcium Homeostasis

Mitochondria have the ability to sequester large quantities of calcium when cytosolic concentrations are high, (Nicholls and Ward, 2000; Duchen, 1999; Duchen, 2000) and are therefore thought to play an important role in buffering cytosolic calcium levels. Early ultrastructural evidence identified in motor nerve terminals from muscle biopsies of ALS patients, showed increased levels of calcium located within mitochondria and increased mitochondrial volume (Siklos et al., 1996b). Mitochondrial damage may therefore result from disrupted calcium homeostasis, in ALS (Manfredi and Xu, 2005; von Lewinski and Keller, 2005; Menzies et al., 2002).

Intracellular calcium can be also buffered by calcium binding proteins, reduced levels of endogenous calcium binding proteins such as parvalbumin and calbindin-D_{28k} have been implicated in ALS (Alexianu et al., 1994b). Post-mortem specimens from ALS patients have shown an absence of immunoreactive calbindin-D28k and parvalbumin in cortical and spinal motoneurons, whereas motoneurons which are relatively spared in ALS (i.e., Onuf's nucleus motoneurons, oculomotor, trochlear, and abducens cranial nerve neurons) express higher levels of calcium binding proteins (Alexianu et al., 1994b). There is evidence from electrophysiological studies, using lumbar spinal cord tissue slices, that spinal motoneurons have a limited ability to buffer intracellular Ca^{2+} (Palecek et al., 1999) which may render motoneurons particularly vulnerable to Ca^{2+} mediated cell death. There is further electrophysiological evidence, from brainstem slices to shown that the oculomotor motoneurons have a 5-6 times greater calcium buffering

capacity compared to the motoneurons in nucleus hypoglossus and spinal cord, which are lost early in ALS (Vanselow and Keller, 2000).

It is well known that in both ALS patients and transgenic mutant SOD1 mice there is a disease-selective resistance in a subset of motoneurons, in particular the extraocular motoneurons, which express abundant levels of parvalbumin and calbindin-D_{28k} (Nimchinsky et al., 2000). Further evidence in mutant SOD1 mice has shown a reduction in parvalbumin in spinal motoneurons compared to oculomotor motoneurons (Siklos et al., 1998). Parvalbumin overexpressing and mutant $SOD1^{G93A}$ double transgenic mice, resulted in a improvement of motoneuron survival and delayed the disease progression of the $SOD1^{G93A}$ mice (Beers et al., 2001). *In vivo* it has been shown that treatment with ALS sera or immunoglobulin (IgG) increases calcium in motor axon terminals (Engelhardt et al., 1991; Engelhardt et al., 1995). In parvalbumin/$SOD1^{G93A}$ mice, following treatment with ALS sera or (IgG) the increase in intracellular calcium in motor axon terminals of the interosseus muscle was attenuated (Beers et al., 2001). The immune-mediated response which results in an increase in calcium was attenuated by expression of parvalbumin in the double transgenic mice. Spinal cord motoneurons in parvalbumin transgenic mice, have also been shown to be protected from excitotoxicity induced cell-death and by injury following a peripheral nerve crush (Van Den et al., 2002a; Dekkers et al., 2004).

It has been proposed that early mitochondrial alterations, observed in SOD1 mice, could result from the increased levels of intracellular calcium (Dal Canto and Gurney, 1994a; Wong et al., 1995; Carri et al., 1997; Kong and Xu, 1998). Indeed early impairments in calcium capacity have been reported from isolated brain and spinal cord mitochondria of mutant SOD1 mice (Damiano et al., 2006). Excessive intracellular calcium in motoneurons leading to mitochondrial calcium overload has been shown to promote increased ROS generation, (Carriedo et al., 2000).

It has been proposed that motoneurons with a low expression of calcium binding proteins may depend to a greater extent on mitochondrial uptake in order to buffer

calcium effectively (von Lewinski and Keller, 2005). Mitochondrial calcium overload could therefore result in mitochondrial depolarisation and decreased levels of ATP synthesis (Beers et al., 2001). This may render mitochondria in motoneurons more susceptible to damage and eventual cell death.

Mitochondria are therefore implicated in ALS, but not very much is known about the involvement of mitochondria in skeletal muscle. There some early evidence of abnormal mitochondrial structure and dysfunction in muscle biopsies from ALS patients. However it is unclear whether this is a primary cause or a contributing factor to the pathogenesis of ALS.

3.1.5 Mechanisms of calcium signalling in skeletal muscle

In skeletal muscle, muscle contraction is triggered by the release of Ca^{2+} ions from the sarcoplasmic reticulum. An action potential propagates along the surface and transverse tubule membranes which results in membrane depolarisation, which can be detected by the 'voltage-sensor' dihydropyridine receptors (DHPRs) in the transverse tubular system. Mechanical conformational coupling DHPRs and the ryanodine receptors (RyR) activate Ca^{2+} release channel RyR located in the sarcoplasmic reticulum and initiate subsequent excitation-contraction coupling (ECC) in skeletal muscle, as shown in **Fig.3.1**. The contraction/relaxation cycle is terminated when Ca^{2+} is taken back into the sarcoplasmic reticulum by the Ca^{2+} pump (Ca^{2+}-ATPase). The initial Ca^{2+} transient can be further amplified by the calcium induced calcium release (CICR), which accounts for the ability in skeletal muscle to generate calcium spikes and calcium waves (Berridge, 1997). However in skeletal muscle the contribution of CICR to excitation-contraction coupling under physiological conditions still remains controversial. Principally there are two intracellular channels responsible for the release of calcium from the internal stores within muscle, RyR and the inositol 1, 4, 5-trisphosphate receptors (IP_3Rs) (Berridge, 1997). Earlier studies have elucidated two separate Ca^{2+} release systems in cultured myotubes, a fast Ca^{2+} transient associated with RyR and a slow Ca^{2+} transients associated with increases in IP_3 concentration and the presence of IP_3Rs (Powell et al., 2001). It now appears the IP_3 is important in the signalling of muscle activity to the

nucleus, particularly important in development, for the initiation of transcription of activity –dependent genes (Jaimovich et al., 2000).

Figure 3.1 Skeletal muscle excitation-contraction coupling

Excitation-contraction coupling is the orchestrated sequence of events, by which an action potential propagates along the plasma membrane and transverse-tubule membrane and subsequent depolarisation of the transverse-tubule results in calcium release and muscle contraction. The depolarisation of the transverse-tubule is transmitted across the triad junction, which is formed between the transverse-tubule membrane and the terminal cisternae membrane of the sarcoplasmic reticulum. The DHPRs detect depolarisation leading to conformational coupling between DHPRs and Ca^{2+} release channel RyR in the sarcoplasmic reticulum. A tetrad of four DHPR opposes every second RyR. Ca^{2+} release from the RyR initiates subsequent excitation-contraction coupling (ECC) in skeletal muscle. The contraction/relaxation cycle is terminated when Ca^{2+} is taken back into the sarcoplasmic reticulum by the Ca^{2+} pump (Ca^{2+}-ATPase). (Schematic diagram adapted (Dulhunty et al., 2002))

FIGURE 3.1

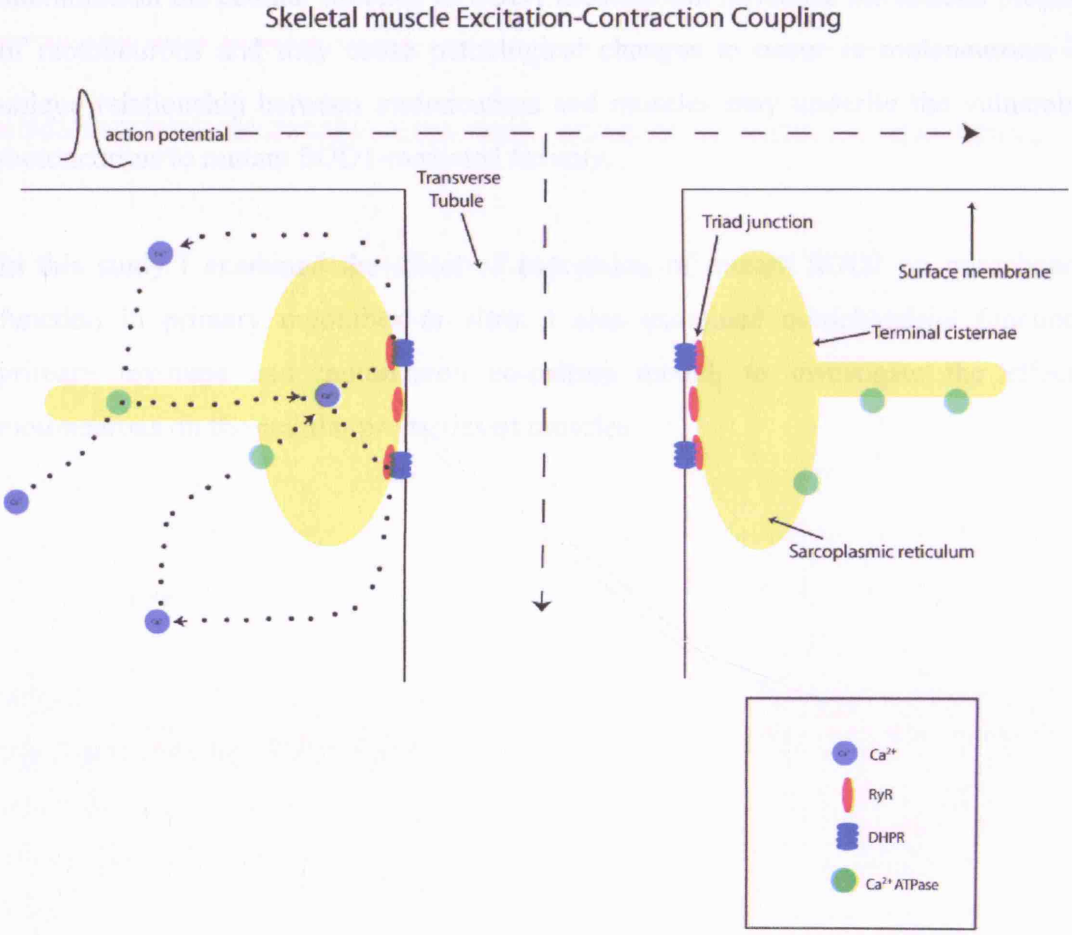
Skeletal muscle Excitation-Contraction Coupling
action potential
Transverse Tubule
Triad junction
Surface membrane
Terminal cisternae
Sarcoplasmic reticulum
Ca2+
RyR
DHPR
Ca2+ ATPase

3.1.6 Hypothesis

Although transgenic $SOD1^{G93A}$ mice express mutant SOD1 in all cells, mutant SOD toxicity results in the selective degeneration of motoneurons. A unique feature of motoneurons is the interaction and contact with skeletal muscle fibres in the periphery. There is evidence for early pathological changes occurring in skeletal muscle, resulting in abnormal mitochondria in ALS patients. The hypothesis of this study is that alterations in the cellular function of SOD1 muscles can influence the cellular properties of motoneurons and may cause pathological changes to occur in motoneurons. This unique relationship between motoneurons and muscles may underlie the vulnerability motoneurons to mutant SOD1-mediated toxicity.

In this study I examined the effect of expression of mutant SOD1 on mitochondrial function in primary myotubes *in vitro*. I also examined mitochondrial function in primary myotube and motoneuron co-culture model, to investigate the effect of motoneurons on the cellular properties of muscles.

3.2 RESULTS

The experiments described in this chapter examine the cellular properties of $SOD1^{G93A}$ skeletal muscle. An *in vitro* co-culture model was established using different combinations of genotypes of $SOD1^{G93A}$ and WT motoneurons with $SOD1^{G93A}$ myotubes and WT myotubes to determine the effect of mutant SOD1 expression on mitochondrial function in motoneurons and muscles. Mitochondrial function and calcium signalling were assessed *in vitro* in separate myotube cultures and also in co-cultures of primary myotubes and motoneurons. All data collected are representative of at least 3 separate experiments from cultures prepared on separate occasions.

3.2.1 Characterisation of primary myotube cultures

Myoblasts were isolated from the hind-limbs of neonatal mice, and within 2 days the myoblasts had formed elongated multinucleated myotubes. To characterise the myotube cultures the expression of skeletal muscle specific proteins and receptors on the myotubes was examined by immuno-staining at 12 days in-vitro. A monoclonal anti-slow myosin antibody was used to identify skeletal muscle-specific slow myosin heavy chain (MHC) expression. AChR were labelled with α-bungarotoxin conjugated-Alexa 488, and nuclei with DAPI. **Figure 3.2** shows typical examples of myotube cultures and shows co-localization of slow MHC immunofluorescence with AChR staining on the surface of the myotubes and nuclei stained with DAPI. The staining pattern of slow MHC was specific, with visible cross-striations indicating the assembly of slow MHC into sarcomeres as shown in **Figure 3.3 (A-C)**. AChR expression was clustered randomly on the myotubes, as would be expected in non-innervated myotubes. The localized expression of muscle-specific MHC and AChR confirms the myotube phenotype in the primary cultures.

Figure 3.2 - Expression of slow myosin heavy chain (MHC) and AChR in primary cultures of myotubes

Images of WT primary myotube cultures were acquired using the Confocal LSM (Zeiss 510) microscope with a 40x oil emersion objective lens. Myoblasts were isolated from hind-limbs of neonatal mice and cultured for 12-13 days, during which time the myoblasts fused to form multinucleated myotubes. The myotubes were stained with DAPI to visualise nuclei. The AChR on the myotubes surfaces were labelled with Alexa 488 conjugated α-bungarotoxin and the cultures were immuno-stained with an antibody to MHC. The co-localization of slow MHC immunofluorescence can be seen with AChR on the surface of the myotubes.

(Scale bar =50μm)

FIGURE 3.2

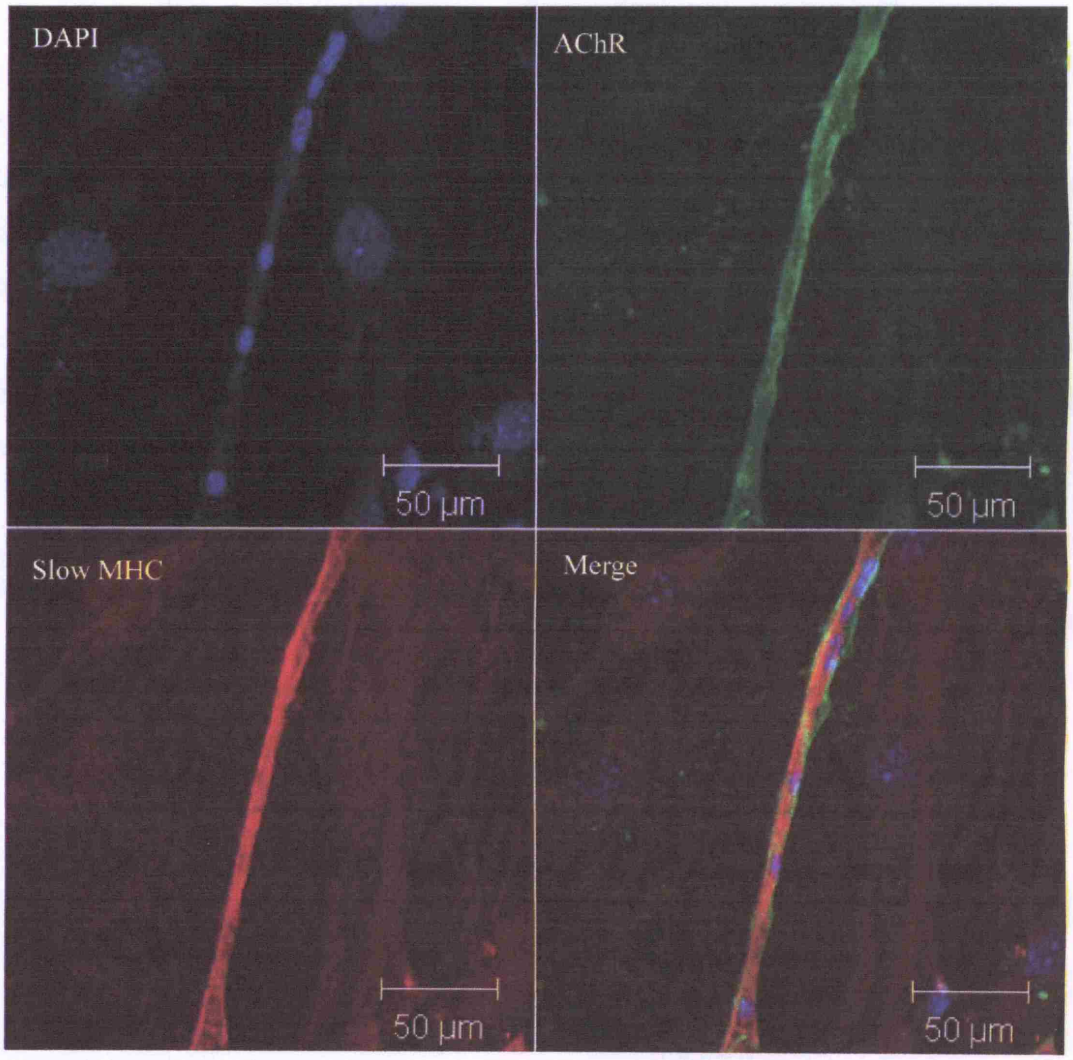

Figure 3.3 Expression of slow myosin heavy chain (MHC) exhibiting cross striations

Images of WT primary myotube cultures **(A)** were acquired on a light microscope (DMR Leica) at 40x/0.7 magnification and images were captured using a digital camera (E995; Nikon). The cultures were immunostained with an antibody for MHC and visualised using ABC kit and 3-3'-diaminobenzidine. Images **(B-C)** were acquired using the Confocal LSM (Zeiss 510) microscope using a 40x oil emersion objective lens (numerical aperture 1.3) and show myotubes stained with a slow MHC antibody conjugated to Alexa-488. The myotubes are clearly multi-nucleated **(A)** and by this stage contain well organised cross striations **(A-C)**.

(Scale bar A=10μm, B= 50 μm, C= 5 μm)

FIGURE 3.3

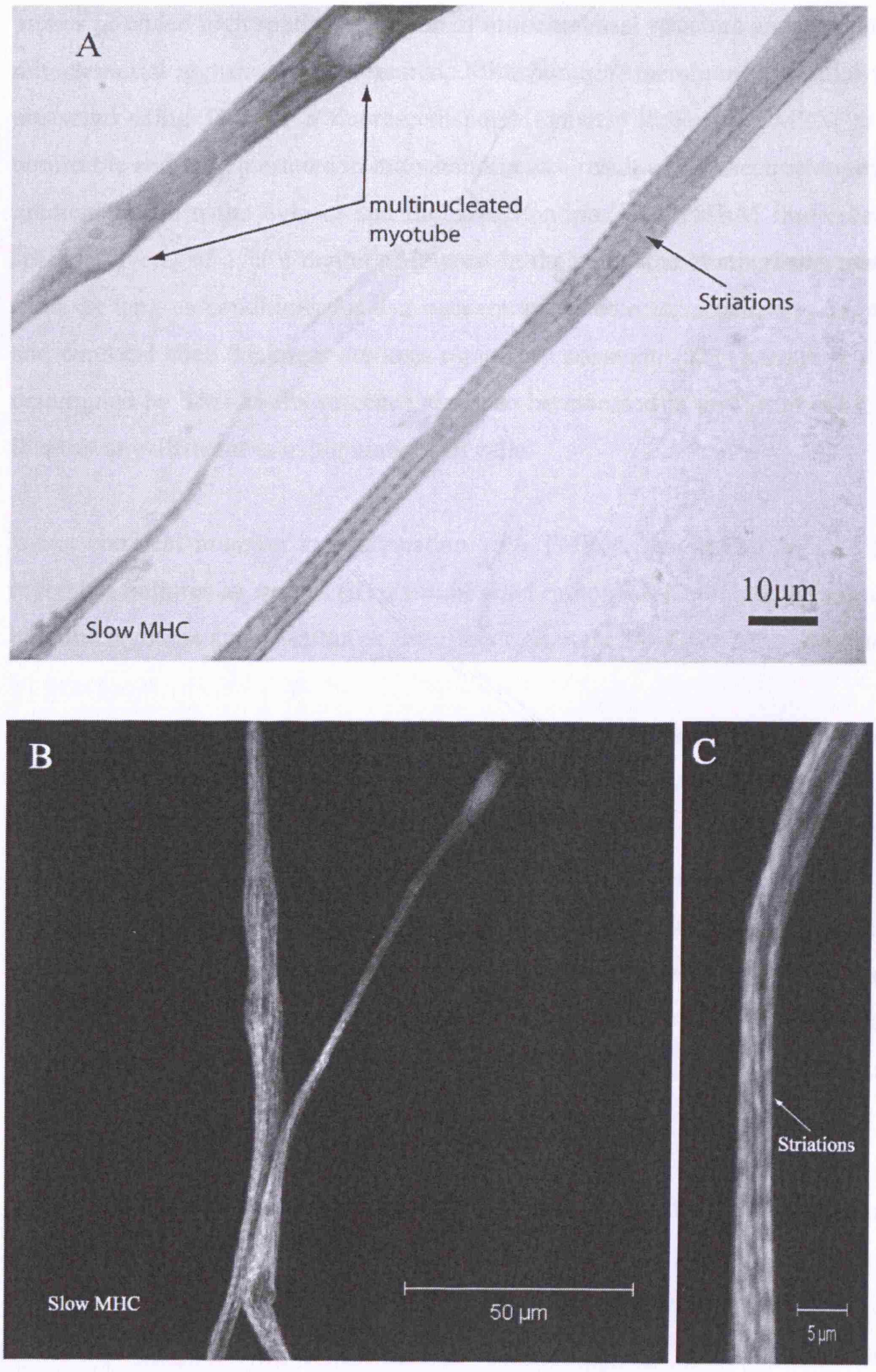
A
multinucleated
myotube
Striations
10µm
Slow MHC
B
Slow MHC
50 µm
C
Striations
5 µm

3.2.2 Resting mitochondrial membrane potential

Measurements of mitochondrial function in cells using confocal imaging and fluorescent probes provided high spatial resolution of mitochondrial structure and permitted discrete mitochondrial signals to be measured. Mitochondrial membrane potential ($\Delta\Psi_m$) was measured using TMRM, a fluorescent potentiometric indicator. TMRM is membrane permeable and is sequestered in mitochondria as a result of the electrochemical potential gradient between the cytosol and the mitochondria. The TMRM fluorescence can be spatially averaged over a region of interest in the cells, and comparisons made between cells, as long as conditions for dye concentration, detector sensitivity, amplifier offset and confocal slice thickness are kept rigorously constant. This permits the $\Delta\Psi_m$ to be determined by TMRM fluorescence signal to be assessed in groups of cells, in order to identify any differences in populations of cells.

Using confocal imaging in combination with TMRM, the resting $\Delta\Psi_m$ of (i) primary myotubes cultures as well as (ii) myotubes and motoneuron co-cultures was assessed. In both the myotube and co-cultures, the effect of mutant SOD1 on $\Delta\Psi_m$ was determined.

3.2.2.1 Resting mitochondrial membrane potential of primary myotube cultures

It is unclear whether deficits in mitochondria in muscles of ALS patients are the primary cause or a contributing factor to the pathogenesis of ALS. The limitation of using human samples is that it is only possible to assess altered muscle mitochondrial function well after disease onset. By using a transgenic mouse model of ALS, mitochondrial function can be examined prior to evidence of disease onset. In these experiments $\Delta\Psi_m$ was assessed in $SOD1^{G93A}$ myotubes and WT myotubes by measuring the TMRM signal, to determine any early changes in the resting $\Delta\Psi_m$ which may indicate altered mitochondrial function.

The myotube cultures were loaded with TMRM (20nM) and were allowed to equilibrate for at least 30mins. Measurements of mitochondrial membrane potential were determined using a confocal microscope and were analyzed using Zeiss 510 Laser Scanning Microscope Image Examiner software. For each experiment a 'z stack' was

acquired through the entire cell and a 3D projection made. The maximum intensity value of each pixel was taken through each point in the cell and a single compressed image was generated. A threshold value for the background fluorescence was subtracted from the fluorescence signal for each image. Regions of interest for each cell were selected and the mean pixel intensity value obtained, corresponded to the fluorescence signal. The fluorescence signal was corrected for the laser power and the resulting value corresponded to the mitochondrial membrane potential.

Typical compressed 3D images are shown in **Fig 3.4(A).** Measurements of the mean resting $\Delta\Psi_m$ determined by TMRM is summarised in the bar chart shown in Fig **3.5 (A)**. The results show that $SOD1^{G93A}$ myotube cultures mitochondria had a significantly reduced $\Delta\Psi_m$, with a 36% reduction in mean TMRM fluorescence compared to WT myotubes. The TMRM signal in the $SOD1^{G93A}$ myotubes was 453 a.u ± 17 (n=29) compared to 712 ± 28 a.u (n=36) in WT myotubes ($P \leq 0.001$). Therefore the resting mitochondrial membrane potential in $SOD1^{G93A}$ myotubes is significantly reduced. In the primary myotube cultures, residual fibroblasts which were not fully removed passaging or by treatment with cytosine arabinoaside (anti-mitotic drug) were also present in the culture preparations together with the myotubes, as shown in **Fig 3.4(B).** The mean resting $\Delta\Psi_m$ in fibroblasts was also examined by TMRM, to investigate whether the deleterious effects of mutant SOD1 on mitochondrial function were specific for myotubes or present in other cell types. The mean measurements TMRM fluorescence for the fibroblasts are summarised in the bar chart in **Fig 3.5(A).** The results show $\Delta\Psi_m$ in $SOD1^{G93A}$ fibroblasts was 395 a.u ± 12 (n=42) which was significantly less than the $\Delta\Psi_m$ WT fibroblasts which was 543 a.u ± 22 (n=40) $P \leq 0.001$). This represents a 27% reduction in the mitochondrial membrane potential in mutant SOD1 expression in fibroblasts compared to WT fibroblasts. Assessment of the $\Delta\Psi_m$ in myotubes and fibroblasts therefore revealed that mutant SOD expression in myotubes had a significantly greater reduction in the TMRM fluorescence signal compared to fibroblasts ($P \leq 0.004$). The results are summarised in the bar chart in **Fig 3.5(B).** This data suggest that the effect of mutant SOD1 is not specific to myotubes and that other cell types are susceptible to alterations in $\Delta\Psi_m$ as a consequence of mutant SOD1

expression. However it is clear that mutant SOD expression has significant deleterious effects on mitochondrial function in myotubes even very early during development.

Figure 3.4 Mitochondrial membrane potential measured using TMRM in myotube cultures

The cells were loaded with TMRM (20nM) and allowed to equilibrate for approximately 30 mins. TMRM crosses the cell membrane easily and localizes to the mitochondrial compartment in response to the electrochemical potential gradient. Images of TMRM loaded $SOD1^{G93A}$ myotubes (A) and $SOD1^{G93A}$ Fibroblasts (B) acquired using the Confocal LSM (Zeiss 510) microscope with excitation at 543nm and emission measured at 560nm using a 40x oil emersion objective lens. For each experiment a 'z stack' was acquired through the entire cell and a 3D projection made. The maximum intensity value of each pixel was taken through each point in the cell and a single compressed image was generated.

(Scale bar = 50μm)

FIGURE 3.4

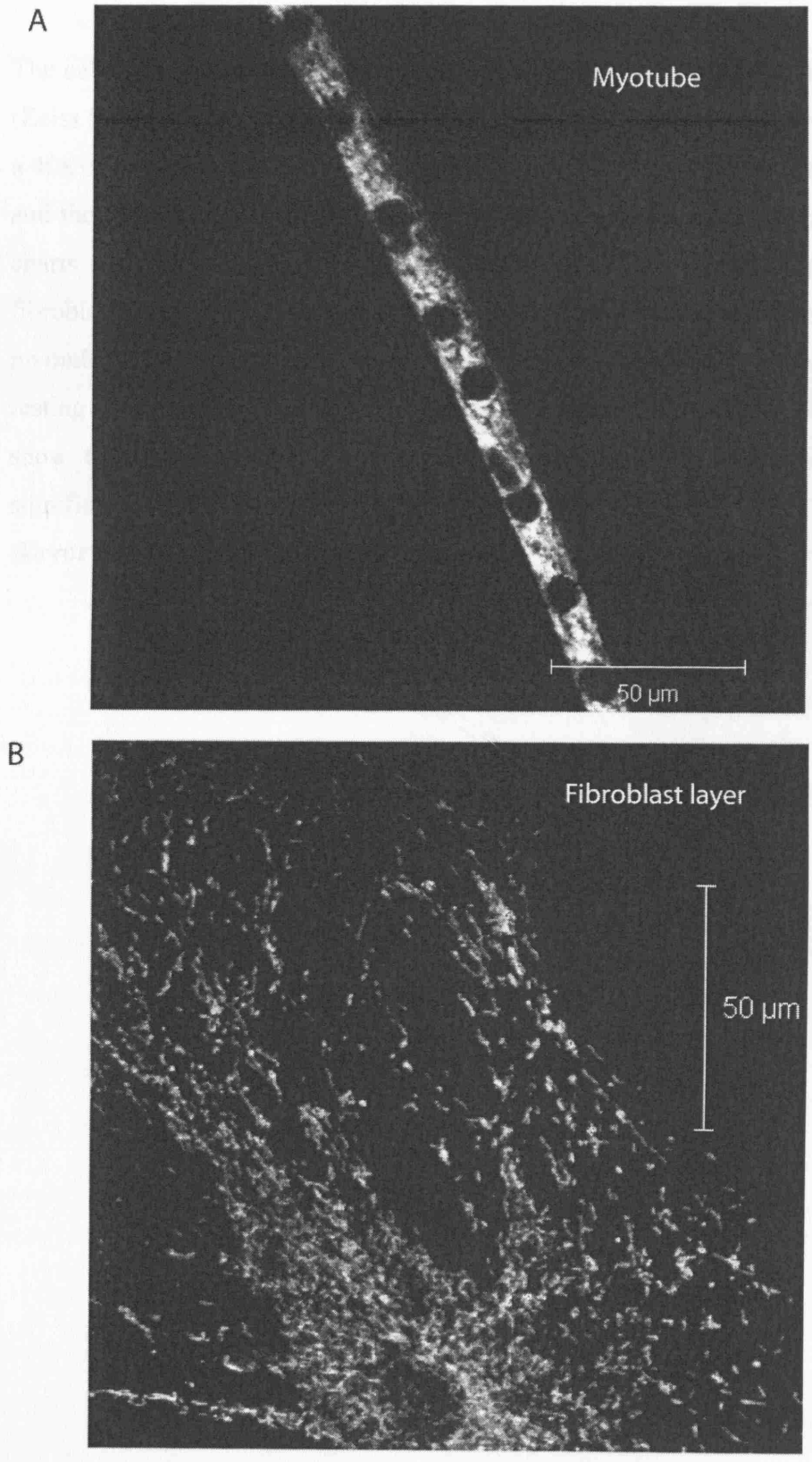

Figure 3.5 Measurements of mitochondrial membrane potential

The cells were loaded with TMRM and images were acquired using the Confocal LSM (Zeiss 510) microscope with excitation at 543nm and emission measured at 560nm using a 40x oil emersion objective lens. The fluorescence signal was corrected for laser power and the resulting value corresponded to the mitochondrial membrane potential. The bar charts summarises mean resting mitochondrial membrane potential (A) myotubes and fibroblasts and is expressed as a percentage of the WT signal. The signal from WT myotubes and fibroblasts is presented as 100%. The bar chart (B) summarises the mean resting mitochondrial membrane potential SOD myotubes and fibroblasts. The results show that mitochondria of mutant SOD1 expressing myotubes and fibroblasts are significantly more depolarised than in WT controls.

(Error bars = standard error of the mean, * $P \leq 0.001$, ** $P \leq 0.001$* P = 0.002)**

FIGURE 3.5

A

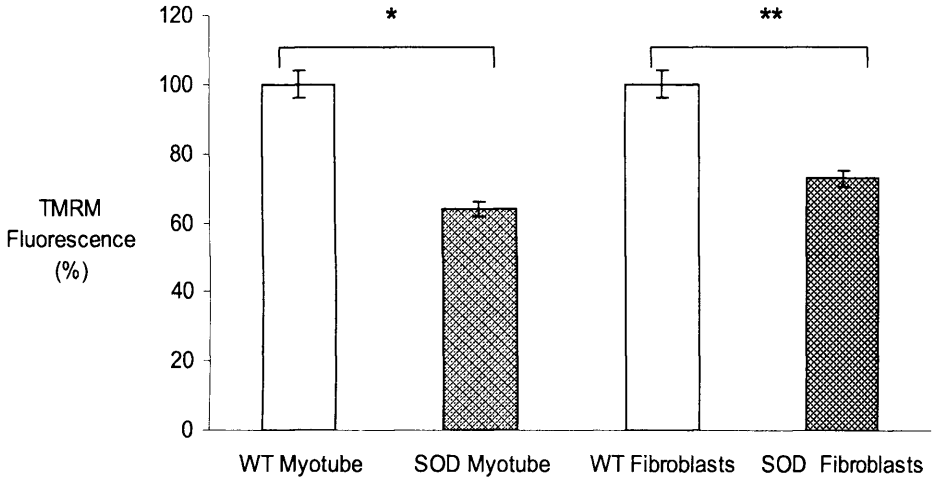
120
100
80
60
40
20
0
TMRM Fluorescence (%)
*
**
WT Myotube
SOD Myotube
WT Fibroblasts
SOD Fibroblasts

B

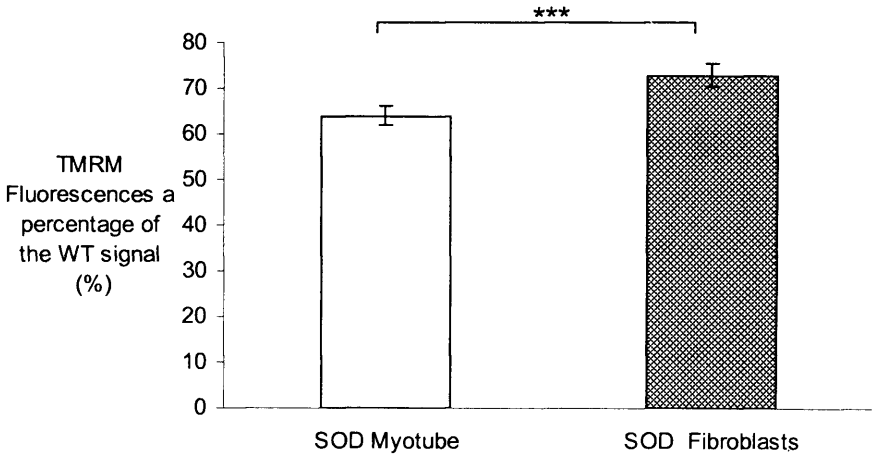
***
80
70
60
50
40
30
20
10
0
TMRM Fluorescences a percentage of the WT signal (%)
SOD Myotube
SOD Fibroblasts

3.2.2.2 Measurements of resting mitochondrial membrane potential of myotube and motoneuron co-cultures

The results from the previous experiment show that the resting $\Delta\Psi_m$ is reduced in $SOD1^{G93A}$ myotubes compared to WT myotubes. In the next set of experiments the effect of co-culturing motoneurons with myotubes on $\Delta\Psi_m$ was examined. In these experiments, SOD1 or WT motoneurons were co-cultured with SOD1 or WT myotubes and the $\Delta\Psi_m$ in both motoneurons and myotubes was examined. Thus there were 4 experimental groups,

(i) WT motoneurons with WT myotubes (WTmnWTm)

(ii) WT motoneurons with SOD myotubes (WTmnSODm)

(iii) SOD motoneurons with SOD myotubes (SODmnSODm)

(iv) SOD motoneurons with WT myotubes (SODmnWTm)

An example of a motoneuron and myotube loaded with TMRM are shown in **Fig 3.6.** The mean resting TMRM fluorescence in the co-cultures was measured and the results are summarised in the bar chart shown in **Fig. 3.7 (A)** myotubes **(B)** motoneurons. The results show that the $SOD1^{G93A}$ myotubes in the co-cultures had significantly reduced $\Delta\Psi_m$ compared to the WT myotubes. The TMRM signal in the myotubes in WTmnWTm cultures was 598 a.u ± 2.7 (n=12) and was significantly reduced by 16.5% to 499 a.u ± 15 (n=13) in WTmnSODm cultures ($P \leq 0.015$). Furthermore the SODmnSODm cultures were more depolarised, so that the $\Delta\Psi_m$ was reduced to 495 a.u ± 10 (n=23) representing a 17.22% reduction compared to WTmnWTm ($P \leq 0.003$).

Interestingly the myotubes cultured in the absence of motoneurons, irrespective of genotype, were more depolarised than the myotubes in co-culture. The $\Delta\Psi_m$ of $SOD1^{G93A}$ myotubes was reduced by 36% when cultured alone and was only reduced by 16% in co-culture. Therefore myotubes cultured in the absence of motoneurons, are more susceptible to the SOD1-induced reductions in $\Delta\Psi_m$.

Examination of $\Delta\Psi_m$ motoneurons in co-cultures showed that the expression of SOD1 in either motoneurons or myotubes significantly decreased the $\Delta\Psi_m$. The $\Delta\Psi_m$ in WTmnWTm co-cultures was 803 a.u ± 4.5 (n=5), however was reduced in WTmnSODm co-cultures the $\Delta\Psi_m$ was reduced by 38% to 500 a.u ± 1.7 (n=3) ($P \leq 0.036$). Furthermore the resting $\Delta\Psi_m$ in SODmnWTm cultures was also reduced by 15% to 682.1 a.u ± 18.45 (n=5) compared to WTmnWTm and in SODmnSODm the $\Delta\Psi_m$ was reduced by 30% to 561 a.u ± 35 (n=4) compared to WTmnWTm ($P \leq 0.032$).

Thus mutant SOD expression in myotubes was sufficient to reduce $\Delta\Psi_m$ even in co-cultured WT motoneurons. Indeed the reduction in the $\Delta\Psi_m$ induced by mutant SOD expression in myotubes was greater in WT motoneurons, than the decrease in $\Delta\Psi_m$ induced by mutant SOD expression in motoneurons themselves. These findings are supported by other studies, which have reported depolarisation in $\Delta\Psi_m$ in motoneurons under basal conditions *in vitro* (Carri et al., 1997; Kruman et al., 1999; Rizzardini et al., 2005). The motoneurons in these previous studies were not in co-culture with muscles, yet the results presented in this chapter, suggest that perturbations in $\Delta\Psi_m$ in motoneurons may be further exacerbated by co-culturing motoneurons with $SOD1^{G93A}$ myotubes. It appears from these results that the expression of mutant SOD in myotubes is able to induce a reduction in $\Delta\Psi_m$ in co-cultured motoneurons. Due to the small sample size of cells examined, it is uncertain to whether these findings are typical of all motoneurons. By increasing the sample size, a more representative interpretation of the findings can be made.

It is apparent from these measurements of mitochondrial function there is an interaction between motoneurons and myotubes *in vitro*. This interaction may specifically underlie the susceptibility of motoneurons to cellular stress, in particular mitochondrial dysfunction in ALS.

Figure 3.6 Image of TMRM loaded motoneurons and myotubes in co-culture

The motoneuron and myotube co-cultures with TMRM (20nM). Images of TMRM loaded (A) motoneurons and (B) myotubes acquired using the Confocal LSM (Zeiss 510) microscope with excitation at 543nm and emission measured at 560nm using a 40x oil emersion objective lens are shown.

(Scale bars = 20 μm and 50 μm)

FIGURE 3.6

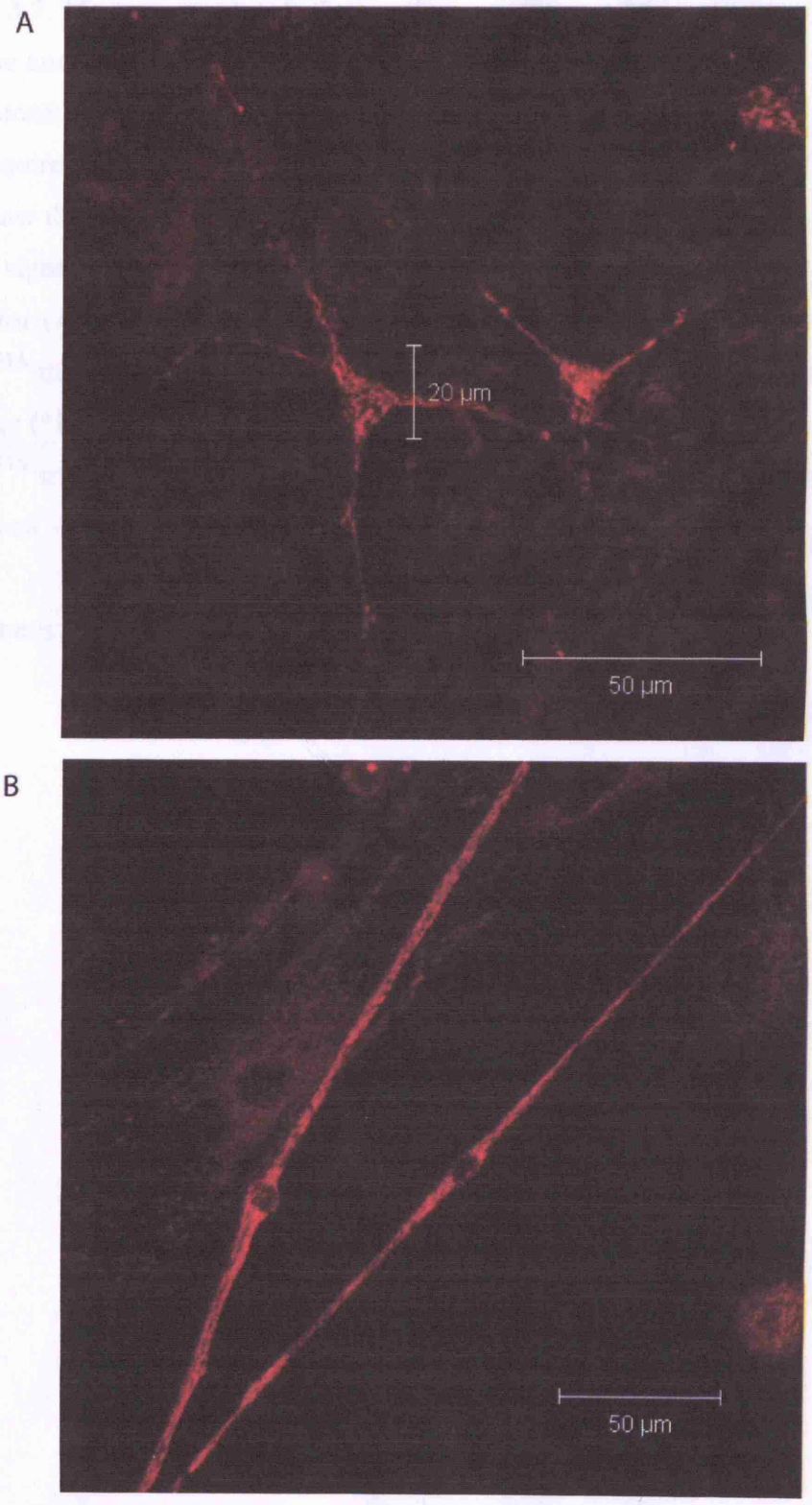

Figure 3.7 Measurements of the resting mitochondrial membrane potential of myotube and motoneuron co-cultures

The motoneuron and myotube co-cultures were loaded with TMRM (20nM). Images were acquired using x 40 oil immersion objective lens on a Zeiss 510 CLSM. The bar chart show the mean resting mitochondrial membrane potential ($\Delta\Psi_m$), as determined by TMRM signal is expressed as a percentage of WT (the signal from WT is represented as 100%) for (A) myotubes and (B) motoneurons. The results show that the $\Delta\Psi_m$ in the $SOD1^{G93A}$ myotubes in the co-cultures were significantly reduced compared to the WT myotubes (*$P \leq 0.015$ and ** $P \leq 0.003$). It can also be seen that motoneurons cultured on $SOD1^{G93A}$ myotubes had a significantly lower resting $\Delta\Psi_m$ compared to motoneurons cultured on WT myotubes (*$P \leq 0.036$ and ** $P \leq 0.032$).

(Error bars = standard error of the mean)

FIGURE 3.7

A

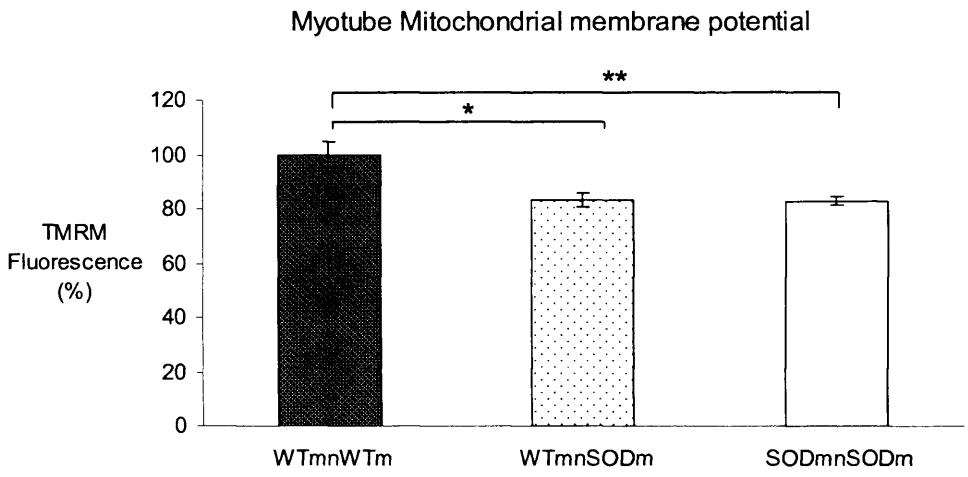
Myotube Mitochondrial membrane potential
**
*
120
100
80
60
40
20
0
TMRM
Fluorescence
(%)
WTmnWTm
WTmnSODm
SODmnSODm

B

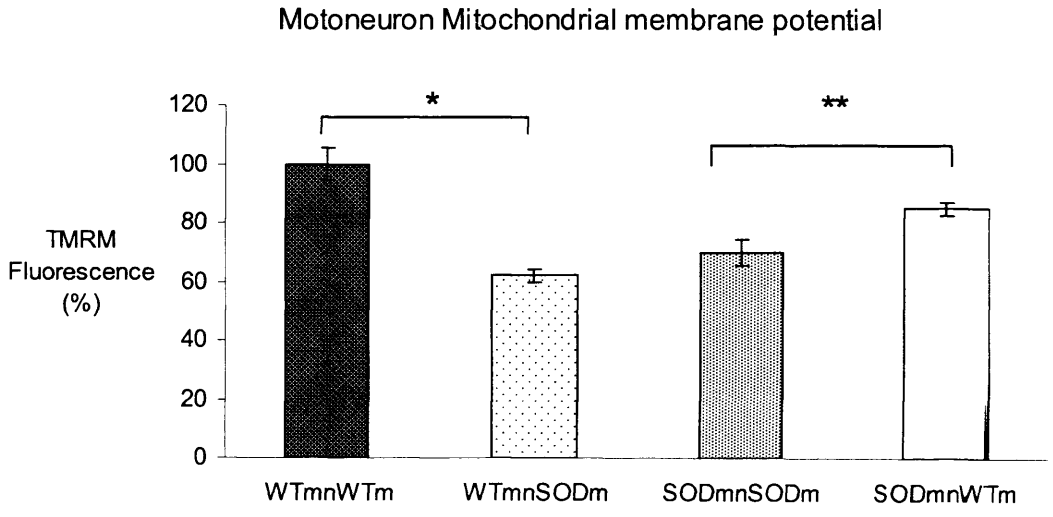
Motoneuron Mitochondrial membrane potential
*
**
120
100
80
60
40
20
0
TMRM
Fluorescence
(%)
WTmnWTm
WTmnSODm
SODmnSODm
SODmnWTm

3.2.3 Assessing redox status by measurements NAD(P)H autofluorescence

Analysis of the resting mitochondrial membrane potential show that the $SOD1^{G93A}$ myotubes were reduced compared to WT myotubes. These results suggest the mitochondria are depolarised, which may result from either mitochondria proton leak due to mitochondrial uncoupling or a deficit in mitochondrial respiration. The electron transport chain and oxidative phosphorylation are coupled by a proton gradient across the inner mitochondrial membrane. When there is a dissipation of the proton gradient or a proton 'leak' in the mitochondria, the mitochondria become uncoupled and there is dissociation between electron transport and ATP synthesis.

To examine the mitochondrial respiration, measurements of the mitochondrial oxygen consumption of these cells would be normally determined. However it is difficult to measure oxygen consumption in groups of cells in culture. To overcome the problem of measuring oxygen consumption, mitochondrial function can be assessed in the $SOD1^{G93A}$ myotubes, by manipulation of the NAD(P)H autofluorescence. Measurements of the change in the redox state can give an indication of the metabolic state of the mitochondria.

In most cells the intrinsic autofluorescence arises from pyridine nucleotide carriers NADH and electron carrier flavoprotein which are located within mitochondria. The autofluorescence signal which is emitted from the mitochondria can be manipulated and changes in the autofluorescence can provide an indication of the mitochondrial metabolism. An example of autofluorescence in the primary myotube cultures is shown in **Fig 3.8**. To assess the redox state in the myotube cultures, the autofluorescence of NADH was exploited. In these experiments the flavoprotein signal was very weak when manipulated with mitochondrial inhibitors or uncouplers, suggesting that the autofluorescence may come from another source and may not be a mitochondrial flavoprotein signal. Therefore in these experiments only the NADH autofluorescence was determined.

NADH was excited in the UV wavelength (peak excitation 350nm) and fluorescence measured (peak emission 450nm). The reduced form, NADH is autofluorescent, whilst the oxidised form, NAD^+, is not fluorescent. An increase in autofluorescence therefore indicates an increase in the ratio of NADH to NAD^+.

Manipulation of the NADH autofluorescence, using compounds that alter mitochondrial function, enabled the metabolic state of mitochondria to be assessed. Application of sodium cyanide (CN^-) blocks cytochrome oxidase (complex V) resulting in the inhibition of respiration preventing the oxidation of NADH to NAD^+ thereby producing a maximal reduced state. CN^- therefore results in NADH accumulation and an increase in NADH autofluorescence. FCCP is a mitochondrial uncoupler, which dissipates membrane potential, stimulating maximal respiration causing oxidation of NADH. Reducing the NADH accumulation and therefore causes a decrease in the NADH autofluorescence signal as illustrated in **Fig 3.9**. In theses experiments the changes in NADH autofluorescence intensity were normalised between the maximally reduced (CN^-) value of 1 and the maximally oxidised (FCCP) signal, assigned a value of 0. A redox index could then be established, by using the fluorescence intensity at baseline and following the response to CN^- and FCCP by the following formulae:
Redox index = (Baseline) - (FCCP)/ (CN^-) - (FCCP)

Measurements of the mean redox index for NADH autofluorescence of $SOD1^{G93A}$ and WT mice myotubes are summarised in the bar chart **Fig 3.10**. The redox index of WT was 0.38 arbitrary units (a.u) (±0.03 n=28) compared to $SOD1^{G93A}$ 0.46 a.u (±0.02 n=22) $P \leq 0.022$. In $SOD1^{G93A}$ myotubes, there was an increase of 21% of the redox index suggesting that the mitochondria were in a more reduced state compared to WT myotubes. The reduction in the mitochondrial redox state may result from an increase in substrate handling. However, as the $\Delta\Psi_m$ is also reduced in $SOD1^{G93A}$ myotubes, it is more likely that the reduction in the mitochondrial redox state is due to impaired respiration. The maintenance of the $\Delta\Psi_m$ is dependent on the mitochondrial respiratory rate. In this study it was not possible to measure the redox state in motoneurons co-cultured with myotubes due a shortage of time. However a previous study from our

group has shown that the mitochondrial redox index was significantly greater in mitochondria of both WT and $SOD1^{G93A}$ motoneurons when co-cultured with $SOD1^{G93A}$ astrocytes. This indicates that the mitochondrial redox state is more reduced in motoneurons co-cultured with $SOD1^{G93A}$ astrocytes. This reduced redox state in motoneurons is a similar finding to that observed in the $SOD1^{G93A}$ myotubes and it is likely that the reduction in the mitochondrial redox state is due to impaired respiration.

Figure 3.8 NADH and Flavoprotein autofluorescence in myotube cultures

Images of NADH and Flavoprotein autofluorescence in myotube cultures were acquired using a Confocal LSM (Zeiss 510) microscope. NADH was excited at 351nm and emission measured at 450nm (blue fluorescence as shown in A). Flavoprotein was excited at 450nm and emission measured at 550nm, (green fluorescence shown in B). NADH and FAD autofluorescence images were merged in C. A typical trace of NADH and FAD autofluorescence in WT myotube in response to cyanide and FCCP is shown in D.

Scale bar =50μm, sec = seconds

FIGURE 3.8

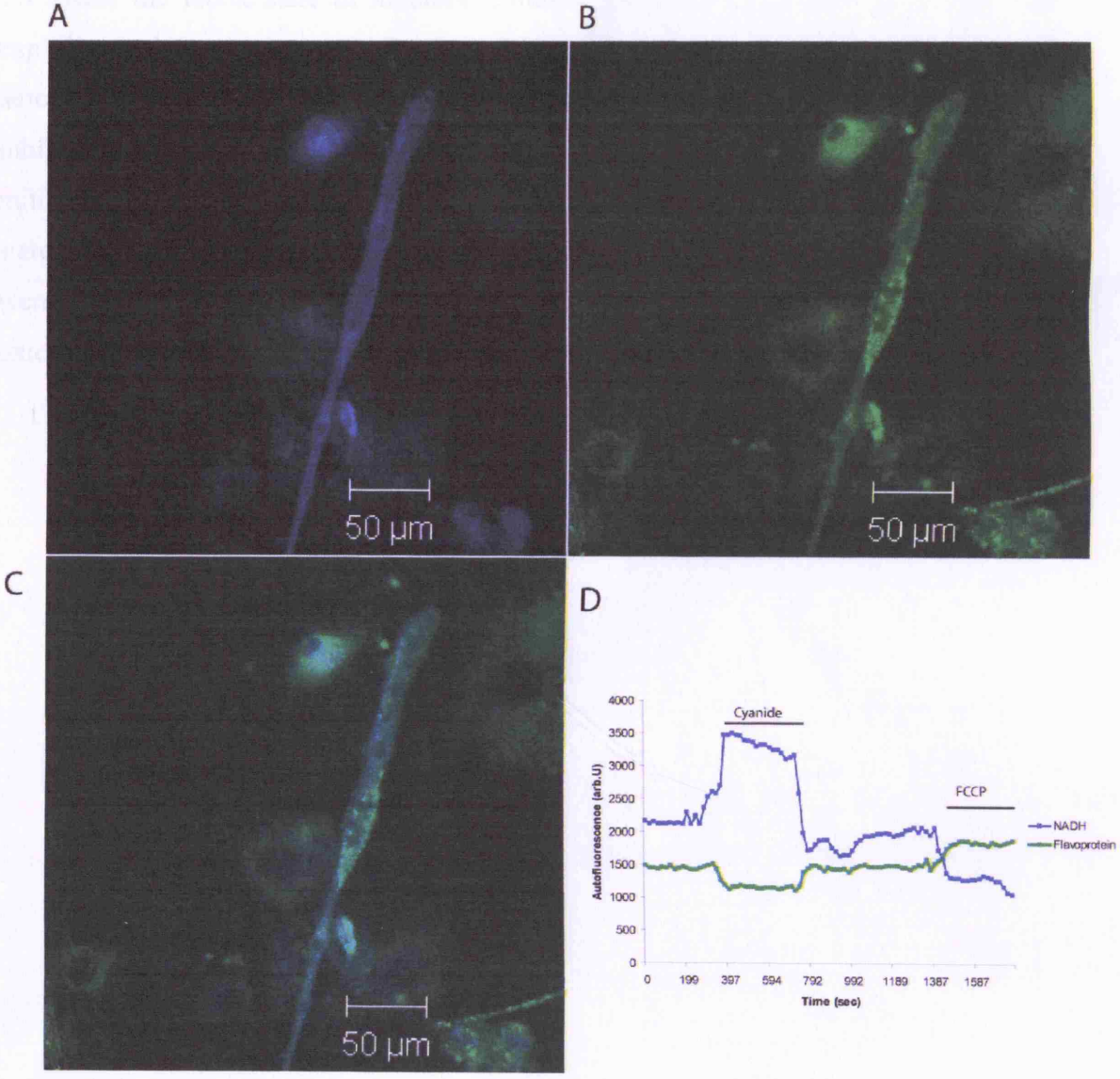
A
B
50 µm
50 µm
C
D
50 µm
Cyanide
FCCP
NADH
Flavoprotein
Autofluorescence (arb.U)
Time (sec)
4000
3500
3000
2500
2000
1500
1000
500
0
0
199
397
594
792
992
1189
1387
1587

Figure 3.9 NADH autofluorescence in myotube cultures

To assess the redox state in myotube cultures, the autofluorescence of NADH was exploited and acquired using a Confocal LSM (Zeiss 510) microscope. Resting NADH autofluorescence (as shown in A), can be manipulated with sodium cyanide (CN^-), inhibits respiration and produces a maximal reduced state (as shown in C). FCCP is a mitochondrial uncoupler, which stimulates maximal respiration resulting in an oxidised state (as shown in D). In these experiments the changes in autofluorescence intensity were normalised between the maximally reduced (CN^-) value of 1 and the maximally oxidised (FCCP) signal assigned a value of 0 (refer in B).

FIGURE 3.9

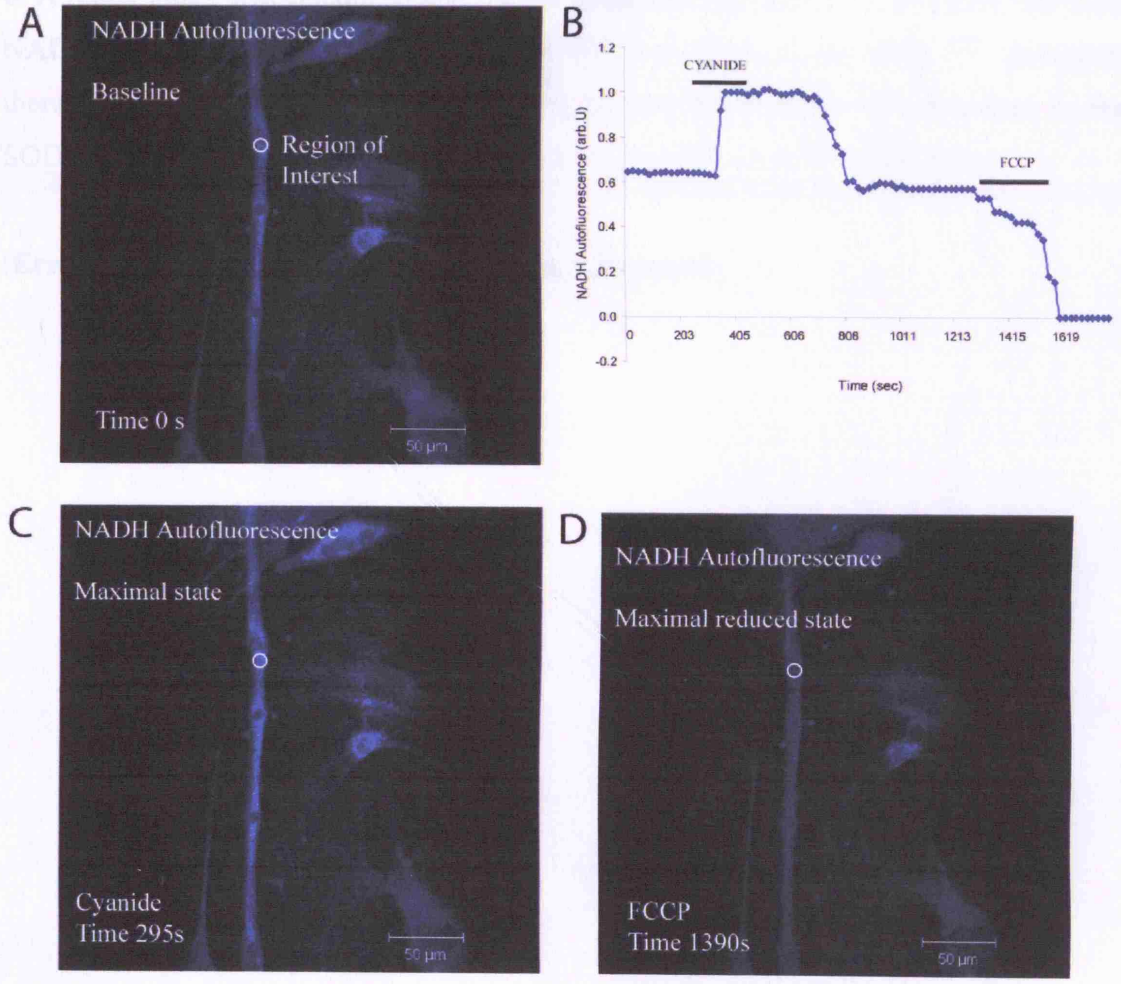
A
NADH Autofluorescence
Baseline
Region of Interest
Time 0 s
50 µm
B
CYANIDE
FCCP
NADH Autofluorescence (arb.U)
1.2
1.0
0.8
0.6
0.4
0.2
0.0
-0.2
0
203
405
606
808
1011
1213
1415
1619
Time (sec)
C
NADH Autofluorescence
Maximal state
Cyanide
Time 295s
50 µm
D
NADH Autofluorescence
Maximal reduced state
FCCP
Time 1390s
50 µm

Figure 3.10 Measurements of the redox status in myotube cultures

Manipulation of NADH autofluorescence, using the respiratory inhibitor CN^- results in a maximal reduced state. FCCP stimulates maximal respiration, resulting in an oxidised state. The changes in autofluorescence intensity were normalised between the maximally reduced (CN^-) value of 1 and the maximally oxidised (FCCP) signal assigned a value of 0. A redox index was calculated and the bar chart summarises the mean redox index for NADH autofluorescence in $SOD1^{G93A}$ and WT myotubes. In the $SOD1^{G93A}$ myotubes there was an increase in the redox index, suggesting that the mitochondria in the $SOD1^{G93A}$ myotubes were in a more reduced state compared to WT myotubes.

(Error bars = standard error of the mean, * $P \leq 0.022$)

FIGURE 3.10

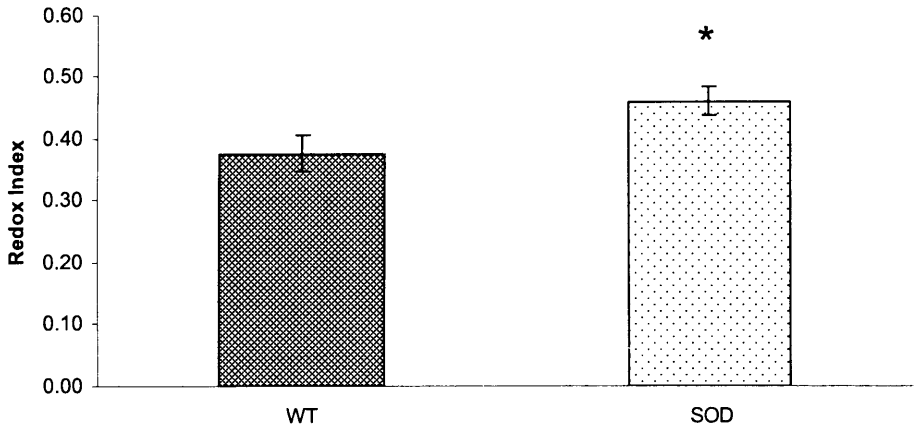

3.2.4 Cytosolic calcium activity

Since mitochondria are involved in the uptake of calcium and mitochondrial calcium uptake is dependent on the $\Delta\Psi_m$, changes in the $\Delta\Psi_m$ may influence the cytosolic calcium signalling. In the next series of experiments calcium homeostasis in both genotypes in myotubes and motoneurons was assessed.

3.2.4.1 Myotube cultures

Intracellular calcium is important for the metabolic function of muscle, and calcium has been suggested to directly stimulate mitochondrial respiration (Kavanagh et al., 2000). As the previous results show that $\Delta\Psi_m$ was reduced in the $SOD1^{G93A}$ myotubes, suggesting altered mitochondrial function, the myotubes were examined to determine whether there was evidence of altered calcium activity in the $SOD1^{G93A}$ myotubes.

Myotube cultures (9-12 DIV) were loaded with the cytosolic calcium indicator Fluo-4 AM and spontaneous calcium activity in the myotubes was recorded. To distinguish spontaneous calcium activity from background noise, the images were normalised with respect to the baseline fluorescence. As there was spontaneous calcium activity throughout the time series, the image analysis software (Lucida) was used to create a virtual image from the darkest value of each pixel throughout the time series as a means of assigning a baseline value. To normalize the fluorescence signal, all images of the time series were then divided by the 'darkest' (baseline) image. The cytosolic calcium signals were measured by identifying the peak amplitude of a calcium transient and the frequency of calcium transients. Examples of typical traces of spontaneous calcium activity in myotubes from different regions of interest (ROI) are shown in **Fig 3.11**.

The myotube cultures were maintained in recording medium (RM), containing $CaCl_2$ (2mM) during the imaging experiments. To determine the effect of external calcium on the spontaneous calcium signals in the myotubes, the recording medium was replaced with Ca^{2+} free recording medium, containing the calcium buffer EGTA (1mM). The spontaneous calcium signals required the presence of external Ca^{2+}, as the removal of extra-cellular Ca^{2+} by the addition of Ca^{2+} free recording medium, containing EGTA

(1mM) dramatically reduced the spontaneous cytosolic calcium activity in myotube cultures. The re-addition of Ca^{2+} containing RM, once again initiated spontaneous cytosolic calcium activity in myotube cultures. This indicates that there is a requirement for external calcium to generate spontaneous calcium signals in the myotubes.

(i) Spontaneous cytosolic calcium: measurements of amplitude and frequency of calcium transients

Spontaneous calcium signals were recorded and the results are summarised in the bar chart shown in **Fig 3.12**. There was no significant difference in the mean peak amplitude of spontaneous cytosolic calcium activity in myotube cultures in WT myotubes which was 4.2 a.u ± 0.5 (n=20), or in wild type human SOD overexpressing myotubes (SOD^{WT}) which was 4.6 a.u ± 0.3 (n=35) and in $SOD1^{G93A}$ myotubes the mean peak amplitude was 4.67 a.u ± 1.8 (n=39).

However the mean frequency of spontaneous cytosolic calcium activity was significantly increased in $SOD1^{G93A}$ myotubes compared to controls. The mean frequency was 10 a.u ± 3.2 (n=10) in WT, 10.7 a.u ± 1.8 (n=35) in SOD^{WT} and this was significantly increased by 105% to 22 a.u ± 2.1 (n=38) in $SOD1^{G93A}$ myotube ($P \leq 0.001$). These results show that the increase in frequency of spontaneous cytosolic calcium activity was specific to mutant $SOD1^{G93A}$ myotubes and was not seen in SOD^{WT} myotubes. These mice express WT human Cu/Zn SOD at levels comparable $SOD1^{G93A}$ and act as a control for elevated levels of human SOD (Dal Canto and Gurney, 1995).

Figure 3.11 Examples of traces of spontaneous cytosolic calcium activity in myotube cultures

The myotube cultures were loaded with the high affinity calcium indicator Fluo-4 AM. Spontaneous calcium activity occurred along the length of the myotubes. A typical example of recordings of a WT myotube is shown in (A). Different regions of interest (ROI) were selected along the myotube (C) and the traces plotted show the relative change in intensity of Fluo-4 AM fluorescence over time (B).

(Scale bar =20 μm, sec= seconds)

FIGURE 3.11

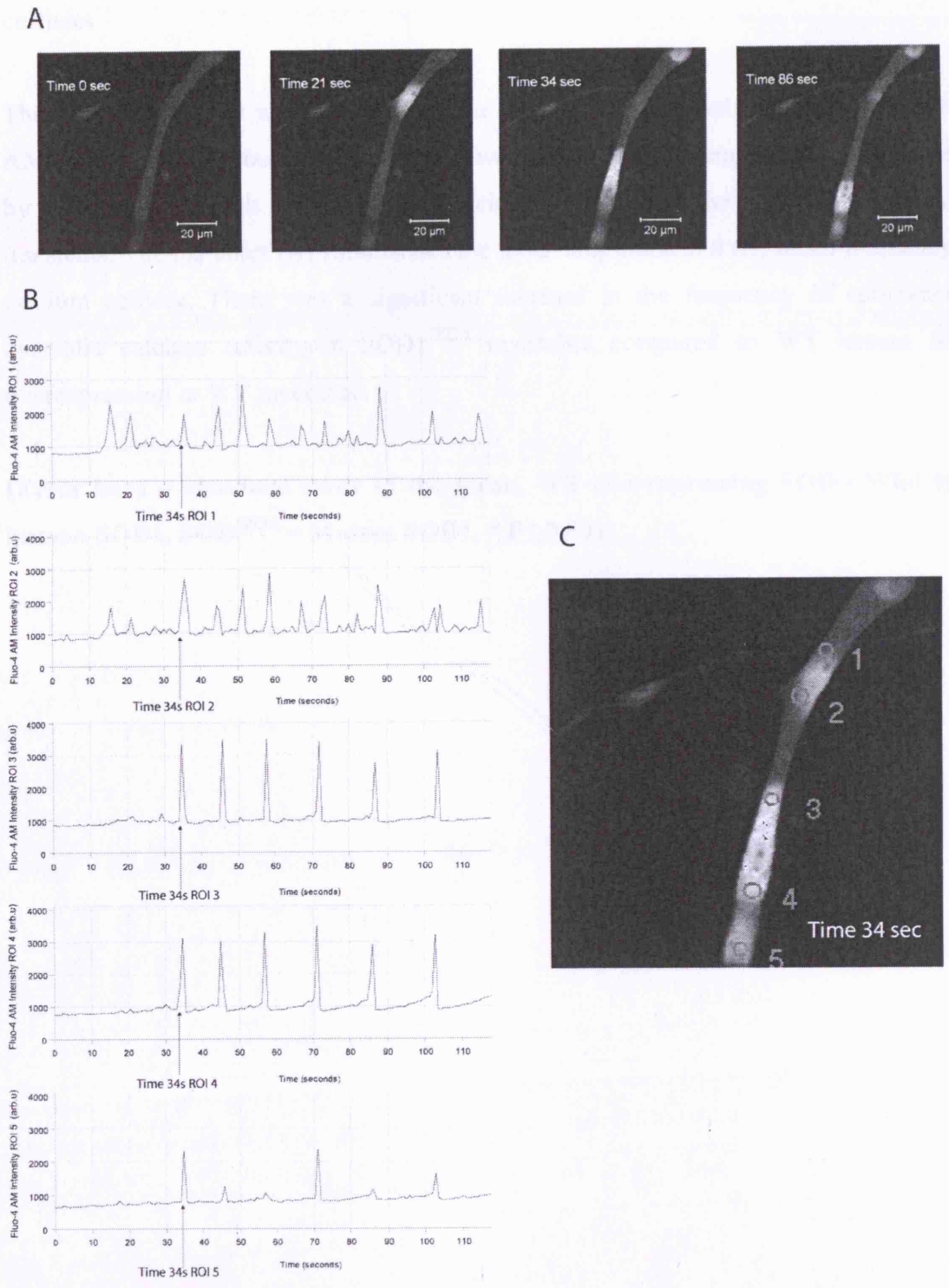
A
Time 0 sec
Time 21 sec
Time 34 sec
Time 86 sec
20 µm
B
Fluo-4 AM Intensity ROI 1 (arb.u)
Time 34s ROI 1
Fluo-4 AM Intensity ROI 2 (arb.u)
Time 34s ROI 2
Fluo-4 AM Intensity ROI 3 (arb.u)
Time 34s ROI 3
Fluo-4 AM Intensity ROI 4 (arb.u)
Time 34s ROI 4
Fluo-4 AM Intensity ROI 5 (arb.u)
Time 34s ROI 5
Time (seconds)
C
1
2
3
4
5
Time 34 sec

Figure 3.12 Measurement of spontaneous cytosolic calcium activity in myotube cultures

The myotube cultures were loaded with the high affinity cytosolic calcium dye Fluo-4 AM and the spontaneous calcium activity was recorded. Calcium activity was assessed by measuring the peak amplitude of a calcium transient and the frequency of calcium transients. The bar chart (A) summarises the mean amplitude and (B) mean frequency of calcium activity. There was a significant increase in the frequency of spontaneous cytosolic calcium activity in $SOD1^{G93A}$ myotubes compared to WT human SOD overexpressing or WT myotubes.

(Error bars = standard error of the mean, WT overexpressing SOD= Wild type human SOD1, SOD^{G93A} = Mutant SOD1, * P≤ 0.001)

FIGURE 3.12

A

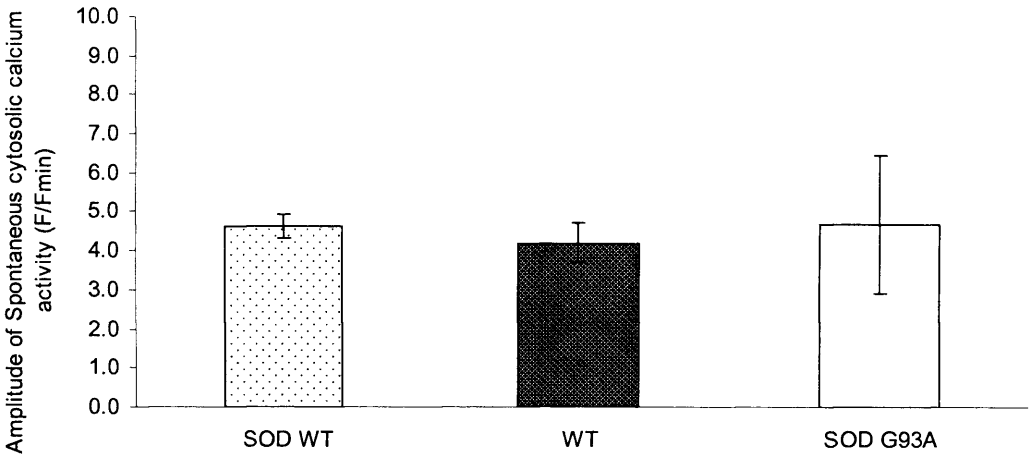

B

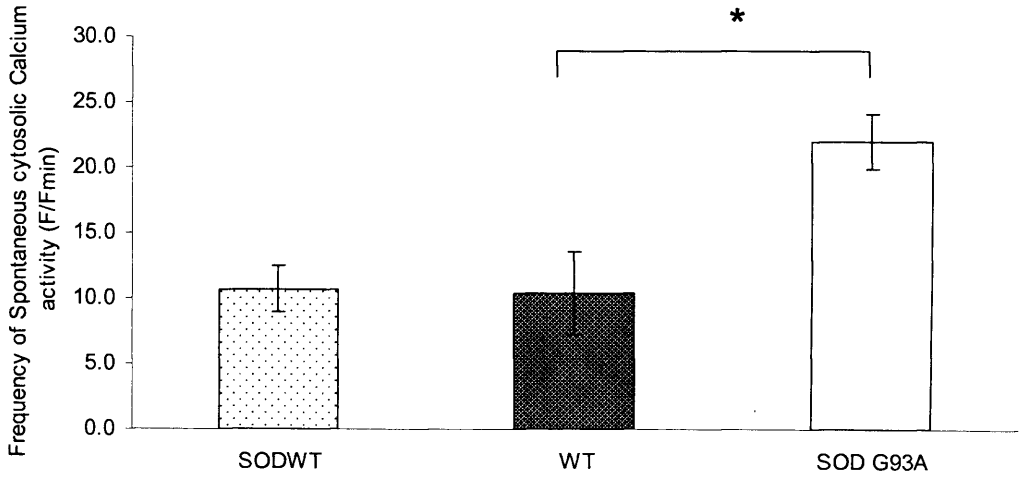

(ii) Rate of propagation of calcium transients in myotube cultures

The calcium transients generated in the myotube cultures, were either (i) fast and propagated along the length of the myotube as a calcium wave or (ii) localised calcium transients that occurred in a small region, and resembled 'sparks' in the myotubes. Previous results from our group have shown that alterations in the mitochondrial $\Delta\Psi_m$ can significantly increase the rate of propagation of the spontaneous cytosolic calcium in cortical astrocytes (Boitier et al., 1999). Furthermore the reduction in the $\Delta\Psi_m$ in $SOD1^{G93A}$ myotubes described in section **3.2.2.1** may also affect the rate of propagation of the spontaneous cytosolic calcium activity in the myotubes. To further characterise the spontaneous calcium transients, the rate of propagation of the transients was calculated for the WT human SOD overexpressing myotubes, WT and mutant $SOD1^{G93A}$ myotubes. The rate of propagation was calculated, measuring the distance travelled (μm) of the calcium wave along the myotube between two regions of interest, and the time taken (seconds). The Zeiss confocal software was used to measure the distances along the myotubes and the time taken.

An example of a propagating, spontaneous calcium transient in WT myotube is shown in **Fig 3.13 (A-C).** The mean propagation velocity of SOD^{WT} was 24μm/s ± 3.4 (n=16) and 22 μm/s ± 2.2 (n=21) in WT myotubes. In the $SOD1^{G93A}$ myotubes the propagation velocity was significantly increased to 35.4 μm/s ± 2 (n=24), this represents a 59% increase in the propagation velocity ($P \leq 0.002$). The mean propagation velocity of the myotubes is summarised in the bar chart Fig 3.13, these values are similar to those obtained in cortical astrocytes (Boitier et al., 1999).

Figure 3.13 Spontaneous cytosolic calcium activity propagates along the length of the myotube

The spontaneous cytosolic calcium transients propagate along the length of the myotube, resulting in an increase in the high affinity cytosolic calcium Fluo- 4AM is revealed by the pseudo-colour scale. An example of the spontaneous cytosolic calcium transients in a myotube is shown (A-C) and propagated at a velocity of 35μm/s.

(Scale bar = 20μm, sec= seconds)

FIGURE 3.13

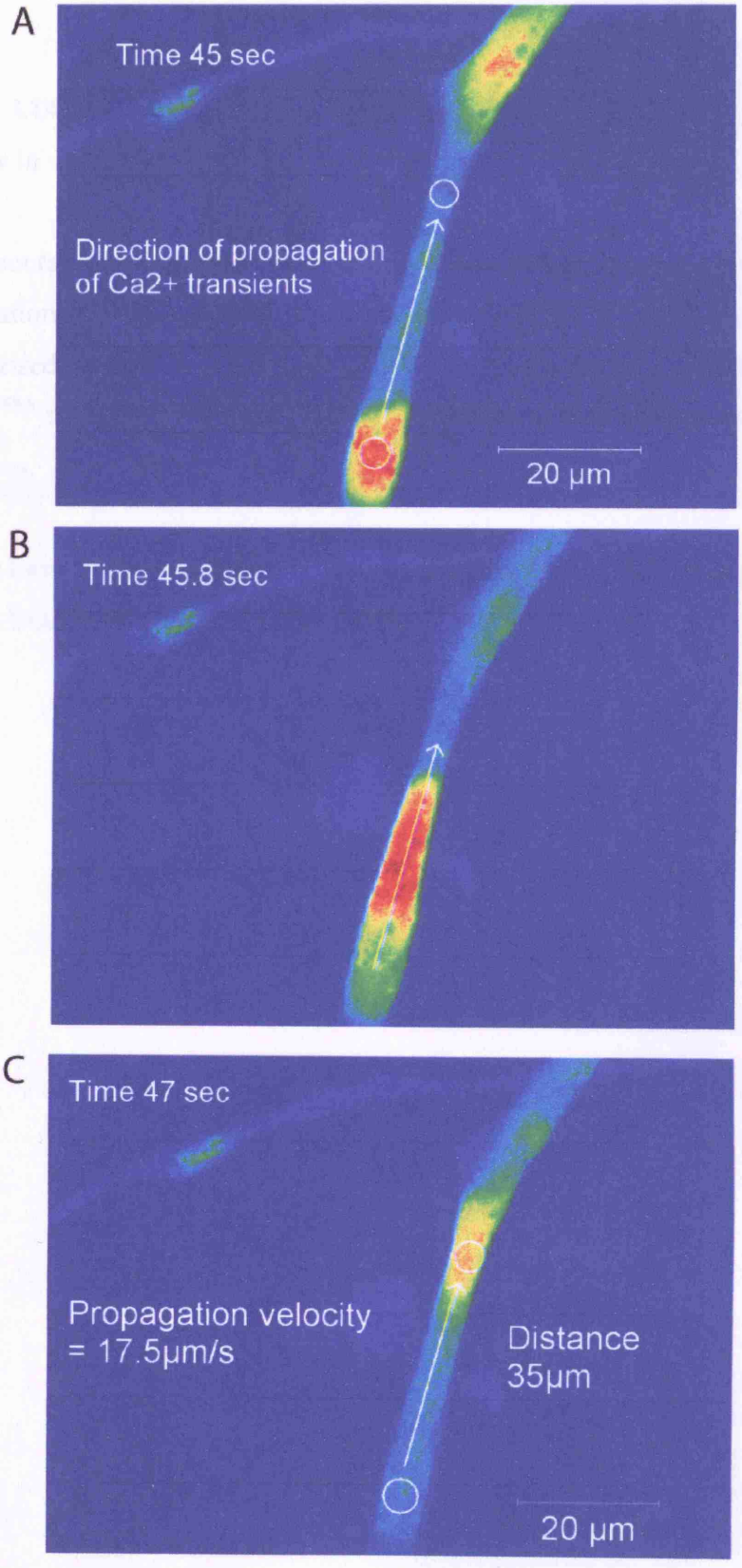
A
Time 45 sec
Direction of propagation
of Ca2+ transients
20 µm
B
Time 45.8 sec
C
Time 47 sec
Propagation velocity
= 17.5µm/s
Distance
35µm
20 µm

Figure 3.14 Measurements of propagation velocity of spontaneous cytosolic calcium activity in myotubes

The spontaneous calcium transient propagated along the myotube. The rate of propagation of the calcium transients was calculated and the mean velocity is summarised in the bar chart. The rate of propagation was significantly increased in $SOD1^{G93A}$ myotubes compared to WT myotubes or WT human SOD1 overexpressing myotubes.

(Error bars = standard error of the mean, WT overexpressing SOD= Wild type human SOD1, SOD^{G93A} = Mutant SOD1,* $P \leq 0.002$)

FIGURE 3.14

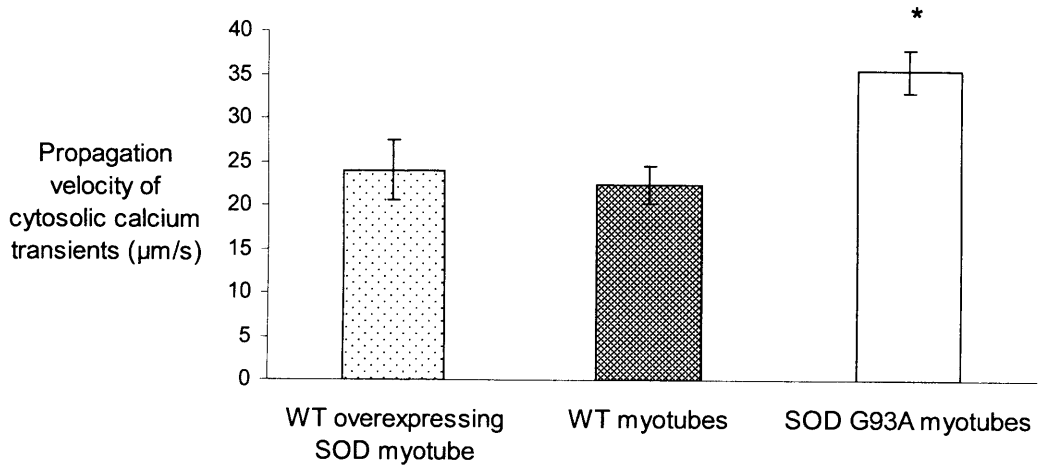
Propagation velocity of cytosolic calcium transients (μm/s)
40
35
30
25
20
15
10
5
0
*
WT overexpressing SOD myotube
WT myotubes
SOD G93A myotubes

(iii) Caffeine-induced increases the frequency of cytosolic calcium transients in myotube cultures

The expression of mutant $SOD1^{G93A}$ in myotubes alters the frequency and propagation velocity of spontaneous cytosolic calcium activity in myotubes. The calcium activity in the myotubes was further examined by stimulating the cells with caffeine. This acts to potentiate calcium-induced calcium release (CICR), which underlies the generation of oscillating calcium signals in myotubes. The intracellular stores of Ca^{2+} in the sarcoplasmic reticulum release Ca^{2+} via CICR, through ryanodine (RyR) receptors. The initial Ca^{2+} transient can be further amplified by the CICR, which accounts for the ability in skeletal muscle to generate calcium spikes and calcium waves (Berridge, 1997). In the next series of experiments the myotubes were treated with caffeine, to investigate whether the expression of mutant SOD1 altered calcium release mechanisms from internal stores and the generation of calcium waves.

The myotubes cultures were loaded with the high affinity cytosolic calcium dye Fluo-4 AM and the caffeine-induced calcium transients recorded. Caffeine releases Ca^{2+} from the RyR by increasing the sensitivity of calcium release. The Ca^{2+} release channels (RyR), open at resting intracellular calcium concentrations. The application of caffeine (1mM) produced an increase in the frequency of cytosolic calcium transients in myotube cultures. Increasing the concentration of caffeine (10mM) increased the frequency of the calcium transients further, as shown in **Fig.3.15**.

To examine the effect of mutant SOD1 expression on the elevated calcium transients the myotubes were treated with 1mM caffeine. There was no difference in the frequency of the calcium transients between WT myotubes and $SOD1^{G93A}$ myotubes, following treatment with caffeine. The mean frequency in WT myotubes was 6.4 a.u ± 0.75 (n=5) and in $SOD1^{G93A}$ myotubes the frequency was 6.25 a.u ± 1.31 (n=4). The results are summarised in the bar chart in **Fig 3.16(A)**.

The mean amplitude of the caffeine-induced calcium transient in WT myotubes was 9.6 a.u ± 0.2 (n=9) and in $SOD1^{G93A}$ myotubes the amplitude was significantly reduced by

46% to 5.2 a.u ± 0.3 (n=9) P≤ 0.001. The results are summarised in the bar chart in Fig 3.15 (B). These results suggest that expression of mutant SOD in myotubes may not alter the CICR mechanisms although further experiments are required to investigate this mechanism further.

Figure 3.15 Caffeine potentiates Ca^{2+} induced calcium release in myotube cultures

The myotube cultures were loaded with the high affinity cytosolic calcium dye Fluo-4 AM and the caffeine-induced calcium transients recorded. The application of caffeine (1mM) produced an increase in the frequency of cytosolic calcium transients in myotube cultures as can be seen in **Fig.3.14 (A)** examples from a WT myotube. Increasing the concentration of caffeine (10mM) increased the frequency of the calcium transients further, as shown in **Fig.3.15 (B)**.

(sec = seconds, mM= millimolar)

FIGURE 3.15

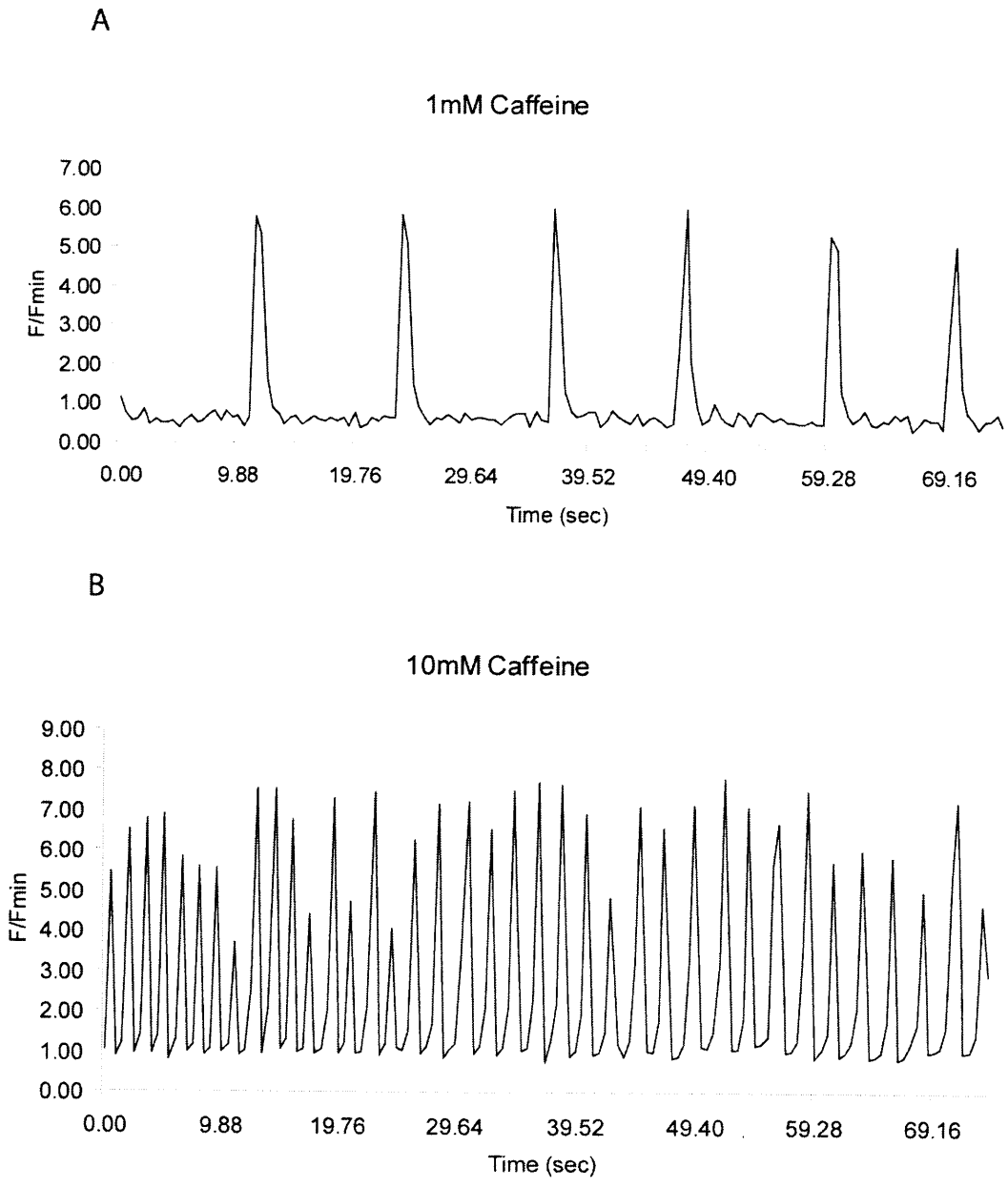
A
1mM Caffeine
7.00
6.00
5.00
4.00
3.00
2.00
1.00
0.00
F/Fmin
0.00
9.88
19.76
29.64
39.52
49.40
59.28
69.16
Time (sec)
B
10mM Caffeine
9.00
8.00
7.00
6.00
5.00
4.00
3.00
2.00
1.00
0.00
F/Fmin
0.00
9.88
19.76
29.64
39.52
49.40
59.28
69.16
Time (sec)

Figure 3.16 Caffeine induced a decrease in amplitude of cytosolic calcium transients in SOD1^{G93A} myotube cultures

The myotube cultures were loaded with the high affinity cytosolic calcium dye Fluo-4 AM and the caffeine-induced calcium transients were recorded. The mean amplitude of the caffeine-induced calcium transient was significantly reduced by 46% in SOD1^{G93A} myotubes compared to WT myotubes. The results are summarised in the bar chart. The application of caffeine (1mM), did not significantly alter the frequency of calcium transient in WT myotubes compared to SOD1^{G93A} myotubes

(Error bars =SEM, mM=millimolar * P≤ 0.001)

FIGURE 3.16

A

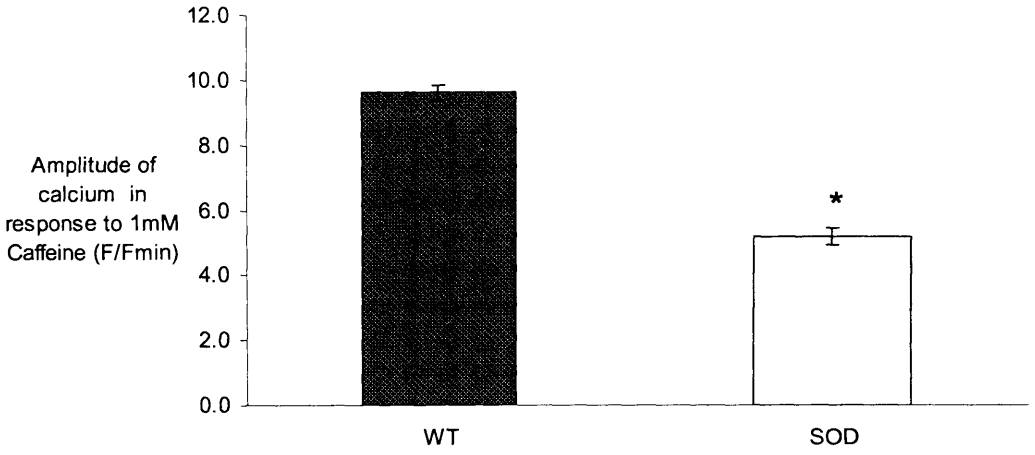

B

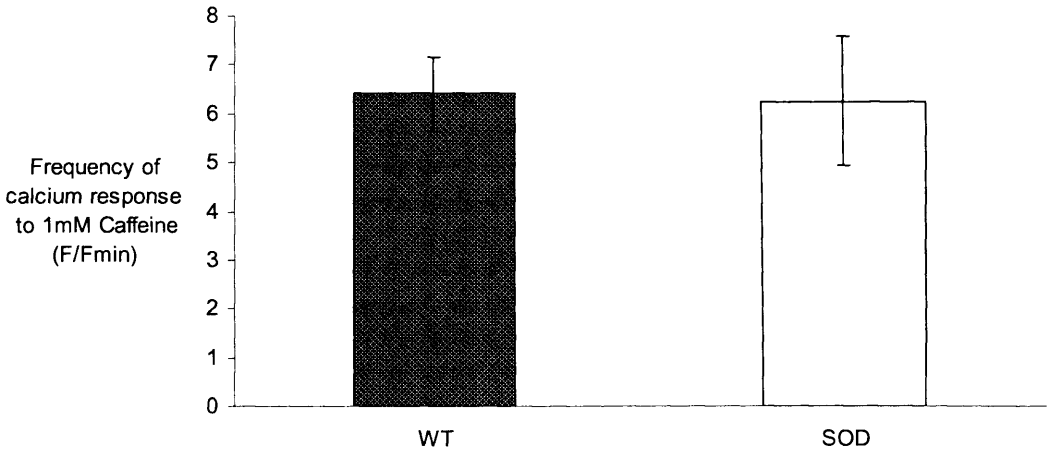

3.2.5 Cytosolic calcium activity in myotubes in co-cultures

In the next series of experiments co-cultures of motoneurons and the myotubes were established and examined for any changes in the cellular properties of these cells. However in the co-cultures only very few motoneurons made contact with myotubes. Therefore the experiments were restricted to measurements of calcium activity.

The previous experiments established that $SOD1^{G93A}$ myotubes have an increased frequency of spontaneous cytosolic calcium activity, which may reflect an increased excitability of the muscle plasma membrane; therefore co-cultures were assessed to determine whether the presence of motoneurons would alter calcium activity in the myotubes. The motoneuron and myotube co-cultures were loaded with the high affinity cytosolic calcium dye Fluo-4 AM and the spontaneous calcium activity was recorded.

(i) Spontaneous cytosolic calcium: measurements of amplitude and frequency of calcium transients in co-cultures

The spontaneous cytosolic calcium in the myotubes was examined in co-cultures either WT or $SOD1^{G93A}$ motoneurons, to determine whether motoneurons change the characteristics of calcium signalling in the myotubes. The spontaneous cytosolic calcium activity in the co-cultures was assessed by measuring the peak amplitude of a calcium transient and the frequency of calcium transients in the myotubes. The results are summarised in the bar chart in **Figure 3.17**. The amplitude in WT motoneurons/SOD myotubes (WTmnSODm) was 4.7 a.u ± 0.1 (n=20). However as shown in **Fig.3.17 (A)** this was significantly decreased by 20%, in SODmnSODm co-cultures where the amplitude was 3.8 a.u ± 0.2 (n=18) $P \leq 0.011$.

The frequency of spontaneous calcium activity in the $SOD1^{G93A}$ myotubes in the co-cultures did not significantly change regardless of the genotype of the motoneurons. In WTmnSODm co-cultures the frequency of calcium activity was 6.5 a.u ± 0.6 (n=17) and the frequency in SODmnSODm was 7.9 a.u ± 1.4 (n=13) which was not significantly different (see **Fig.3.17 (B)**).

Figure 3.17 Measurements of spontaneous cytosolic calcium activity in myotubes co-cultured with motoneurons

The motoneuron and myotube co-cultures were loaded with the high affinity cytosolic calcium dye Fluo-4 AM and the spontaneous calcium activity were recorded. The spontaneous cytosolic calcium activities were quantified in the co-cultures by measuring the peak amplitude of a calcium transient and the frequency of calcium transients in the myotubes. The bar chart (A) summarises the mean amplitude and (B) mean frequency of calcium activity in myotubes

(Error bars = standard error of the mean, MN = motoneuron, m=myotubes,* P≤ 0.011)

FIGURE 3.17

A

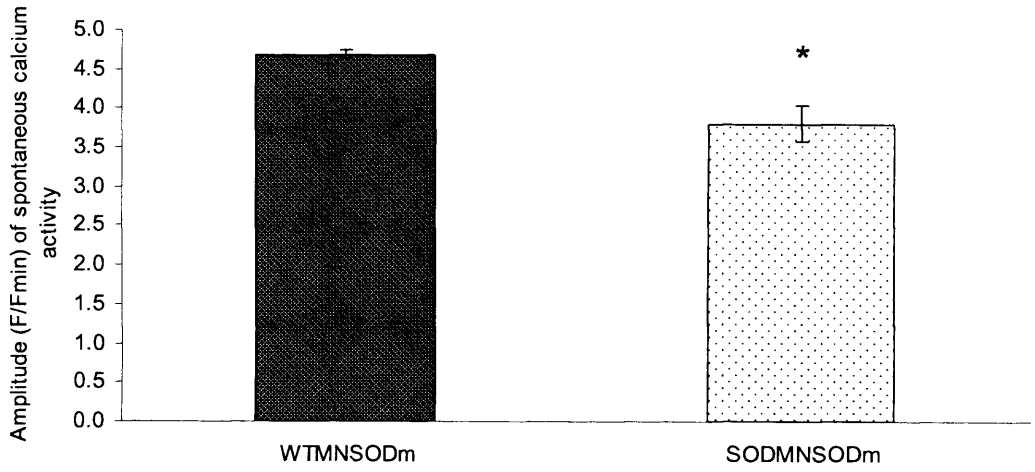

B

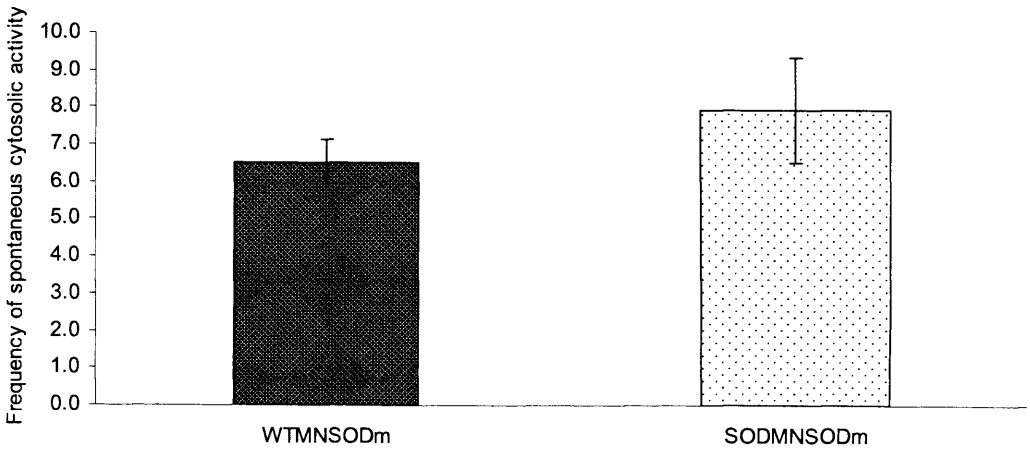

ii) Cytosolic calcium measurements following stimulation with glutamate

To determine whether motoneurons in co-culture formed functional contacts with the myotubes, the co-cultures were treated with glutamate (5μM). Motoneurons can respond to glutamate and a corresponding calcium response measured in the myotubes, indicating there is a functional connection between the motoneurons and myotubes. Myotubes that were successfully innervated by motoneurons, showed an elevated calcium response to glutamate stimulation. In the next series of experiments the effect of mutant SOD1 in motoneurons co-cultured with myotubes was assessed, following stimulation with glutamate in both motoneurons and myotubes co-cultures of either genotype of both cell types.

Therefore in these experiments following stimulation with glutamate the response of motoneuron of either genotype and myotubes of either genotype in culture were examined. Motoneurons (10DIV) and myotubes (16DIV) co-cultures were loaded with the high affinity cytosolic calcium dye Fluo-4 AM. Motoneurons were identified by their morphological appearance, characteristically a large cell body diameter >20μm, pyramidal shape and extensive dentritic arborisation. Calcium homeostasis has previously been shown to be perturbed in $SOD1^{G93A}$ motoneurons (Kruman et al., 1999). In these experiments the calcium response following stimulation with glutamate was assessed in the $SOD1^{G93A}$ motoneurons in the co-cultures, to identify any altered calcium response.

Following exposure to glutamate (5μM) and there was a marked increase in the intensity of the fluorescent cytosolic calcium indicator Fluo-4 AM in motoneurons as shown in **Fig 3.18 (A)**. The change in fluorescence in the cell soma was measured as a function of time.

The peak amplitude of response was significantly greater in $SOD1^{G93A}$ motoneurons compared to WT motoneurons, cultured with either $SOD1^{G93A}$ or WT myotubes. The results are summarised in **Fig. 3.19 (A)**. The mean peak amplitude in motoneurons exposed to glutamate was 10.5 a.u ± 0.82 (n=9) in SODmnSODm and 9.6 a.u ± 1.92

(n=2) in SODmnWTm. The calcium response was decreased in WTmnSODm to 5.6 a.u ± 0.6 (n=3) and 4 a.u ± 0.3 (n=5) in WTmnWTm. The calcium in response to glutamate was significantly increased by 162% in SODmnSODm compared to WTmnWTm ($P \leq 0.003$). In addition, following exposure to glutamate, there was a significant increase (87%) in calcium response in motoneurons in SODmnSODm compared to WTmnSODm ($P \leq 0.016$).

There was an increase in calcium observed in some but not all myotubes in response to glutamate stimulation, suggesting that at least some motoneurons were innervated the myotubes. The results are summarised in **Fig. 3.19 (B)**. There was no significant difference in the peak amplitude in myotube responses to glutamate stimulation in WTmnWTm 4.24 a.u ± 0.5 (n=7) and SODmnSODm 4.9 a.u ± 0.3 (n=7). However in co-cultures of SODmnWTm co-cultured, there was an increase 39% in the peak amplitude in response to glutamate compared to WTmnWTm. The peak amplitude in SODmnWTm was 5.9 a.u ± 0.25 (n=3). The difference in the mean values of SODmnWTm and SODmnSODm is not great enough to reject the possibility that the difference is due to random sampling variability. There is not a statistically significant difference between SODmnWTm and SODmnSODm ($P = 0.117$).

These results suggest that the presence of expression of SOD in motoneurons increases the amplitude of calcium response specifically in WT myotubes.

Figure 3.18 Increase in the cytosolic calcium in co-cultures following stimulation with glutamate

The motoneuron and myotube co-cultures were loaded with the high affinity cytosolic calcium dye Fluo-4AM. The co-cultures were exposed to glutamate (5μM) resulting in a marked increase in the fluorescence intensity of the cytosolic calcium indicator Fluo-4 AM, in the motoneurons. The motoneuron in **(A)** shows an elevation in Fluo-4 AM fluorescence intensity over time following stimulation with glutamate **(B)**. The Fluo-4 AM fluorescence intensity following stimulation was elevated, and regions of interest were drawn over the motoneuron cell body and myotubes. An example of a typical trace of the fluorescence intensity over time in motoneurons and myotubes is shown **(C)**.

(Scale bar = 20μm, sec= seconds)

FIGURE 3.18

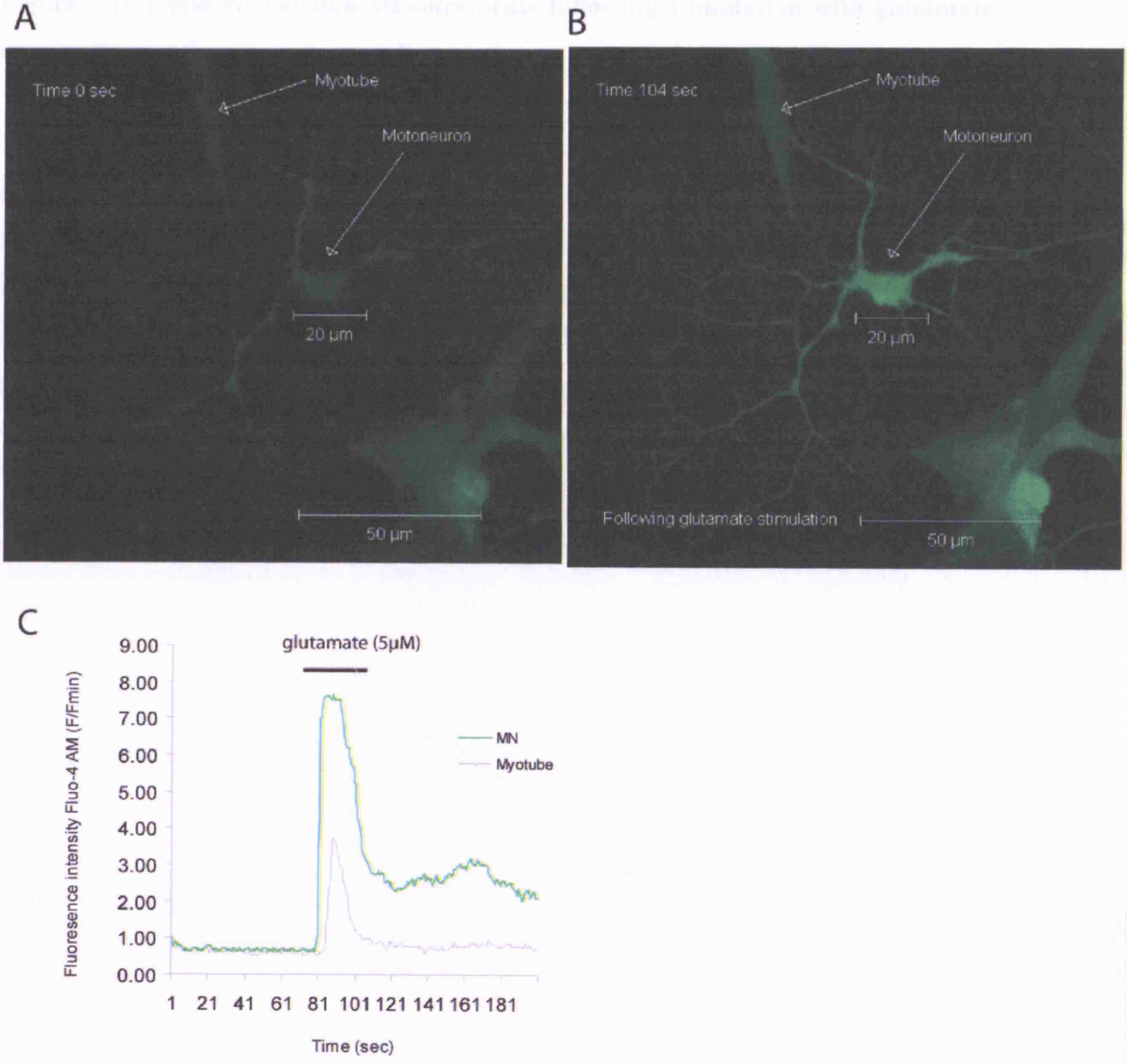
A
Time 0 sec
Myotube
Motoneuron
20 µm
50 µm
B
Time 104 sec
Myotube
Motoneuron
20 µm
Following glutamate stimulation
50 µm
C
glutamate (5µM)
MN
Myotube
Fluoresence intensity Fluo-4 AM (F/Fmin)
9.00
8.00
7.00
6.00
5.00
4.00
3.00
2.00
1.00
0.00
1 21 41 61 81 101 121 141 161 181
Time (sec)

Figure 3.19 Cytosolic calcium measurements following stimulation with glutamate in co-cultures of motoneurons and myotubes

The co-cultures were loaded with the high affinity cytosolic calcium dye Fluo-4 AM and exposed to glutamate (5μM). Glutamate simulation resulted in a marked increase in the fluorescence intensity of the cytosolic calcium indicator Fluo-4 AM. The increase in fluorescence intensity was assessed by measuring the peak amplitude of the calcium response. The bar chart summarises the mean peak amplitude of calcium in response to glutamate stimulation in motoneurons (A) and in myotubes (B). The peak amplitude was significantly increased in $SOD1^{G93A}$ motoneurons cultured with either $SOD1^{G93A}$ or WT myotubes.

(Error bars = standard error of the mean,* P≤0.003, **P≤0.016, ***P≤0.033)

FIGURE 3.19

A

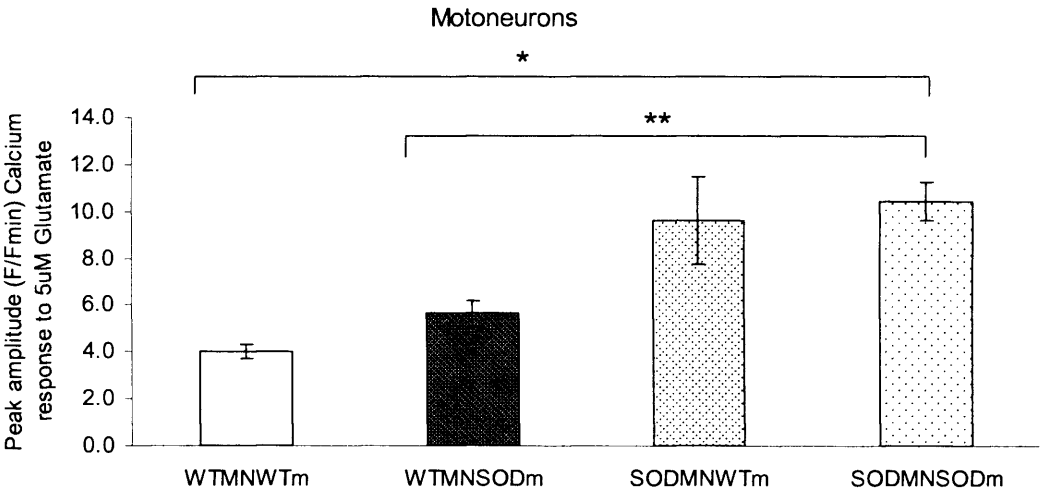

B

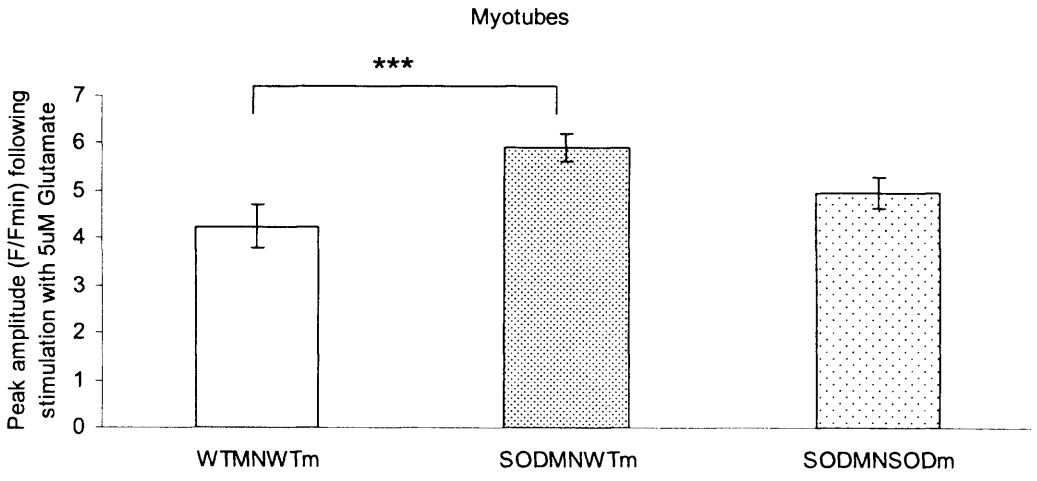

3.3 DISCUSSION

The experiments described in this chapter examined the effect of mutant SOD1 expression in myotubes on mitochondrial function and calcium signalling. In addition in order to examine the effect of motoneurons on the cellular properties of muscles, an *in vitro* co-culture system was established. The results show that expression of mutant SOD1 in myotubes and motoneurons has a profound effect on cellular function. In primary myotube cultures and co-cultures, there was evidence of mutant SOD1 induced calcium dysregulation and mitochondrial dysfunction.

3.3.1 The expression of SOD1^{G93A} disrupts mitochondrial function in myotubes

Measurements of mitochondrial function were assessed in primary myotube cultures $\Delta\Psi_m$ was assessed using the potentiometric indicator TMRM, to determine any changes in resting $\Delta\Psi_m$ induced by SOD1^{G93A} myotubes. In SOD1^{G93A} myotubes the mean $\Delta\Psi_m$ was significantly decreased compared to WT myotubes. These results suggest that expression of SOD1^{G93A} disrupts mitochondrial function in myotubes even during a very early stage of development, prior to onset of any symptoms.

In the primary myotube cultures, residual fibroblasts were also present in the culture preparations alongside the myotubes. Therefore the resting $\Delta\Psi_m$ of fibroblasts was also measured simultaneously with the myotubes. Measurements of mitochondrial function in fibroblasts allowed a different cell type that is not known to be involved in ALS pathogenesis to be examined. Interestingly, the $\Delta\Psi_m$ of SOD1^{G93A} fibroblasts was also significantly reduced compared to WT fibroblasts. These results therefore show that the reduction in $\Delta\Psi_m$ is not exclusive to muscles and occurs in other cell types that express mutant SOD1. These findings support the possibility that the mutant SOD1-mediated toxicity affects other neighbouring non-neuronal cells and is not exclusive to motoneurons. The consequence of SOD1-induced disruption in $\Delta\Psi_m$ in fibroblasts is unclear.

The mechanisms by which mutant SOD1 induces a decrease in $\Delta\Psi_m$ in myotubes and fibroblasts is unclear. However $\Delta\Psi_m$ was more reduced in myotubes than the fibroblasts, which may imply a selective vulnerability in the $\Delta\Psi_m$ between the different cell types. A decrease in $\Delta\Psi_m$ may arise through various mechanisms, for example inhibition of respiration, reduced substrate availability, or leaky mitochondria due to mitochondrial uncoupling. All these mechanisms would act to dissipate $\Delta\Psi_m$.

Further measurements of mitochondrial function in myotubes showed that expression of $SOD1^{G93A}$ in myotubes was associated with a more reduced redox state, compared to WT myotubes. The altered redox state may be due to either an increased availability of mitochondrial substrates or to a reduced rate of oxidation by the respiratory chain, which would result in an increase in the ratio of NADH to NAD+, therefore shifting the balance of the pyridine nucleotide pool towards a reduced state. The combination of a reduced $\Delta\Psi$m and a more reduced redox state, suggest that in $SOD1^{G93A}$ myotubes mitochondrial respiration is inhibited, since the maintenance of the $\Delta\Psi$m is dependent on the respiratory rate. Thus $SOD1^{G93A}$ induced mitochondrial dysfunction in myotubes is an early feature of SOD1-induced ALS pathogenesis that is present even at an early stage in development. These results also show that mitochondrial dysfunction in $SOD1^{G93A}$ myotubes can occur even in the absence of motoneuron contact with myotubes. Expression of mutant SOD1 enzyme in myotubes may heighten or predispose motoneurons to mitochondrial dysfunction, once functional contact is made with myotubes.

Previous studies have also shown mitochondrial dysfunction in $SOD1^{G93A}$ muscle at a presymptomatic stage. For example uncoupling protein 3 (UCP3) mRNA is up-regulated at 75 days of age (Dupuis et al., 2003). Consistent with mitochondrial uncoupling, reductions in respiratory control ratio and reduced ATP levels have also been identified in mutant SOD1 muscle at 90 days of age (Dupuis et al., 2003). The findings were also supported by imaging NADH autofluorescence in muscle from ALS patients, which found an elevated redox state in the mitochondrial NAD system and identified a deficiency of complex I electron transport chain (Wiedemann et al., 1998). These studies

support the results presented in this study which show that expression of $SOD1^{G93A}$ disrupts mitochondrial function in myotubes Previous studies have also reported further changes in mitochondrial electron chain, in particular involving complex I and IV in ALS patients, SOD1G93A mice and neuronal cell lines (Kirkinezos et al., 2005; Higgins et al., 2002; Jung et al., 2002; Mattiazzi et al., 2002; Menzies et al., 2002; Vielhaber et al., 2000).

3.3.2 The expression of $SOD1^{G93A}$ disrupts mitochondrial function in motoneurons and myotubes in co-cultures

The expression of mutant SOD1 in both motoneurons and myotubes in co-culture resulted in decrease in $\Delta\Psi_m$ in both cell types under basal conditions. In SODmnSODm co-cultures there was a significant decrease of $\Delta\Psi_m$ in myotubes and in motoneurons compared to WTmnWTm co-cultures. However the decrease in the $\Delta\Psi_m$ in motoneurons was greater than the decrease in the $\Delta\Psi_m$ in myotubes.

Interestingly the expression of $SOD1^{G93A}$ in myotubes cultured in the absence of motoneurons resulted in a greater reduction in $\Delta\Psi_m$ than in $SOD1^{G93A}$ myotubes in co-culture with $SOD1^{G93A}$ motoneurons. These results suggest that motoneurons influence mitochondrial function of $SOD1^{G93A}$ myotubes. The change in $\Delta\Psi_m$ in $SOD1^{G93A}$ myotubes may reflect an activity dependent change, so that the $\Delta\Psi_m$ is increased when contact between myotubes and motoneurons are made. Therefore, myotubes are more susceptible to a reduction in $\Delta\Psi_m$ in the absence of motoneurons.

The reduction in $\Delta\Psi_m$ in motoneurons in co-cultures revealed that the expression of mutant SOD1 disrupts $\Delta\Psi_m$ of motoneurons to a greater extent than SOD1 myotubes. This reduction in $\Delta\Psi_m$ shown in motoneurons may at least in part be responsible for the mitochondrial dysfunction observed in motoneurons in the pathogenesis of ALS.

These findings are in agreement with previous studies, where mutant SOD1 expression resulted in depolarisation of the $\Delta\Psi$m under basal conditions in motoneurons in vitro (Carri et al., 1997; Kruman et al., 1999; Rizzardini et al., 2005). These previous findings

together with those presented in this chapter, suggest that perturbations in $\Delta\Psi m$ may underlie a selective vulnerability to cellular stress in motoneurons in ALS. Furthermore the depolarisation of $\Delta\Psi m$ in motoneurons is further exacerbated by co-culturing motoneurons with $SOD1^{G93A}$ myotubes. Therefore mitochondrial dysfunction in myotubes results in even greater mitochondrial dysfunction in motoneurons.

3.3.3 Spontaneous cytosolic calcium activity in myotubes

After 3-4 days *in vitro* the myotube cultures exhibited widespread spontaneous contractions which were sustained for over 12-14 days in culture. Spontaneous contractile activity in skeletal muscle is crucial for *in vitro* myogenesis, in particular for the assembly and maintenance of the sarcomeres and the transition between myosin isoforms (Torgan and Daniels, 2001). Previous studies using rodent primary myotube cultures have shown that spontaneous contractions can be prevented by treatment with the voltage-gated Na^+ channel blocker, tetrodotoxin (TTX) (Daniels et al., 2000; Zhou et al., 2006; Torgan and Daniels, 2001). In this study presented TTX was not used and the myotubes remained spontaneously active in culture throughout the experiments. The spontaneous contractions were associated with propagating calcium transients in the myotubes.

The results from this study show that there was an increased frequency of cytosolic Ca^{2+} transients in $SOD1^{G93A}$ myotubes compared to WT myotubes. This may reflect an increased excitability of the muscle plasma membrane in $SOD1^{G93A}$ myotubes. Interestingly, the increased frequency of Ca^{2+} transients was not observed in wild type human SOD overexpressing myotubes which suggests that it is specific to the expression of mutant SOD1 rather than over-expression of the SOD1 protein it self.

3.3.4 Propagation velocity of spontaneous cytosolic calcium transients is increased in myotubes expressing mutant SOD1

The increased frequency of spontaneous cytosolic Ca^{2+} transients in the $SOD1^{G93A}$ myotubes was accompanied by an increased rate of propagation of the cytosolic Ca^{2+} transients. There was a significant increase in rate of propagation of the cytosolic Ca^{2+}

transients in SOD1^{G93A} myotubes, which may result from the decreased $\Delta\Psi_m$. Mitochondrial calcium uptake acts as a spatial buffering system that can limit the spread of a calcium signal through the cell (Boitier et al., 1999). As mitochondrial Ca^{2+} uptake is dependent on $\Delta\Psi_m$, a decreased $\Delta\Psi_m$ will reduce mitochondrial Ca^{2+} uptake, reduce calcium buffering and so increase the rate of propagation of Ca^{2+} waves (Boitier et al., 1999). Taken together, these results suggest that mitochondrial Ca^{2+} uptake may be impaired in SOD1^{G93A} myotubes as a result of decreased $\Delta\Psi_m$.

In the SOD1^{G93A} myotubes, the mean velocity of propagation Ca^{2+} transients was 35.4 μm/s ± 2. This value is comparable to the propagation velocity of caffeine-induced cytosolic Ca^{2+} waves in a muscle cell-line culture where the velocity was 35 μm/s (Flucher and Andrews, 1993). Furthermore, in cortical astrocytes, the mean propagation velocity was 36 μm/s (Boitier et al., 1999), which is also comparable to the mean value obtained SOD1^{G93A} myotubes. The increased rate of propagation of the cytosolic Ca^{2+} transients was not observed in either WT human SOD1 overexpressing myotubes or WT myotubes, which indicates that it is specific effect of the expression of mutant SOD1.

3.3.6 Caffeine-induced increases of cytosolic calcium in myotube cultures

The response of myotubes to calcium-induced calcium release from sarcoplasmic reticulum was examined by stimulating the myotubes with caffeine. This results in an increase in cytosolic calcium, and increased frequency of cytosolic calcium transients in the myotubes. Although no difference in the frequency of cytosolic calcium transients was found between SOD1^{G93A} myotubes and WT myotubes. Interestingly there was increased caffeine-induced calcium transient amplitude value in the WT (Figure 3.16 A) compared to baseline (Figure 3.12 A), but not in the SOD1^{G93A} myotubes. However upon stimulation with caffeine SOD1^{G93A} myotubes were shown to have reduced amplitude compared to WT myotubes. There appears to be a clear difference in these caffeine-induced amplitude results. This may suggest that there is an altered calcium release mechanisms in SOD1^{G93A} myotubes from internal stores which in not evident in the WT myotubes, however further experiments are required to investigate the calcium release mechanism. By using antagonists of intracellular calcium stores, such as

Thapsigarin and depleting external calcium (calcium free recording medium), it is possible to identify other possible calcium release mechanisms, which may also contribute to calcium release. To improve this particular experiment, measuring the basal cytosolic calcium levels prior to stimulating with caffeine, would give a better indication of the relative effect of caffeine on the amplitude in each genotype of the myotubes.

3.3.7 Elevated intracellular calcium levels in co-cultures following stimulation with glutamate

To determine whether motoneurons were able to successfully innervate myotubes, intracellular Ca^{2+} levels were measured in the motoneurons and myotubes following stimulation with glutamate (5μM) since myotubes show no intrinsic sensitivity to glutamate and can therefore only be excited by glutamate via innervating motoneurons. The results showed that Ca^{2+} levels rose in some but not all myotubes. There was no difference in the peak Ca^{2+} amplitude in myotubes in response to glutamate in WTmnWTm compared to SODmnSODm. However in SODmnWTm co-cultures, the amplitude of the $[Ca^{2+}]_c$ response in myotubes following stimulation with glutamate, was significantly increased compared to WTmnWTm. These results suggest that expressing mutant SOD1 in motoneurons increased the Ca^{2+} amplitude to the greatest extent in WT myotubes. There may therefore be an increased vulnerability to mutant SOD1 in WT myotubes when innervated by SOD1 motoneurons, which does not occur when SODmnSODm are co-cultured. The exact cause for this vulnerability in WT myotubes when innervated by SOD1 motoneurons is unclear.

Ca^{2+} levels were also measured in motoneurons following stimulation with glutamate which showed a marked increase in the amplitude of intracellular Ca^{2+} levels. The peak amplitude of the Ca^{2+} response was significantly greater in $SOD1^{G93A}$ motoneurons compared to WT motoneurons in co-culture co-cultured with myotubes of either genotype. The Ca^{2+} response in motoneurons to glutamate stimulation was significantly greater in SODmnSODm compared to WTmnWTm co-cultures.

In the peak amplitude in SOD motoneurons in co-culture with WT myotubes is not statistically different (P = 0.095) from WTmnWTm, as the difference in the median values between the two groups is not great enough to exclude the possibility that the difference is due to random sampling variability. The sample size of SODmnWTm is very small (n=2) therefore more experiments need to be carried out to determine any significant difference between the two groups.

These experiments provide evidence that there is an increased intracellular Ca^{2+} response in mutant SOD1-expressing motoneurons following exposure to glutamate. This may therefore suggest that there is a disruption in intracellular Ca^{2+} homeostasis in SOD1 motoneurons. Previous reports have also shown in $SOD1^{G93A}$ motoneurons an elevated intracellular response to glutamate (Kruman et al., 1999). High concentrations of glutamate are known to cause neuronal cell death predominantly as a result of excessive inflow of Ca^{2+} through NMDA channels. Motoneuron susceptibility to glutamate may also be exacerbated by a reduction in expression of Ca^{2+} binding proteins (Ince et al., 1993; Alexianu et al., 1994a) accompanied by a low Ca^{2+} buffering capacity of mitochondria (Damiano et al., 2006)

The findings outlined in this experiment are in agreement with the data on elevated intracellular Ca^{2+} response to glutamate reported by Kruman et al (1999), in which glutamate stimulation induced a larger peak Ca^{2+} amplitude. Elevated intracellular Ca^{2+} was also associated with a decreased $\Delta\Psi_m$ in $SOD1^{G93A}$ motoneurons (Kruman et al., 1999). It follows that a disruption in mitochondrial function may therefore influence the intracellular Ca^{2+} signalling (Jacobson and Duchen, 2004).

3.3.8 Mitochondria and local calcium signalling

Electron microscopy studies have shown that skeletal muscle is densely packed with mitochondria which are in close proximity to the sarcoplasmic reticulum (SR) (Ogata and Yamasaki, 1985). Mitochondria may therefore play an important role in regulating

intracellular signals in skeletal muscle and muscle contraction. There is accumulating evidence for the importance of mitochondrial Ca^{2+} uptake during the contraction and relaxation cycle in mammalian skeletal muscle (Bruton et al., 2003; Rudolf et al., 2004). During muscle contraction *in vivo*, mitochondria have been shown to be able to sequester and rapidly release Ca^{2+} during relaxation in mammalian skeletal muscle under physiological conditions (Rudolf et al., 2004). The uptake of mitochondrial Ca^{2+} is mediated by the uniporter (Nicholls and Crompton, 1980), and is driven by the potential difference that exists across the mitochondrial membrane (Babcock and Hille, 1998). Under physiological conditions, the Ca^{2+} uniporter has been shown to shape intracellular calcium signalling' in various cells (Babcock and Hille, 1998; Duchen, 1999; Rizzuto et al., 2000).

There are alternative mechanisms by which mitochondria can influence intracellular homeostasis, for example through ATP synthesis, accumulation of Ca^{2+}, generation of superoxide radicals, disruption of mitochondrial function due to the collapse of the mitochondrial membrane potential, of which can alter the pattern of intracellular Ca^{2+} signalling.

The disruption of mitochondrial Ca^{2+} uptake may promote spontaneous Ca^{2+} release in skeletal muscle. Inhibition of the mitochondrial Ca^{2+} uniporter with Ru360 and pharmacological uncoupling agents (FCCP) act to dissipate $\Delta\Psi_m$ and attenuate mitochondrial Ca^{2+} uptake, resulting in an increase the frequency of Ca^{2+} sparks (spontaneous Ca^{2+} transients) in permeabilized skeletal muscle fibres (Isaeva and Shirokova, 2003). Pharmacological agents which disrupt mitochondrial Ca^{2+} uptake were also shown to promote Ca^{2+} release back into the cytosol (Montero et al., 2001). Mitochondria may therefore normally act to suppress spontaneous Ca^{2+} transients by buffering intracellular Ca^{2+} near Ca^{2+} release sites (Isaeva and Shirokova, 2003).

The results from this study support the existing evidence which suggests that skeletal muscle may be involved in the pathogenesis of ALS. Expression of mutant SOD1 in myotubes was found to alter cellular function, including both calcium signalling and

mitochondrial function. However a recent study showed that the specific knockdown of mutant SOD1 specifically in muscle using siRNA has no affect on disease onset or progression (Miller et al., 2006). This finding suggests that muscle alone is not the primary target for SOD1 mutant mediated disease. Therefore it is possible that the impairments in cellular function in SOD1 muscle reported in this study may not be primary cause for the pathogenesis of ALS, but rather a contributing factor. It is likely that early metabolic dysfunction in skeletal muscle may play a role in the progression of the disease in vulnerable motoneurons.

3.3.9 Futher Research

It appears from these results that the expression of mutant SOD in myotubes is able to induce a reduction in $\Delta\Psi_m$ in co-cultured motoneurons. Due to the small sample size of cells examined, it is uncertain to whether these findings are typical of all motoneurons. By increasing the sample size of this experiment, a more representative interpretation of the findings could be made. In this study it was not possible to measure the redox state in motoneurons co-cultured with myotubes due a shortage of time. It would be of interest to measure the mitochondrial redox state in the co-cultures and examine the effect of expression of mutant SOD in myotubes on co-cultured motoneurons. As a consequence of mitochondrial dysfunction and an inhibition of respiration there is a reduction in ATP generation. It would be of interest to measure ATP levels in the motoneuron and myotube co-cultures using a luciferase/luciferin-based approach.

Calcium overload may account for the mitochondrial dysfunction observed in motoneurons; therefore it would be of interest to measure mitochondrial calcium in the motoneuron and myotube co-cultures. Using rhod 5N-AM ester, a cationic calcium indicator, the rhod 5N-AM accumulates in mitochondria in response to $\Delta\Psi_m$. A higher resting level of mitochondrial calcium may be the result of a high resting cytosolic calcium level or increased mitochondrial calcium signaling. To examine this, co-cultures could be loaded with indo-1 AM, a high affinity, ratiometric calcium indicator and resting cytosolic calcium level in motoneurons and myotubes could be measured.

3.4 CONCLUSION

The experiments presented in this chapter show that expression of mutant SOD1 results in a deficit in cellular function in mitochondria and calcium handling in presymptomatic skeletal muscle. Expression of mutant SOD1 in myotubes resulted in:

- A decrease in mitochondrial membrane potential, accompanied by an reduced redox state – consistent with a defect in mitochondrial respiration
- Increased frequency and rate of propagation of cytosolic Ca^{2+} transients, which may reflect and heighten excitability in the muscle membrane and/or a deficit in mitochondrial Ca^{2+} uptake

Expression of mutant SOD1 in embryonic motoneurons in co-cultures with primary myotubes irrespective of genotype thus results in:

- A decrease in mitochondrial membrane potential, consistent with a defect in mitochondrial respiration
- An increased amplitude of Ca^{2+} in innervated myotubes
- An increased amplitude of Ca^{2+} transients in motoneurons in response to glutamate stimulation

The findings outlined in this chapter thus provide evidence for the involvement of mitochondrial dysfunction and aberrant calcium handling arising from the expression of the mutant SOD1 enzyme, in motoneurons and muscles at an early stage in development prior to the manifestation of a pathological state.

Chapter 4

The effect of treatment with Mechano-growth factor (MGF), an IGF-I splice variant, in mouse model of Amyotrophic Lateral Sclerosis

4.1 INTRODUCTION

Neurons are known to be dependent on neurotrophic factors for their development and survival (Oppenheim, 1991). The therapeutic potential of several neurotrophic factors has been examined in models of ALS and the most promising results have been obtained following treatment of $SOD1^{G93A}$ mice with IGF-I (Kaspar et al., 2003; Kaspar et al., 2005; Dobrowolny et al., 2005; Nagano et al., 2005; Narai et al., 2005). The expression of IGF-I is highly regulated, including gene transcription, splicing and translation. In this chapter, the effect of treatment with a muscle-derived growth factor called mechano-growth factor (MGF), a splice variant of insulin-like growth factor (IGF-I), was assessed in $SOD1^{G93A}$ mice. Alternative isoforms of IGF-I have different functional roles (Yang and Goldspink, 2002; Aperghis et al., 2004; Ates et al., 2007), therefore a direct comparison of treatment with IGF-I and MGF in $SOD1^{G93A}$ mice was made to determine the most effective isoform in ameliorating the disease progression in $SOD1^{G93A}$ mice.

4.1.1 Neurotrophic factors as potential therapeutic agents for ALS

Motoneuron survival is subject to retrograde trophic influence derived from target muscle. The pioneering studies of Victor Hamburger and Rita Levi-Montalcini (Hamburger V and Levi-Montalcini R, 1949) recognised that target tissue mass is related proportionally to motoneuron survival during normal programmed cell death. Studies by Levi-Montalcini in the 1960s later identified the first neurotrophic factor, nerve growth factor (NGF) as crucial for the survival of sympathetic and sensory neurons. The discovery of NGF prompted the search for other neurotrophic factors. Several studies have shown that neurotrophic factors can protect motoneurons from injury-induced cell death during postnatal development (Hughes et al., 1993; Li et al., 1994; Ikeda et al., 1996; Koliatsos et al., 1993; Koliatsos et al., 1994; Sendtner et al., 1990; Sendtner et al., 1992; Tan et al., 1996; Vejsada et al., 1995; Yan et al., 1992; Baumgartner and Shine, 1998). Furthermore GDNF and BDNF were also shown to promote survival of motoneurons in the adult animals following ventral root avulsion (Novikov et al., 1995; Novikov et al., 1997). These initial studies in the mid 1990's were promising, showing neurotrophic factors were capable of preventing the degeneration of motoneurons,

however the beneficial effects were only shown to be effective in the short term. The experimental animal studies, lead to the initiation of clinical trials of subcutaneous recombinant neurotrophic factors (refer to Table 4.1) in ALS patients that failed to show any benefit. The failure of neurotrophic factors in the clinical trials may be due to the short plasma half-life of the recombinant proteins or poor delivery of neurotrophic factors to motoneurons. To overcome the inadequate delivery to motoneurons, and sustain levels of the neurotrophic factors, gene-therapy approaches have been investigated.

TABLE 4.1 Early clinical trials of neurotrophic factors

Neurotrophic factor	Delivery	Outcome	References
BDNF	Subcutaneous	Negative	BDNF study group* (1999)
IGF-I	Subcutaneous	Beneficial	(Lai et al., 1997)
IGF-I	Subcutaneous	Negative	(Borasio et al., 1998)
CNTF	Subcutaneous	Negative	CNTF study group ** (1996)
			(Miller et al., 1996)
CNTF	Intrathecal	Negative	(Aebischer et al., 1996)

Early clinical trials of neurotrophic factors in ALS patients failed to show conclusive evidence of therapeutic potential. The delivery method predominately used was subcutaneous however intrathecal delivery was also tested without success. (BDNF= Brain-derived neurotrophic factor, CNTF= Ciliary neurotrophic factor, IGF-I= Insulin-like growth factor)

* (1999) A controlled trial of recombinant methionyl human BDNF in ALS: The BDNF Study Group (Phase III). Neurology 52:1427-1433. (no authors listed), **(1996) A double-blind placebo-controlled clinical trial of subcutaneous recombinant human ciliary neurotrophic factor (rHCNTF) in amyotrophic lateral sclerosis. ALS CNTF Treatment Study Group. Neurology 46:1244-1249. (no authors listed)

4.1.2 The neuroprotective effects of IGF-I in ALS

Several studies have reported the beneficial effects of IGF-I treatment in the $SOD1^{G93A}$ mice (Kaspar et al., 2003; Kaspar et al., 2005; Dobrowolny et al., 2005; Nagano et al., 2005; Narai et al., 2005). The most promising results to date have been obtained following viral delivery of IGF-I to skeletal muscle in $SOD1^{G93A}$ mice. In $SOD1^{G93A}$ mice treatment with IGF-I results in a delay in disease progression and a significant extension in lifespan (Kaspar et al., 2003). However, delivery of IGF-I AAV virus to skeletal muscle resulted in only ~1% of the virus being retrogradely transported to the motoneurons. It is therefore possible that the beneficial effects of IGF-I arose predominately from local expression of IGF-I in the muscle of the $SOD1^{G93A}$ mice (Kaspar et al., 2003) with only a modest effect of IGF-I in to motoneurons within the spinal cord. Muscle performance and endurance may also play an important feature in ameliorating the disease progression in $SOD1^{G93A}$ mice. This is supported by the finding that IGF-I treatment combined with moderate exercise, dramatically enhances the neuroprotective effect of IGF-I in $SOD1^{G93A}$ mice, with a 69% increase in lifespan (Kaspar et al., 2005). However there is considerable debate as to the involvement of exercise in the pathogenesis of ALS. For example there is evidence to show that high intensity endurance exercise in fact hastens disease progression in male $SOD1^{G93A}$ mice (Mahoney et al., 2004), although other lines of research indicate that exercise may in fact be beneficial (Bello-Haas et al., 2007). Exercise and physical activity has been shown to increase serum IGF-I and provide neuroprotection in other neurodegenerative diseases (Kirkinezos et al., 2003; Carro et al., 2001; Veldink et al., 2003; van Dellen et al., 2000; Lee et al., 2004).

The beneficial effects of IGF-I may in part depend on the direct delivery of IGF-I to spinal motoneurons. The continuous infusion of recombinant human IGF-I into the spinal cord, directly into the intrathecal space in $SOD1^{G93A}$ mice, delayed the disease progression, increased motoneuron survival and extended the lifespan by 11%, using a high dose IGF-I (1mg/kg body weight per day) (Nagano et al., 2005). The neuroprotective effects IGF-I were accompanied by increased expression levels of several signalling cascades including phosphorylated-Akt and ERK, therefore suggesting

that IGF-I treatment promoted cell survival, via the MEK/ERK and PI3/AKT signalling pathways (Nagano et al., 2005). In $SOD1^{G93A}$ mice treated with IGF-I, the IGF-I signalling transduction system was further examined, in particular the IGF-IRβ (IGF-I receptor β subunit) and the intracellular downstream protein IRS-I (Insulin receptor substrate protein I). Decreased IGF-IRβ and IRS-I expression levels were identified following IGF-I treatment in $SOD1^{G93A}$ mice (Narai et al., 2005). This may be explained by an increased availability of free IGF-I, which would down-regulate IGF-IR levels (Narai et al., 2005). This study revealed that treatment with IGF-I in $SOD1^{G93A}$ mice involved the signal transduction pathway via the IGF-IR and downstream signalling protein IRS-I.

The muscle restricted expression of IGF-I has also been shown to have beneficial effects in $SOD1^{G93A}$ mice. In double transgenic $SOD1^{G93A}$ mice, with muscle restricted expression of the class 1 isoform (IGF-IEa), disease progression was significantly ameliorated (Dobrowolny et al., 2005). The results from this study showed attenuated muscle atrophy, maintenance of neuromuscular contact, increased survival of motoneurons and an extension in the lifespan of the $SOD1^{G93A}$/mIGF-I mice (Dobrowolny et al., 2005).

Thus there is considerable evidence to show the beneficial effects of IGF-I in $SOD1^{G93A}$ mice. However, this is in disagreement with a recently published study, where the sustained overexpression of IGF-I in either skeletal muscle or CNS in $SOD1^{G93A}$ mice failed to show any improvement in disease progression or lifespan (Messi et al., 2007). This discrepancy may arise from the difference in IGF-I administration. For example it is possible that exposure of IGF-I throughout development could alter receptor expression and down-regulate the actions of IGF-I. The mIGF-I/ $SOD1^{G93A}$ used by Dobrowolny et al., 2005, also expressed IGF-I throughout development, although a myosin light chain regulatory enhancer element was used, which might also explain the differences in the actions of IGF-I. The negative results of IGF-I (Messi et al., 2007) further strengthen the importance of carefully designing therapeutic strategies for

$SOD1^{G93A}$ mice and equally as importantly, choosing the appropriate approach for administrating IGF-I delivery.

In view of the positive findings with IGF-I in $SOD1^{G93A}$ mice, several clinical trials of IGF-I in have been initiated in ALS patients. However the clinical trials of subcutaneous administration of recombinant human IGF-I in ALS have led to conflicting results. A North American trial concluded that treatment with IGF-I delayed disease progression, as determined by the Appel ALS rating score (Lai et al., 1997). In contrast a European clinical trial found no significant effect of IGF-I (Borasio et al., 1998). The discrepancies of these two clinical trials may in part be due to differences in the trial design and/or ineffective delivery of IGF-I to the CNS. A third clinical trial of IGF-I is currently underway with ALS patients in North America and aims to finally establish whether IGF-I can delay the disease progression in patients with ALS.

The failure of the clinical trials may also be possibly related to the high concentrations of IGFBP, which sequester IGF-I and perhaps limit the trophic actions of IGF-I. In post-mortem studies from SALS patients, the concentration of free IGF-I in ventral horn homogenates was found to be decreased and there was an increase in IGFBP 2, 5 and 6 (Wilczak et al., 2003). Furthermore serum IGF-I and insulin levels were also shown to be decreased in ALS patients (Torres-Aleman et al., 1998). In ALS patients, serum concentration of IGF-I was found to be either normal or slightly decreased (Braunstein and Reviczky, 1987). The expression levels of IGF-I was found to be normal in spinal cords from ALS patients, however the expression of the receptor IGF-IR was increased (Adem et al., 1994). Therefore the levels of endogenous IGF-I, IGF-IR and IGF-I binding proteins change with disease progression in ALS patients. This evidence may support the application of IGF-I to promote neuronal survival and regulate altered IGF-I signalling in ALS patients.

4.1.3 MGF is a splice variant of IGF-I

Alternative splicing of messenger RNA (mRNA) allows several gene products with different functions to be produced from a single gene coding sequence. This form of

post-translational modification occurs in the IGF-I gene which can generate several spliced exons, with different combinations from the primary RNA transcripts. In rodent muscle there are two splice variants expressed, IGF-IEa which corresponds to the main systemic liver isoform of IGF-I and the IGF-Ib commonly known as mechano-growth factor (MGF). MGF was first identified and cloned in stretched adult rabbit tibialis anterior (TA) muscle, which was electrically stimulated, and immobilised by a plaster cast (Yang et al., 1996; Mckoy et al., 1999). There was a marked upregulation in expression of the two isoforms IGF-IEa and MGF (IGF-Ib) only in the stimulated muscle. The newly identified splice variant of IGF-I was termed 'mechano-growth factor', as the expression in muscle was induced following mechanical overload.

In response to mechanical stimulation, muscle injury or exercise, the IGF-I gene is initially spliced to MGF and then to the IGF-IEa splice variant (Hill and Goldspink, 2003). Structurally the IGF-I rodent gene has six exons, separated by five introns, as shown in **Figure 4.1**. Alternative splicing of the IGF-I gene to MGF results in a different 3' exon to the IGF-IEa (liver isoform) and this has a 52 base insert in rodents, in the E domain of exon 5. Therefore MGF has a different carboxy (C) terminal sequence than that of IGF-IEa.

4.1.4 MGF

Muscle is a post-mitotic tissue that requires an efficient local repair mechanism to respond to damage. MGF is thought to act as a local tissue repair factor and, following damage, MGF increases the pool of satellite cells (Ates et al., 2007) or muscle progenitor cells, facilitating repair and maintenance of this postmitotic tissue (Hill and Goldspink, 2003). Satellite cells are mulitpotent stem cells that reside in the periphery of muscle fibres between the basement membrane and the plasma membrane (Mauro A, 1961). Following activation they proliferate and fuse with the muscle fibres and initiate muscle regenerative pathways. In response to local muscle injury, up-regulation of MGF expression precedes the increase in expression of markers for activation of satellite cells as identified by M-Cad mRNA levels, indicating that MGF is involved in initiating satellite cell activation in muscle (Hill and Goldspink, 2003).

MGF has been shown to be functionally distinct from the IGF-IEa isoform, as MGF promotes rapid proliferation of myoblasts but inhibits terminal differentiation. In contrast, the systemic IGF-IEa isoform enhances terminal differentiation in the myoblasts of the C2C12 muscle cell line (Yang and Goldspink, 2002). MGF is also a potent inducer of muscle hypertrophy. Plasmid-based gene transfer was used to introduce MGF cDNA into muscle in normal and dystrophic mice, resulting in 20% increase in muscle weight and increase in muscle fibres size within 2 weeks of injection (Goldspink, 2001). Previously it has been shown that MGF mRNA expression is upregulated following high resistance exercise in young human subjects, but not in the elderly subjects (Hameed et al., 2003). In contrast to MGF, the IGFIa isoform mRNA showed no significant change with exercise. Therefore an attenuated expression of MGF may underlie the age related loss of muscle mass.

In addition to its ability to promote muscle repair, MGF has been shown to have neuroprotective effects in the CNS. Following facial nerve avulsion, intramuscular plasmid-based gene transfer was used to introduce MGF cDNA and thus rescued 88% of motoneurons that would otherwise die due to nerve avulsion. However treatment with IGF-Ia rescued only 37% of the injured facial motoneurons (Aperghis et al., 2004). In this model of acute motoneuron degeneration, MGF is therefore markedly more effective than IGF-Ia in rescuing motoneurons from cell death. MGF has also been shown to have a strong neuroprotective effects in other models of neuronal death (Aperghis et al., 2004). In a gerbil model of transient brain ischemia *in vivo* treatment with a synthetic MGF C-terminal peptide resulted in an increased survival of CA1 hippocampal neurons following an ischaemic insult (Dluzniewska et al, 2005). Moreover, ischaemia resulted in increased expression of endogenous MGF in the ischemia-resistant hippocampal neurons, suggesting that the endogenous MGF may have an important neuroprotective function. MGF has also been shown to protect neurons, *in vitro*, and in organotypic cultures MGF was found to rescue hippocampal neurons from oxidative stress and NMDA-excitotoxic insults (Dluzniewska et al, 2005).

Figure 4.1 Insulin-like growth factor gene (IGF-I) is alternatively spliced and forms distinct circulating and tissue specific isoforms

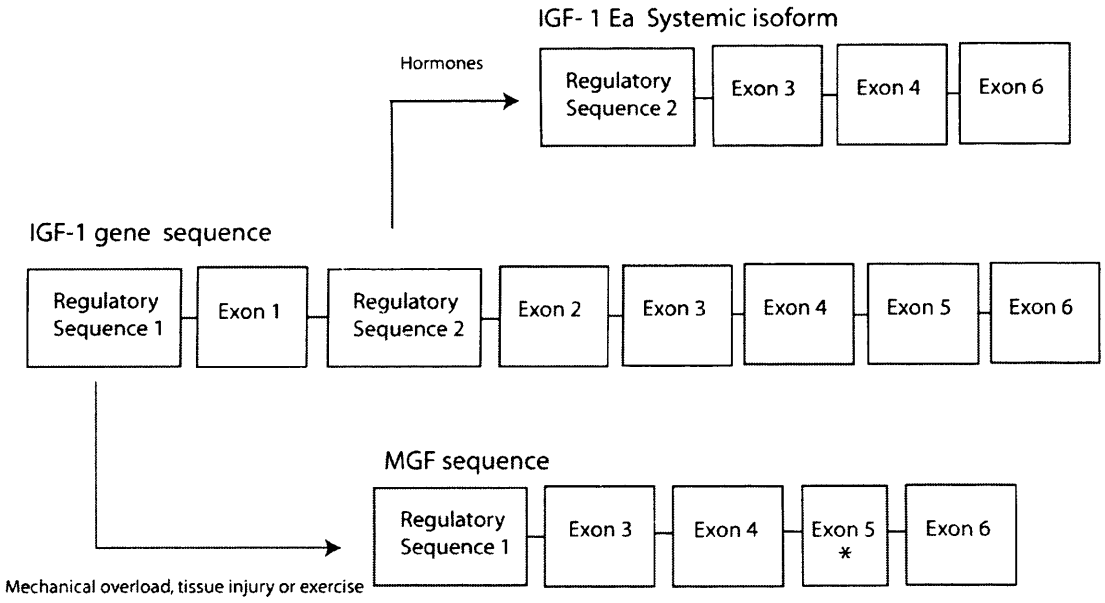

The rodent IGF-I gene contains six exons separated by five introns. Following mechanical overload, tissue injury or exercise the IGF-I gene is initially spliced to MGF, which has a 52 base pair insert in the E domain, which alters the reading frame, resulting in a different 3'sequence and carboxy peptide sequence. * 52 base pair insert in the E domain

4.1.5 Hypothesis to be tested

Amyotrophic lateral sclerosis is characterised by significant muscle atrophy accompanied by extensive degeneration of motoneurons. The muscle-derived growth factor MGF is known to protect neurons from a variety of insults and promote muscle repair and regeneration. In this study the effect of treatment with MGF is examined in the $SOD1^{G93A}$ mouse model of ALS. Since global administration of MGF plasmids to all muscles was not feasible, we determined the ability of MGF to improve function and rescue motoneurons of specific hindlimb muscles that we have previously shown to be severely affected in $SOD1^{G93A}$ mice (Sharp et al., 2005). In order to establish whether MGF was more effective than IGF-I in ameliorating disease in $SOD1^{G93A}$ mice a direct comparison of the effectiveness of IGF-I and MGF was made to evaluate which IGF-I isoform was the most effective and suitable for development of a therapy for ALS.

4.2 RESULTS

At 70 days of age randomly assigned male and female $SOD1^{G93A}$ mice and WT littermates were injected bilaterally with pcDNA3.1/NT vectors containing either the C-terminal cDNA sequence of MGF, full length IGF-I cDNA sequence, or vehicle control plasmid, into the tibialis anterior (TA), extensor digitorum longus (EDL), gastrocnemius and quadriceps muscles. The effect of treatment with MGF and IGF-I on disease progression, hind limb muscle function, and motoneuron survival were examined at 120 days of age in both $SOD1^{G93A}$ and WT mice.

4.2.1 Expression of MGF in skeletal muscle of $SOD1^{G93A}$ mice

Intramuscular injections of MGF cDNA pcDNA3.1/NT or vehicle plasmid were administered into the hindlimb muscle of $SOD1^{G93A}$ mice at 70 days of age. Plasmid driven expression of MGF was determined from muscle tissue and spinal cord protein homogenates at approximately 2 weeks post-injection. At ~ 84 days of age (2 weeks post- injection) the optimum level of plasmid driven expression MGF is expected to be achieved in the skeletal muscle (communication of Dr SY Yang). The results from the western blot analysis are shown in **Figure 4.2** from **(A)** TA muscle of vehicle treated $SOD1^{G93A}$ mice, **(B)** TA muscle of MGF treated $SOD1^{G93A}$ mice, **(C)** spinal cord of vehicle treated $SOD1^{G93A}$ mice and **(D)** spinal cord of MGF treated $SOD1^{G93A}$ mice. Western blot analysis of protein extracts showed increased levels of MGF expression only in MGF treated TA muscle. There were no elevated levels of MGF protein expression detected in spinal cord samples from MGF treated $SOD1^{G93A}$ mice.

Figure 4.2 Western blot analysis of the expression of MGF in TA muscle and spinal cord from MGF or vehicle treated SOD1^{G93A} mice

Representative western blot analysis of the expression of MGF in TA and spinal cord protein extracts from SOD1^{G93A} mice treated with either plasmid containing MGF cDNA sequence, or vehicle control plasmid. Protein homogenates were examined 2 weeks post-injected. The western blot analysis compared protein levels of MGF expression in **(A)** TA muscle of vehicle treated SOD1^{G93A} mice, **(B)** TA muscle of MGF treated SOD1^{G93A} mice, **(C)** spinal cord of vehicle treated SOD1^{G93A} mice and **(D)** spinal cord of MGF treated SOD1^{G93A} mice. There is a marked increase in MGF expression in TA muscle from MGF treated SOD1^{G93A} mice, there was no elevation of MGF expression in spinal cord. MGF Band ~25kDa and loading control used was actin.
(Minus symbol = vehicle treated SOD1^{G93A} mice and plus symbol = MGF treated SOD1^{G93A} mice)

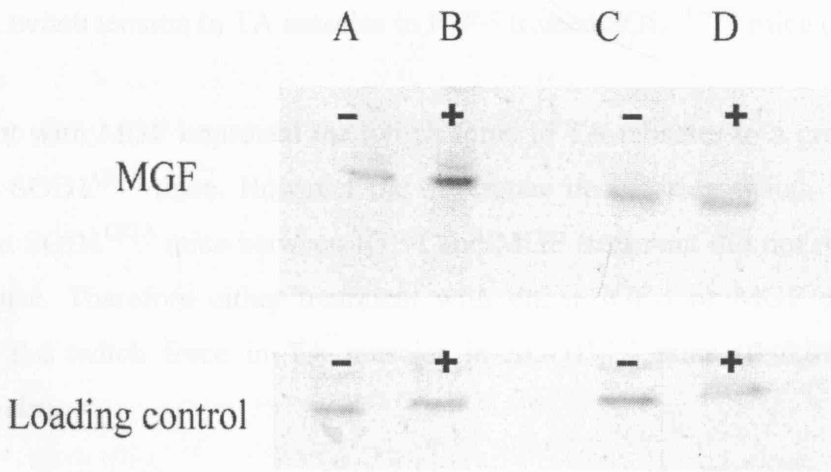

4.2.2 Isometric tension recordings

At 120 days of age $SOD1^{G93A}$ mice and WT mice were anaesthetized and prepared for in-vivo physiological recordings, to assess the hind limb twitch and tetanic muscle force in the TA and EDL muscles.

4.2.3 Maximum Twitch and Tetanic tension in TA muscle

Maximal twitch contractions were elicited by stimulation of the sciatic nerve, using square-wave pulses of 0.02 ms duration and supra-maximal intensity via silver wire electrodes. The results of the mean maximal twitch tension are summarized in the bar chart in **Figure 4.3(A)**. At 120 days of age, the vehicle treated $SOD1^{G93A}$ mice had significantly reduced twitch tension compared to WT littermates. In the TA muscles from WT mice the mean twitch force was 32g (± 2.9 n=9), whereas in $SOD1^{G93A}$ mice this was reduced to 7.06g (± 0.94 n=16). This represented a 77.9% reduction in maximal twitch tension in TA muscles compared with WT at 120 days of age. Treatment with MGF in $SOD1^{G93A}$ mice significantly improves the twitch force in TA muscles to 13.8 g (± 1.62 n=16), which represents a 95.5% increase in maximal twitch tension compared to vehicle treated $SOD1^{G93A}$ mice ($P \leq 0.001$). Whereas in IGF-I treated $SOD1^{G93A}$ mice the maximal twitch tension was 12.8g (± 1.5 n=14). This represented an 81% increase in maximal twitch tension in TA muscles in IGF-I treated $SOD1^{G93A}$ mice ($P \leq 0.010$).

Treatment with MGF improved the twitch force in TA muscles to a greater extent than IGF-I in $SOD1^{G93A}$ mice. However the difference in restoring twitch force of the TA muscle in $SOD1^{G93A}$ mice between IGF-I and MGF treatment did not reach statistically significance. Therefore either treatment with either IGF-I or MGF can significantly improve the twitch force in TA muscles in $SOD1^{G93A}$ mice ($P \leq 0.010$ and $P \leq 0.001$ respectively).

The maximal tetanic tension of TA muscle was determined next. Maximal tetanic contractions of TA muscles were elicited by trains of stimuli at increasing frequencies of 40, 80 and 100 Hz. The results are summarized in the bar chart in **Figure 4.3(B)**. In WT mice there was no significant difference found in the maximal tetanic tension between

WT mice treated with MGF or with control vehicle plasmid. At 120 days of age, the $SOD1^{G93A}$ mice treated with vehicle plasmid, had a significantly weaker tetanic tension 19.5g (± 2.2 n=16) compared 138g (±16.58 n=7) in the vehicle treated WT muscle. This represented an 85.9% reduction in the TA maximal tetanic tension compared with WT mice at 120 days of age. However treatment with MGF in $SOD1^{G93A}$ mice, significantly improved the muscle force to 38.1g (± 4.6 n=10) this represents a 95% improvement in muscle function compared to vehicle treated $SOD1^{G93A}$ mice ($P \leq 0.001$). The maximal tetanic tension in the TA muscles in IGF-I treated mice was 41.2g ± 6.75 n=14) ($P \leq 0.003$) thus treatment with IGF-I resulted in a 111% increase in the mean tetanic tension compared with vehicle treated $SOD1^{G93A}$ mice at 120 days of age.

The maximal tetanus tension in the TA muscle, in the IGF-I treated $SOD1^{G93A}$ mice was improved by 16% compared to the MGF treated $SOD1^{G93A}$ mice. However the difference in restoring tetanic force of the TA muscle in $SOD1^{G93A}$ mice between IGF-I and MGF treatment did not reach statistically significance. Therefore either treatment with either IGF-I or MGF can both significantly improve the tetanic force in TA muscles in $SOD1^{G93A}$ mice ($P \leq 0.003$ and $P \leq 0.001$ respectively).

4.2.4 Maximum Twitch and Tetanic tension in EDL muscle

The maximum twitch and tetanic tension in EDL muscle were assessed and examples of traces from EDL muscle of are shown in **Fig. 4.4** from vehicle treated WT mice, MGF treated WT mice, vehicle treated $SOD1^{G93A}$ mice, MGF treated $SOD1^{G93A}$ mice and IGF-I treated $SOD1^{G93A}$ mice, assessed at 120 days of age. The results of the mean maximal twitch tension are summarized in the bar chart in **Fig. 4.5(A)**. In the vehicle treated WT mice there was no significant difference found between the MGF treated WT mice, although there was a 20% reduction in twitch force in the MGF treated WT mice. At 120 days of age, vehicle treated $SOD1^{G93A}$ mice had reduced twitch tension compared to WT littermates. In vehicle treated $SOD1^{G93A}$ mice there was a reduction in the twitch tension to 3.62g (± 0.4 n=16), compared vehicle treated WT mice, this represented a 34% reduction in maximal twitch tension in the EDL muscles compared with WT at 120 days of age. Treatment with MGF in $SOD1^{G93A}$ mice improved the

twitch force in EDL muscles to 4.45g (± 0.62 n=9) this represents a 22.9% increase in maximal twitch tension compared to vehicle treated $SOD1^{G93A}$ mice, although it did not reach statistical significance. The mean maximal twitch tension improved to 4.4g (± 0.33 n=12) in IGF-I treated $SOD1^{G93A}$ mice, a 38% increase in muscle force although it failed to reach statistical significance.

Treatment with both IGF-I and MGF in $SOD1^{G93A}$ mice improved the twitch force in EDL muscles. The difference between IGF-I and MGF treatment in the twitch force of the TA muscle in $SOD1^{G93A}$ mice did not reach statistical significance. Therefore both IGF-I and MGF are equally as effective in improving twitch force in the EDL muscle in $SOD1^{G93A}$ mice.

The maximal tetanic tension of the EDL muscle was determined next. The results are summarized in the bar chart in **Fig. 4.5(B)**. In WT mice there was no significant difference found in the maximal tetanic tension between WT mice treated with MGF and WT mice treated with vehicle. At 120 days of age, the EDL tetanic tension in the vehicle treated $SOD1^{G93A}$ mice was significantly weaker 13.5g (± 1.2 n=15) than vehicle treated WT littermates 22.45g (± 4.75 n=7). This represented a 40% reduction in maximal tetanic tension compared with WT mice at 120 days of age. Treatment with MGF in the $SOD1^{G93A}$ mice, improved the muscle force to 15.21g (± 1.74 n=9) this represents a 12% improvement in muscle function compared to vehicle treated $SOD1^{G93A}$ mice although it did not reach statistical significance. Similarly, treatment with IGF-I treated $SOD1^{G93A}$ mice improved the muscle force to 15.1g (±1.77 n=13). This represented an 11.8% improvement in tetanic tension in IGF-I treated mice, although this did not reach statistical significance.

Treatment with either IGF-I or MGF in $SOD1^{G93A}$ mice improved the tetanic force in EDL muscles. The difference in the twitch force of the TA muscle in $SOD1^{G93A}$ mice between IGF-I and MGF treatment did not reach statistical significance. Therefore treatments with either IGF-I or MGF in $SOD1^{G93A}$ mice are equally effective in

improving the tetanic force in the EDL muscles, although this improvement does not reach statistical significance.

Figure 4.3 Maximum twitch and tetanic tension of TA muscles from WT and SOD1 ^{G93A} mice, treated with vehicle, MGF or IGF-I assessed at 120 days of age

Isometric twitch contractions were elicited by stimulation of the sciatic nerve using square-wave pulses of 0.02 ms duration and supra-maximal intensity via silver wire electrodes. Maximal tetanic contractions of TA muscles were elicited by trains of stimuli at increasing frequency of 40, 80 and 100 Hz. The bar chart **Fig 4.3(A)** summarizes the mean maximum twitch tension and **Fig 4.3(B)** shows the mean maximum tetanic tension generated in the TA muscle. At 120 days of age, SOD1^{G93A} mice show a significant reduction in maximal twitch and tetanic force compared to WT littermates. However, treatment with MGF and IGF-I in SOD1^{G93A} mice significantly improves maximal twitch and tetanic muscle force in the TA muscles.

(Error bars = ± standard error of the mean, g=grams, A* P≤0.001 A P≤0.010 B* P≤0.001 B** P≤0.001)**

FIGURE 4.3

A

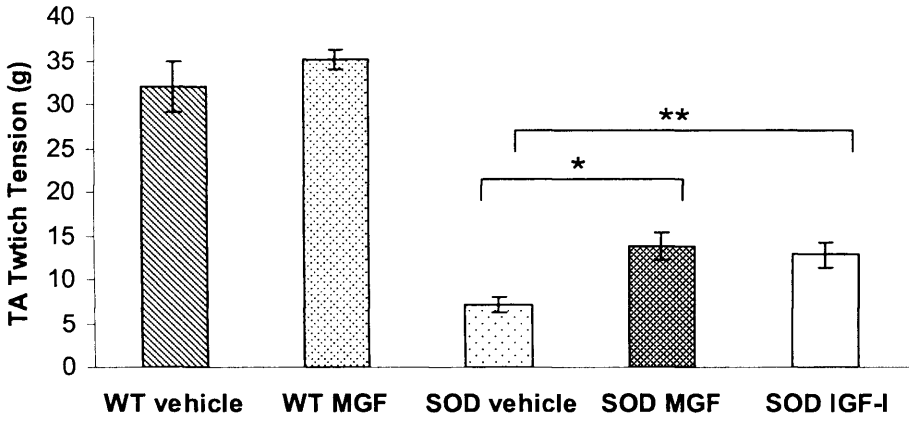
TA Twtich Tension (g)
40
35
30
25
20
15
10
5
0
**
*
WT vehicle
WT MGF
SOD vehicle
SOD MGF
SOD IGF-I

B

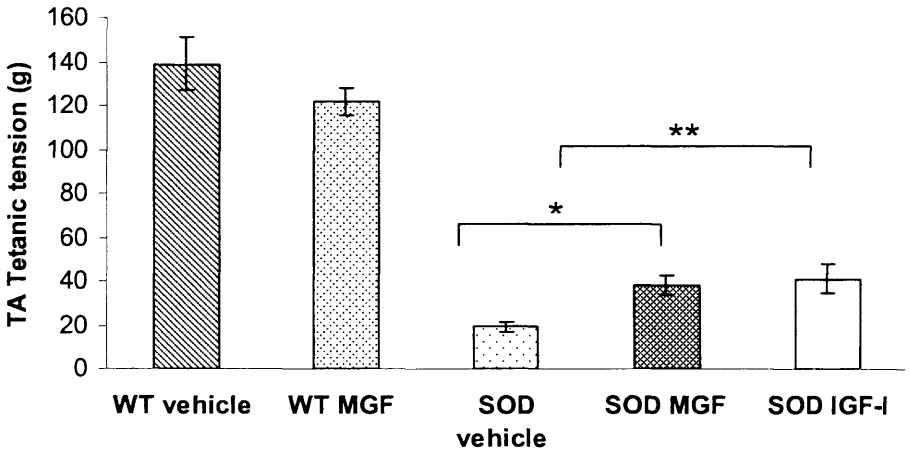
TA Tetanic tension (g)
160
140
120
100
80
60
40
20
0
**
*
WT vehicle
WT MGF
SOD vehicle
SOD MGF
SOD IGF-I

Figure 4.4 Maximum twitch and tetanic tension traces of EDL muscles of WT mice and SOD1^{G93A} mice, treated with vehicle, MGF, or IGF-I assessed at 120 days of age

The maximum twitch and tetanic tension of the EDL muscle was assessed in WT and SOD1^{G93A} mice, treated with vehicle or MGF. Maximum twitch contractions were elicited by stimulating the sciatic nerve using square-wave pulses of 0.02 ms duration and supra-maximal intensity via silver wire electrodes. Maximal tetanic contractions of EDL muscles were elicited by trains of stimuli at increasing frequency of 40, 80 and 100 Hz. Maximum twitch and tetanic traces are shown from **(A)** vehicle treated WT mice **(B)** MGF treated WT mice **(C)** vehicle treated SOD1^{G93A} mice **(D)** MGF treated SOD1^{G93A} mice and **(E)** IGF-I treated SOD1^{G93A} mice.

(Scale bars, g=grams, ms= milliseconds)

FIGURE 4.4

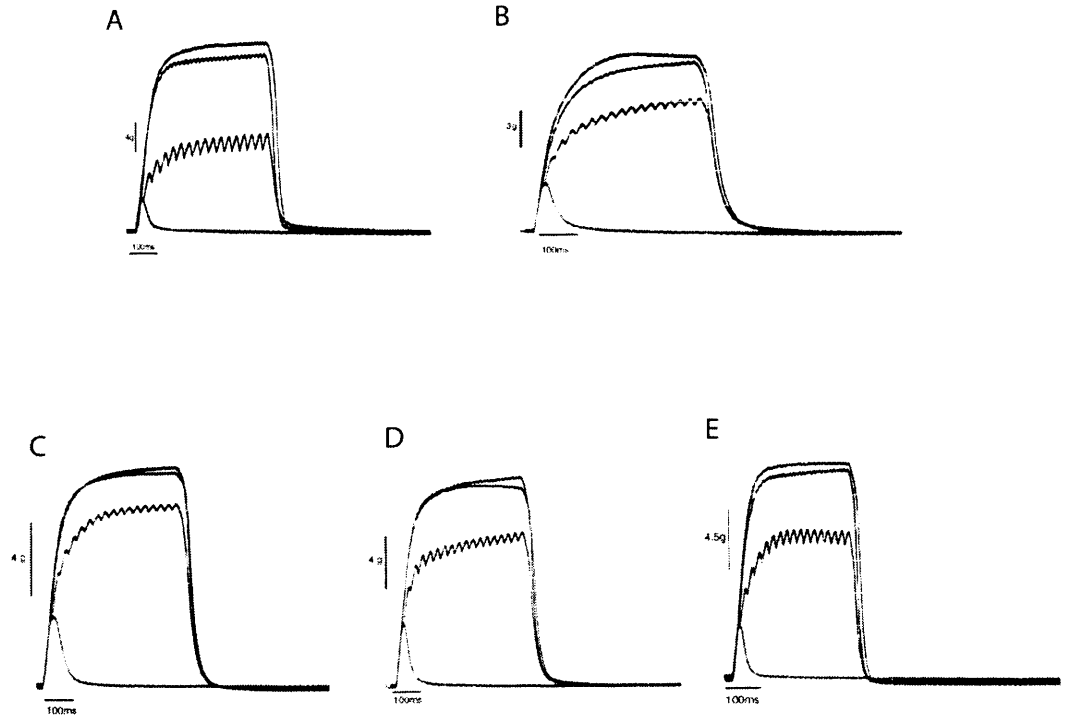

Figure 4.5 Maximum twitch and tetanic tension traces of EDL muscles from WT mice and SOD1^{G93A} mice, treated with vehicle, MGF, or IGF-I assessed at 120 days of age

The maximum twitch and tetanic traces were assessed in the EDL muscle from vehicle treated WT mice, MGF treated WT mice, vehicle treated SOD1^{G93A} mice, MGF treated SOD1^{G93A} mice and IGF-I treated SOD1^{G93A} mice. The bar chart **Fig.4.5(A)** summarises the mean maximum twitch tension and **Fig.4.5(B)** mean tetanic tension in the EDL muscle.

(Error bars = standard error of the mean)

FIGURE 4.5

A

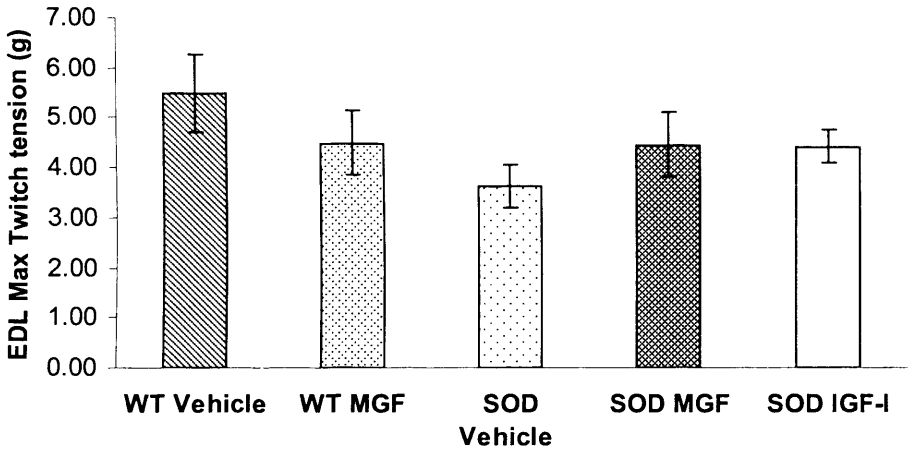
EDL Max Twitch tension (g)
7.00
6.00
5.00
4.00
3.00
2.00
1.00
0.00
WT Vehicle
WT MGF
SOD Vehicle
SOD MGF
SOD IGF-I

B

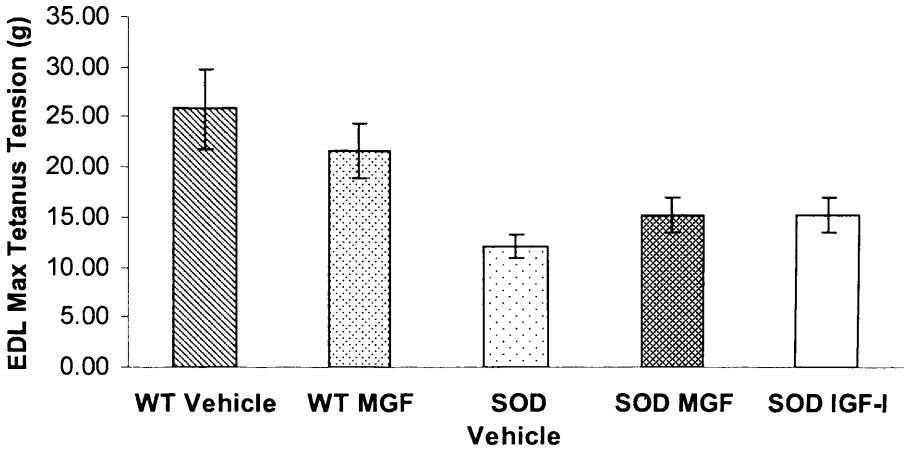
EDL Max Tetanus Tension (g)
35.00
30.00
25.00
20.00
15.00
10.00
5.00
0.00
WT Vehicle
WT MGF
SOD Vehicle
SOD MGF
SOD IGF-I

4.2.5 Contractile characteristics of TA and EDL muscles in WT mice and SOD1^{G93A} mice treated with vehicle, MGF or IGF-I assessed at 120 days of age

The contractile characteristics of TA and EDL muscles were assessed in WT mice and SOD1^{G93A} mice, treated with vehicle, MGF or IGF-I and the results are summarized in **Table 4.2(A)** TA muscle and **(B)** EDL muscle at 120 days of age.

(i) Time to peak

The time to peak is determined by measuring the time taken (ms) for the muscle to elicit peak twitch tension. In WT mice treatment with MGF had no effect on the time to peak in the TA or EDL muscles compared to vehicle treated WT mice. In SOD1^{G93A} mice as disease progresses the speed of contractions of the TA and EDL muscles becomes significantly slower. In SOD1^{G93A} mice both the TA and EDL muscles had significantly slower time to peak compared to WT mice ($P \leq 0.014$ and $P \leq 0.045$ respectively). However following treatment with MGF there was a no significance difference in the time to peak in the TA and EDL muscles in the vehicle treated SOD1^{G93A} mice compared to the MGF treated SOD1^{G93A} mice. Similarly there was no significant difference in the time to peak of TA muscles in SOD1^{G93A} mice treated with, IGF-I, however treatment with IGF-I significantly improved the time to reach peak contraction (TTP) of EDL muscle compared to vehicle treated SOD1^{G93A} mice ($P \leq 0.005$). The TTP in the IGF-I treated SOD1^{G93A} mice is significantly faster compared to MGF treated SOD1^{G93A} mice ($P \leq 0.013$). Therefore IGF-I is more effective than MGF in improving the speed of contraction in the EDL muscle.

(ii) ½ Relaxation Time

The ½ relaxation time is the time taken (ms) for the peak twitch tension to decrease to half of the initial value. Treatment with MGF had no effect on the ½ relaxation time in WT mice in both the TA and EDL muscles. In SOD1^{G93A} mice there was a significant increase in the ½ relaxation time in the TA ($P \leq 0.022$) and EDL muscles ($P \leq 0.002$) compared to WT mice. There was no significant difference in the ½ relaxation time in

either the TA or EDL muscles, in $SOD1^{G93A}$ mice treated with MGF. However the ½ relaxation time was decreased in the TA and EDL muscles of $SOD1^{G93A}$ mice treated with MGF and IGF-I, yet this improvement in the time to peak, did not reach statistical significance.

As a consequence of the disease progression in $SOD1^{G93A}$ mice, there is an increase in the time to peak and the ½ relaxation time in both the TA and EDL muscles. In $SOD1^{G93A}$ mice treatment with MGF and IGF-I decrease the ½ relaxation time compared to vehicle treated $SOD1^{G93A}$ mice, in both the TA and EDL muscles; however despite this improvement in speed of contraction there was a failure to reach statistical significance. There was no statistically significant difference between treatment with either IGF-I or MGF in the half relaxation time in the TA or EDL muscles. Therefore treatments with either IGF-I or MGF were equally unsuccessful in significantly improving the half relaxation time in the TA and EDL muscle.

Table 4.2 Contractile characteristics of TA and EDL muscles from WT and SOD1^{G93A} mice treated with vehicle, MGF, or IGF-I assessed at 120 days of age

The contractile characteristics of the TA and EDL muscle were assessed in WT vehicle and SOD1^{G93A} mice, treated with either vehicle or MGF, assessed at 120 days of age. The time to peak is determined by the time taken (ms) for a muscle to elicit peak twitch tension. The ½ relaxation time is the time taken (ms) for the peak twitch tension to decrease to half of the initial value. The table shows the mean time to peak and the half relaxation time for (A) TA and (B) EDL muscles in WT mice and SOD1^{G93A} mice at 120 days of age.

(TTP= time to peak, ± standard error of the mean, ms= milliseconds, *P ≤ 0.014, **P ≤0.022, ***P ≤ 0.045, ****P ≤ 0.002 # P ≤ 0.005)

TABLE 4.2

A

	WT vehicle	WT MGF	SOD vehicle	SOD MGF	SOD IGF-I
TA TTP (ms)	**22.72** ±1.52 (n=10)	**26.0** ± 1.3 (n=8)	**30.03** ± 2.01* (n=16)	**25.85** ±0.82 (n=10)	**27.24** ± 2.4 (n=14)
TA ½ RT (ms)	**22.68** ± 2.88 (n=10)	**26.8** ± 2.46 (n=8)	**33.58** ± 2.97** (n=16)	**28.99** ±1.98 (n=10)	**32.19** ±3.1 (n=14)

B

	WT vehicle	WT MGF	SOD vehicle	SOD MGF	SOD IGF-I
EDL TTP (ms)	**21.57** ± 0.95 (n=7)	**24.29** ± 2.16 (n=7)	**26.25** ± 1.4*** (n=16)	**24.8** ± 1.7 (n=9)	**21.2** ± 0.69 (n=13) #
EDL ½ RT (ms)	**14.43** ± 1.5 (n=7)	**19.75** ± 3.12 (n=8)	**24.73** ±1.9 **** (n=16)	**20.11** ±2.2 (n=9)	**21.7** ± 1.01 (n=13)

Figure 4.6 Contractile characteristics of TA and EDL muscles from WT and $SOD1^{G93A}$ mice treated with vehicle, MGF, or IGF-I assessed at 120 days of age

The contractile characteristics of the TA and EDL muscle were assessed in WT vehicle and $SOD1^{G93A}$ mice, treated with either vehicle or MGF, assessed at 120 days of age. The bar charts shows the mean time to peak and the half relaxation time for (A) TA muscle Time to peak (B) TA muscle ½ relaxation time (C) EDL muscle Time to peak (D) EDL muscle ½ relaxation time.

(Error bars = ±standard error of the mean, ms= milliseconds, *P ≤ 0.014, **P ≤0.022, ***P ≤ 0.045 ****P ≤ 0.005, *****P ≤ 0.002

FIGURE 4.6 (i)

A

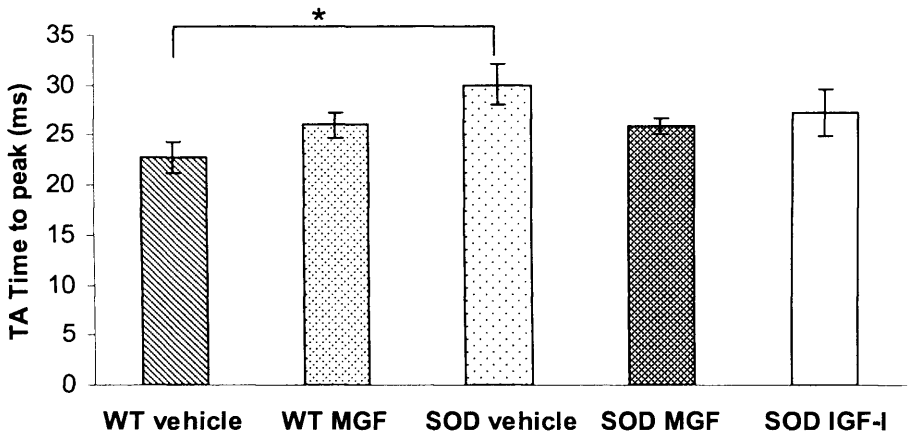

B

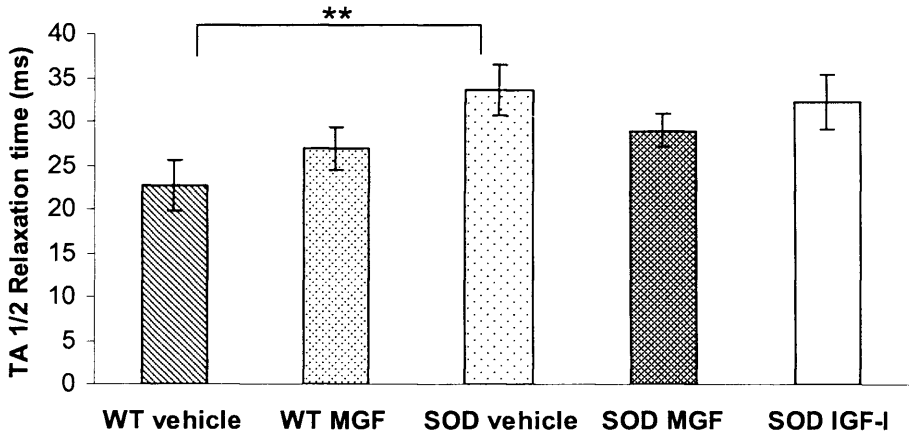

FIGURE 4.6. (ii)

C

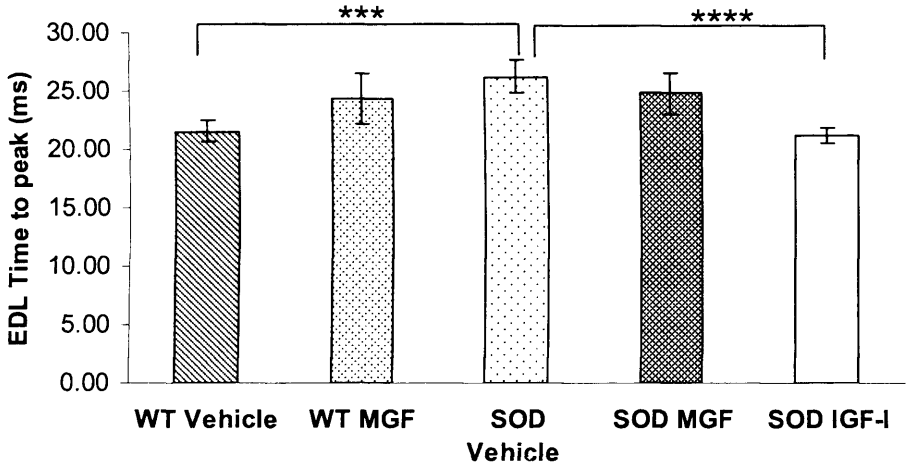

D

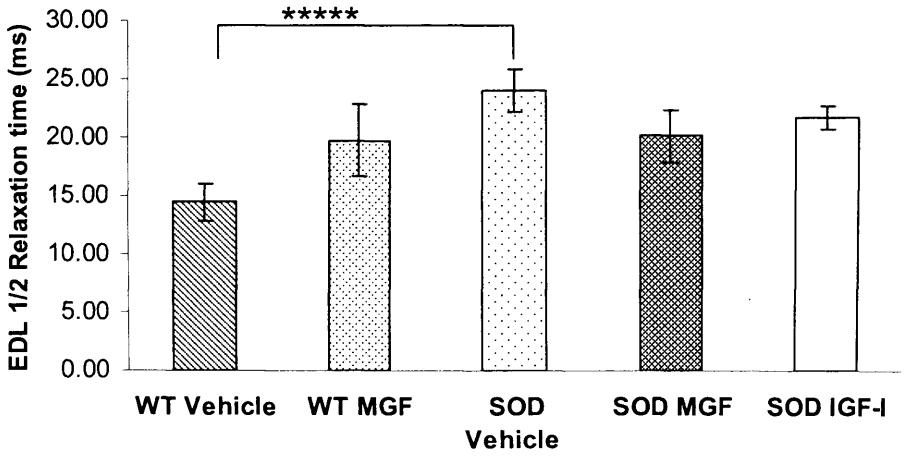

4.2.6 Motor unit number

The number of functional motor units in the EDL muscle in WT and $SOD1^{G93A}$ mice, treated with either MGF or the vehicle was examined at 120 days of age. Examples of typical motor unit traces are shown in **Fig. 4.7** and the results of the mean motor unit survival are summarized in the bar chart **Fig. 4.8**. In vehicle treated WT mice, the EDL muscle is innervated on average by 30 (±2.43, n=7) motor units. Treatment with MGF has no effect on the number of motor units in EDL so that 32 (±3.3, n=6) motor units survive in the MGF treated WT mice. In contrast in the vehicle treated $SOD1^{G93A}$ mice there is a reduction in motor unit survival, so that at 120 days of age only 10 (±0.618 n=16) motor units survive. However following treatment with MGF, there is a significant improvement in the number of motor units in EDL of $SOD1^{G93A}$ mice and on average 15 (±1.56 n=9) motor units survive ($P \leq 0.006$). Thus treatment of $SOD1^{G93A}$ mice with MGF significantly improves the motor unit survival in $SOD1^{G93A}$ mice. Similarly in IGF-I treated $SOD1^{G93A}$ mice there was a significant improvement and 15 (±0.77 n=13) motor units survived ($P \leq 0.001$), an increase of 50%.

Thus treatment with either IGF-I or MGF significantly improved the number of functional motor units surviving in the $SOD1^{G93A}$ mice. There was no statistically significant difference in the number of surviving motor units between IGF-I or MGF treated $SOD1^{G93A}$ mice. Thus treatment with either IGF-I or MGF was equally as effective in rescuing motor units in $SOD1^{G93A}$ mice. In both IGF-I and MGF treated $SOD1^{G93A}$ mice, 15 motor units survived.

Figure 4.7 Motor Unit traces from WT and SOD1^{G93A} mice treated with either vehicle, MGF or IGF-I, assessed at 120 days of age

The number of functional motor units that innervate the EDL muscle was assessed in WT and SOD1^{G93A} mice at 120 days of age. Examples of motor unit traces are shown from **(A)** vehicle treated WT mice **(B)** MGF treated WT mice **(C)** vehicle treated SOD1^{G93A} mice, **(D)** MGF treated SOD1^{G93A} mice and **(E)** IGF-I treated SOD1^{G93A} mice

(ms= milliseconds)

FIGURE 4.7

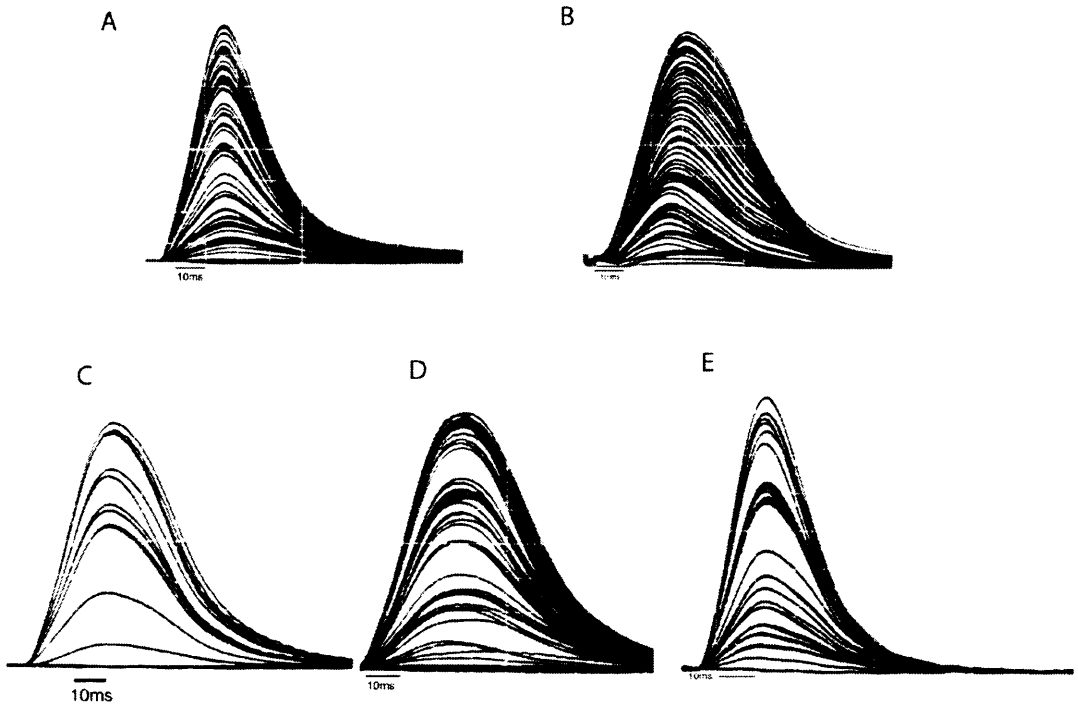

Figure 4.8 Survival of motor units from WT mice and SOD1^{G93A} mice treated with vehicle, MGF, or IGF-I assessed at 120 days of age

The number of functional motor units that innervate the EDL muscle was assessed in WT mice and SOD1^{G93A} mice at 120 days of age. The MGF treated SOD1^{G93A} mice have a significantly greater number of motor units compared to the vehicle treated mice at 120 days of age.

(Error bars ± standard error of the mean,*P≤ 0.006)

FIGURE 4.8

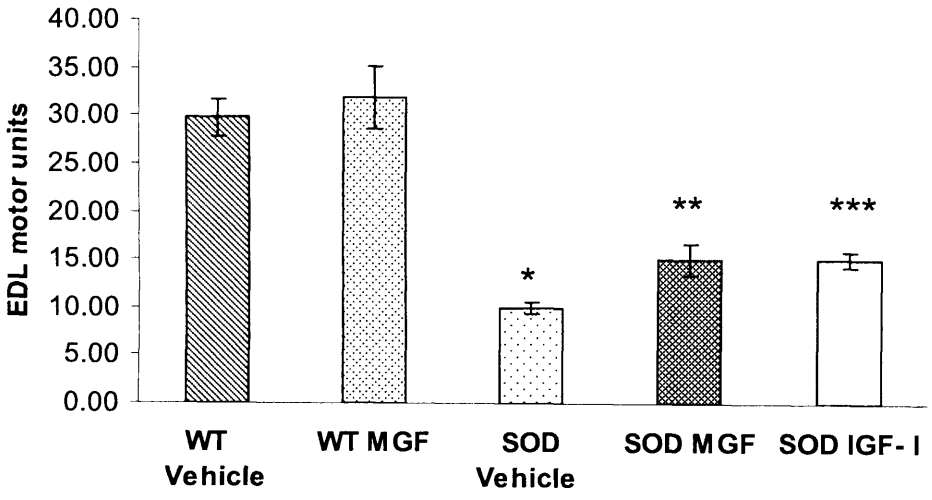
40.00
35.00
30.00
25.00
20.00
15.00
10.00
5.00
0.00
EDL motor units
*
**
***
WT Vehicle
WT MGF
SOD Vehicle
SOD MGF
SOD IGF-I

4.2.7 EDL muscle fatigue pattern

The EDL muscle is a fast fatigable (glycolytic) muscle that fatigues rapidly when repeatedly stimulated producing a characteristic fatigue pattern. The effect of treatment with MGF on this characteristic fatigue pattern of the EDL muscle was examined in WT mice and $SOD1^{G93A}$ mice at 120 days of age by repetitively stimulating the EDL muscle at 40 Hz for 250 ms every second for 3 mins. Examples of fatigue traces from WT mice and $SOD1^{G93A}$ mice treated with MGF or vehicle are shown in **Fig. 4.9**. The fatigue trace of the WT mice shows that the EDL muscle fatigues rapidly when stimulated repeatedly. In contrast, the typical fatigue pattern of EDL changes quite markedly in the vehicle treated $SOD1^{G93A}$ mice and becomes a fatigue resistant muscle. Treatment with MGF and IGF-I in the $SOD1^{G93A}$ mice prevents this change in the fatigue characteristic of EDL.

There was no difference seen in the typical fatigue pattern between IGF-I and MGF treated $SOD1^{G93A}$ mice, the fatigability of the EDL muscle can be quantified by calculating a fatigue index, which is a ratio of the force of tetanic contractions at the beginning of stimulation compared to the force of tetanic contractions at the end of the 3 minute stimulation. It was not possible to compare fatigue index for the treated $SOD1^{G93A}$ mice as the slope of the traces, which reflects the decrease in tetanic tension, were markedly different in individual experimental groups. In order to determine a reliable fatigue index, for each experimental group it is necessary for the traces to have a consistent pattern.

The fatigue test indicates that treatment with either IGF-I or MGF can prevent the disease related changes in the EDL muscle phenotype which change markedly as a consequence of disease progression of the $SOD1^{G93A}$ mice. Both IGF-I and MGF are equally as effective in preventing the changes in the fatigue characteristics and the EDL muscle fatigues rapidly when repeatedly stimulated in both IGF-I and MGF treated $SOD1^{G93A}$ mice.

Figure 4.9 Fatigue traces from WT mice and SOD1^{G93A} mice treated with vehicle MGF or IGF-I assessed at 120 days of age

The fatigue pattern of the EDL muscle was examined by repeatedly stimulating the EDL muscle at 40 Hz for 250 ms every second for 3 mins. EDL is normally a fast fatigable (glycolytic) muscle, which has a characteristic fatigue pattern when repetitively stimulated. The force of contraction is greater at the beginning of the fatigue test, and as the EDL muscle cannot maintain the force of contraction it is seen to fatigue through the duration of the fatigue test. Examples of fatigue traces are shown from **(A)** vehicle treated WT mice **(B)** MGF treated WT mice **(C)** vehicle treated SOD1^{G93A} mice **(D)** MGF treated SOD1^{G93A} mice and **(E)** IGF-I treated SOD1^{G93A} mice. Treatment with MGF and IGF-I in the SOD1^{G93A} mice, results in the normal fatigue characteristic of the EDL muscle being preserved MGF treated SOD1^{G93A} mouse.
(g=grams, s= seconds)

FIGURE 4.9

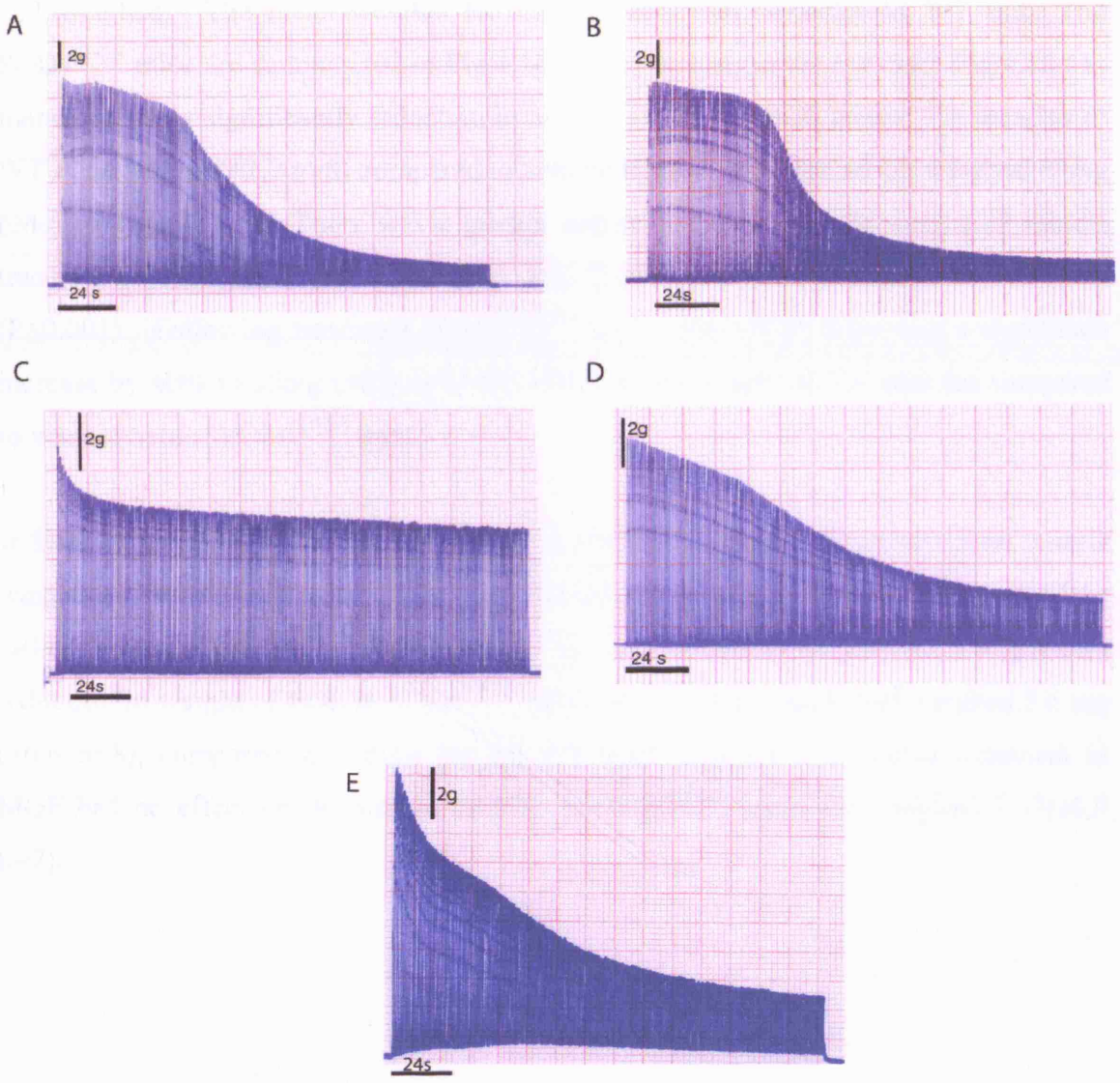

4.2.8 Muscle weights

Following the physiological tension recordings, the TA and EDL muscles were removed and weighed. The mean weights for the TA and EDL muscles in WT mice and $SOD1^{G93A}$ mice are summarized in **Fig 4.10**. It can be seen in the bar chart **Fig 4.10 (A)** that there was a significantly reduction in muscle weight in MGF treated TA muscles of WT mice, 43 mg (±2.9 n=8) compared to vehicle treated WT mice which weighed 58mg (±4.6 n=8) ($P \leq 0.023$). There was a greater reduction in TA muscle weight of vehicle treated $SOD1^{G93A}$ mice, which weighed only 25mg (±1.3 n=8) compared to WT mice ($P \leq 0.001$). Following treatment of $SOD1^{G93A}$ mice with MGF, there was a significant increase by 40% to 35mg (±0.9 n=8) ($P \leq 0.001$) in the weight of TA muscles compared to vehicle treated $SOD1^{G93A}$ mice

In EDL muscles of WT mice treatment with MGF had no significant effect on muscle weight, so that vehicle treated EDL weighed 10.8mg (±0.5 n=8), compared to 9.67mg (±0.63 n=7) in MGF treated WT mice. Similar to the TA there was a significant reduction in weight of EDL in $SOD1^{G93A}$ mice treated with vehicle and weighed 8.6 mg (±0.6 n=8), compared to vehicle treated WT mice ($P \leq 0.021$). However treatment in MGF had no effect on the weight of EDL in $SOD1^{G93A}$ mice and weighed 7.57(±0.7 n=7).

Figure 4.10 Weights of TA and EDL muscles from WT mice and SOD1^{G93A} mice, treated with vehicle, MGF, or IGF-I assessed at 120 days of age

The weights of TA and EDL muscles were assessed in vehicle treated WT mice, MGF treated WT mice, vehicle treated SOD1^{G93A} mice, MGF treated SOD1^{G93A} mice, and IGF-I treated SOD1^{G93A} mice. Surprisingly a significantly reduction in muscle weight in MGF treated TA muscles of WT mice was found. This decrease in muscle weight may be attributed to an insufficient uptake of MGF cDNA into the TA muscle of WT mice. Alternatively it is possible that the effect of MGF as a potent inducer of muscle hypertrophy is more effective in SOD1^{G93A} mice than in WT mice. The bar charts show the mean muscle weights (mg) for both the TA **(A)** and EDL **(B)** muscles.

(Error bars = ± standard error of the mean, mg= milligrams, * P≤0.023, ** P≤0.001 ***P≤0.001, **** P≤0.021)

FIGURE 4.10

A

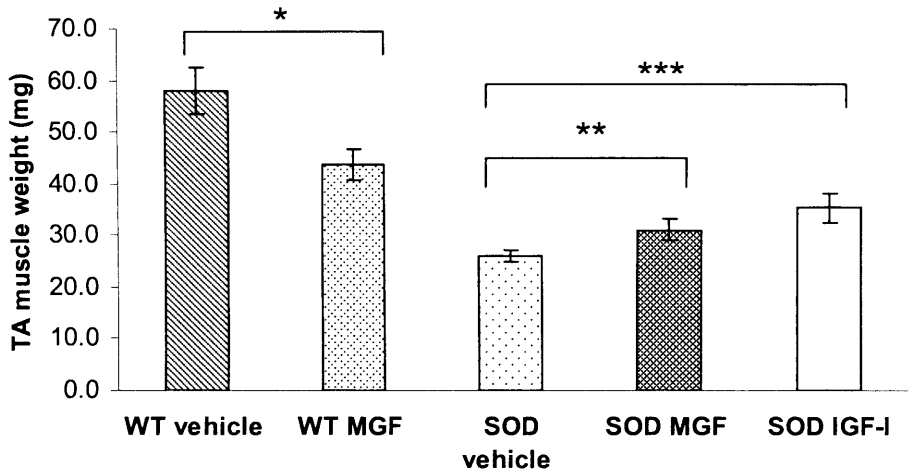

B

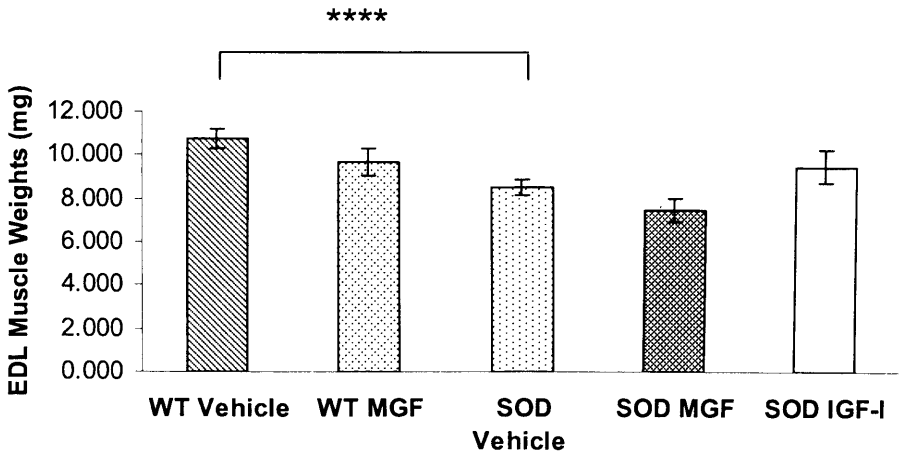

4.2.9 Muscle Histology

To determine whether there was any evidence of satellite cell activation, such as centralized nuclei in the $SOD1^{G93A}$ mice treated with MGF, transverse muscle sections were stained with Haematoxylin & Van Gieson for overall morphological assessment of TA muscle. Representative examples of TA muscles stained with Haematoxylin & Van Gieson are shown in **Fig 4.11** The Haematoxylin & Van Gieson stains the cytoplasm yellow, the nuclei black and collagen red. In WT mice, vehicle treated $SOD1^{G93A}$ mice and IGF-I $SOD1^{G93A}$ mice there are peripheral located nuclei surrounding the muscle fibres. Histological analysis of muscle sections in the MGF treated $SOD1^{G93A}$ mice revealed centralised nuclei, as indicated by an arrow in **Fig 4.11(C)** centralised nuclei represents a hallmark of satellite cell activation in the muscle fibers. The observed centralised nuclei indicate recent fusion of activated satellite cells to existing myofibers and suggest that the muscles are undergoing a process of regeneration (Barton et al., 1999).

Figure 4.11 Haematoxylin & Van Gieson staining of TA muscles from vehicle, IGF-I or MGF treated SOD1^{G93A} mice, assessed at 120 days of age

Transverse cross sections of TA muscles were stained with Haematoxylin & Van Gieson, which stains the cytoplasm yellow, nuclei black and collagen red. The TA muscles show a typical pattern of peripherally located nuclei in **(A)** vehicle treated WT, **(B)** vehicle treated SOD1^{G93A} mice, **(C)** IGF-I treated SOD1^{G93A} mice. In contrast in the SOD1^{G93A} mice treated with the MGF **(D)** the muscle has centralized nuclei, as indicated by arrow, which is a hallmark of satellite activation of regenerating muscle fibres.

(Scale bar =100μm)

FIGURE 4.11

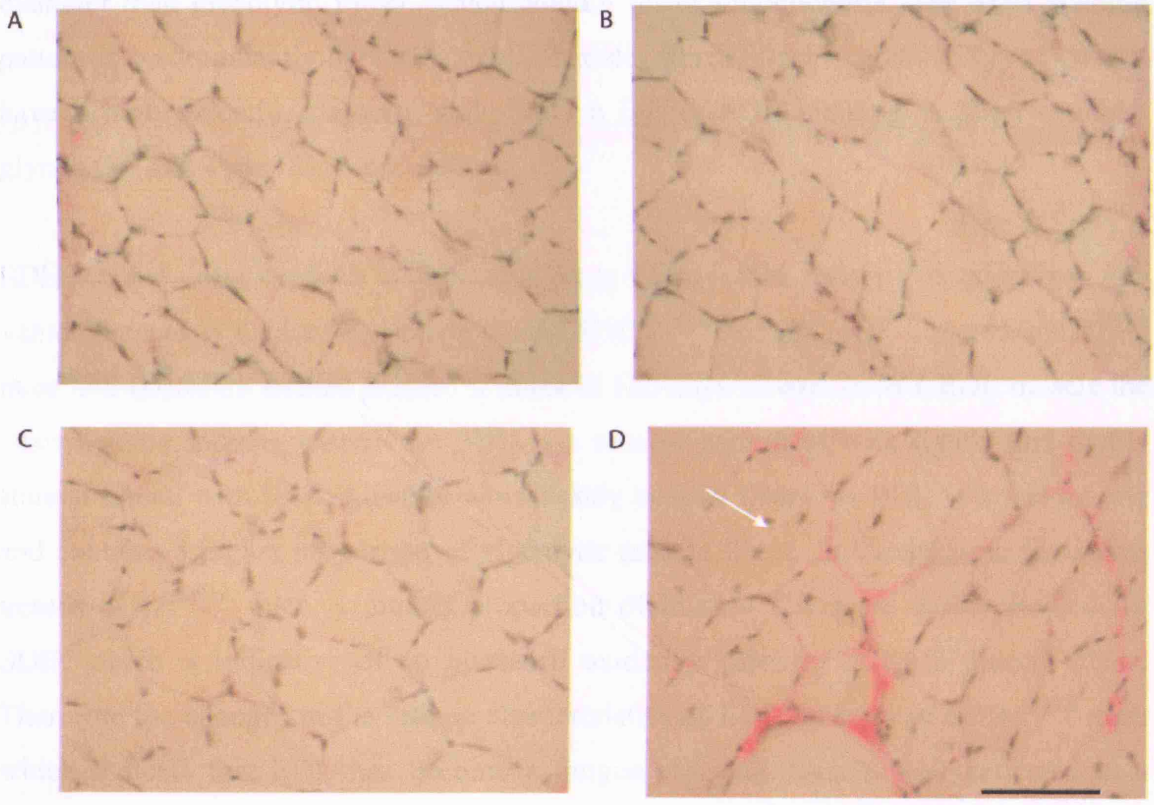

4.2.10 Muscle histochemistry

The oxidative capacity of EDL muscle was assessed by staining transverse cross sections of muscle with succinate dehydrogenase (SDH). SDH is an enzymatic intermediate of the mitochondrial Krebs cycle, which acts as a marker of the oxidative capacity of the muscle. Oxidative muscles fibres which contain numerous mitochondria and thus have a high capacity for oxidative phosphorylation are normally smaller in diameter than glycolytic fibres, which contain fewer mitochondria. The SDH staining pattern is predominantly darker in small diameter fibres (slow oxidative, Type I) which have a high oxidative capacity and shows a lighter SDH staining in large diameter glycolytic (fast Type IIB) muscle fibres.

SDH stained cross sections of EDL muscle in **Figure 4.11** shows examples from (A) vehicle treated WT mice (B) vehicle treated $SOD1^{G93A}$ mice (C) IGF-I treated $SOD1^{G93A}$ mice and (D) MGF treated $SOD1^{G93A}$ mice at 120 days of age. In WT EDL muscle the characteristic staining pattern for SDH is a mosaic pattern of both lightly and darkly stained fibers, with predominately more lightly stained fibers, as EDL is a fast muscle and contains a higher proportion of glycolytic muscle fibres. In comparison, in vehicle treated $SOD1^{G93A}$ mice, a greater proportion of muscle fibers are darkly stained for SDH, which is indicative of an increased oxidative capacity of these muscle fibers. Therefore the changes in the fatigue characteristics of EDL muscles of $SOD1^{G93A}$ mice which indicate that EDL has become a fatigue resistant muscle were reflected in a change in the histochemical properties of the muscle fibers.

In MGF and IGF-I treated $SOD1^{G93A}$ mice the staining pattern of SDH resembled that of WT mice, with a greater proportion of lightly stained muscle fibres. Therefore, the staining pattern of EDL of $SOD1^{G93A}$ mice treated with either MGF or IGF-I, shows a preservation of the oxidative capacity of these muscle fibers and the maintenance of the glycolytic muscle phenotype.

Furthermore in IGF-I treated $SOD1^{G93A}$ mice there appears to be a greater proportion of darkly stained SDH muscle fibres with smaller diameters compared to MGF treated

$SOD1^{G93A}$ mice. Therefore IGF-I treatment in $SOD1^{G93A}$ mice appears to also effect the size and intensity of SDH stained muscle fibres in $SOD1^{G93A}$ mice. In direct comparison, in the EDL muscle MGF preserves the size of the muscle fibres and there appear to be proportionally less small diameter darkly stained SDH muscle fibres than IGF-I treated $SOD1^{G93A}$ mice.

The IGF-I treated muscle fibres appear to be undergoing denervation/reinnervation as indicated by the muscle fibre type grouping of darkly and lightly stained muscle fibres. It is consistent that the small darkly stained SDH muscle fibres, which are grouped together in IGF-I treated $SOD1^{G93A}$ mice occur as a consequence of denervation/reinnervation. Whereas in the MGF treated $SOD1^{G93A}$ mice there appears to be a preservation of innervation and there is a heterogeneous combination of darkly and lightly stained muscle fibres.

Figure 4.12 Succinate dehydrogenase staining of EDL muscle sections from WT mice and vehicle, IGF-I or MGF treated SOD1^{G93A} mice, assessed at 120 days of age

Transverse cross sections of EDL muscle sections from (A) vehicle treated WT mice (B) vehicle treated SOD1^{G93A} mice (C) IGF-I treated SOD1^{G93A} mice and (D) MGF treated SOD1^{G93A} mice assessed at 120 days of age, stained for succinate dehydrogenase (SDH) activity, an indicator of oxidative capacity of muscle fibres. The vehicle treated WT mice EDL muscles showed a mosaic pattern of SDH activity, with the majority of fibres staining lightly. In the vehicle treated SOD1^{G93A} mice EDL muscle fibres, there is an increased oxidative capacity, reflected by a greater proportion of darkly stained muscle fibres. In contrast, EDL muscles treated with IGF-I and MGF showed a pattern of SDH staining similar to that observed in WT EDL muscles, with a greater proportion lightly stained muscle fibres.

(Scale bar = 100μm)

FIGURE 4.12

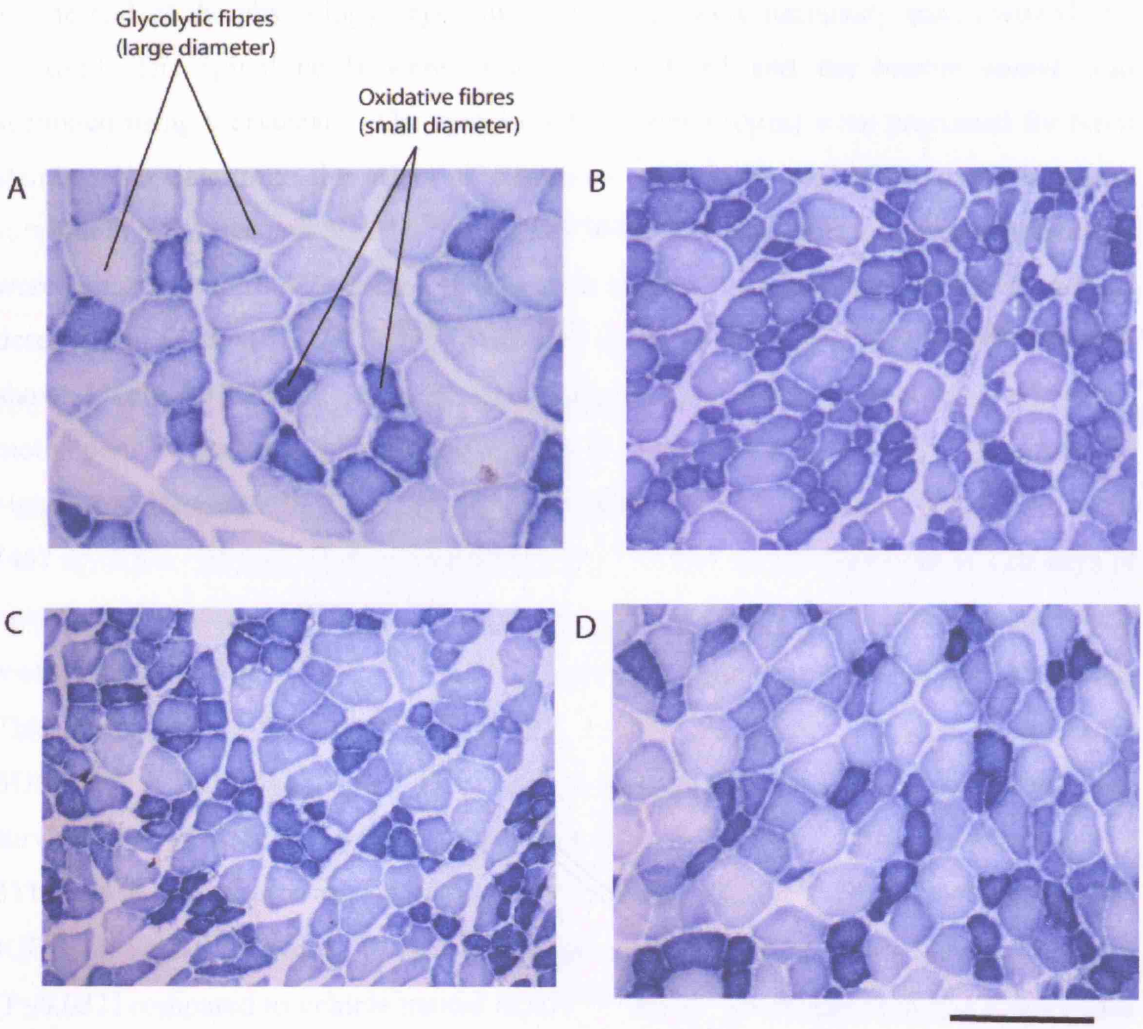
Glycolytic fibres
(large diameter)
Oxidative fibres
(small diameter)
A
B
C
D

4.2.11 Motoneuron survival

At the end of the physiology experiments the mice were terminally anaesthetized and perfused. The spinal cords were removed post-fixed and the lumbar spinal cord sectioned using a cryostat. The spinal cord sections (20μm) were processed for Nissl staining. To determine the effect of treatment with MGF and IGF-I on motoneuron survival in WT mice and $SOD1^{G93A}$ mice at 120 days of age, the number of motoneurons were counted in the sciatic motor pool in each ventral horn from lumber spinal cord (as described in **Chapter 2: 2.5.12**). Examples of spinal cord sections stained with Nissl are shown in **Fig 4.13 (A-D)** and the mean number of motoneurons surviving in the sciatic motor pool of each group is summarized in the bar chart **(Fig 4.13E)**. There was no significant difference in the extent of motoneuron survival in vehicle treated WT mice (467 ± 36.5 n= 2) and MGF treated WT mice (553 ±11 n =2). However at 120 days of age, the vehicle treated $SOD1^{G93A}$ mice have significantly less motoneurons in the sciatic motor pool and only 202 (± 15 n = 4) motoneurons survive compared to WT littermates. This represents a 57% loss of motoneuron survival in $SOD1^{G93A}$ mice. However, in $SOD1^{G93A}$ mice treated with MGF there was a significant increase in motoneuron survival, so that 350 (±15 n=5) motoneurons survive ($P \leq 0.016$). This represents only a 31% loss in motoneuron survival compared to vehicle treated WT mice. Treatment with IGF-I in $SOD1^{G93A}$ mice, have on average 286 (±17 n=5) motoneurons surviving ($P \leq 0.032$) compared to vehicle treated $SOD1^{G93A}$ mice. Treatment with IGF-I represents only a 44% loss in motoneurons compared to WT mice. Thus treatment with MGF in the $SOD1^{G93A}$ mice has a greater neuroprotective effect than IGF-I. The difference in the average number of surviving motoneurons between the IGF-I and MGF treated $SOD1^{G93A}$ mice is statistically significant ($P \leq 0.016$). Thus MGF is more effective in rescuing motoneurons in the sciatic motor pool in $SOD1^{G93A}$ mice than MGF.

Figure 4.13 Motoneuron survival in WT, vehicle treated SOD1^{G93A} mice, IGF-I treated SOD1^{G93A} mice and MGF treated SOD1 ^{G93A} mice, assessed at 120 days of age

Motoneuron survival was assessed by counting the number of Nissl stained motoneurons within the sciatic motor pool in each ventral horn in cross sections of lumber spinal cord of 120 day old mice. Examples of spinal cord sections are shown from **(A)** vehicle treated WT mice **(B)** vehicle treated SOD1^{G93A} mice, **(C)** IGF-I treated SOD1^{G93A} mice and **(D)** MGF treated SOD1^{G93A} mice. The bar chart **(E)** shows the mean number of surviving motoneurons counted in 60 spinal cord sections. The number of surviving motoneurons decreases as the disease progresses in the SOD1^{G93A} mice and a large proportion are lost at 120 days of age. In IGF-I and MGF treated SOD1^{G93A} mice there are a significantly greater number of surviving motoneurons at 120 days of age compared to vehicle treated SOD1^{G93A} mice. However significantly more motoneurons survive in MGF treated SOD1^{G93A} mice compared to IGF-I treated SOD1^{G93A} mice.

(Error bars = ± standard error of the mean, scale bar = 200μm, * P≤0.032 **P≤0.016 and ***P≤0.016)

FIGURE 4.13

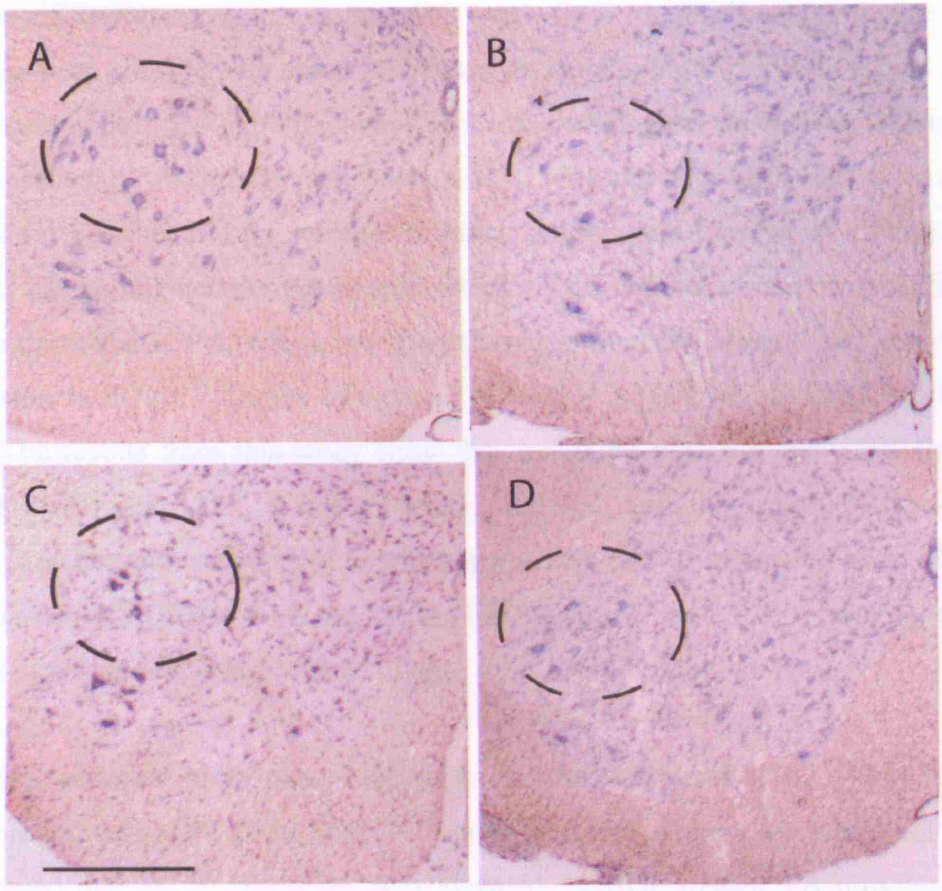
A
B
C
D

E

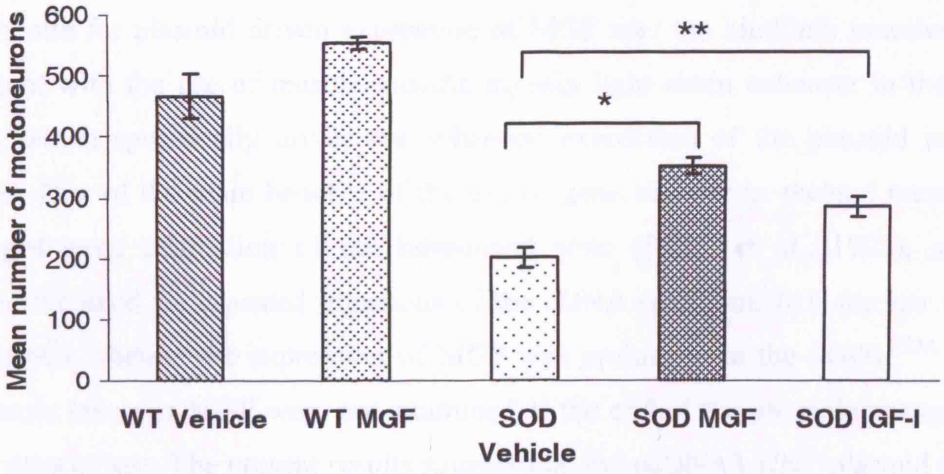
Mean number of motoneurons
600
500
400
300
200
100
0
**
*
WT Vehicle
WT MGF
SOD Vehicle
SOD MGF
SOD IGF-I

4.3 DISCUSSION

There has been considerable research focused on developing therapeutic agents in ALS. SOD1 transgenic mice exhibit phenotypic and pathological characteristics similar to those presented by ALS patients (Gurney et al., 1994) and have been used extensively as a model for preclinical drug screens (Nirmalananthan and Greensmith, 2005). Recent evidence has highlighted the therapeutic potential of a number of neurotrophic factors in ALS, in particular IGF-I, which has been shown to increase lifespan and delay disease progression in $SOD1^{G93A}$ mice (Kaspar et al., 2003; Nagano et al., 2005; Narai et al., 2005). The results from this study show that treatment with a mammalian expression plasmid containing MGF, a splice variant of IGF-I, and full length IGF-I improves muscle function and additionally protects against the loss of motoneurons in $SOD1^{G93A}$ mice. However MGF has a greater neuroprotective effect than IGF-I, rescuing a greater number of motoneurons at 120 days of age.

4.3.1 Expression of MGF protein levels in skeletal muscle of $SOD1^{G93A}$ mice

The protein levels of MGF in $SOD1^{G93A}$ mice were examined by western blot analysis and showed that MGF expression was elevated in MGF treated TA muscle 2 weeks post-injection. There was no increase in expression of protein levels of MGF in $SOD1^{G93A}$ mice treated with MGF in the spinal cord, suggesting that there was no retrograde transport of MGF to the motoneurons in the spinal cord. Therefore, following intramuscular injections with MGF cDNA pcDNA3.1/NT plasmid, it is likely that the primary site for plasmid driven expression of MGF was the hindlimb muscles. This is consistent with the use of muscle-specific myosin light chain enhancer in the plasmid vector, which specifically drives the enhanced expression of the plasmid in skeletal muscle. One of the main benefits of the use of gene transfer in skeletal muscle is the prolonged gene expression of the introduced gene (Skarli et al., 1998), ultimately limiting the need for repeated injections of the cDNA construct. It is unclear from our experiments whether the expression of MGF was prolonged in the $SOD1^{G93A}$ mice, as the protein levels of MGF were not examined at the end of the physiology experiments at 120 days of age. The present results suggest that the pcDNA3.1/NT plasmid construct was an efficient vector for the introduction and expression of MGF in skeletal muscle.

Although further investigations are required to determine whether there was prolonged gene expression of the introduced gene.

4.3.2 MGF improves hind limb muscle function in SOD1^{G93A} mice

There is a dramatic reduction in the muscle force in hind limbs as a consequence of disease progression in SOD1^{G93A} mice (Sharp et al., 2005). The results of this study confirm these results and show a significant reduction in muscle force in hind limb muscles of SOD1^{G93A} mice at 120 days of age. The maximal tetanic force of TA and EDL muscles of vehicle treated SOD1^{G93A} mice is reduced by 85% and 40% respectively, compared to muscles of vehicle treated WT mice. Therefore the TA muscle is more affected than the EDL muscle. Treatment with MGF and IGF-I preferentially improves muscle force in the TA muscle compared to the EDL muscle. Previous studies of disease progression have reported a greater vulnerability in the TA muscles in SOD1^{G93A} mice, whereby muscle weakness occurs at an earlier stage in the TA than the EDL muscle (Sharp et al., 2005). The increased vulnerability of the TA muscle in SOD1^{G93A} mice may be due to a greater proportion of motoneurons innervating the TA muscle having larger peripheral fields compared to EDL. The peripheral field is defined as the muscle fibre territory, which a single motoneuron innervates. During postnatal development motoneurons have large peripheral fields and these are reduced during the period when elimination of poly-neuronal innervation occurs. Having larger peripheral fields may increase the metabolic demands on motoneurons, possibly rendering the motoneurons more susceptible to pathogenic mechanisms, such as increased levels oxidative stress (Sharp et al., 2005).

Fast-fatigue resistant motoneuron axons are affected at symptom-onset, whereas axons of slow motoneurons are disease-resistant in SOD1^{G93A} mice (Pun et al., 2006). Previous studies have shown that a sub-group of fast-fatigue-resistant neuromuscular synapses are lost early on in the disease, whereas the slow-type synapses were resistant and were not lost at disease end-stage (Frey et al., 2000; Pun et al., 2006). It is suggested that slow twitch neuromuscular synapses exhibit a particular plasticity and can undergo collateral sprouting to reinnervated vacated synapses. However fast-twitch neuromuscular

synapses exhibit less plasticity, ultimately resulting in the early loss of the neuromuscular synapse. Axonal sprouting, induced by BoTx, failed to cause sprouting in fast-twitch neuromuscular synapses, whereas in the soleus muscle, the slow-type synapses readily sprouted (Frey et al., 2000). As the mouse soleus muscle contains both slow and fast fatigue resistant motor units, sprouting in response to BoTx, is determined by both the muscle type and motor unit type (Frey et al., 2000).

There is also further evidence to suggest an associated vulnerability of fast twitch EDL muscles, compared to slow twitch soleus muscles in $SOD1^{G93A}$ mice (Derave et al., 2003). Using electrical stimulation of a single skinned muscle fibre from $SOD1^{G93A}$ mice (at disease end stage) it was revealed that the fast-twitch EDL muscle had reduced muscle mass and muscle force, compared to the soleus muscle, which was unaffected (Derave et al., 2003). These studies indicate the involvement of different muscle subtypes rendering specific motoneurons susceptible to degeneration in ALS.

4.3.3 Muscle contractile characteristics change as a consequence of disease progression in $SOD1^{G93A}$ mice

The contractile properties of the TA and EDL muscles were assessed in WT mice and $SOD1^{G93A}$ mice. The results presented here show a marked change in the speed of contraction of $SOD1^{G93A}$ mice muscles at 120 days of age. The TA and EDL muscles in $SOD1^{G93A}$ mice were slower to reach peak twitch tension and similarly the half relaxation time was considerably slower than WT mice. It is known from a previous study (Sharp et al., 2005), that the half relaxation time of a single twitch of the EDL and TA muscles in $SOD1^{G93A}$ mice was significantly slower at a late stage disease at 130 days, whilst no difference was observed at 90 days of age (Sharp et al., 2005). These results suggest that as hindlimb muscles of the $SOD1^{G93A}$ mice become progressively weaker in the course of disease progression, and significant changes occur to the contractile characteristics of the hindlimb muscles.

The results presented here also show that treatment with MGF did not significantly change the contractile characteristics of $SOD1^{G93A}$ mice hind limb muscles. However, in

EDL muscles there was a significant improvement in the speed of contraction in IGF-I treated $SOD1^{G93A}$ mice compared to vehicle treated $SOD1^{G93A}$ mice. The time to peak in the IGF-I treated $SOD1^{G93A}$ mice is significantly faster compared to MGF treated $SOD1^{G93A}$ mice. Therefore IGF-I is more effective than MGF in improving the speed of contraction, in the EDL muscle. However although the results did not reach significance there was a trend towards an improvement in the ½ relaxation time in TA muscles of MGF and IGF-I treated $SOD1^{G93A}$ mice.

The prolonged half relaxation time in the hind limb muscles $SOD1^{G93A}$ mice may be the result of a slower rate of calcium reuptake by the sarcoplasm reticulum. The speed of relaxation of the muscle requires calcium to be rapidly pumped back into the sarcoplasmic reticulum by calcium pump (Ca^{2+}ATPase). The Ca^{2+}ATPase activity has a faster rate in fast twitch muscles and slower rate in slow twitch muscles. Therefore at end-stage, the prolonged half relaxation time in TA and EDL muscles may result from the disease-related changes in muscle phenotype, which shifts towards a slow muscle phenotype.

4.3.4 Fatigue characteristics of EDL muscles in MGF and IGF-I treated $SOD1^{G93A}$ mice

The results of this study show that treatment with MGF and IGF-I in the $SOD1^{G93A}$ mice, at 70 days of age, preserves the fast fatigable phenotype of the EDL muscle. EDL is normally a fast muscle that fatigues rapidly when repeatedly stimulated, producing a characteristic fatigue pattern. In $SOD1^{G93A}$ mice there is a marked change in the characteristic fatigue pattern of the EDL muscle as a consequence of disease progression (Sharp et al., 2005). At 120 days the EDL muscle in the $SOD1^{G93A}$ mice, has an increased fatigue resistance that resembles a phenotype of a slow muscle. The changes in the muscle fatigability are likely to be the result of altered muscle function. Since muscle fibre phenotype is known to be determined by the activity of innervating motoneurons (Navarrete and Vrbova, 1984), changes in the muscle phenotype can reflect altered motoneuron activity.

The changes in EDL fatigue characteristics in $SOD1^{G93A}$ mice are similar to those that occur in the EDL following neonatal nerve injury. It is well established that during early postnatal development nerve injury results in denervation and the loss of a large number of motoneurons (Lowrie et al., 1987). Postnatal nerve injury also results in a marked change in the reinnervated muscle phenotype. The fast fatigable EDL muscle changes towards a slower fatigue resistant muscle, although slow twitch muscles do not alter thier phenotype (Lowrie and Vrbova, 1984; Lowrie et al., 1987). The change in phenotype of fast muscles, towards a phenotype characteristic of a slow muscle, may result from an altered firing pattern of the surviving motoneurons. The firing pattern of normal motor units in fast fatigable muscle is phasic and high frequency, accompanied by the expression of muscles fibres with a low oxidative capacity and fast myosin. Slow fatigue-resistant muscles normally have a tonic low frequency motor unit activity pattern, and express slow myosin. Postnatal nerve injury dramatically alters the firing patterns of fast fatigable muscle, resulting in a tonic motor activity pattern, which is associated with slow twitch muscle (Navarrete and Vrbova, 1983) and altered myosin composition. The changes of the motor unit activity patterns, in fast fatigable muscle, are associated predominately with an increased oxidative capacity of muscle fibers and slow myosin expression (Lowrie et al., 1987). The marked changes in muscle phenotype which occur as a result of neonatal nerve injury are similar to those shown in this study of the $SOD1^{G93A}$ EDL muscle. Alterations in the motoneuron firing pattern may occur prior to or as a direct result of motoneuron degeneration and have a dramatic effect on muscle function.

It is well established that the excitability of motoneurons is related to morphology, small motoneurons have a lower threshold for excitation and a sustained firing pattern compared to larger motoneurons (Henneman et al., 1965). Large α motoneurons are known to be preferentially vulnerable to cell death in ALS (Kieran et al., 2004; Fischer et al., 2004; Mohajeri et al., 1998). Motoneuron degeneration may preferentially preserve small motoneurons and the size of the remaining motoneurons can directly relate to the higher excitability of motoneurons. An increased excitability in motoneuron activity could possibly be the result of reduction in the size of motoneurons which

normally innervate fast muscles. The altered excitability of the motoneurons could underline the change in muscle phenotype observed as a consequence of disease progression in the $SOD1^{G93A}$ mice.

It is also possible that there is a selective loss of particular motoneuron subtypes. Previous studies have shown an increased selective loss of fast fatigable motoneurons compared to slow fatigue-resistant motoneurons (Frey et al., 2000; Pun et al., 2006). These authors reported a preferential denervation at neuromuscular synapse of fast fatigable motoneurons, occurring prior to symptom onset in the $SOD1^{G93A}$ mice (Frey et al., 2000; Pun et al., 2006). The remaining motoneuron innervating muscles are slow fatigue-resistant motoneurons.

The changes in the EDL muscle phenotype in the $SOD1^{G93A}$ mice may be due to the selective denervation/reinnervation in skeletal muscle that occurs in $SOD1^{G93A}$ mice prior to the loss of motoneurons (Chiu et al., 1995). As the disease proceeds and there is a progressive degeneration of motoneurons, the axons of the remaining motoneurons sprout. Due to the progressive nature of the disease, continued sprouting of motor axons occurs, and this compensatory sprouting may compromise motoneurons and render them susceptible to cell death (White et al., 2000).

The oxidative capacity of the EDL muscle in $SOD1^{G93A}$ mice is known to dramatically alter as a consequence of disease progression, as shown by the staining pattern of succinate dehydrogenase (SDH), a marker of the oxidative capacity of the muscle. In WT EDL muscle there is a mosaic pattern for SDH staining, with the majority of muscles fibres staining lightly. This characteristic staining pattern is dramatically altered in the EDL muscle from vehicle treated $SOD1^{G93A}$ mice at 120 days of age, where there are a greater proportion of darkly stained muscles fibres, indicating an increased oxidative capacity in the EDL muscle of the $SOD1^{G93A}$ mice. This change in the oxidative metabolism of EDL muscle of the $SOD1^{G93A}$ mice has been observed in previous studies (Kieran et al., 2004; Sharp et al., 2005; Bilsland et al., 2006) and is associated with changes in the myosin isoforms, indicative of a change in the muscle

phenotype. The results from this study show that treatment with MGF, in the EDL muscle of the $SOD1^{G93A}$ mice, results in distinctly heterogeneous, staining patterns similar to that observed in the WT muscle, with both darkly and lightly stained muscle fibers, indicating a preservation of the fast fatigable glycolytic muscle phenotype.

It is known that during the disease progression of the $SOD1^{G93A}$ mice there is age-related change in the muscle phenotype, at a symptomatic stage; fast fatigable glycolytic muscle becomes converted towards a slow oxidative and fatigue resistant muscle. The results from this study show that treatment with MGF and IGF-I at 70 days of age preserves muscle fibre phenotype in the EDL muscle of the $SOD1^{G93A}$ mice.

The staining pattern of succinate dehydrogenase (SDH), shows both treatment with IGF-I and MGF increase lightly stained muscle fibers, however IGF-I does not preserve fibre size, there are a large proportion of smaller diameter muscle fibres . It appears that IGF-I muscle fibres also have a pattern of muscle fibre grouping which may be due to the selective denervation/reinnervation in skeletal muscle occurring. Whereas MGF preserves muscle fibers size and contractile force, the maintenance of muscle phenotype may be attributed to a promotion of innervation.

4.3.5 MGF preserves motor units in $SOD1^{G93A}$ mice

The number of motor units that innervated the EDL muscle was assessed at 120 days of age. In $SOD1^{G93A}$ mice there was a significant reduction (66%) in the number of surviving motor units in the EDL muscle compared to EDL muscle wild-type mice. This is in agreement with previous reports, wherein a reduction by 60% number of surviving motor units was shown in the EDL muscle (Kieran et al., 2004; Sharp et al., 2003; Bilsland et al., 2006). There is a selective and progressive loss of motor units in the hindlimb muscles of $SOD1^{G93A}$ mice as the disease progresses. In MGF and IGF-I treated $SOD1^{G93A}$ mice there was a significant increase in motor unit survival, so that 33%, more motor units survived compared to vehicle treated $SOD1^{G93A}$ mice. Thus treatment with MGF and IGF-I were equally as effective in rescuing motor units in $SOD1^{G93A}$ mice.

4.3.6 MGF expression improves motoneuron survival in SOD1^{G93A} mice

In addition to its beneficial effects on muscle function in SOD1^{G93A} mice, IGF-I is also known to have significant neuroprotective effects on motoneurons (Kaspar et al., 2003; Kaspar et al., 2005; Nagano et al., 2005; Narai et al., 2005). In this study, following treatment at 70 days, IGF-I treatment resulted in a 41% improvement in motoneuron survival. However following treatment with MGF, more motoneurons survived, so that there was a 73% improvement in motoneuron survival in MGF treated SOD1^{G93A} mice compared to vehicle treated mice at 120 days of age. Both IGF-I and MGF significantly improved motoneuron survival in SOD1^{G93A} mice, yet MGF rescues significantly more motoneurons than IGF-I ($P \leq 0.016$), suggesting a greater neuroprotective potency.

4.3.7 MGF expression promotes muscle regeneration in SOD1^{G93A} mice

There is considerable muscle weakness and atrophy in skeletal muscle, as a consequence of disease progression in SOD1^{G93A} mice. This study shows that treatment with MGF is able to preserve the phenotype and some of the normal functional properties of TA and EDL muscles. It is known that skeletal muscle has the ability to repair itself following injury or disease. In response to mechanical overload or muscle injury, MGF, a splice variant of IGF-1, is upregulated and acts to promote skeletal muscle regeneration (Hill and Goldspink, 2003). The upregulation of MGF can be considered as a "local tissue repair factor" for skeletal muscle. This study shows that enhanced levels of MGF, by gene transfer, proved effective in preventing the disease-related changes in skeletal muscle that occur in SOD1^{G93A} mice. There is further evidence, in this study, to suggest that treatment with MGF, promotes regeneration of muscles. Histological examination shows the presence of centralized nuclei, a hallmark of satellite cell activation, in the TA muscle of MGF treated SOD1^{G93A} mice at 120 days of age. The existence of centralized nuclei in muscle is indicative of recent fusion of activated satellite cells to existing myofibres (Barton et al., 1999). The capacity of quiescent satellite cells to be activated and enter the cell cycle and provide the precursors, needed for the formation of new muscles, underlies the regenerative capacity of skeletal muscle (Wozniak et al., 2005). Previous studies have shown that MGF is involved in the activation of satellite cells

(Hill and Goldspink, 2003). IGF-I has also been shown to activate satellite cells, and is believed to underlie the functional hypertrophy in muscle, by increased muscle regeneration (Barton et al., 1999). In double transgenic mice, with muscle restricted expression of IGF-IEa and the $SOD1^{G93A}$ mutation, muscle atrophy was substantially attenuated and in addition there were hallmarks of satellite cell activity and fibre maturation, centralized nuclei, Pax7, desmin, myogenin and neonatal myosin heavy chain.

The contribution of satellite cells to sustaining the mass of denervated muscle is one proposed mechanism for the maintenance of muscle phenotype. However a crucial factor for the restoration of muscle phenotype is reinnervation. It is possible that MGF expression promotes muscle regeneration in $SOD1^{G93A}$ mice, but may also act to reduce denervation and promote innervation at the level of the neuromuscular junction.

4.3.8 MGF mechanism for neuroprotection

The results presented here show that gene transfer of MGF to the hind limb muscles of $SOD1^{G93A}$ mice clearly delays disease progression by improving motoneuron survival resulting in an increase in muscle force and motor unit survival. The muscle-restricted expression of MGF indicates that the neuroprotective effects of MGF may act via mechanisms that are independent of retrograde transport to the motoneuron cell body. Examination of the spinal cord showed no evidence of MGF expression within motoneurons or glial cells of MGF treated $SOD1^{G93A}$ mice. The neuroprotective mechanism for MGF is not completely understood. However IGF-I, is known to act through the phosphatidylinositol 3-kinase (PI3-K)/Akt pathway to promote neuronal survival (Dudek et al., 1997) and activate anti-apoptotic cascades (Trejo et al., 2004). The binding and activation of IGF-1 to the extracellular domain IGF-I receptor (IGF-IR), results in the phosphorylation of the insulin receptor substrates IRS-1 IRS-2, which leads to the activation of two downstream signalling cascades for neuronal survival: mitogen-activated protein kinase (MAPK) kinase (MEK)/ extracellular-signal-regulated kinase (ERK) and PI3-K/Akt pathways (Dudek et al., 1997).

In a recent study comparing IGF-IEa to MGF using viral mediated delivery targeted at TA and EDL muscles, there was an increased activation of PI3-K /AKT and MAPK pathways following treatment with both IGF-1 isoforms. Surprisingly, MGF significantly promoted the phosphorylated ERK1/2 and the IGF-I receptor (IGF-IR) in muscle compared to IGF-Ia isoform (Barton, 2006). These results are not in agreement with previous studies, that suggest that the MGF C-terminal lacks the domain responsible for IGF-I receptor binding, (Yang and Goldspink, 2002) and signals through an IGF-I receptor independent mechanism. Further studies have shown that MGF exerts neuroprotective effects independent of the IGF-I receptor (Dluzniewska et al., 2005). Therefore the neuroprotective potential of MGF may act through a novel receptor independent of the known IGF-I receptor. Further studies are required to determine the precise mechanisms for the neuroprotective potential of MGF.

4.3.9 Therapeutic potential of MGF for ALS patients

ALS is a relentless disease, for which, disappointingly there is no effective treatment or cure to date, therefore there is considerable research aimed at developing potential therapies to ameliorate the disease progression. ALS is characterized by a decline in muscle function resulting in muscle weakness. The results in this study show MGF can promote muscle repair and regeneration, in addition to protecting neurons from cell death. This study aimed to evaluate the treatment with MGF in a particular group of hind limb muscles in $SOD1^{G93A}$ mice and to determine the potential of MGF to ameliorate the disease progression.

The results, presented in this study, show that increasing expression levels of MGF in skeletal muscle of $SOD1^{G93A}$ mice improved muscle function and furthermore protected motoneurons from cell death. MGF therefore delayed the disease progression in $SOD1^{G93A}$ mice. This is proof of principle that MGF may be of therapeutic value for both delaying muscle atrophy and degeneration of motoneurons. Further evidence is required to confirm the therapeutic potential of MGF, and determine whether MGF could extend the lifespan in $SOD1^{G93A}$ mice.

Treatment with a stable synthetic MGF c-terminal peptide, has been used previously in a gerbil model of transient brain ischemia (Dluzniewska et al., 2005). The modified PEGylated c-terminal MGF peptide was administered as a single bolus injection, intra-arterially following an ischemic insult and resulted in an increased survival of CA1 hippocampal neurons. Furthermore, neuronal survival after global brain ischemia was associated with increased expression of endogenous MGF (Dluzniewska et al., 2005).

It would appear that strategies to specifically up-regulate MGF expression in both muscle and motoneurons, could be a viable approach for ALS therapies. There are two possible mechanisms to up-regulate MGF expression, either by directly augmenting exogenous MGF, or alternately up-regulating endogenous MGF expression. Gene therapy techniques, such as using cDNA or viral vectors, may not be a feasible method for patients, due to risks of tumor growth. There are several other alternatives for administering exogenous MGF: using the stable peptide either intramuscularly via injections or continuously by intrathecal infusion using an osmotic mini-pump.

A failure of IGF-I in previous clinical trials may be due not only to ineffective delivery of IGF-I to the CNS. And it may be that a successful therapeutic strategy, requires combined therapies (Carri et al., 2006). The most appropriate administration method to deliver MGF requires further investigation. Further studies are required to determine the mechanism by which muscle restricted expression of MGF exerts neuroprotection.

4.3.10 Further research

There are further investigations which can be carried out to determine the additional mechanisms of MGF in $SOD1^{G93A}$ mice. It still remains unknown whether treatment with MGF in $SOD1^{G93A}$ mice, provides any beneficial effect to non-neuronal cells in the CNS. The therapeutic potential of MGF could be further investigated in non-neuronal cells, such as microglia and astrocytes, as neuroinflammation and astrogliosis are prominent features in ALS (Appel and Simpson, 2001). Since IGF-I has been shown to attenuate the increased in TNF-α expression at end-stage in $SOD1^{G93A}$ mice

(Dobrowolny et al., 2005). There may be altered levels of the pro-inflammatory cytokine such as TNF-α and interleukin (IL)-1beta in MGF treated $SOD1^{G93A}$ mice. At present there are no studies that have shown whether MGF can alter the release of pro-inflammatory cytokines. IGF-I has also been shown to significantly reduce astrogliosis in $SOD1^{G93A}$ mice (Kaspar et al., 2003). Further studies could determine the extent of astrogliosis by GFAP staining in MGF treated $SOD1^{G93A}$ mice and identify whether MGF has the potential to modulate the inflammatory response in $SOD1^{G93A}$ mice.

There is evidence that IGF-I promotes neuronal survival by inhibiting apoptosis, through a PI3-kinase/Akt pathway (Dudek et al., 1997). IGF-I has been reported to increase the phosphorylated state of Akt, a protein kinase that is involved in blocking pro-apoptotic pathways, through a receptor mediated PI3-kinase pathway (Kulik and Weber, 1998; Palazzolo et al., 2007). Akt has been shown to stimulate the phosphorylation of the pro-apoptotic protein Bad, thereby inhibiting the pro-apoptotic functions of Bad (Datta et al., 1997; del Peso et al., 1997). Further studies could be carried out to identify whether MGF has anti-apoptotic actions in $SOD1^{G93A}$ mice. By examining spinal cord homogenates of MGF treated $SOD1^{G93A}$ mice, using western blot analysis levels of phosphorylated Akt could be determined. A feature of apoptosis includes the cleavage of caspase -3 and caspase -9 and using western blot analysis levels of caspase cleavage could be determined in MGF treated $SOD1^{G93A}$ mice. Together these studies could determine the possible anti-apoptotic actions of MGF in $SOD1^{G93A}$ mice, an increased level of phosphorylated Akt and suppressing activation of caspases would provide evidence for an anti- apoptotic mechanism.

The observation of centralized nuclei in muscle exclusively of MGF treated $SOD1^{G93A}$ mice, suggests activation of satellite cells. To confirm this possible mechanism of muscle regeneration other hallmarks of satellite cell activity and fibre maturation could be investigated. Makers of muscle regeneration such as Pax7, desmin, myogenin and neonatal myosin heavy chain could be analyzed by western blot analysis using muscle protein lysate. An increase in these markers would suggest that the activation of satellite

cells and muscle regeneration is likely mechanism for the maintenance of muscle phenotype in $SOD1^{G93A}$ mice.

The modified PEGylated c-terminal MGF peptide used previously (Dluzniewska et al., 2005) may be an alternatives method for administering MGF to $SOD1^{G93A}$ mice either intramuscularly via injections or continuously by intrathecal infusion using an osmotic mini-pump. Administering MGF in a peptide form may extend the lifespan in $SOD1^{G93A}$ mice, as well as ameliorating the disease progression. Treatment with MGF administered at a symptomatic stage in $SOD1^{G93A}$ mice, may prove to be affective at ameliorating the muscle atrophy and protecting motoneuron loss. However it remains to be shown whether MGF is affective at a symptomatic stage in $SOD1^{G93A}$ mice. The modified PEGylated c-terminal MGF peptide could be used at 90 days of age a symptomatic stage in $SOD1^{G93A}$ mice to examine the efficacy of MGF at this stage in the disease.

4.4 CONCLUSIONS

The results of this study show that treatment with MGF in $SOD1^{G93A}$ mice at 70 days of age, an presymptomatic stage, rescues motoneurons and results in a substantial functional improvement in muscle force, contractile characteristics, and motor unit number. This study highlights the potential therapeutic role of MGF for patients with ALS and identifies the muscle as an accessible target for intervention in therapeutic strategies for motoneuron disease.

CHAPTER 5

GENERAL DISCUSSION

5.1. Aims of Thesis

The aim of this thesis was to investigate the possible involvement of skeletal muscle in the pathogenesis of ALS and determine whether targeting skeletal muscle could be a successful therapeutic strategy for the treatment of ALS.

ALS is characterised by the degeneration of motoneurons accompanied by significant muscle atrophy. The precise molecular mechanism underlying the selective vulnerability of motoneurons in ALS remains unclear however it seems increasingly apparent that the pathogenesis of ALS is not exclusive to motoneurons, but is a multi-system disorder. In the CNS mutant SOD1-mediated toxicity occurs in motoneurons as well as surrounding non-neuronal cells. However our understanding of the effect that expression of mutant SOD1 on interaction between motoneurons and skeletal muscle has not previously been directly investigated. The experiments presented in Chapter 3 investigated the effect of mutant SOD1 in muscle and the influence of motoneurons on the cellular properties of muscle in an *in vitro* co-culture model. In Chapter 4 the experiments examined the potential neuroprotective effects of treatment with an IGF-I splice variant, MGF in $SOD1^{G93A}$ mice. Since previous studies have established the efficacy of treatment with IGF-I in $SOD1^{G93A}$ mice, in order to evaluate the relative efficacy of MGF, a direct comparison of IGF-I and MGF was made. Taken together the results presented in this thesis contribute to our understanding of the involvement of skeletal muscle in the pathogenesis of ALS and furthermore identify the skeletal muscle as a potential therapeutic target for ALS.

5.2 The effect of mutant SOD1 expression on the cellular properties of skeletal muscle and motoneurons

The main evidence for the involvement of skeletal muscle in the pathogenesis of ALS has arisen from the analysis of muscle biopsies from symptomatic ALS patients or from autopsy/post-mortem studies (Afifi et al., 1966; Siklos et al., 1996b; Vielhaber et al., 2000; Wiedemann et al., 1998). However, it remains unclear whether changes observed in ALS muscles are specific to ALS patients, or whether similar changes can be

observed in muscle from patients with chronic denervated muscle (Krasnianski et al., 2006). Interestingly, one of the earliest pathological changes observed in tissue from ALS patients is abnormal mitochondrial structure and mitochondrial dysfunction in muscle biopsies from ALS patients (Afifi et al., 1966; Siklos et al., 1996b; Vielhaber et al., 2000; Wiedemann et al., 1998; Dupuis et al., 2003; Soraru et al., 2007). However, it is unclear whether this is a primary cause or a contributing factor to the pathogenesis of ALS. The major limitation of using human samples is that it is usually only possible to assess alterations in muscle well after disease onset. Therefore, in this thesis using a transgenic mouse model of ALS, the cellular function of muscle was determined prior to disease onset, at an early presymptomatic stage of development.

The findings outlined in Chapter 3, provide evidence for the involvement of mitochondrial dysfunction and aberrant calcium handling arising from the expression of the mutant SOD1 enzyme, in skeletal muscles at an early stage in development. The reductions in the mitochondrial redox state and reduced mitochondrial membrane potential, suggest an inhibition of respiration, which may result from reduced ATP generation. In line with these results, mitochondrial uncoupling, reductions in respiratory control ratio and reduced ATP levels have also been identified in mutant SOD1 muscle (Dupuis et al., 2003).

Interestingly, mutant SOD1 muscles cultured in the absence of motoneurons had a greater reduction in the mitochondrial membrane potential, than muscles in co-cultured with motoneurons of either genotype. Therefore non-innervated muscle may be more vulnerable to mitochondrial dysfunction, and interaction with the motoneuron may act to reduce metabolic stress of muscle cells. It is possible that un-innervated skeletal muscle cells are in a heighten state of metabolic stress, so that the reciprocal interaction between motoneurons and muscles improves the cellular function of muscles.

Under basal conditions there is a reduction in mitochondrial membrane potential in motoneurons of either genotype. Moreover this reduction in mitochondrial membrane potential is further exacerbated by co-culturing motoneurons of either genotype with

$SOD1^{G93A}$ myotubes. This may reflect a defective mechanism in maintaining the mitochondrial membrane potential in motoneurons which cannot be rectified by contact with muscle cells, or may be a direct influence of mutant SOD1 muscles on motoneurons. These results show that the expression of mutant SOD1 disrupts the mitochondrial membrane potential of motoneurons, and this may be responsible for the enhanced mitochondrial dysfunction observed in motoneurons in the pathogenesis of ALS.

Importantly the results from **Chapter 3** also show that the reduction in mitochondrial membrane potential is not exclusive to motoneurons and muscles, but also occurs in other cell types that express mutant SOD1, such as fibroblasts which are not thought to play a role in ALS pathogenesis. These findings support the possibilities that mutant SOD1-mediated toxicity affects cells that are not implicated in ALS. It is also possible that the reduction in mitochondrial membrane potential is not necessarily a pathological feature and always detrimental to cellular function. A further explanation is that fibroblasts may be involved in the pathogenesis although there is no evidence to date. The most likely explanation for these findings are that motoneurons have a heighten vulnerability to alterations in mitochondrial function compared to other cells. Previous studies have also shown that embryonic motoneurons already have an increased excitability, possibly due to an increased persistent sodium conductance increasing excitability in motoneurons (Pieri et al., 2003; Kuo et al., 2004; Kuo et al., 2005). Embryonic motoneurons have also been shown to have deficits in axonal transport (Kieran et al., 2005; De Vos et al., 2007) and mitochondrial dysfunction. It is therefore well established that motoneurons are susceptible cell to many cellular functions and a reduction in mitochondrial membrane potential shown in this study may affect motoneurons to a greater extent than other cell types.

Mitochondrial calcium uptake depends on mitochondrial membrane potential and changes in the mitochondrial membrane potential can influence cytosolic calcium signalling. In **Chapter 3**, the results showed that a reduction in mitochondrial membrane potential correlated with a significantly increased the rate of propagation of the calcium

waves in mutant SOD1 muscle. This may imply an impaired mitochondrial calcium uptake mechanism. There was also evidence of dysregulated cytosolic calcium activity in motoneurons in co-cultures. Mutant SOD1-expressing motoneurons co-cultured with mutant SOD1 or WT muscle were shown to have an increased intracellular calcium response of to glutamate, which may indicate that there is a disruption in intracellular calcium homeostasis.

The findings in **Chapter 3** therefore highlight the involvement of mitochondrial dysfunction and aberrant calcium handling arising from the expression of the mutant SOD1 enzyme, in motoneurons and muscles at an early stage in development. The specific knockdown of mutant SOD1 specifically in muscle using siRNA has been shown to have no effect on disease progression (Miller et al., 2006). This finding suggests that muscle alone is not the primary target for mutant SOD1-mediated disease. However impairments in cellular function in mutant SOD1 muscle, reported in **Chapter 3** are likely to be major contributing factor in the pathogenesis of ALS.

In $SOD1^{G93A}$ mice motoneuron degeneration is preceded by the retraction of presynaptic terminals from muscle, leading to hypothesis that ALS is a "dying–back" axonopathy (Fischer et al., 2004). The results presented in this study do not support this hypothesis and rather support the possibility that there is a pre-existing mitochondrial dysfunction in both embryonic motoneurons and postnatal muscles and that peripheral denervation is the direct consequence of cellular dysfunction in both cell types. Alterations in mitochondrial function in motoneurons and muscle may accumulate over time and increase their susceptibility to other pathological factors.

5.3 The neuroprotective effects of treatment with Mechano-Growth Factor (MGF), in $SOD1^{G93A}$ mice

The muscle-derived growth factor MGF is known to protect neurons from a variety of insults, promoting muscle repair and regeneration (Aperghis et al., 2004; Ates et al., 2007; Cheema et al., 2005; Dluzniewska et al., 2005; Hameed et al., 2003; Hill and Goldspink, 2003; Mckoy et al., 1999; Yang et al., 1996; Yang and Goldspink, 2002). In

view of the unsuccessful clinical trials of a number of neurotrophic factors (Borasio et al., 1998; Miller et al., 1996; Aebischer et al., 1996) and the beneficial effects of targeting IGF-I directly to motoneurons and muscle in $SOD1^{G93A}$ mice (Kaspar et al., 2003; Kaspar et al., 2005; Dobrowolny et al., 2005; Nagano et al., 2005; Narai et al., 2005), the effect of treatment with MGF was examined in the $SOD1^{G93A}$ mouse model of ALS. MGF cDNA delivered via a mammalian expression plasmid to skeletal muscle in $SOD1^{G93A}$ mice, resulted in an improvement in muscle strength, an increase in motor unit survival and motoneuron survival. These results highlight the potential of MGF to ameliorate disease progression and confirm the neuroprotective effects of MGF in $SOD1^{G93A}$ mice. These results represent a "proof of principle" and show that MGF can delay muscle atrophy and motoneuron degeneration in $SOD1^{G93A}$ mice. As a therapeutic strategy, augmenting levels of MGF in skeletal muscles of ALS patients may prove beneficial to muscles and motoneurons. In this study, only a restricted number of muscles were treated with MGF in order to establish the potential of MGF in this model. Clearly for MGF to have any therapeutic significance, an effective system of delivery to all muscles must be developed. One possibility is that the delivery of exogenous MGF may be achieved by using a stable peptide either continuously by intrathecal infusion, using a mini-pump or injections intramuscularly to ameliorate the disease progression. These results identify skeletal muscle as a target cell to deliver exogenous neurotrophic factors and support the hypothesis that neurotrophic support is limited in ALS.

5.4 Conclusion

The results presented in this thesis support previous findings that suggest that skeletal muscle play an important role in the pathogenesis of ALS. In summary, in this thesis I have established that:

i) Mutant SOD1 expression in skeletal muscle significantly influences mitochondrial function and calcium signalling in skeletal muscles at an early stage in development.

ii) Interaction with muscle influences the cellular function of motoneurons

iii) Enhancement of neurotrophic support to muscles, by treatment with a muscle derived growth factor, MGF, delays the disease-associated reduction in muscle function and improves motoneuron survival.

iv) Treatment with MGF is more effective at rescuing motoneurons in SOD1 mice than IGF-I.

v) Skeletal muscle is identified as an accessible and suitable target for the development of therapeutic strategies for the treatment of motoneuron diseases

Taken together, these findings support the hypothesis that ALS is a multi-system disorder, where alterations in the cellular function of different cell types occur. Therefore therapeutic strategies that involve multi-cellular targeting are likely to be more successful in the treatment of ALS than approaches that involve specific cellular populations such as motoneurons alone.

Reference List

(1999) A controlled trial of recombinant methionyl human BDNF in ALS: The BDNF Study Group (Phase III). Neurology 52:1427-1433.

(1996) A double-blind placebo-controlled clinical trial of subcutaneous recombinant human ciliary neurotrophic factor (rHCNTF) in amyotrophic lateral sclerosis. ALS CNTF Treatment Study Group. Neurology 46:1244-1249.

Abalkhail H, Mitchell J, Habgood J, Orrell R, de Belleroche J (2003) A new familial amyotrophic lateral sclerosis locus on chromosome 16q12.1-16q12.2. Am J Hum Genet 73:383-389.

Abe K, Pan LH, Watanabe M, Kato T, Itoyama Y (1995) Induction of nitrotyrosine-like immunoreactivity in the lower motor neuron of amyotrophic lateral sclerosis. Neurosci Lett 199:152-154.

Abe K, Pan LH, Watanabe M, Konno H, Kato T, Itoyama Y (1997) Upregulation of protein-tyrosine nitration in the anterior horn cells of amyotrophic lateral sclerosis. Neurol Res 19:124-128.

Acsadi G, Anguelov RA, Yang H, Toth G, Thomas R, Jani A, Wang Y, Ianakova E, Mohammad S, Lewis RA, Shy ME (2002) Increased survival and function of SOD1 mice after glial cell-derived neurotrophic factor gene therapy. Hum Gene Ther 13:1047-1059.

Adams L, Goldman D (1998) Role for calcium from the sarcoplasmic reticulum in coupling muscle activity to nicotinic acetylcholine receptor gene expression in rat. J Neurobiol 35:245-257.

Adem A, Ekblom J, Gillberg PG, Jossan SS, Hoog A, Winblad B, Aquilonius SM, Wang LH, Sara V (1994) Insulin-like growth factor-1 receptors in human spinal cord: changes in amyotrophic lateral sclerosis. J Neural Transm Gen Sect 97:73-84.

Aebischer P, Schluep M, Deglon N, Joseph JM, Hirt L, Heyd B, Goddard M, Hammang JP, Zurn AD, Kato AC, Regli F, Baetge EE (1996) Intrathecal delivery of CNTF using encapsulated genetically modified xenogeneic cells in amyotrophic lateral sclerosis patients. Nat Med 2:696-699.

Afifi AK, Aleu FP, Goodgold J, MacKay B (1966) Ultrastructure of atrophic muscle in amyotrophic lateral sclerosis. Neurology 16:475-481.

Alexianu ME, Ho BK, Mohamed AH, La Bella V, Smith RG, Appel SH (1994a) The role of calcium-binding proteins in selective motoneuron vulnerability in Amyotrophic lateral sclerosis. Ann Neurol 36:846-858.

Alexianu ME, Ho BK, Mohamed AH, La B, V, Smith RG, Appel SH (1994b) The role of calcium-binding proteins in selective motoneuron vulnerability in amyotrophic lateral sclerosis. Ann Neurol 36:846-858.

Alexianu ME, Kozovska M, Appel SH (2001) Immune reactivity in a mouse model of familial ALS correlates with disease progression. Neurology 57:1282-1289.

Anderson MJ, Cohen MW (1977) Nerve-induced and spontaneous redistribution of acetylcholine receptors on cultured muscle cells. J Physiol 268:757-773.

Andreassen OA, Ferrante RJ, klivenyi P, klein A, Shinobu LA, Epstein CJ, Beal MF (2000) Partial deficiency of manganese superoxide dismutase exacerbates a transgenic mouse model of Amyotrophic lateral sclerosis. Ann Neurol 47:447-455.

Aperghis M, Johnson IP, Cannon J, Yang SY, Goldspink G (2004) Different levels of neuroprotection by two insulin-like growth factor-I splice variants. Brain Res 1009:213-218.

Appel SH, Simpson EP (2001) Activated microglia: the silent executioner in neurodegenerative disease? Curr Neurol Neurosci Rep 1:303-305.

Arai T, Hasegawa M, Akiyama H, Ikeda K, Nonaka T, Mori H, Mann D, Tsuchiya K, Yoshida M, Hashizume Y, Oda T (2006) TDP-43 is a component of ubiquitin-positive tau-negative inclusions in frontotemporal lobar degeneration and amyotrophic lateral sclerosis. Biochem Biophys Res Commun 351:602-611.

Arakawa Y, Sendtner M, Thoenen H (1990) Survival effect of ciliary neurotrophic factor (CNTF) on chick embryonic motoneurons in culture: comparison with other neurotrophic factors and cytokines. J Neurosci 10:3507-3515.

Arrasate M, Mitra S, Schweitzer ES, Segal MR, Finkbeiner S (2004) Inclusion body formation reduces levels of mutant huntingtin and the risk of neuronal death. Nature 431:805-810.

Ates K, Yang SY, Orrell RW, Sinanan AC, Simons P, Solomon A, Beech S, Goldspink G, Lewis MP (2007) The IGF-I splice variant MGF increases progenitor cells in ALS, dystrophic, and normal muscle. FEBS Lett 581:2727-2732.

Atsumi T (1981) The ultrastructure of intramuscular nerves in amyotrophic lateral sclerosis. Acta Neuropathol (Berl) 55:193-198.

Azzouz M, Hottinger A, Paterna JC, Zurn AD, Aebischer P, Bueler H (2000) Increased motoneuron survival and improved neuromuscular function in transgenic ALS mice after intraspinal injection of an adeno-associated virus encoding Bcl-2. Hum Mol Genet 9:803-811.

Azzouz M, Ralph GS, Storkebaum E, Walmsley LE, Mitrophanous KA, Kingsman SM, Carmeliet P, Mazarakis ND (2004) VEGF delivery with retrogradely transported lentivector prolongs survival in a mouse ALS model. Nature 429:413-417.

Babcock DF, Hille B (1998) Mitochondrial oversight of cellular Ca2+ signaling. Curr Opin Neurobiol 8:398-404.

Barber SC, Mead RJ, Shaw PJ (2006) Oxidative stress in ALS: a mechanism of neurodegeneration and a therapeutic target. Biochim Biophys Acta 1762:1051-1067.

Barton D, Shoturma, Sweeney (1999) Contribution of satellite cells to IGF-I induced hypertrophy of skeletal muscle. Acta Physiologica Scandinavica 167:301-305.

Barton ER (2006) Viral expression of insulin-like growth factor-I isoforms promotes different responses in skeletal muscle. J Appl Physiol 100:1778-1784.

Baumgartner BJ, Shine HD (1998) Neuroprotection of spinal motoneurons following targeted transduction with an adenoviral vector carrying the gene for glial cell line-derived neurotrophic factor. Exp Neurol 153:102-112.

Beal MF, Ferrante RJ, Browne SE, Matthews RT, Kowall NW, Brown RH, Jr. (1997) Increased 3-nitrotyrosine in both sporadic and familial amyotrophic lateral sclerosis. Ann Neurol 42:644-654.

Beaulieu JM, Nguyen MD, Julien JP (1999) Late onset of motor neurons in mice overexpressing wild-type peripherin. J Cell Biol 147:531-544.

Bedlack RS, Traynor BJ, Cudkowicz ME (2007) Emerging disease-modifying therapies for the treatment of motor neuron disease/amyotropic lateral sclerosis. Expert Opin Emerg Drugs 12:229-252.

Beers DR, Henkel JS, Xiao Q, Zhao W, Wang J, Yen AA, Siklos L, McKercher SR, Appel SH (2006) Wild-type microglia extend survival in PU.1 knockout mice with familial amyotrophic lateral sclerosis. Proc Natl Acad Sci U S A 103:16021-16026.

Beers DR, Ho BK, Siklos L, Alexianu ME, Mosier DR, Mohamed AH, Otsuka Y, Kozovska ME, McAlhany RE, Smith RG, Appel SH (2001) Parvalbumin overexpression alters immune-mediated increases in intracellular calcium, and delays disease onset in a transgenic model of familial amyotrophic lateral sclerosis. J Neurochem 79:499-509.

Bello-Haas VD, Florence JM, Kloos AD, Scheirbecker J, Lopate G, Hayes SM, Pioro EP, Mitsumoto H (2007) A randomized controlled trial of resistance exercise in individuals with ALS. Neurology 68:2003-2007.

Beretta S, Sala G, Mattavelli L, Ceresa C, Casciati A, Ferri A, Carri MT, Ferrarese C (2003) Mitochondrial dysfunction due to mutant copper/zinc superoxide dismutase associated with amyotrophic lateral sclerosis is reversed by N-acetylcysteine. Neurobiol Dis 13:213-221.

Berridge MJ (1997) Elementary and global aspects of calcium signalling. J Physiol 499 (Pt 2):291-306.

Bilsland LG, Dick JR, Pryce G, Petrosino S, Di M, V, Baker D, Greensmith L (2006) Increasing cannabinoid levels by pharmacological and genetic manipulation delay disease progression in SOD1 mice. FASEB J 20:1003-1005.

Boillee S, Vande VC, Cleveland DW (2006) ALS: a disease of motor neurons and their nonneuronal neighbors. Neuron 52:39-59.

Boitier E, Rea R, Duchen MR (1999) Mitochondria exert a negative feedback on the propagation of intracellular Ca2+ waves in rat cortical astrocytes. J Cell Biol 145:795-808.

Borasio GD, Robberecht W, Leigh PN, Emile J, Guiloff RJ, Jerusalem F, Silani V, Vos PE, Wokke JH, Dobbins T (1998) A placebo-controlled trial of insulin-like growth factor-I in amyotrophic lateral sclerosis. European ALS/IGF-I Study Group. Neurology 51:583-586.

Braunstein GD, Reviczky AL (1987) Serum insulin-like growth factor-I levels in amyotrophic lateral sclerosis. J Neurol Neurosurg Psychiatry 50:792-794.

Brown MD (1973) Role of activity in the differentiation of slow and fast muscles. Nature 244:178-179.

Bruening W, Roy J, Giasson B, Figlewicz DA, Mushynski WE, Durham HD (1999) Up-regulation of protein chaperones preserves viability of cells expressing toxic Cu/Zn-superoxide dismutase mutants associated with amyotrophic lateral sclerosis. J Neurochem 72:693-699.

Bruijn LI, Becher MW, Lee MK, Anderson KL, Jenkins NA, Copeland NG, Sisodia SS, Rothstein JD, Borchelt DR, Price DL, Cleveland DW (1997) ALS-linked SOD1 mutant G85R mediates damage to astrocytes and promotes rapidly progressive disease with SOD1-containing inclusions. Neuron 18:327-338.

Bruijn LI, Houseweart MK, Kato S, Anderson KL, Anderson SD, Ohama E, Reaume AG, Scott RW, Cleveland DW (1998) Aggregation and motor neuron toxicity of an ALS-linked SOD1 mutant independent from wild-type SOD1. Science 281:1851-1854.

Bruton J, Tavi P, Aydin J, Westerblad H, Lannergren J (2003) Mitochondrial and myoplasmic [Ca2+] in single fibres from mouse limb muscles during repeated tetanic contractions. J Physiol 551:179-190.

Buchanan J, Sun YA, Poo MM (1989) Studies of nerve-muscle interactions in Xenopus cell culture: fine structure of early functional contacts. J Neurosci 9:1540-1554.

Buckingham M (2001) Skeletal muscle formation in vertebrates. Curr Opin Genet Dev 11:440-448.

Buckingham M, Bajard L, Chang T, Daubas P, Hadchouel J, Meilhac S, Montarras D, Rocancourt D, Relaix F (2003) The formation of skeletal muscle: from somite to limb. J Anat 202:59-68.

Buffelli M, Burgess RW, Feng G, Lobe CG, Lichtman JW, Sanes JR (2003) Genetic evidence that relative synaptic efficacy biases the outcome of synaptic competition. Nature 424:430-434.

Burt AM (1975) Choline acetyltransferase and acetylcholinesterase in the developing rat spinal cord. Exp Neurol 47:173-180.

Butovsky O, Talpalar AE, Ben Yaakov K, Schwartz M (2005) Activation of microglia by aggregated beta-amyloid or lipopolysaccharide impairs MHC-II expression and renders them cytotoxic whereas IFN-gamma and IL-4 render them protective. Mol Cell Neurosci 29:381-393.

Callaway EM, Soha JM, Van Essen DC (1987) Competition favouring inactive over active motor neurons during synapse elimination. Nature 328:422-426.

Camu W, Henderson CE (1992) Purification of embryonic rat motoneurons by panning on a monoclonal antibody to the low-affinity NGF receptor. J Neurosci Methods 44:59-70.

Canton T, Bohme GA, Boireau A, Bordier F, Mignani S, Jimonet P, Jahn G, Alavijeh M, Stygall J, Roberts S, Brealey C, Vuilhorgne M, Debono MW, Le Guern S, Laville M, Briet D, Roux M, Stutzmann JM, Pratt J (2001) RPR 119990, a novel alpha-amino-3-hydroxy-5-methyl-4-isoxazolepropionic acid antagonist: synthesis, pharmacological properties, and activity in an animal model of amyotrophic lateral sclerosis. J Pharmacol Exp Ther 299:314-322.

Cardona AE, Pioro EP, Sasse ME, Kostenko V, Cardona SM, Dijkstra IM, Huang D, Kidd G, Dombrowski S, Dutta R, Lee JC, Cook DN, Jung S, Lira SA, Littman DR, Ransohoff RM (2006) Control of microglial neurotoxicity by the fractalkine receptor. Nat Neurosci 9:917-924.

Caroni P, Becker M (1992) The downregulation of growth-associated proteins in motoneurons at the onset of synapse elimination is controlled by muscle activity and IGF1. J Neurosci 12:3849-3861.

Carri MT, Ferri A, Battistoni A, Famhy L, Gabbianelli R, Poccia F, Rotilio G (1997) Expression of a Cu, Zn superoxide dismutase typical of familial amyotrophic lateral sclerosis induces mitochondrial alteration and increase of cytosolic calcium concentration in transfected neuroblastoma SH-SY5Y cells. FEBS Lett 414:365-368.

Carri MT, Grignaschi G, Bendotti C (2006) Targets in ALS: designing multidrug therapies. Trends Pharmacol Sci 27:267-273.

Carriedo SG, Sensi SL, Yin HZ, Weiss JH (2000) AMPA exposures induce mitochondrial Ca^{2+} overload and ROS generation in spinal motor neurons in vitro. J Neurosci240-250.

Carriedo SG, Yin HZ, Weiss JH (1996) Motor neurons are selectively vulnerable to AMPA/kainate receptor-mediated injury in vitro. J Neurosci 16:4069-4079.

Carro E, Trejo JL, Busiguina S, Torres-Aleman I (2001) Circulating insulin-like growth factor I mediates the protective effects of physical exercise against brain insults of different etiology and anatomy. J Neurosci 21:5678-5684.

Chance PF, Rabin BA, Ryan SG, Ding Y, Scavina M, Crain B, Griffin JW, Cornblath DR (1998) Linkage of the gene for an autosomal dominant form of juvenile amyotrophic lateral sclerosis to chromosome 9q34. Am J Hum Genet 62:633-640.

Cheema U, Brown R, Mudera V, Yang SY, McGrouther G, Goldspink G (2005) Mechanical signals and IGF-I gene splicing in vitro in relation to development of skeletal muscle. J Cell Physiol 202:67-75.

Chen YZ, Bennett CL, Huynh HM, Blair IP, Puls I, Irobi J, Dierick I, Abel A, Kennerson ML, Rabin BA, Nicholson GA, Auer-Grumbach M, Wagner K, De Jonghe P, Griffin JW, Fischbeck KH, Timmerman V, Cornblath DR, Chance PF (2004) DNA/RNA helicase gene mutations in a form of juvenile amyotrophic lateral sclerosis (ALS4). Am J Hum Genet 74:1128-1135.

Cheroni C, Peviani M, Cascio P, Debiasi S, Monti C, Bendotti C (2005) Accumulation of human SOD1 and ubiquitinated deposits in the spinal cord of SOD1G93A mice during motor neuron disease progression correlates with a decrease of proteasome. Neurobiol Dis 18:509-522.

Chevalier-Larsen E, Holzbaur EL (2006) Axonal transport and neurodegenerative disease. Biochim Biophys Acta 1762:1094-1108.

Chiu AY, Zhai P, Dal Canto MC, Peters TM, Kwon YW, Prattis SM, Gurney ME (1995) Age-dependent penetrance of disease in a transgenic mouse model of familial amyotrophic lateral sclerosis. Mol Cell Neurosci 6:349-362.

Choi DW (1992) Excitotoxic cell death. J Neurobiol 23:1261-1276.

Chow I, Poo MM (1985) Release of acetylcholine from embryonic neurons upon contact with muscle cell. J Neurosci 5:1076-1082.

Clement AM, Nguyen MD, Roberts EA, Garcia ML, Boillee S, Rule M, McMahon AP, Doucette W, Siwek D, Ferrante RJ, Brown RH, Jr., Julien JP, Goldstein LS, Cleveland DW (2003) Wild-type nonneuronal cells extend survival of SOD1 mutant motor neurons in ALS mice. Science 302:113-117.

Cleveland DW (1999) From Charcot to SOD1: mechanisms of selective motor neuron death in ALS. Neuron 24:515-520.

Cleveland DW, Rothstein JD (2001) From Charcot to Lou Gehrig: deciphering selective motor neuron death in ALS. Nat Rev Neurosci 2:806-819.

Close R. (1964) Dynamic properties of fast and slow skeletal muscles of the rat during development. J Physiol 173:74-95.

Connold AL, Evers JV, Vrbova G (1986) Effect of low calcium and protease inhibitors on synapse elimination during postnatal development in the rat soleus muscle. Brain Res 393:99-107.

Corbo M, Hays AP (1992) Peripherin and neurofilament protein coexist in spinal spheroids of motor neuron disease. J Neuropathol Exp Neurol 51:531-537.

Cossu G, Tajbakhsh S, Buckingham M (1996) How is myogenesis initiated in the embryo? Trends Genet 12:218-223.

Cote F, Collard JF, Julien JP (1993) Progressive neuronopathy in transgenic mice expressing the human neurofilament heavy gene: a mouse model of amyotrophic lateral sclerosis. Cell 73:35-46.

Couillard-Despres S, Zhu Q, Wong PC, Price DL, Cleveland DW, Julien JP (1998) Protective effect of neurofilament heavy gene overexpression in motor neuron disease induced by mutant superoxide dismutase. Proc Natl Acad Sci U S A 95:9626-9630.

Cozzolino M, Ferri A, Ferraro E, Rotilio G, Cecconi F, Carri MT (2006) Apaf1 mediates apoptosis and mitochondrial damage induced by mutant human SOD1s typical of familial amyotrophic lateral sclerosis. Neurobiol Dis 21:69-79.

Dai Z, Peng HB (1993) Elevation in presynaptic Ca2+ level accompanying initial nerve-muscle contact in tissue culture. Neuron 10:827-837.

Dai Z, Peng HB (1995) Presynaptic differentiation induced in cultured neurons by local application of basic fibroblast growth factor. J Neurosci 15:5466-5475.

Dal Canto MC, Gurney ME (1994a) Developement of central Nervous system pathology in a murine transgenic mouse model of human amyotrophic lateral sclerosis. Am J Pathol1271-1279.

Dal Canto MC, Gurney ME (1995) Neuropathological changes in two lines of mice carrying a transgene for mutant human Cu,Zn SOD, and in mice overexpressing wild type human SOD: a model of familial amyotrophic lateral sclerosis (FALS). Brain Res 676:25-40.

Dal Canto MC, Gurney ME (1994b) Development of central nervous system pathology in a murine transgenic model of human amyotrophic lateral sclerosis. Am J Pathol 145:1271-1279.

Damiano M, Starkov AA, Petri S, Kipiani K, Kiaei M, Mattiazzi M, Flint BM, Manfredi G (2006) Neural mitochondrial Ca2+ capacity impairment precedes the onset of motor symptoms in G93A Cu/Zn-superoxide dismutase mutant mice. J Neurochem 96:1349-1361.

Daniels MP, Lowe BT, Shah S, Ma J, Samuelsson SJ, Lugo B, Parakh T, Uhm CS (2000) Rodent nerve-muscle cell culture system for studies of neuromuscular junction development: refinements and applications. Microsc Res Tech 49:26-37.

Datta SR, Dudek H, Tao X, Masters S, Fu H, Gotoh Y, Greenberg ME (1997) Akt phosphorylation of BAD couples survival signals to the cell-intrinsic death machinery. Cell 91:231-241.

De Vos KJ, Chapman AL, Tennant ME, Manser C, Tudor EL, Lau KF, Brownlees J, Ackerley S, Shaw PJ, McLoughlin DM, Shaw CE, Leigh PN, Miller CC, Grierson AJ (2007) Familial amyotrophic lateral sclerosis-linked SOD1 mutants perturb fast axonal transport to reduce axonal mitochondria content. Hum Mol Genet.

Dekkers J, Bayley P, Dick JR, Schwaller B, Berchtold MW, Greensmith L (2004) Over-expression of parvalbumin in transgenic mice rescues motoneurons from injury-induced cell death. Neuroscience 123:459-466.

del Peso L, Gonzalez-Garcia M, Page C, Herrera R, Nunez G (1997) Interleukin-3-induced phosphorylation of BAD through the protein kinase Akt. Science 278:687-689.

Derave W, Van Den BL, Lemmens G, Eijnde BO, Robberecht W, Hespel P (2003) Skeletal muscle properties in a transgenic mouse model for amyotrophic lateral sclerosis: effects of creatine treatment. Neurobiol Dis 13:264-272.

Di Giorgio FP, Carrasco MA, Siao MC, Maniatis T, Eggan K (2007) Non-cell autonomous effect of glia on motor neurons in an embryonic stem cell-based ALS model. Nat Neurosci 10:608-614.

Dluzniewska J, Sarnowska A, Beresewicz M, Johnson I, Srai SK, Ramesh B, Goldspink G, Gorecki DC, Zablocka B (2005) A strong neuroprotective effect of the autonomous C-terminal peptide of IGF-1 Ec (MGF) in brain ischemia. FASEB J 19:1896-1898.

Dobrowolny G, Giacinti C, Pelosi L, Nicoletti C, Winn N, Barberi L, Molinaro M, Rosenthal N, Musaro A (2005) Muscle expression of a local Igf-1 isoform protects motor neurons in an ALS mouse model. J Cell Biol 168:193-199.

Drachman DB, Frank K, Dykes-Hoberg M, Teismann P, Almer G, Przedborski S, Rothstein JD (2002) Cyclooxygenase 2 inhibition protects motor neurons and prolongs survival in a transgenic mouse model of ALS. Ann Neurol 52:771-778.

Duchen MR (2000) Mitochondria and Ca(2+)in cell physiology and pathophysiology. Cell Calcium 28:339-348.

Duchen MR (1999) Contribution of mitochondria to animal physiology: from homeostatic sensor to calcium signalling and cell death. J Physiol1-17.

Duchen MR (2004) Mitochondria in heath and disease: perspectives on a new mitochondrial biology. Mol Aspects of Med 25:451.

Dudek H, Datta SR, Franke TF, Birnbaum MJ, Yao R, Cooper GM, Segal RA, Kaplan DR, Greenberg ME (1997) Regulation of neuronal survival by the serine-threonine protein kinase Akt. Science 275:661-665.

Dulhunty AF, Haarmann CS, Green D, Laver DR, Board PG, Casarotto MG (2002) Interactions between dihydropyridine receptors and ryanodine receptors in striated muscle. Prog Biophys Mol Biol 79:45-75.

Dupuis L, Di Scala F, Rene F, de Tapia M, Oudart H, Pradat PF, Meininger V, Loeffler JP (2003) Up-regulation of mitochondrial uncoupling protein 3 reveals an early muscular metabolic defect in amyotrophic lateral sclerosis. FASEB J 17:2091-2093.

Dupuis L, Gonzalez de Aguilar JL, Oudart H, de Tapia M, Barbeito L, Loeffler JP (2004) Mitochondria in amyotrophic lateral sclerosis: a trigger and a target. Neurodegener Dis 1:245-254.

Duxson MJ, Vrbova G (1985) Inhibition of acetylcholinesterase accelerates axon terminal withdrawal at the developing rat neuromuscular junction. J Neurocytol 14:337-363.

Echtay KS, Roussel D, St Pierre J, Jekabsons MB, Cadenas S, Stuart JA, Harper JA, Roebuck SJ, Morrison A, Pickering S, Clapham JC, Brand MD (2002) Superoxide activates mitochondrial uncoupling proteins. Nature 415:96-99.

Engelhardt JI, Appel SH (1990) IgG reactivity in the spinal cord and motor cortex in amyotrophic lateral sclerosis. Arch Neurol 47:1210-1216.

Engelhardt JI, Appel SH, Jakab K, Garcia J, Stefani E (1991) Immune-mediated models of motor neuron destruction in the guinea pig. Adv Neurol 56:369-379.

Engelhardt JI, Siklos L, Komuves L, Smith RG, Appel SH (1995) Antibodies to calcium channels from ALS patients passively transferred to mice selectively increase intracellular calcium and induce ultrastructural changes in motoneurons. Synapse 20:185-199.

Ericson J, Morton S, Kawakami A, Roelink H, Jessell TM (1996) Two critical periods of Sonic Hedgehog signaling required for the specification of motor neuron identity. Cell 87:661-673.

Esteves TC, Brand MD (2005) The reactions catalysed by the mitochondrial uncoupling proteins UCP2 and UCP3. Biochim Biophys Acta 1709:35-44.

Facchinetti F, Sasaki M, Cutting FB, Zhai P, MacDonald JE, Reif D, Beal MF, Huang PL, Dawson TM, Gurney ME, Dawson VL (1999) Lack of involvement of neuronal nitric oxide synthase in the pathogenesis of a transgenic mouse model of familial amyotrophic lateral sclerosis. Neuroscience 90:1483-1492.

Ferrante RJ, Browne SE, Shinobu LA, Bowling AC, Baik MJ, MacGarvey U, Kowall NW, Brown RH, Jr., Beal MF (1997) Evidence of increased oxidative damage in both sporadic and familial amyotrophic lateral sclerosis. J Neurochem 69:2064-2074.

Fischer LR, Culver DG, Tennant P, Davis AA, Wang M, Castellano-Sanchez A, Khan J, Polak MA, Glass JD (2004) Amyotrophic lateral sclerosis is a distal axonopathy: evidence in mice and man. Exp Neurol 185:232-240.

Flanagan SW, Anderson RD, Ross MA, Oberley LW (2002) Overexpression of manganese superoxide dismutase attenuates neuronal death in human cells expressing mutant (G37R) Cu/Zn-superoxide dismutase. J Neurochem 81:170-177.

Flucher BE, Andrews SB (1993) Characterization of spontaneous and action potential-induced calcium transients in developing myotubes in vitro. Cell Motil Cytoskeleton 25:143-157.

Fray AE, Ince PG, Banner SJ, Milton ID, Usher PA, Cookson MR, Shaw PJ (1998) The expression of the glial glutamate transporter protein EAAT2 in motor neuron disease: an immunohistochemical study. Eur J Neurosci 10:2481-2489.

Frey D, Schneider C, Xu L, Borg J, Spooren W, Caroni P (2000) Early and selective loss of neuromuscular synapse subtypes with low sprouting competence in motoneuron diseases. J Neurosci 20:2534-2542.

Friedlander RM, Brown RH, Gagliardini V, Wang J, Yuan J (1997) Inhibition of ICE slows ALS in mice. Nature 388:31.

Garbuzova-Davis S, Willing AE, Zigova T, Saporta S, Justen EB, Lane JC, Hudson JE, Chen N, Davis CD, Sanberg PR (2003) Intravenous administration of human umbilical cord blood cells in a mouse model of amyotrophic lateral sclerosis: distribution, migration, and differentiation. J Hematother Stem Cell Res 12:255-270.

Gautam M, Noakes PG, Mudd J, Nichol M, Chu GC, Sanes JR, Merlie JP (1995) Failure of postsynaptic specialization to develop at neuromuscular junctions of rapsyn-deficient mice. Nature 377:232-236.

Glazner GW, Yadav K, Fitzgerald S, Coven E, Brenneman DE, Nelson PG (1997) Cholinergic stimulation increases thrombin activity and gene expression in cultured mouse muscle. Brain Res Dev Brain Res 99:148-154.

Goldspink G (2001).

Gong YH, Parsadanian AS, Andreeva A, Snider WD, Elliott JL (2000) Restricted expression of G86R Cu/Zn superoxide dismutase in astrocytes results in astrocytosis but does not cause motoneuron degeneration. J Neurosci 20:660-665.

Gordon T, Perry R, Tuffery AR, Vrbova GGG (1974) Possible mechanisms determining synapse formation in developing skeletal muscles of the chick. Cell Tissue Res 155:13-25.

Green DR, Kroemer G (2004) The pathophysiology of mitochondrial cell death. Science 305:626-629.

Greensmith L, Dick J, Emanuel AO, Vrbova G (1996) Induction of transmitter release at the neuromuscular junction prevents motoneuron death after axotomy in neonatal rats. Neuroscience 71:213-220.

Greensmith L, Hasan HI, Vrbova G (1994a) Nerve injury increases the susceptibility of motoneurons to N-methyl-D-aspartate-induced neurotoxicity in the developing rat. Neuroscience 58:727-733.

Greensmith L, Mentis GZ, Vrbova G (1994b) Blockade of N-methyl-D-aspartate receptors by MK-801 (dizocilpine maleate) rescues motoneurones in developing rats. Brain Res Dev Brain Res 81:162-170.

Greensmith L, Ng P, Mohaghegh P, Vrbova G (2000) Reducing transmitter release from nerve terminals influences motoneuron survival in developing rats. Neuroscience 97:357-362.

Greensmith L, Vrbova G (1992) Alterations of nerve-muscle interaction during postnatal development influence motoneurone survival in rats. Brain Res Dev Brain Res 69:125-131.

Greensmith L, Vrbova G (1996) Motoneurone survival: a functional approach. Trends Neurosci 19:450-455.

Greensmith L, Vrbova G (1991) Neuromuscular contacts in the developing rat soleus depend on muscle activity. Brain Res Dev Brain Res 62:121-129.

Gros-Louis F, Lariviere R, Gowing G, Laurent S, Camu W, Bouchard JP, Meininger V, Rouleau GA, Julien JP (2004) A frameshift deletion in peripherin gene associated with amyotrophic lateral sclerosis. J Biol Chem 279:45951-45956.

Guegan C, Vila M, Rosoklija G, Hays AP, Przedborski S (2001) Recruitment of the mitochondrial-dependent apoptotic pathway in amyotrophic lateral sclerosis. J Neurosci 21:6569-6576.

Gurney ME, Fleck TJ, Himes CS, Hall ED (1998) Riluzole preserves motor function in a transgenic model of familial amyotrophic lateral sclerosis. Neurology 50:62-66.

Gurney ME, Pu H, Chiu AY, Dal Canto MC, Polchow CY, Alexander DD, Caliendo J, Hentati A, Kwon YW, Deng HX, . (1994) Motor neuron degeneration in mice that express a human Cu,Zn superoxide dismutase mutation. Science 264:1772-1775.

Hadano S, et al. (2001) A gene encoding a putative GTPase regulator is mutated in familial amyotrophic lateral sclerosis 2. Nat Genet 29:166-173.

Hafezparast M, et al. (2003) Mutations in dynein link motor neuron degeneration to defects in retrograde transport. Science 300:808-812.

Hall ED, Oostveen JA, Gurney ME (1998b) Relationship of microglial and astrocytic activation to disease onset and progression in a transgenic model of familial ALS. Glia 23:249-256.

Hall ED, Oostveen JA, Gurney ME (1998a) Relationship of microglial and astrocytic activation to disease onset and progression in a transgenic model of familial ALS. Glia 23:249-256.

Hall ED, Oostveen JA, Gurney ME (1998c) Relationship of microglial and astrocytic activation to disease onset and progression in a transgenic model of familial ALS. Glia 23:249-256.

Hamburger V, Levi-Montalcini R (1949) Proliferation differentiation and degeneration in the spinal ganglia of the chick embryo under normal and experimental conditions. J Exp Zoology 111:457-501.

Hameed M, Orrell RW, Cobbold M, Goldspink G, Harridge SD (2003) Expression of IGF-I splice variants in young and old human skeletal muscle after high resistance exercise. J Physiol 547:247-254.

Heath PR, Tomkins J, Ince PG, Shaw PJ (2002) Quantitative assessment of AMPA receptor mRNA in human spinal motor neurons isolated by laser capture microdissection. Neuroreport 13:1753-1757.

Henkel JS, Beers DR, Siklos L, Appel SH (2006) The chemokine MCP-1 and the dendritic and myeloid cells it attracts are increased in the mSOD1 mouse model of ALS. Mol Cell Neurosci 31:427-437.

Henkel JS, Engelhardt JI, Siklos L, Simpson EP, Kim SH, Pan T, Goodman JC, Siddique T, Beers DR, Appel SH (2004) Presence of dendritic cells, MCP-1, and activated microglia/macrophages in amyotrophic lateral sclerosis spinal cord tissue. Ann Neurol 55:221-235.

Henneman E, Somjen G, Carpenter DOC (1965) Functional significance of cell size in spinal motoneurons. J Neurophysiol 28:560-580.

Hentati A, Ouahchi K, Pericak-Vance MA, Nijhawan D, Ahmad A, Yang Y, Rimmler J, Hung W, Schlotter B, Ahmed A, Ben Hamida M, Hentati F, Siddique T (1998) Linkage of a commoner form of recessive amyotrophic lateral sclerosis to chromosome 15q15-q22 markers. Neurogenetics 2:55-60.

Higgins CM, Jung C, Ding H, Xu Z (2002) Mutant Cu, Zn superoxide dismutase that causes motoneuron degeneration is present in mitochondria in the CNS. J Neurosci 22:RC215.

Hill M, Goldspink G (2003) Expression and splicing of the insulin-like growth factor gene in rodent muscle is associated with muscle satellite (stem) cell activation following local tissue damage. J Physiol 549:409-418.

Hirano A (1996) Neuropathology of ALS: an overview. Neurology 47:S63-S66.

Hirano A (1991) Cytopathology of amyotrophic lateral sclerosis. Adv Neurol 56:91-101.

Hirano A, Donnenfeld H, Sasaki S, Nakano I (1984a) Fine structural observations of neurofilamentous changes in amyotrophic lateral sclerosis. J Neuropathol Exp Neurol 43:461-470.

Hirano A, Nakano I, Kurland LT, Mulder DW, Holley PW, Saccomanno G (1984b) Fine structural study of neurofibrillary changes in a family with amyotrophic lateral sclerosis. J Neuropathol Exp Neurol 43:471-480.

Holzbaur EL, Howland DS, Weber N, Wallace K, She Y, Kwak S, Tchistiakova LA, Murphy E, Hinson J, Karim R, Tan XY, Kelley P, McGill KC, Williams G, Hobbs C, Doherty P, Zaleska MM, Pangalos MN, Walsh FS (2006) Myostatin inhibition slows muscle atrophy in rodent models of amyotrophic lateral sclerosis. Neurobiol Dis 23:697-707.

Hottinger AF, Fine EG, Gurney ME, Zurn AD, Aebischer P (1997) The copper chelator d-penicillamine delays onset of disease and extends survival in a transgenic mouse model of familial amyotrophic lateral sclerosis. Eur J Neurosci 9:1548-1551.

Howland DS, Liu J, She Y, Goad B, Maragakis NJ, Kim B, Erickson J, Kulik J, DeVito L, Psaltis G, DeGennaro LJ, Cleveland DW, Rothstein JD (2002) Focal loss of the glutamate transporter EAAT2 in a transgenic rat model of SOD1 mutant-mediated amyotrophic lateral sclerosis (ALS). Proc Natl Acad Sci U S A 99:1604-1609.

Huang CF, Flucher BE, Schmidt MM, Stroud SK, Schmidt J (1994) Depolarization-transcription signals in skeletal muscle use calcium flux through L channels, but bypass the sarcoplasmic reticulum. Neuron 13:167-177.

Hughes RA, Sendtner M, Thoenen H (1993) Members of several gene families influence survival of rat motoneurons in vitro and in vivo. J Neurosci Res 36:663-671.

Ikeda K, Iwasaki Y, Shiojima T, Kinoshita M (1996) Neuroprotective effect of various cytokines on developing spinal motoneurons following axotomy. J Neurol Sci 135:109-113.

Ince PG, Stout N, Shaw PJ, Slade J, Hunziker W, Heizmann CW, Baimbridge KG (1993) Parvalbumin and calbindin-D_{28k+}in the human motor system and in motor neuron disease. Neuropathol Appl Neurobiol 19:291-299.

Isaeva EV, Shirokova N (2003) Metabolic regulation of Ca2+ release in permeabilized mammalian skeletal muscle fibres. J Physiol 547:453-462.

Jaarsma D, Haasdijk ED, Grashorn JA, Hawkins R, van Duijn W, Verspaget HW, London J, Holstege JC (2000) Human Cu/Zn superoxide dismutase (SOD1) overexpression in mice causes mitochondrial vacuolization, axonal degeneration, and premature motoneuron death and accelerates motoneuron disease in mice expressing a familial amyotrophic lateral sclerosis mutant SOD1. Neurobiol Dis 7:623-643.

Jaarsma D, Rognoni F, van Duijn W, Verspaget HW, Haasdijk ED, Holstege JC (2001) CuZn superoxide dismutase (SOD1) accumulates in vacuolated mitochondria in transgenic mice expressing amyotrophic lateral sclerosis-linked SOD1 mutations. Acta Neuropathol (Berl) 102:293-305.

Jacobson J, Duchen MR (2004) Interplay between mitochondria and cellular calcium signalling. Mol Cell Biochem 256-257:209-218.

Jaimovich E, Reyes R, Liberona JL, Powell JA (2000) IP3 receptors, IP(3) transients and nucleus-associated Ca^{2+} signals in cultured skeletal muscle. Am J Physiol Cell PhysiolC998-C1010.

Jung C, Higgins CM, Xu Z (2002) Mitochondrial electron transport chain complex dysfunction in a transgenic mouse model for amyotrophic lateral sclerosis. J Neurochem 83:535-545.

Kabashi E, Agar JN, Taylor DM, Minotti S, Durham HD (2004) Focal dysfunction of the proteasome: a pathogenic factor in a mouse model of amyotrophic lateral sclerosis. J Neurochem 89:1325-1335.

Kanazawa I (2001) How do neurons die in neurodegenerative diseases? Trends Mol Med 7:339-344.

Karki S, Holzbaur EL (1995) Affinity chromatography demonstrates a direct binding between cytoplasmic dynein and the dynactin complex. J Biol Chem 270:28806-28811.

Kashihara Y, Kuno M, Miyata Y (1987) Cell death of axotomized motoneurones in neonatal rats, and its prevention by peripheral reinnervation. J Physiol 386:135-148.

Kaspar BK, Frost LM, Christian L, Umapathi P, Gage FH (2005) Synergy of insulin-like growth factor-1 and exercise in amyotrophic lateral sclerosis. Ann Neurol 57:649-655.

Kaspar BK, Llado J, Sherkat N, Rothstein JD, Gage FH (2003) Retrograde viral delivery of IGF-1 prolongs survival in a mouse ALS model. Science 301:839-842.

Kassar-Duchossoy L, Gayraud-Morel B, Gomes D, Rocancourt D, Buckingham M, Shinin V, Tajbakhsh S (2004) Mrf4 determines skeletal muscle identity in Myf5:Myod double-mutant mice. Nature 431:466-471.

Kasthuri N, Lichtman JW (2003) The role of neuronal identity in synaptic competition. Nature 424:426-430.

Kavanagh NI, Ainscow EK, Brand MD (2000) Calcium regulation of oxidative phosphorylation in rat skeletal muscle mitochondria. Biochim Biophys Acta 1457:57-70.

Kawahara Y, Ito K, Sun H, Aizawa H, Kanazawa I, Kwak S (2004) Glutamate receptors: RNA editing and death of motor neurons. Nature 427:801.

Kawamata T, Akiyama H, Yamada T, McGeer PL (1992) Immunologic reactions in amyotrophic lateral sclerosis brain and spinal cord tissue. Am J Pathol 140:691-707.

Kelly AM, Zacks SI (1969) The fine structure of motor endplate morphogenesis. J Cell Biol 42:154-169.

Kidokoro Y, Yeh E (1982) Initial synaptic transmission at the growth cone in Xenopus nerve-muscle cultures. Proc Natl Acad Sci U S A 79:6727-6731.

Kieran D, Hafezparast M, Bohnert S, Dick JR, Martin J, Schiavo G, Fisher EM, Greensmith L (2005) A mutation in dynein rescues axonal transport defects and extends the life span of ALS mice. J Cell Biol 169:561-567.

Kieran D, Kalmar B, Dick JR, Riddoch-Contreras J, Burnstock G, Greensmith L (2004) Treatment with arimoclomol, a coinducer of heat shock proteins, delays disease progression in ALS mice. Nat Med 10:402-405.

Kim HJ, Hwang NR, Lee KJ (2007) Heat shock responses for understanding diseases of protein denaturation. Mol Cells 23:123-131.

Kirkinezos IG, Bacman SR, Hernandez D, Oca-Cossio J, Arias LJ, Perez-Pinzon MA, Bradley WG, Moraes CT (2005) Cytochrome c association with the inner mitochondrial membrane is impaired in the CNS of G93A-SOD1 mice. J Neurosci 25:164-172.

Kirkinezos IG, Hernandez D, Bradley WG, Moraes CT (2003) Regular exercise is beneficial to a mouse model of amyotrophic lateral sclerosis. Ann Neurol 53:804-807.

Klivenyi P, Ferrante RJ, Matthews RT, Bogdanov MB, Klein AM, Andreassen OA, Mueller G, Wermer M, Kaddurah-Daouk R, Beal MF (1999) Neuroprotective effects of creatine in a transgenic animal model of amyotrophic lateral sclerosis. Nat Med 5:347-350.

Klivenyi P, Kiaei M, Gardian G, Calingasan NY, Beal MF (2004) Additive neuroprotective effects of creatine and cyclooxygenase 2 inhibitors in a transgenic mouse model of amyotrophic lateral sclerosis. J Neurochem 88:576-582.

Ko CP (1985) Formation of the active zone at developing neuromuscular junctions in larval and adult bullfrogs. J Neurocytol 14:487-512.

Koliatsos VE, Cayouette MH, Berkemeier LR, Clatterbuck RE, Price DL, Rosenthal A (1994) Neurotrophin 4/5 is a trophic factor for mammalian facial motor neurons. Proc Natl Acad Sci U S A 91:3304-3308.

Koliatsos VE, Clatterbuck RE, Winslow JW, Cayouette MH, Price DL (1993) Evidence that brain-derived neurotrophic factor is a trophic factor for motor neurons in vivo. Neuron 10:359-367.

Kong J, Xu Z (1998) Massive mitochondrial degeneration in motor neurons triggers the onset of amyotrophic lateral sclerosis in mice expressing a mutant SOD1. J Neurosci 18:3241-3250.

Kostic V, Jackson-Lewis V, de Bilbao F, Dubois-Dauphin M, Przedborski S (1997) Bcl-2: prolonging life in a transgenic mouse model of familial amyotrophic lateral sclerosis. Science 277:559-562.

Krasnianski A, Deschauer M, Krasnianski M, Zierz S (2006) Reply to 'Mitochondrial changes in skeletal muscle in amyotrophic lateral sclerosis and other neurogenic atrophies--a comment'. Brain 129:E41.

Kriz J, Gowing G, Julien JP (2003) Efficient three-drug cocktail for disease induced by mutant superoxide dismutase. Ann Neurol 53:429-436.

Kriz J, Nguyen MD, Julien JP (2002) Minocycline slows disease progression in a mouse model of amyotrophic lateral sclerosis. Neurobiol Dis 10:268-278.

Kroemer G, Galluzzi L, Brenner C (2007) Mitochondrial membrane permeabilization in cell death. Physiol Rev 87:99-163.

Kruman II, Pedersen WA, Springer JE, Mattson MP (1999) ALS-linked Cu/Zn-SOD mutation increases vulnerability of motor neurons to excitotoxicity by a mechanism involving increased oxidative stress and perturbed calcium homeostasis. Exp Neurol 160:28-39.

Kulik G, Weber MJ (1998) Akt-dependent and -independent survival signaling pathways utilized by insulin-like growth factor I. Mol Cell Biol 18:6711-6718.

Kuo JJ, Schonewille M, Siddique T, Schults AN, Fu R, Bar PR, Anelli R, Heckman CJ, Kroese AB (2004) Hyperexcitability of cultured spinal motoneurons from presymptomatic ALS mice. J Neurophysiol 91:571-575.

Kuo JJ, Siddique T, Fu R, Heckman CJ (2005) Increased persistent Na(+) current and its effect on excitability in motoneurones cultured from mutant SOD1 mice. J Physiol 563:843-854.

Lai EC, Felice KJ, Festoff BW, Gawel MJ, Gelinas DF, Kratz R, Murphy MF, Natter HM, Norris FH, Rudnicki SA (1997) Effect of recombinant human insulin-like growth factor-I on progression of ALS. A placebo-controlled study. The North America ALS/IGF-I Study Group. Neurology 49:1621-1630.

Lambrechts D, et al. (2003) VEGF is a modifier of amyotrophic lateral sclerosis in mice and humans and protects motoneurons against ischemic death. Nat Genet 34:383-394.

LaMonte BH, Wallace KE, Holloway BA, Shelly SS, Ascano J, Tokito M, Van Winkle T, Howland DS, Holzbaur EL (2002) Disruption of dynein/dynactin inhibits axonal transport in motor neurons causing late-onset progressive degeneration. Neuron 34:715-727.

Langman J, Haden CC (1970) Formation and migration of neuroblasts in the spinal cord of the chick embryo. J Comp Neurol 138:419-425.

Lariviere RC, Beaulieu JM, Nguyen MD, Julien JP (2003) Peripherin is not a contributing factor to motor neuron disease in a mouse model of amyotrophic lateral sclerosis caused by mutant superoxide dismutase. Neurobiol Dis 13:158-166.

Lee MK, Marszalek JR, Cleveland DW (1994) A mutant neurofilament subunit causes massive, selective motor neuron death: implications for the pathogenesis of human motor neuron disease. Neuron 13:975-988.

Lee S, Barton ER, Sweeney HL, Farrar RP (2004) Viral expression of insulin-like growth factor-I enhances muscle hypertrophy in resistance-trained rats. J Appl Physiol 96:1097-1104.

Leigh PN, Whitwell H, Garofalo O, Buller J, Swash M, Martin JE, Gallo JM, Weller RO, Anderton BH (1991) Ubiquitin-immunoreactive intraneuronal inclusions in amyotrophic lateral sclerosis. Morphology, distribution, and specificity. Brain 114 (Pt 2):775-788.

Levine JB, Kong J, Nadler M, Xu Z (1999) Astrocytes interact intimately with degenerating motor neurons in mouse amyotrophic lateral sclerosis (ALS). Glia 28:215-224.

Li L, Oppenheim RW, Lei M, Houenou LJ (1994) Neurotrophic agents prevent motoneuron death following sciatic nerve section in the neonatal mouse. J Neurobiol 25:759-766.

Li M, Ona VO, Guegan C, Chen M, Jackson-Lewis V, Andrews LJ, Olszewski AJ, Stieg PE, Lee JP, Przedborski S, Friedlander RM (2000) Functional role of caspase-1 and caspase-3 in an ALS transgenic mouse model. Science 288:335-339.

Ligon LA, LaMonte BH, Wallace KE, Weber N, Kalb RG, Holzbaur EL (2005) Mutant superoxide dismutase disrupts cytoplasmic dynein in motor neurons. Neuroreport 16:533-536.

Lino MM, Schneider C, Caroni P (2002) Accumulation of SOD1 mutants in postnatal motoneurons does not cause motoneuron pathology or motoneuron disease. J Neurosci 22:4825-4832.

Linseman DA, Phelps RA, Bouchard RJ, Le SS, Laessig TA, McClure ML, Heidenreich KA (2002) Insulin-like growth factor-I blocks Bcl-2 interacting mediator of cell death (Bim) induction and intrinsic death signaling in cerebellar granule neurons. J Neurosci 22:9287-9297.

Liu J, Lillo C, Jonsson PA, Vande VC, Ward CM, Miller TM, Subramaniam JR, Rothstein JD, Marklund S, Andersen PM, Brannstrom T, Gredal O, Wong PC, Williams DS, Cleveland DW (2004) Toxicity of familial ALS-linked SOD1 mutants from selective recruitment to spinal mitochondria. Neuron 43:5-17.

Liu J, Shinobu LA, Ward CM, Young D, Cleveland DW (2005) Elevation of the Hsp70 chaperone does not effect toxicity in mouse models of familial amyotrophic lateral sclerosis. J Neurochem 93:875-882.

Liu Y, Fields RD, Festoff BW, Nelson PG (1994) Proteolytic action of thrombin is required for electrical activity-dependent synapse reduction. Proc Natl Acad Sci U S A 91:10300-10304.

Lobsiger CS, Garcia ML, Ward CM, Cleveland DW (2005) Altered axonal architecture by removal of the heavily phosphorylated neurofilament tail domains strongly slows superoxide dismutase 1 mutant-mediated ALS. Proc Natl Acad Sci U S A 102:10351-10356.

Loeb JA, Fischbach GD (1995) ARIA can be released from extracellular matrix through cleavage of a heparin-binding domain. J Cell Biol 130:127-135.

Lohof AM, Ip NY, Poo MM (1993) Potentiation of developing neuromuscular synapses by the neurotrophins NT-3 and BDNF. Nature 363:350-353.

Lowrie MB, Krishnan S, Vrbova G (1987) Permanent changes in muscle and motoneurones induced by nerve injury during a critical period of development of the rat. Brain Res 428:91-101.

Lowrie MB, Vrbova G (1984) Different pattern of recovery of fast and slow muscles following nerve injury in the rat. J Physiol 349:397-410.

Lu B, Czernik AJ, Popov S, Wang T, Poo MM, Greengard P (1996) Expression of synapsin I correlates with maturation of the neuromuscular synapse. Neuroscience 74:1087-1097.

Lupa MT, Gordon H, Hall ZW (1990) A specific effect of muscle cells on the distribution of presynaptic proteins in neurites and its absence in a C2 muscle cell variant. Dev Biol 142:31-43.

Lupa MT, Hall ZW (1989) Progressive restriction of synaptic vesicle protein to the nerve terminal during development of the neuromuscular junction. J Neurosci 9:3937-3945.

Mahoney DJ, Rodriguez C, Devries M, Yasuda N, Tarnopolsky MA (2004) Effects of high-intensity endurance exercise training in the G93A mouse model of amyotrophic lateral sclerosis. Muscle Nerve 29:656-662.

Manfredi G, Xu Z (2005) Mitochondrial dysfunction and its role in motor neuron degeneration in ALS. Mitochondrion 5:77-87.

Maragakis NJ, Dykes-Hoberg M, Rothstein JD (2004) Altered expression of the glutamate transporter EAAT2b in neurological disease. Ann Neurol 55:469-477.

Martin LJ (1999) Neuronal death in amyotrophic lateral sclerosis is apoptosis: possible contribution of a programmed cell death mechanism. J Neuropathol Exp Neurol 58:459-471.

Martinou JC, Falls DL, Fischbach GD, Merlie JP (1991) Acetylcholine receptor-inducing activity stimulates expression of the epsilon-subunit gene of the muscle acetylcholine receptor. Proc Natl Acad Sci U S A 88:7669-7673.

Martinou JC, Martinou I, Kato AC (1992) Cholinergic differentiation factor (CDF/LIF) promotes survival of isolated rat embryonic motoneurons in vitro. Neuron 8:737-744.

Matthews RT, Yang L, Browne S, Baik M, Beal MF (1998) Coenzyme Q10 administration increases brain mitochondrial concentrations and exerts neuroprotective effects. Proc Natl Acad Sci U S A 95:8892-8897.

Mattiazzi M, D'Aurelio M, Gajewski CD, Martushova K, Kiaei M, Beal MF, Manfredi G (2002) Mutated human SOD1 causes dysfunction of oxidative phosphorylation in mitochondria of transgenic mice. J Biol Chem 277:29626-29633.

Mauro A (1961) Satellite cell of skeletal muscle fibers. J Biophys Biochem Cytol 9:493-495.

McClive PJ, Sinclair AH (2001) Rapid DNA extraction and PCR-sexing of mouse embryos. Mol Reprod Dev 60:225-226.

McGeer PL, McGeer EG, Kawamata T, Yamada T, Akiyama H (1991) Reactions of the immune system in chronic degenerative neurological diseases. Can J Neurol Sci 18:376-379.

McHanwell S, Biscoe TJ (1981) The localization of motoneurons supplying the hindlimb muscles of the mouse. Philos Trans R Soc Lond B Biol Sci 293:477-508.

Mckoy G, Ashley W, Mander J, Yang SY, Williams N, Russell B, Goldspink G (1999) Expression of insulin growth factor-1 splice variants and structural genes in rabbit skeletal muscle induced by stretch and stimulation. J Physiol 516 (Pt 2):583-592.

Mentis GZ, Greensmith L, Vrbova G (1993) Motoneurons destined to die are rescued by blocking N-methyl-D-aspartate receptors by MK-801. Neuroscience 54:283-285.

Menzies FM, Ince PG, Shaw PJ (2002) Mitochondrial involvement in amyotrophic lateral sclerosis. Neurochem Int 40:543-551.

Messi ML, Clark HM, Prevette DM, Oppenheim RW, Delbono O (2007) The lack of effect of specific overexpression of IGF-1 in the central nervous system or skeletal muscle on pathophysiology in the G93A SOD-1 mouse model of ALS. Exp Neurol.

Migheli A, Atzori C, Piva R, Tortarolo M, Girelli M, Schiffer D, Bendotti C (1999) Lack of apoptosis in mice with ALS. Nat Med 5:966-967.

Miller RG, Petajan JH, Bryan WW, Armon C, Barohn RJ, Goodpasture JC, Hoagland RJ, Parry GJ, Ross MA, Stromatt SC (1996) A placebo-controlled trial of recombinant human ciliary neurotrophic (rhCNTF) factor in amyotrophic lateral sclerosis. rhCNTF ALS Study Group. Ann Neurol 39:256-260.

Miller TM, Kaspar BK, Kops GJ, Yamanaka K, Christian LJ, Gage FH, Cleveland DW (2005) Virus-delivered small RNA silencing sustains strength in amyotrophic lateral sclerosis. Ann Neurol 57:773-776.

Miller TM, Kim SH, Yamanaka K, Hester M, Umapathi P, Arnson H, Rizo L, Mendell JR, Gage FH, Cleveland DW, Kaspar BK (2006) Gene transfer demonstrates that muscle is not a primary target for non-cell-autonomous toxicity in familial amyotrophic lateral sclerosis. Proc Natl Acad Sci U S A.

Mohajeri MH, Figlewicz DA, Bohn MC (1998) Selective loss of alpha motoneurons innervating the medial gastrocnemius muscle in a mouse model of amyotrophic lateral sclerosis. Exp Neurol 150:329-336.

Montero M, Alonso MT, Albillos A, Garcia-Sancho J, Alvarez J (2001) Mitochondrial Ca(2+)-induced Ca(2+) release mediated by the Ca(2+) uniporter. Mol Biol Cell 12:63-71.

Munch C, Sedlmeier R, Meyer T, Homberg V, Sperfeld AD, Kurt A, Prudlo J, Peraus G, Hanemann CO, Stumm G, Ludolph AC (2004) Point mutations of the p150 subunit of dynactin (DCTN1) gene in ALS. Neurology 63:724-726.

Murakami T, Nagano I, Hayashi T, Manabe Y, Shoji M, Setoguchi Y, Abe K (2001) Impaired retrograde axonal transport of adenovirus-mediated E. coli LacZ gene in the mice carrying mutant SOD1 gene. Neurosci Lett 308:149-152.

Muresan V, Stankewich MC, Steffen W, Morrow JS, Holzbaur EL, Schnapp BJ (2001) Dynactin-dependent, dynein-driven vesicle transport in the absence of membrane proteins: a role for spectrin and acidic phospholipids. Mol Cell 7:173-183.

Nachlas MM, TSOU KC, DE SOUZA E, CHENG CS, SELIGMAN AM (1957) Cytochemical demonstration of succinic dehydrogenase by the use of a new p-nitrophenyl substituted ditetrazole. J Histochem Cytochem 5:420-436.

Nagai M, Re DB, Nagata T, Chalazonitis A, Jessell TM, Wichterle H, Przedborski S (2007) Astrocytes expressing ALS-linked mutated SOD1 release factors selectively toxic to motor neurons. Nat Neurosci 10:615-622.

Nagano I, Ilieva H, Shiote M, Murakami T, Yokoyama M, Shoji M, Abe K (2005) Therapeutic benefit of intrathecal injection of insulin-like growth factor-1 in a mouse model of Amyotrophic Lateral Sclerosis. J Neurol Sci 235:61-68.

Narai H, Nagano I, Ilieva H, Shiote M, Nagata T, Hayashi T, Shoji M, Abe K (2005) Prevention of spinal motor neuron death by insulin-like growth factor-1 associating with the signal transduction systems in SODG93A transgenic mice. J Neurosci Res 82:452-457.

Navarrete R, Vrbova G (1983) Changes of activity patterns in slow and fast muscles during postnatal development. Developmental Brain Research 8:11-19.

Navarrete R, Vrbova G (1993) Activity-dependent interactions between motoneurones and muscles: their role in the development of the motor unit. Prog Neurobiol 41:93-124.

Navarrete R, Vrbova G (1984) Differential effect of nerve injury at birth on the activity pattern of reinnervated slow and fast muscles of the rat. J Physiol 351:675-685.

Neff NT, Prevette D, Houenou LJ, Lewis ME, Glicksman MA, Yin QW, Oppenheim RW (1993) Insulin-like growth factors: putative muscle-derived trophic agents that promote motoneuron survival. J Neurobiol 24:1578-1588.

Neumann M, Sampathu DM, Kwong LK, Truax AC, Micsenyi MC, Chou TT, Bruce J, Schuck T, Grossman M, Clark CM, McCluskey LF, Miller BL, Masliah E, Mackenzie IR, Feldman H, Feiden W, Kretzschmar HA, Trojanowski JQ, Lee VM (2006) Ubiquitinated TDP-43 in frontotemporal lobar degeneration and amyotrophic lateral sclerosis. Science 314:130-133.

Nguyen MD, D'Aigle T, Gowing G, Julien JP, Rivest S (2004) Exacerbation of motor neuron disease by chronic stimulation of innate immunity in a mouse model of amyotrophic lateral sclerosis. J Neurosci 24:1340-1349.

Nicholls DG, Crompton M (1980) Mitochondrial calcium transport. FEBS Lett 111:261-268.

Nicholls DG, Ward MW (2000) Mitochondrial membrane potential and neuronal glutamate excitotoxicity: mortality and millivolts. Trends Neurosci 23:166-174.

Nimchinsky EA, Young MW, Yeung G, Shah RA, Gordon JW, Bloom FE, Morrison JH, Hof PR (2000) Differential vulnerability of oculomotor, facial, and hypoglossal nuclei G86R superoxide dismutase transgenic mice. J Comp Neurol112-125spinal cord motoneurons.

Nirmalananthan N, Greensmith L (2005) Amyotrophic lateral sclerosis: recent advances and future therapies. Curr Opin Neurol 18:712-719.

Nishimura AL, Mitne-Neto M, Silva HC, Oliveira JR, Vainzof M, Zatz M (2004a) A novel locus for late onset amyotrophic lateral sclerosis/motor neurone disease variant at 20q13. J Med Genet 41:315-320.

Nishimura AL, Mitne-Neto M, Silva HC, Richieri-Costa A, Middleton S, Cascio D, Kok F, Oliveira JR, Gillingwater T, Webb J, Skehel P, Zatz M (2004b) A mutation in the vesicle-trafficking protein VAPB causes late-onset spinal muscular atrophy and amyotrophic lateral sclerosis. Am J Hum Genet 75:822-831.

Novikov L, Novikova L, Kellerth JO (1995) Brain-derived neurotrophic factor promotes survival and blocks nitric oxide synthase expression in adult rat spinal motoneurons after ventral root avulsion. Neurosci Lett 200:45-48.

Novikov L, Novikova L, Kellerth JO (1997) Brain-derived neurotrophic factor promotes axonal regeneration and long-term survival of adult rat spinal motoneurons in vivo. Neuroscience 79:765-774.

O'Brien RA, Ostberg A, Vrbova G (1982) The reorganization of the neuromuscular junctions during development in Rats. pp 247-257.

O'Brien RA, Vrbova G (1978) Acetylcholine synthesis in nerve endings to slow and fast muscles of developing chicks: effect of muscle activity. Neuroscience 3:1227-1230.

Oeda T, Shimohama S, Kitagawa N, Kohno R, Imura T, Shibasaki H, Ishii N (2001) Oxidative stress causes abnormal accumulation of familial amyotrophic lateral sclerosis-related mutant SOD1 in transgenic Caenorhabditis elegans. Hum Mol Genet 10:2013-2023.

Ogata T, Yamasaki Y (1985) Scanning electron-miscroscopic studies on the three-dimensional structure of mitochondria in the mammalian red,white and intermediate muscle fibers. Cell Tissue Res 241:251-256.

Okado-Matsumoto A, Fridovich I (2001) Subcellular distribution of superoxide dismutases (SOD) in rat liver: Cu,Zn-SOD in mitochondria. J Biol Chem 276:38388-38393.

Okado-Matsumoto A, Fridovich I (2002) Amyotrophic lateral sclerosis: a proposed mechanism. Proc Natl Acad Sci U S A 99:9010-9014.

Oosthuyse B, et al. (2001) Deletion of the hypoxia-response element in the vascular endothelial growth factor promoter causes motor neuron degeneration. Nat Genet 28:131-138.

Oppenheim RW (1991) Cell death during development of the nervous system. Annu Rev Neurosci 14:453-501.

Palazzolo I, Burnett BG, Young JE, Brenne PL, La Spada AR, Fischbeck KH, Howell BW, Pennuto M (2007) Akt blocks ligand binding and protects against expanded polyglutamine androgen receptor toxicity. Hum Mol Genet 16:1593-1603.

Palecek J, Lips MB, Keller BU (1999) Calcium dynamics and buffering in motoneurones of the mouse spinal cord. J Physiol 520 Pt 2:485-502.

Pasinelli P, Belford ME, Lennon N, Bacskai BJ, Hyman BT, Trotti D, Brown RH, Jr. (2004) Amyotrophic lateral sclerosis-associated SOD1 mutant proteins bind and aggregate with Bcl-2 in spinal cord mitochondria. Neuron 43:19-30.

Pasinelli P, Brown RH (2006) Molecular biology of amyotrophic lateral sclerosis: insights from genetics. Nat Rev Neurosci 7:710-723.

Pieri M, Albo F, Gaetti C, Spalloni A, Bengtson CP, Longone P, Cavalcanti S, Zona C (2003) Altered excitability of motor neurons in a transgenic mouse model of familial amyotrophic lateral sclerosis. Neurosci Lett 351:153-156.

Porter BE, Weis J, Sanes JR (1995) A motoneuron-selective stop signal in the synaptic protein S-laminin. Neuron 14:549-559.

Powell JA, Carrasco MA, Adams DS, Drouet B, Rios J, Muller M, Estrada M, Jaimovich E (2001) IP(3) receptor function and localization in myotubes: an unexplored Ca(2+) signaling pathway in skeletal muscle. J Cell Sci 114:3673-3683.

Pramatarova A, Laganiere J, Roussel J, Brisebois K, Rouleau GA (2001) Neuron-specific expression of mutant superoxide dismutase 1 in transgenic mice does not lead to motor impairment. J Neurosci 21:3369-3374.

Puls I, Jonnakuty C, LaMonte BH, Holzbaur EL, Tokito M, Mann E, Floeter MK, Bidus K, Drayna D, Oh SJ, Brown RH, Jr., Ludlow CL, Fischbeck KH (2003) Mutant dynactin in motor neuron disease. Nat Genet 33:455-456.

Puls I, Oh SJ, Sumner CJ, Wallace KE, Floeter MK, Mann EA, Kennedy WR, Wendelschafer-Crabb G, Vortmeyer A, Powers R, Finnegan K, Holzbaur EL, Fischbeck KH, Ludlow CL (2005) Distal spinal and bulbar muscular atrophy caused by dynactin mutation. Ann Neurol 57:687-694.

Pun S, Santos AF, Saxena S, Xu L, Caroni P (2006) Selective vulnerability and pruning of phasic motoneuron axons in motoneuron disease alleviated by CNTF. Nat Neurosci 9:408-419.

Ralph GS, Radcliffe PA, Day DM, Carthy JM, Leroux MA, Lee DC, Wong LF, Bilsland LG, Greensmith L, Kingsman SM, Mitrophanous KA, Mazarakis ND, Azzouz M (2005) Silencing mutant SOD1 using RNAi protects against neurodegeneration and extends survival in an ALS model. Nat Med 11:429-433.

Raoul C, Abbas-Terki T, Bensadoun JC, Guillot S, Haase G, Szulc J, Henderson CE, Aebischer P (2005) Lentiviral-mediated silencing of SOD1 through RNA interference retards disease onset and progression in a mouse model of ALS. Nat Med 11:423-428.

Raoul C, Buhler E, Sadeghi C, Jacquier A, Aebischer P, Pettmann B, Henderson CE, Haase G (2006) Chronic activation in presymptomatic amyotrophic lateral sclerosis (ALS) mice of a feedback loop involving Fas, Daxx, and FasL. Proc Natl Acad Sci U S A 103:6007-6012.

Raoul C, Estevez AG, Nishimune H, Cleveland DW, deLapeyriere O, Henderson CE, Haase G, Pettmann B (2002) Motoneuron death triggered by a specific pathway downstream of Fas. potentiation by ALS-linked SOD1 mutations. Neuron 35:1067-1083.

Raoul C, Henderson CE, Pettmann B (1999) Programmed cell death of embryonic motoneurons triggered through the Fas death receptor. J Cell Biol 147:1049-1062.

Reaume AG, Elliott JL, Hoffman EK, Kowall NW, Ferrante RJ, Siwek DF, Wilcox HM, Flood DG, Beal MF, Brown RH, Jr., Scott RW, Snider WD (1996) Motor neurons in Cu/Zn superoxide dismutase-deficient mice develop normally but exhibit enhanced cell death after axonal injury. Nat Genet 13:43-47.

Rizzardini M, Mangolini A, Lupi M, Ubezio P, Bendotti C, Cantoni L (2005) Low levels of ALS-linked Cu/Zn superoxide dismutase increase the production of reactive oxygen species and cause mitochondrial damage and death in motor neuron-like cells. J Neurol Sci 232:95-103.

Rizzuto R, Bernardi P, Pozzan T (2000) Mitochondria as all round- players of the calcium game. J Physiol 529:47.

Robertson J, Doroudchi MM, Nguyen MD, Durham HD, Strong MJ, Shaw G, Julien JP, Mushynski WE (2003) A neurotoxic peripherin splice variant in a mouse model of ALS. J Cell Biol 160:939-949.

Robertson J, Sanelli T, Xiao S, Yang W, Horne P, Hammond R, Pioro EP, Strong MJ (2007) Lack of TDP-43 abnormalities in mutant SOD1 transgenic mice shows disparity with ALS. Neurosci Lett 420:128-132.

Rosen DR (1993) Mutations in Cu/Zn superoxide dismutase gene are associated with familial amyotrophic lateral sclerosis. Nature 364:362.

Rothstein JD, Jin L, Dykes-Hoberg M, Kuncl RW (1993) Chronic inhibition of glutamate uptake produces a model of slow neurotoxicity. Proc Natl Acad Sci U S A 90:6591-6595.

Rothstein JD, Patel S, Regan MR, Haenggeli C, Huang YH, Bergles DE, Jin L, Dykes HM, Vidensky S, Chung DS, Toan SV, Bruijn LI, Su ZZ, Gupta P, Fisher PB (2005) Beta-lactam antibiotics offer neuroprotection by increasing glutamate transporter expression. Nature 433:73-77.

Rothstein JD, Van Kammen M, Levey AI, Martin LJ, Kuncl RW (1995) Selective loss of glial glutamate transporter GLT-1 in amyotrophic lateral sclerosis. Ann Neurol 38:73-84.

Ruddy DM, Parton MJ, Al Chalabi A, Lewis CM, Vance C, Smith BN, Leigh PN, Powell JF, Siddique T, Meyjes EP, Baas F, de J, V, Shaw CE (2003) Two families with familial amyotrophic lateral sclerosis are linked to a novel locus on chromosome 16q. Am J Hum Genet 73:390-396.

Rudolf R, Mongillo M, Magalhaes PJ, Pozzan T (2004) In vivo monitoring of Ca(2+) uptake into mitochondria of mouse skeletal muscle during contraction. J Cell Biol 166:527-536.

Sapp PC, Hosler BA, McKenna-Yasek D, Chin W, Gann A, Genise H, Gorenstein J, Huang M, Sailer W, Scheffler M, Valesky M, Haines JL, Pericak-Vance M, Siddique T, Horvitz HR, Brown RH, Jr. (2003) Identification of two novel loci for dominantly inherited familial amyotrophic lateral sclerosis. Am J Hum Genet 73:397-403.

Sasaki S, Iwata M (1996) Impairment of fast axonal transport in the proximal axons of anterior horn neurons in amyotrophic lateral sclerosis. Neurology 47:535-540.

Sasaki S, Komori T, Iwata M (2000) Excitatory amino acid transporter 1 and 2 immunoreactivity in the spinal cord in amyotrophic lateral sclerosis. Acta Neuropathol (Berl) 100:138-144.

Sasaki S, Warita H, Abe K, Iwata M (2005) Impairment of axonal transport in the axon hillock and the initial segment of anterior horn neurons in transgenic mice with a G93A mutant SOD1 gene. Acta Neuropathol (Berl) 110:48-56.

Schiffer D, Cordera S, Cavalla P, Migheli A (1996) Reactive astrogliosis of the spinal cord in amyotrophic lateral sclerosis. J Neurol Sci 139 Suppl:27-33.

Sendtner M, Holtmann B, Kolbeck R, Thoenen H, Barde YA (1992) Brain-derived neurotrophic factor prevents the death of motoneurons in newborn rats after nerve section. Nature 360:757-759.

Sendtner M, Kreutzberg GW, Thoenen H (1990) Ciliary neurotrophic factor prevents the degeneration of motor neurons after axotomy. Nature 345:440-441.

Sharp PS, Dekkers J, Dick JR, Greensmith L (2003) Manipulating transmitter release at the neuromuscular junction of neonatal rats alters the expression of ChAT and GAP-43 in motoneurons. Brain Res Dev Brain Res 146:29-38.

Sharp PS, Dick JR, Greensmith L (2005) The effect of peripheral nerve injury on disease progression in the SOD1(G93A) mouse model of amyotrophic lateral sclerosis. Neuroscience 130:897-910.

Shaw PJ, Ince PG, Falkous G, Mantle D (1995) Oxidative damage to protein in sporadic motor neuron disease spinal cord. Ann Neurol 38:691-695.

Shi X, Garry DJ (2006) Muscle stem cells in development, regeneration, and disease. Genes Dev 20:1692-1708.

Shinder GA, Lacourse MC, Minotti S, Durham HD (2001) Mutant Cu/Zn-superoxide dismutase proteins have altered solubility and interact with heat shock/stress proteins in models of amyotrophic lateral sclerosis. J Biol Chem 276:12791-12796.

Siklos L, Engelhardt J, Alexianu ME, Gurney ME, Siddique T, Appel SH (1998) Intracellular calcium parallels motoneuron degeneration in SOD-1 mutant mice. J Neuropathol Exp Neurol 57:571-587.

Siklos L, Engelhardt J, Harati Y, Smith RG, Joo F, Appel SH (1996a) Ultrastructural evidence for altered calcium in motor nerve terminals in amyotropic lateral sclerosis. Ann Neurol 39:203-216.

Siklos L, Engelhardt J, Harati Y, Smith RG, Joo F, Appel SH (1996b) Ultrastructural evidence for altered calcium in motor nerve terminals in amyotropic lateral sclerosis. Ann Neurol 39:203-216.

Skarli M, Kiri A, Vrbova G, Lee CA, Goldspink G (1998) Myosin regulatory elements as vectors for gene transfer by intramuscular injection. Gene Ther 5:514-520.

Smith RA, Miller TM, Yamanaka K, Monia BP, Condon TP, Hung G, Lobsiger CS, Ward CM, McAlonis-Downes M, Wei H, Wancewicz EV, Bennett CF, Cleveland DW (2006) Antisense oligonucleotide therapy for neurodegenerative disease. J Clin Invest 116:2290-2296.

Soraru G, Vergani L, Fedrizzi L, D'Ascenzo C, Polo A, Bernazzi B, Angelini C (2007) Activities of mitochondrial complexes correlate with nNOS amount in muscle from ALS patients. Neuropathol Appl Neurobiol 33:204-211.

Sterneck E, Kaplan DR, Johnson PF (1996) Interleukin-6 induces expression of peripherin and cooperates with Trk receptor signaling to promote neuronal differentiation in PC12 cells. J Neurochem 67:1365-1374.

Storkebaum E, et al. (2005) Treatment of motoneuron degeneration by intracerebroventricular delivery of VEGF in a rat model of ALS. Nat Neurosci 8:85-92.

Swanson GJ, Vrbova G (1987) Effects of low calcium and inhibition of calcium-activated neutral protease (CANP) on mature nerve terminal structure in the rat sternocostalis muscle. Brain Res 430:199-203.

Swett JE, Wikholm RP, Blanks RH, Swett AL, Conley LC (1986) Motoneurons of the rat sciatic nerve. Exp Neurol 93:227-252.

Takeuchi H, Kobayashi Y, Yoshihara T, Niwa J, Doyu M, Ohtsuka K, Sobue G (2002) Hsp70 and Hsp40 improve neurite outgrowth and suppress intracytoplasmic aggregate formation in cultured neuronal cells expressing mutant SOD1. Brain Res 949:11-22.

Talbot K (2002) Motor neurone disease. Postgrad Med J 78:513-519.

Tan SA, Deglon N, Zurn AD, Baetge EE, Bamber B, Kato AC, Aebischer P (1996) Rescue of motoneurons from axotomy-induced cell death by polymer encapsulated cells genetically engineered to release CNTF. Cell Transplant 5:577-587.

Tanabe Y, William C, Jessell TM (1998) Specification of motor neuron identity by the MNR2 homeodomain protein. Cell 95:67-80.

Tanaka M, Kim YM, Lee G, Junn E, Iwatsubo T, Mouradian MM (2004) Aggresomes formed by alpha-synuclein and synphilin-1 are cytoprotective. J Biol Chem 279:4625-4631.

Torgan CE, Daniels MP (2001) Regulation of myosin heavy chain expression during rat skeletal muscle development in vitro. Mol Biol Cell 12:1499-1508.

Torres-Aleman I, Villalba M, Nieto-Bona MP (1998) Insulin-like growth factor-I modulation of cerebellar cell populations is developmentally stage-dependent and mediated by specific intracellular pathways. Neuroscience 83:321-334.

Trejo JL, Carro E, Garcia-Galloway E, Torres-Aleman I (2004) Role of insulin-like growth factor I signaling in neurodegenerative diseases. J Mol Med 82:156-162.

Trieu VN, Liu R, Liu XP, Uckun FM (2000) A specific inhibitor of janus kinase-3 increases survival in a transgenic mouse model of amyotrophic lateral sclerosis. Biochem Biophys Res Commun 267:22-25.

Troost D, Claessen N, van den Oord JJ, Swaab DF, de Jong JM (1993) Neuronophagia in the motor cortex in amyotrophic lateral sclerosis. Neuropathol Appl Neurobiol 19:390-397.

Trotti D, Rolfs A, Danbolt NC, Brown RH, Jr., Hediger MA (1999) SOD1 mutants linked to amyotrophic lateral sclerosis selectively inactivate a glial glutamate transporter. Nat Neurosci 2:848.

Troy CM, Brown K, Greene LA, Shelanski ML (1990a) Ontogeny of the neuronal intermediate filament protein, peripherin, in the mouse embryo. Neuroscience 36:217-237.

Troy CM, Muma NA, Greene LA, Price DL, Shelanski ML (1990b) Regulation of peripherin and neurofilament expression in regenerating rat motor neurons. Brain Res 529:232-238.

Tu PH, Raju P, Robinson KA, Gurney ME, Trojanowski JQ, Lee VM (1996) Transgenic mice carrying a human mutant superoxide dismutase transgene develop neuronal cytoskeletal pathology resembling human amyotrophic lateral sclerosis lesions. Proc Natl Acad Sci U S A 93:3155-3160.

Turner MR, Cagnin A, Turkheimer FE, Miller CC, Shaw CE, Brooks DJ, Leigh PN, Banati RB (2004) Evidence of widespread cerebral microglial activation in amyotrophic lateral sclerosis: an [11C](R)-PK11195 positron emission tomography study. Neurobiol Dis 15:601-609.

Tyc F, Vrbova G (1995) Stabilisation of neuromuscular junctions by leupeptin increases motor unit size in partially denervated rat muscles. Brain Res Dev Brain Res 88:186-193.

Van Damme P, Leyssen M, Callewaert G, Robberecht W, Van Den BL (2003) The AMPA receptor antagonist NBQX prolongs survival in a transgenic mouse model of amyotrophic lateral sclerosis. Neurosci Lett 343:81-84.

van Dellen A, Blakemore C, Deacon R, York D, Hannan AJ (2000) Delaying the onset of Huntington's in mice. Nature 404:721-722.

Van Den BL, Robberecht W (2000) Different receptors mediate motor neuron death induced by short and long exposures to excitotoxicity. Brain Res Bull 53:383-388.

Van Den BL, Schwaller B, Vleminckx V, Meijers B, Stork S, Ruehlicke T, Van Houtte E, Klaassen H, Celio MR, Missiaen L, Robberecht W, Berchtold MW (2002a) Protective effect of parvalbumin on excitotoxic motor neuron death. Exp Neurol 174:150-161.

Van Den BL, Tilkin P, Lemmens G, Robberecht W (2002b) Minocycline delays disease onset and mortality in a transgenic model of ALS. Neuroreport 13:1067-1070.

Van Den BL, Vandenberghe W, Klaassen H, Van Houtte E, Robberecht W (2000) Ca(2+)-permeable AMPA receptors and selective vulnerability of motor neurons. J Neurol Sci 180:29-34.

Vandenberghe W, Ihle EC, Patneau DK, Robberecht W, Brorson JR (2000a) AMPA receptor current density, not desensitization, predicts selective motoneuron vulnerability. J Neurosci 20:7158-7166.

Vandenberghe W, Robberecht W, Brorson JR (2000b) AMPA receptor calcium permeability, GluR2 expression, and selective motoneuron vulnerability. J Neurosci 20:123-132.

Vanselow BK, Keller BU (2000) Calcium dynamics and buffering in oculomotor neurones from mouse that are particularly resistant during amyotrophic lateral sclerosis (ALS)-related motoneurone disease. J Physiol 525 Pt 2:433-445.

Vejsada R, Sagot Y, Kato AC (1995) Quantitative comparison of the transient rescue effects of neurotrophic factors on axotomized motoneurons in vivo. Eur J Neurosci 7:108-115.

Veldink JH, Bar PR, Joosten EA, Otten M, Wokke JH, van den Berg LH (2003) Sexual differences in onset of disease and response to exercise in a transgenic model of ALS. Neuromuscul Disord 13:737-743.

Vielhaber S, Kunz D, Winkler K, Wiedemann FR, Kirches E, Feistner H, Heinze HJ, Elger CE, Schubert W, Kunz WS (2000) Mitochondrial DNA abnormalities in skeletal muscle of patients with sporadic amyotrophic lateral sclerosis. Brain 123 (Pt 7):1339-1348.

Vijayvergiya C, Beal MF, Buck J, Manfredi G (2005) Mutant superoxide dismutase 1 forms aggregates in the brain mitochondrial matrix of amyotrophic lateral sclerosis mice. J Neurosci 25:2463-2470.

von Lewinski F, Keller BU (2005) Ca2+, mitochondria and selective motoneuron vulnerability: implications for ALS. Trends Neurosci 28:494-500.

Vukosavic S, Dubois-Dauphin M, Romero N, Przedborski S (1999) Bax and Bcl-2 interaction in a transgenic mouse model of familial amyotrophic lateral sclerosis. J Neurochem 73:2460-2468.

Wang LJ, Lu YY, Muramatsu S, Ikeguchi K, Fujimoto K, Okada T, Mizukami H, Matsushita T, Hanazono Y, Kume A, Nagatsu T, Ozawa K, Nakano I (2002) Neuroprotective effects of glial cell line-derived neurotrophic factor mediated by an adeno-associated virus vector in a transgenic animal model of amyotrophic lateral sclerosis. J Neurosci 22:6920-6928.

Watanabe M, Dykes-Hoberg M, Culotta VC, Price DL, Wong PC, Rothstein JD (2001) Histological evidence of protein aggregation in mutant SOD1 transgenic mice and in amyotrophic lateral sclerosis neural tissues. Neurobiol Dis 8:933-941.

Waterman-Storer CM, Karki S, Holzbaur EL (1995) The p150Glued component of the dynactin complex binds to both microtubules and the actin-related protein centractin (Arp-1). Proc Natl Acad Sci U S A 92:1634-1638.

Waterman-Storer CM, Karki SB, Kuznetsov SA, Tabb JS, Weiss DG, Langford GM, Holzbaur EL (1997) The interaction between cytoplasmic dynein and dynactin is required for fast axonal transport. Proc Natl Acad Sci U S A 94:12180-12185.

West M, Mhatre M, Ceballos A, Floyd RA, Grammas P, Gabbita SP, Hamdheydari L, Mai T, Mou S, Pye QN, Stewart C, West S, Williamson KS, Zemlan F, Hensley K (2004) The arachidonic acid 5-lipoxygenase inhibitor nordihydroguaiaretic acid inhibits tumor necrosis factor alpha activation of microglia and extends survival of G93A-SOD1 transgenic mice. J Neurochem 91:133-143.

Weydt P, Yuen EC, Ransom BR, Moller T (2004) Increased cytotoxic potential of microglia from ALS-transgenic mice. Glia 48:179-182.

White CM, Greensmith L, Vrbova G (2000) Repeated stimuli for axonal growth causes motoneuron death in adult rats: the effect of botulinum toxin followed by partial denervation. Neuroscience 95:1101-1109.

Wiedemann FR, Winkler K, Kuznetsov AV, Bartels C, Vielhaber S, Feistner H, Kunz WS (1998) Impairment of mitochondrial function in skeletal muscle of patients with amyotrophic lateral sclerosis. J Neurol Sci 156:65-72.

Wilczak N, de Vos RA, De Keyser J (2003) Free insulin-like growth factor (IGF)-I and IGF binding proteins 2, 5, and 6 in spinal motor neurons in amyotrophic lateral sclerosis. Lancet 361:1007-1011.

Williams TL, Ince PG, Oakley AE, Shaw PJ (1996) An immunocytochemical study of the distribution of AMPA selective glutamate receptor subunits in the normal human motor system. Neuroscience 74:185-198.

Williamson TL, Cleveland DW (1999) Slowing of axonal transport is a very early event in the toxicity of ALS-linked SOD1 mutants to motor neurons. Nat Neurosci 2:50-56.

Wong PC, Pardo CA, Borchelt DR, Lee MK, Copeland NG, Jenkins NA, Sisodia SS, Cleveland DW, Price DL (1995) An adverse property of a familial ALS-linked SOD1 mutation causes motor neuron disease characterized by vacuolar degeneration of mitochondria. Neuron 14:1105-1116.

Wong V, Arriaga R, Ip NY, Lindsay RM (1993) The neurotrophins BDNF, NT-3 and NT-4/5, but not NGF, up-regulate the cholinergic phenotype of developing motor neurons. Eur J Neurosci 5:466-474.

Wood-Allum CA, Barber SC, Kirby J, Heath P, Holden H, Mead R, Higginbottom A, Allen S, Beaujeux T, Alexson SE, Ince PG, Shaw PJ (2006) Impairment of

mitochondrial anti-oxidant defence in SOD1-related motor neuron injury and amelioration by ebselen. Brain 129:1693-1709.

Wozniak AC, Kong J, Bock E, Pilipowicz O, Anderson JE (2005) Signaling satellite-cell activation in skeletal muscle: markers, models, stretch, and potential alternate pathways. Muscle Nerve 31:283-300.

Xia X, Zhou H, Huang Y, Xu Z (2006) Allele-specific RNAi selectively silences mutant SOD1 and achieves significant therapeutic benefit in vivo. Neurobiol Dis 23:578-586.

Xiao Q, Zhao W, Beers DR, Yen AA, Xie W, Henkel JS, Appel SH (2007) Mutant SOD1(G93A) microglia are more neurotoxic relative to wild-type microglia. J Neurochem.

Xie ZP, Poo MM (1986) Initial events in the formation of neuromuscular synapse: rapid induction of acetylcholine release from embryonic neuron. Proc Natl Acad Sci U S A 83:7069-7073.

Xu Z, Cork LC, Griffin JW, Cleveland DW (1993) Increased expression of neurofilament subunit NF-L produces morphological alterations that resemble the pathology of human motor neuron disease. Cell 73:23-33.

Yamanaka K, Miller TM, McAlonis-Downes M, Chun SJ, Cleveland DW (2006) Progressive spinal axonal degeneration and slowness in ALS2-deficient mice. Ann Neurol 60:95-104.

Yan Q, Elliott J, Snider WD (1992) Brain-derived neurotrophic factor rescues spinal motor neurons from axotomy-induced cell death. Nature 360:753-755.

Yan Q, Matheson C, Lopez OT (1995) In vivo neurotrophic effects of GDNF on neonatal and adult facial motor neurons. Nature 373:341-344.

Yang S, Alnaqeeb M, Simpson H, Goldspink G (1996) Cloning and characterization of an IGF-1 isoform expressed in skeletal muscle subjected to stretch. J Muscle Res Cell Motil 17:487-495.

Yang SY, Goldspink G (2002) Different roles of the IGF-I Ec peptide (MGF) and mature IGF-I in myoblast proliferation and differentiation. FEBS Lett 522:156-160.

Yang Y, Hentati A, Deng HX, Dabbagh O, Sasaki T, Hirano M, Hung WY, Ouahchi K, Yan J, Azim AC, Cole N, Gascon G, Yagmour A, Ben Hamida M, Pericak-Vance M, Hentati F, Siddique T (2001) The gene encoding alsin, a protein with three guanine-nucleotide exchange factor domains, is mutated in a form of recessive amyotrophic lateral sclerosis. Nat Genet 29:160-165.

Yrjanheikki J, Tikka T, Keinanen R, Goldsteins G, Chan PH, Koistinaho J (1999) A tetracycline derivative, minocycline, reduces inflammation and protects against focal

cerebral ischemia with a wide therapeutic window. Proc Natl Acad Sci U S A 96:13496-13500.

Zamzami N, Marchetti P, Castedo M, Hirsch T, Susin SA, Masse B, Kroemer G (1996) Inhibitors of permeability transition interfere with the disruption of the mitochondrial transmembrane potential during apoptosis. FEBS Lett 384:53-57.

Zhang B, Tu P, Abtahian F, Trojanowski JQ, Lee VM (1997) Neurofilaments and orthograde transport are reduced in ventral root axons of transgenic mice that express human SOD1 with a G93A mutation. J Cell Biol 139:1307-1315.

Zhang W, Narayanan M, Friedlander RM (2003) Additive neuroprotective effects of minocycline with creatine in a mouse model of ALS. Ann Neurol 53:267-270.

Zhao W, Xie W, Xiao Q, Beers DR, Appel SH (2006) Protective effects of an anti-inflammatory cytokine, interleukin-4, on motoneuron toxicity induced by activated microglia. J Neurochem 99:1176-1187.

Zhou J, Yi J, Royer L, Launikonis BS, Gonzalez A, Garcia J, Rios E (2006) A probable role of dihydropyridine receptors in repression of Ca2+ sparks demonstrated in cultured mammalian muscle. Am J Physiol Cell Physiol 290:C539-C553.

Zhu S, Stavrovskaya IG, Drozda M, Kim BY, Ona V, Li M, Sarang S, Liu AS, Hartley DM, Wu DC, Gullans S, Ferrante RJ, Przedborski S, Kristal BS, Friedlander RM (2002) Minocycline inhibits cytochrome c release and delays progression of amyotrophic lateral sclerosis in mice. Nature 417:74-78.

Zimmerman MC, Oberley LW, Flanagan SW (2007) Mutant SOD1-induced neuronal toxicity is mediated by increased mitochondrial superoxide levels. J Neurochem 102:609-618.

Zoubine MN, Ma JY, Smirnova IV, Citron BA, Festoff BW (1996) A molecular mechanism for synapse elimination: novel inhibition of locally generated thrombin delays synapse loss in neonatal mouse muscle. Dev Biol 179:447-457.

Zurn AD, Baetge EE, Hammang JP, Tan SA, Aebischer P (1994) Glial cell line-derived neurotrophic factor (GDNF), a new neurotrophic factor for motoneurones. Neuroreport 6:113-118.